UNIVERSITY OF SOUTHAMPTON

FACULTY OF PHYSICAL AND APPLIED SCIENCES

Electronics and Computer Science

An Investigation into Solid Dielectrics

by

Tobias A. Kleemann

Thesis for the degree of Doctor of Philosophy

July 2012

UNIVERSITY OF SOUTHAMPTON

ABSTRACT

FACULTY OF PHYSICAL AND APPLIED SCIENCES
Electronics and Computer Science

Doctor of Philosophy

AN INVESTIGATION INTO SOLID DIELECTRICS

by Tobias A. Kleemann

Direct measurement techniques for the investigation of electrical processes in solid dielectrics are reviewed and their respective strengths and weaknesses are discussed, particularly the complementary nature of thermally stimulated current measurements. The successful design and construction of a new Thermally Stimulated Discharge Current (TSDC) Spectrometer at the University of Southampton is presented and its correct function validated with experimental measurements of the well known and often characterized synthetic polymers low density polyethylene (LDPE) and polyethylene terephtalate (PET). Results were found to correspond well to published data. First TSDC observations of filled and oil impregnated papers are presented.

The second aspect of this work is the investigation of natural polymer insulation materials, specifically paper for oil-paper insulation systems. For the first time, electrical insulation papers with filler contents up to 50% were investigated. Bentonite and talcum were compared as filler materials and found to have negative and positive effects respectively. The superior electrical strength of a talcum filled kraft paper was verified, and a series of constructive modifications was undertaken to further maximise its electrical strength at comparable or improved dielectric performance. An increase in electrical breakdown strength of 20 % to 30 % has been observed, but the substitution of such great amounts of fiber with fillers also lead to a reduction in mechanical strength of the paper. Further trials with chemical additives were conducted to counteract this effect and polyvinyl alcohol and starch were found to enhance the paper strength. Additional trials also comprised sizing agents, guar gum and wet strength agents. Uncharged or slightly charged chemical additives provided best results with regard to dielectric performance. The significance of the trialled paper modifications is judged in light of statistical analysis.

Contents

List of Figures

List of Tables

Listings

Declaration of Authorship

I, Tobias A. Kleemann, declare that the thesis entitled

An Investigation into Solid Dielectrics

and the work presented in the thesis are both my own, and have been generated by me as the result of my own original research.

I confirm that:

1. this work was done wholly or mainly while in candidature for a research degree at this University;
2. where any part of this thesis has previously been submitted for a degree or any other qualification at this University or any other institution, this has been clearly stated;
3. where I have consulted the published work of others, this is always clearly attributed;
4. where I have quoted from the work of others, the source is always given. With the exception of such quotations, this thesis is entirely my own work;
5. I have acknowledged all main sources of help;
6. where the thesis is based on work done by myself jointly with others, I have made clear exactly what was done by others and what I have contributed myself;
7. parts of this work have been published. Please see references below.

Signed:

Date:

T. Kleemann, P. Lewin, S. Badak, and S. Kleemann. Paper & Power: Modifying Electrical Insulation Paper. Professional Papermaking, 9:21–24, 2012.

T. Kleemann, P. Lewin, S. Badak, and S. Kleemann. Paper & Power: Optimierung von Isolationspapieren. Wochenblatt für Papierfabrikation, 6:468–471, 2012.

Presentations at the *International Munich Paper Symposium 2012* in Munich,Germany; and the congress of the Italian paper industry, *Congresso Aticelca 2012* in Ascoli Piceno, Italy.

Acknowledgements

I would like to thank the people at the Tony Davies High Voltage Laboratory for their company and support during the time of my work. Particularly, Prof. Dr. Paul Lewin for his assistance and encouragement as my supervisor; Neil Palmer, for many a helpful engineering suggestion and general support as laboratory manager. Mike and Brian, as the people who make the concepts take shape; and Ian, Mark and Chris, for their various help around the laboratory. Thank you also to everyone at the IVP, especially to Sachin Badakh from PaCon, for his help in the manufacture and characterisation of the paper samples, and Anke Lind for the support with the scanning electron microscope.

To my parents, whose unwavering support made it all possible; and to my grandfather, who cultivated my interest in physics and engineering from an early age.

Abbreviations

AC	Alternating Current
ANOVA	Analysis Of Variance
BNC	Bayonet Neill-Concelman (BNC) connector
BSCCO	Bismuth Strontium Calcium Copper Oxide
DC	Direct Current
DMRT	Dynamical Mechanical Rheological Testing
DMTA	Dynamical Mechanical Thermal Analysis
DSC	Differentially Scanning Calorimetry
DUT	Device Under Test
ECF	Elementary Chlorine Free
FLIMM	Focused Laser Intensity Modulation Method
FRA	Frequency Response Analyser
GPIB	General Purpose Interface Bus (IEEE-488)
GUI	Graphical User Interface
HTS	High-Temperature Superconductivity
HV	High Voltage
IIR	Infinite Impulse Response
IVP	Institute for Papertechnology
laser	Light Amplification by Stimulated Emission of Radiation
LDPE	Low–Density Polyethylene
lHe	Liquid Helium
LIMM	Laser Intensity Modulation Method
LIPP	Laser Induced Pressure Pulse (method)
liquid-N_2	Liquid Nitrogen
LTS	Low Temperature Superconductivity
MEB	Scanning Electron Microscope (French abbr.)
NPLC	Number of Power Line Cycles
OS	Operating System
PAAE	Poylamidoamine–Epichlorohydrin
PD	Partial Discharge
PE	Polyethylene
PEA	Pulse-Electroacoustic (method)

PET	Polyethylene Terephthalate
PI	Polyimide
PIPP	Piezoelectrically Induced Pressure Pulse (method)
PIPS	Piezoelectrically Induced Pressure Step (method)
PPS	Polyphenylene Sulfide
PTFE	Polytetrafluoroethylene
PVA	Polyvinyl Alcohol
PWM	Pulse Width Modulation
PWP	Pressure Wave Propagation (measurement method)
SEM	Scanning Electron Microscope
SF_6	Sulfur Hexafluoride
SI	International System of Units (French: le Système international d'unités)
SID	Sample Identification (number)
SNR	Signal-to-Noise ratio
SR	Schopper Riegler Value
SSR	Solid State Relay
TDM	Thermal Diffusion Method(s)
TEC	Thermoelectric cooler/cooling Element
TPM	Thermal Pulse Method
TRX	Triaxial i.e. three concentric conductors
TSC	Thermally Stimulated Current
TSCS	Thermally Stimulated Current Spectroscopy
TSDC	Thermally Stimulated Discharge Current
TSM	Thermal Step Method
TSM-IHT	Thermal Step Method – Inner Heating Technique
TSM-OCT	Thermal Step Method – Outer Cooling Technique
TSPC	Thermally Stimulated Polarisation Current
UHMW-PE	Ultra High Molecular Weight Polyethylene
WSA	Wet–Strength Agent (Chemical Additive)
XLPE	Cross–Linked Polyethylene
YBCO	Yttrium barium copper oxide

Symbols

T_C	Curie point or Curie temperature
T_{glass}	Glass transition temperature
E_{con}	Conduction band
E_{val}	Valence band
E_f	Fermi energy (level)
ρ_c	Charge density (Cm^{-3})
ϵ	Permittivity
ϵ_0	Vacuum permittivity or permittivity of free space
ϵ_r	Relative permittivity or dielectric constant
P_{FD}	Fermi–Dirac distribution function
ϕ_{metal}	Dielectric work function
χ_{dielec}	Dielectric electron affinity

Chapter 1

Introduction

The concurrent effects of growing energy demands, technological progress and the deregulation of the energy market provoke proactive utility companies to maintain, upgrade or install transmission and distribution capacity in order to ensure robustness and flexibility in their networks. In order to reduce the risk of blackouts and to provide a continuous supply of electricity, the power industry is looking to research to provide better solutions for current problems and future challenges in the energy sector. In order to improve existing electrical application and to further the general understanding of dielectric materials in the electrical industry, it is necessary and desirable to find and characterise new and existing solid dielectrics that are mechanically and electrically robust over the entire temperature range and life-span in which high-voltage power devices operate.

Amorphous and semi-crystalline polymers are favoured as insulation materials in a variety of electrical applications due to their reasonable cost and ease of manufacture. While being extremely suitable for alternate current (AC) operations, their tendency to accumulate charge in the bulk of the material introduces problems in direct current (DC) operation. This excess charge can severely and prematurely deteriorate the breakdown strength of the insulation. It is therefore desirable to investigate the propensity of different solid dielectrics to accumulate electrical charge, and to characterise the nature of that charge in order to better understand the aging phenomenon, and to develop better dielectric insulation materials. To that end, this work introduces a custom built instrument for the measurement of thermally stimulated discharge currents that is now available at the University of Southampton for the observation of thin layers of solid dielectric materials. A number of candidate materials have been measured in the instrument and their responses are presented and discussed in the light of published data.

In the context of this work on solid dielectrics, the term polymers encompasses both synthetic polymers as well as natural polymers. While the former has gained increasing popularity and use in the form of extruded or cast insulation elements, one should

not forget the latter. Of the class of natural polymers, the economic and sustainable polymeric material cellulose is employed most in the electrical industry. It is well known and still actively being used for the manufacture of paper-oil insulation and transformer boards. With the deployment and industrial use of superconducting power devices progressing slowly, the potential to improve electrical insulation systems based around the familiar natural polyanhydroglucose polymer should not be neglected. The electrical industry currently favours insulation papers that are made only from pure cellulose, not taking advantage of possible financial savings or performance gains that may be attained by a suitable substitution of fibres or intelligent use of chemical additives, both of which are common in the paper industry. This research investigates the feasibility of improving the performance of paper-oil insulation systems through the development of paper technology. A series of constructive trials have been conducted in which paper was modified and the electrical performance tested and compared to zero-sheets of virgin laboratory paper as well as to commercially available insulation papers. Due to the fact that paper is almost exclusively employed in conjunction with a liquid impregnating agent, most commonly oil, the properties of the modified papers were determined for dry as well as oil impregnated paper where possible. The newly built TSDC Spectrometer has been employed for the first time to test to what extent paper-oil insulation may be investigate using thermally stimulated discharge current measurements, and whether its propensity for the accumulation of space charge may be determined in that way.

1.1 Research Aims and Objectives

The aims of this research are to provide an introduction into the mechanism of charge transport in solid dielectric materials, to give an overview of different space charge measurement methods, and generally to gain an insight into the behaviour of solid polymer dielectrics in their function as electrical insulation materials. The objective is twofold. Firstly, to build a Thermally Stimulated Discharge Current (TSDC) Spectrometer and to use it to characterise synthetic as well as natural polymers; and secondly, to find ways in which the performance of natural polymer dielectric systems, more precisely cellulose based electrical insulation paper, may be improved. To that end, a series of comparative trials is set to explore and quantify the effects of different mechanical and chemical modifications on the electrical and dielectric performance of paper–oil insulation. Desirable are the identification of new electrical insulation papers that are either more economical to manufacture but have the same electrical performance, or papers with much improved electrical performance.

1.2 Contributions of this Thesis

This research study describes in detail the construction, development and improvement of a large–electrode TSDC spectrometer, and in this way adds to the practical knowledge of instrumentation and measurement science. A series of constructive trials assess possible modifications of paper for their impact on the electrical performance of this natural polymeric dielectric material. For the very first time, the application of talcum in filled papers is introduced as a successful modification of cellulose insulation systems for electrical purposes and its electrical properties are demonstrated. Considered in more detail, the major contributions are as follows:

The custom TSDC spectrometer is employed for measurements of natural polymer composite materials. TSDC spectra of oil soaked and vacuum oil–impregnated cellulose paper systems are presented. For the very first time, TSDC results of highly filled papers using a talcum filler are presented and compared with pulp–only papers.

Different types of pulp are tested for their electrical breakdown strength and mechanical tensile strength. The industry standard of unbleached softwood kraft pulp is shown to perform better than either the bleached kind, or the hardwood pulp.

Papers modified to include a hydrophilic bentonite powder or a hydrophobic talcum powder are trialled against unfilled paper and commercial reference papers. The talcum filled paper samples are shown to have comparable or increased electrical breakdown strength. Dielectric spectroscopy results for talcum filled papers of different filler contents are presented. Different filler contents are explored for an optimisation of electrical breakdown strength against a concomitant loss in tensile strength.

Calendering, a mechanical processing step in the paper production, is introduced and investigated for its effect on the electrical breakdown strength, permittivity and dissipation factor of talcum filled paper for electrical purposes. Results for different pressure settings and number of iterations are presented. Analysis shows that electrical breakdown strength is improved, but dielectric performance reduced by calendering. Furthermore, the magnitude of the pressure setting appears more significant than the number of calendering applications.

Starch and polyvinyl alcohol are explored as chemical additives in talcum filled papers for electrical purposes. Their effects on mechanical tensile strength, electrical breakdown strength, real relative permittivity and the dissipation factor are discussed. A further trial compares polyvinyl alcohols with different degrees of hydrolysis, viscosity and ash content for their effects on electrical breakdown strength and finds that no decisive statistical difference can be ascertained between the different compounds.

The popular sizing agents Alkenyl Succinic Anhydride and Alkyl Ketene Dimer are investigated for effects on the electrical breakdown strength of electrical paper–oil

insulation. Neither compound is found to have statistically significant beneficial effects.

A comparative trial of dry–strength agents, specifically cationized starch, native starch and guar gum, shows no positive effect on the breakdown strength in comparison to paper filled only with talcum powder. The positive effect of talcum filler on electrical breakdown strength is demonstrated again by a comparison with unfilled paper.

An examination of talcum filled papers that are modified by either a polymer sizing agent, a cationic dry–strength agent or a wet–strength agent is presented. Results show that the dry–strength agent has a statistically significant negative effect on the electrical breakdown strength of the paper–oil insulation, whereas both the wet–strength additive as well as the polymer sizing agent has a statistically significant positive effect.

In summary, this thesis contributes the results of an investigation that explores a number of different mechanical and chemical modifications for their impact on the electrical and dielectric characteristics of paper for electrical applications. The results suggest that the use of talcum as a filler in electrical paper–oil insulation may yield financial as well as technical advantages.

1.3 Thesis Outline

Chapter 1 introduces the topic and context of this work, and provides statements on the research aims and objective as well as the thesis contribution. A literature review of solid dielectric materials at room and low temperatures is covered by Chapter 2. Chapter 3 provides an overview on theories behind charge transportation in solid dielectrics. It is followed, with Chapter 4, by a discussion on measurement methods and technologies that are suitable for the investigation of electrical processes in solid dielectrics. Chapter 5 describes the design and construction as well as various post-processing procedures of a thermally stimulated discharge current measurement system developed at the University of Southampton. Chapter 6 presents measurement results recorded with that instrument, of synthetic as well as natural polymer systems. An investigation into improving electrical insulation paper is presented in Chapter 7. Chapter 8 concludes the thesis and outlines future work. It is followed by appendices and the bibliography.

Some of the results in Chapter 7 were presented at the International Munich Paper Symposium (IMPS) 2012 [1] and at Aticelca 2012 [2], the 43^{rd} annual congress of the Italian Paper Association. The same work also underlies two of the author's published journal papers [3, 4].

Chapter 2

Solid Electrical Insulation Materials

Solid electrical insulation is the most ubiquitous form of dielectric materials in that even liquid or gaseous insulation systems require solid elements for mechanical support. Despite their importance, almost a century of research and numerous detailed theories on the breakdown behaviour of solids have yielded a state-of-the-art understanding that has been described as "crude and inconclusive"[5]. Material testing is ongoing and a lot of dielectric materials have been characterised over a wide range of temperatures, including extremes such as liquid nitrogen temperature (77 K at 1 atm), or at liquid helium temperature (4.2 K at 1 atm) [6, 7]. This tentative comprehension of solid dielectrics is even more concerning for an industry that relies on solid dielectrics and their continued performance at not only room temperature, but at extreme temperatures such as the cryogenic domain for electrical insulation of superconductors, or the use of upgraded paper-oil insulation running close to the point of premature aging in high-voltage transformers. Unfortunately the behaviour of materials at low or very high temperatures cannot simply be extrapolated from their behaviour at room temperature, since most materials undergo phase transformations when cooled far below room temperature, or loose crystallinity at high temperatures. On the other hand, some analytical methods, such as for example thermally stimulated current spectrometry, make active use of the low temperature domain in the material characterisation process. In view of that, the following general introduction of solid dielectric systems is expanded by a consideration of the behaviour of solid dielectrics at low temperature. A categorical overview of polymers, ceramics and glasses, as well as polymer composites is then followed by a closer look at a number of synthetic or natural materials that are commonly characterised by thermally stimulated current measurements.

2.1 Solid Dielectric Systems

In order for any solid material to be suitable for insulation purposes, it is desirable for it to perform well with regard to the following criteria as summarised here [8]:

It must provide sufficient mechanical strength and toughness to withstand the design stresses at the desired operating temperatures without losing structural or dimensional qualities. This may include scheduled and unscheduled heating and cooling cycles that create stresses which the dielectric must be able to withstand without its mechanical or dielectric properties being adversely affected or prematurely altered.

Thermal insulation properties must be sufficient, or tailored to the application. The dielectric material must be able to cope with sudden temperature and high-voltage transients concomitant with lighting strike events or quenching, the latter being the sudden loss of the superconducting state in a superconductor. The material must not only withstand the mechanical stress created by such an event, but depending on the design of the application, may be required to conduct the thermal energy away from the conductor so it can be removed by ambient medium circulation, or an active refrigeration system.

In addition to the above, the following characteristics are commonly required for a material to be considered a good dielectric. It ought to exhibit:

- Low electrical losses.
- High electrical strength.
- High resistance to surface tracking or treeing.
- No or negligible water treeing.
- High resistance to space charge injection.
- None, or reduced thermal and chemical degradation.

Finally, for the material to be economically feasible, it is desired to be:

- Processable by a commercial manufacturing process in order to keep production costs low.
- Made of materials that are easily available so that procurement costs are viable and enough resources can be gathered to satisfy the market demand.

2.2 Solid Dielectrics at Low Temperature

The low temperature domain entails a number of challenges for dielectric materials, both mechanically and electrically. Solid dielectrics engineered for applications in the low temperature environment will henceforth be referred to as cryogenic dielectrics. This section introduces a number of characteristics of the cryogenic domain, some that are helpful, and some that are detrimental in their effects. It should be noted, that a general problem of material testing at such low temperatures is that long term tests are very expensive and it is thus not uncommon for conclusions and lifetime estimations of several decades to be based on a few days of testing [9].

The power dissipation in materials that form part of AC electrical systems at cryogenic temperatures is generally smaller than that at room temperature, since the molecular motion of the dielectric solid is reduced in the low temperature domain. The dissipation of electromagnetic energy inherent in the material may be quantified by the measure of the dissipation factor, also $\tan\delta$. Figure 2.1 illustrates this trend for glass fibre reinforced plastic at three different temperatures: 4.2 K, 77 K and 300 K. Heat generated due to power loss in the dielectric is thus commonly negligible compared to AC losses in the conductor, or to the influx of external heat. Figure 2.2 shows the electric strength of a number of polymers. It can be seen that electric breakdown strength in polymers is improved in the cryogenic domain. Non-polar polymers exhibit a temperature independent electrical breakdown strength; that of polar polymers, while elevated, decreases with decreasing temperature. Composite polymers show an increase in breakdown strength with decreasing temperature [10]. Thermal contraction of the solid dielectric due to the low temperature is usually undesirable, but it may also have positive effects. Cryotreatment of polymers has been found to increase hardness i.e. wear resistance, and the increased electrical breakdown strength of some composites is thought to be due to micro-voids being reduced by the internal compressive stress at low temperatures [11]. Electrical breakdown via treeing progresses at a slower rate at cryogenic temperatures, on the other hand, the induced mechanical stresses may lead to premature cracking of the insulation material due to its increased brittle character at low temperatures [10]. It follows, that crack initiation and propagation characteristics as well as their relative importance in the desired design should be taken into account when choosing a material for low temperature applications [12].

Penetration of water into the solid dielectric is less of a problem in a cryogenic environment, since operating temperatures are well below the freezing point, and water is thus only present as a solid. This naturally assumes that the water was not previously present as a contaminant inside the material. The previous argument also holds for any water-soluble chemical agent that would cause a chemical degradation. Furthermore, the reduced ambient energy at low temperatures will slow down or prevent thermally activated reactions as well as thermal degradation [10].

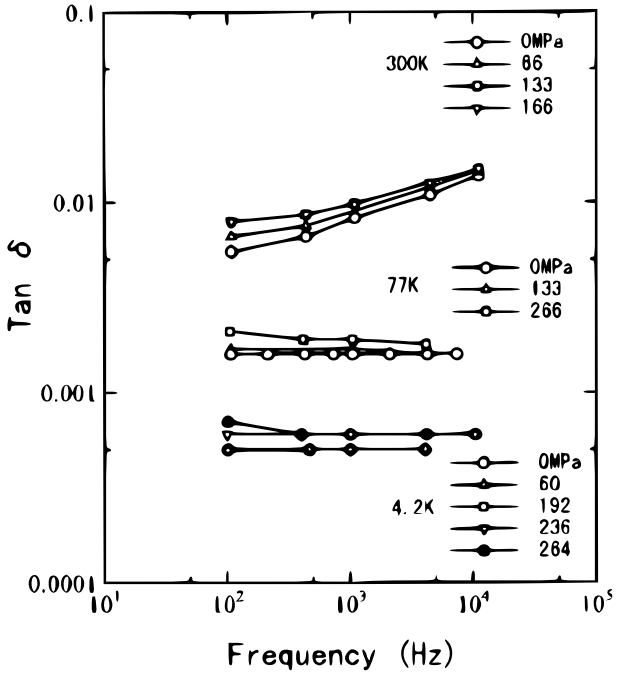

FIGURE 2.1: Temperature dependence of the energy dissipation in glass fibre reinforced plastics, as quantified by $\tan\delta$. [13]

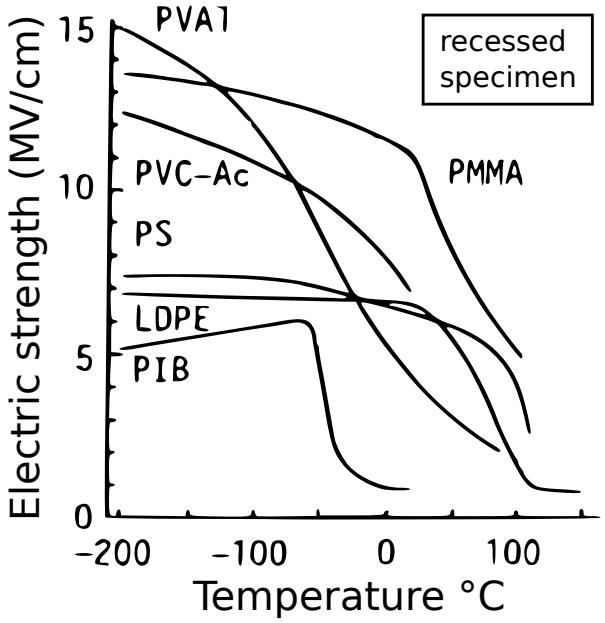

FIGURE 2.2: The dependence of DC electric strength on temperature. Non-polar polymers: LDPE - low density polyethylene, PS - polystyrene, PIB - polyisobutylene. Polar polymers: PVAl - polyvinyl alcohol, PMMA - polymethyl methacrylate, PVC-Ac - polyvinylchloride-acetate. [10, 14]

2.3 Polymers

Polymers are already popular in a number of applications in the power industry and have been used for low temperature applications for some time. However, new applications in the aerospace industry and the field of superconductivity pose new challenges to the design of adequate dielectric materials. Knowledge of their behaviour at low temperatures has not yet achieved the same maturity as that of their behaviour at room temperature. Thus even though cryogenics as well as dielectric material research are well established fields of research, the interface between the two deserves more attention. For most polymers, the cryogenic domain lies well below the glass transition temperature (T_{glass}). At such temperatures the molecular chains of a polymeric material stiffen, and their response to mechanical or electrical stress as well as their ageing behaviour is different to that at higher temperatures.

Polymers that are able to change the bond angles on their main chain, i.e. are composed of oxygen, sulphur or various hetero cyclic linkages, have been shown empirically to excel at low temperatures due to their retained flexibility after the main segmental motion of the polymer macro-molecule has been frozen out. Aromatic polymers have been shown to exhibit such prominent mechanical characteristics at cryogenic temperatures [15].

Thermal gradients and rapid changes in temperature are another type of stress that dielectrics have to accommodate at low temperatures. Thinner sections of bulk polymer material are generally tougher and better able to cope with thermal shock than thicker sections. Also, small corners and other stress concentrators are best avoided in the planning stage of the physical component, since local concentration of mechanical or electrical stresses increases the risk of failure [12].

Creep due to thermal activation processes is not common at cryogenic temperatures. At such temperatures creep rates are considerably smaller than at room temperature. When creep is observed, it is accompanied by crack growth and thus also results in a degradation of the electric breakdown strength of the dielectric. The introduction of mechanical defects is the major mechanism that degrades the performance of dielectrics. In composites, creep at cryogenic temperature is mainly due to the growth of cracks and not due to molecular relaxation. Crack inception and propagation naturally differs with the form and material of the composite. Wrapping dielectric film e.g. polyimide, around the composite component, can improve the dielectric breakdown strength and the long term performance of the part or material in question [13].

2.3.1 Thermoplastics and Thermosets

Thermoplastics and thermosets are two very different classes into which polymers may be categorised. The difference may be succinctly described by their melt behaviour. The

former class of polymers turns liquid when sufficiently heated, while the latter does not (once cured into a solid).

The mechanical properties of thermoplastics are strongly dependent upon temperature and loading conditions. They all undergo a phase transition to the brittle state at their material specific glass transition temperature. In many cases this is more of a range than a distinct point. In the glass/brittle state, the inability of the polymers to deform limits the use of most thermoplastics below their T_{glass}. Exceptions like polytetrafluoroethylene, which is able to accommodate small amounts of deformation below T_{glass}, are being used at liquid helium temperatures for seals or gaskets [12].

Thermosets are made up from shorter, highly interconnected polymer chains. The extensive cross–linking[1] during the curing process results in a plastic which behaves like an organic glass at room temperature and not unlike thermoplastic materials well below T_{glass}. After a thermoset has been cured, if forms a strong and rigid but brittle solid. Its mechanical properties are less affected by changes in temperature. Heating an amorphous thermoset above the glass transition temperature will render it rubber-like but not liquid. Due to its inherently brittle nature, thermosets are rarely used by themselves for low temperature applications. When employed with a filler e.g. phenolic impregnated cloths or paper, it results in a very tough composite material that is suitable for load bearing, dielectric structures [12]. Refer to Section 2.5 for more information on composite materials.

2.3.2 Crystallinity

Crystallinity describes a solid, or regions in a solid, where atoms or molecules are arranged in an ordered, periodic fashion. This is in contrast to amorphous regions or materials where the arrangement is completely random. An amorphous thermoplastic is either a liquid or, if slightly cross–linked, a rubber, at temperatures above the glass transition temperature. At these temperatures the thermal excitations are strong enough to disrupt van der Waals' bonding. If the polymer chains of the thermoplastic are long enough to be sufficiently entangled with neighbouring chains, or if the polymer is cross–linked, then individual chains are constrained in their motion and true liquid behaviour is never achieved. In this case the plastics behave as rubbers above T_{glass}. When an amorphous, unlinked polymer is slowly cooled below T_{glass}, the loss in thermal excitation reduces the segmental motion of the macro-molecular chains and turns the polymer into a super-cooled liquid, i.e. a glass [16].

Manufacturing processes also play a major role in determining crystallinity. Common fabrication techniques such as extrusion or injection moulding impart a preferred direction on the macro-molecular chains inside the plastic, increasing toughness in the

[1] Cross–linking: a way of covalently connecting individual molecular chains to form a larger macromolecule.

direction of extrusion while weakening the material in the perpendicular direction. As a consequence, plastics that may generally be regarded as amorphous may exhibit limited crystallinity after manufacturing. Figure 2.3 illustrates the difference between amorphous and crystalline regions in a polymer. Toughness also diminishes with an increasing level of crystallinity inside the polymer, a characteristic that is generally dictated by the cooling rate during fabrication [12].

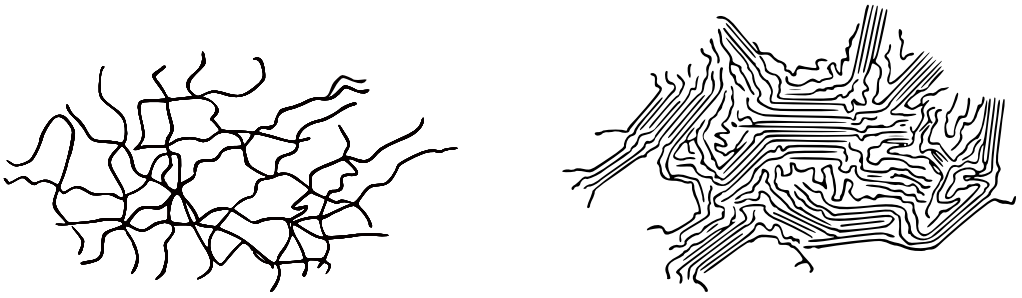

(a) Amorphous polymer. [17]

(b) A crystalline polymer showing regions of molecular order embedded in a matrix of amorphous polymer. [17]

FIGURE 2.3: Two-dimensional illustration of amorphous and crystalline polymers.

The degree of crystallinity in the polymer has a significant impact on its physical behaviour. Figure 2.4 shows its effect on a number of material properties in conjunction with the influence of cross-linking. The use of cross-linking agents in solid polymers and the use of crystalline fillers in polymer composites are popular tools employed to harness this effect.

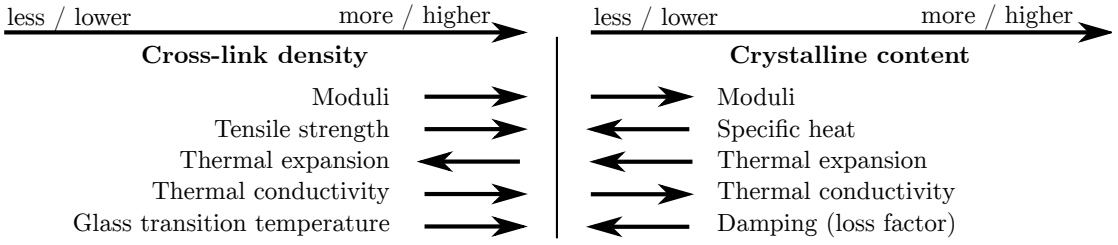

FIGURE 2.4: Influence of cross-link density and crystalline content on selected polymer properties. [18]

2.4 Ceramics and Glasses

Ceramics have a micro-crystalline structure while glasses have an amorphous structure. Both are usually brittle since stress concentrations around defects can not be relieved through plastic deformation and consequently their resilience to failure under compressive strain is better then under tension. Due to the generally poor thermal conductivity and consequent proneness to thermal shock, both ceramics and glasses are more popular as thermal insulation in the form of powders, foams or granules, than as bulk material

at low temperatures. However, glass is used in low temperature applications such as for viewing ports in cryogenic bubble chambers. Special manufacturing techniques like stress removal by annealing or induced residual compressive stresses are employed to toughen the glass for such applications [12]. They are also used extensively as fillers in composites.

2.5 Composites

Composites consist of two or more materials and are designed to combine the individual material characteristics to achieve a synergetic effect. Desired material characteristics can thus be enhanced or added to the composite.

Polytetrafluoroethylene (PTFE) of the flurorocarbon family of polymers is a good example for how combining two materials can result in a superior composite. PTFE is an excellent electrical insulator and inert to most chemicals and solvents. Small crystallites sit between the individual polymer chains and prevent them from packing closely together during the phase transition to the glassy state, thus retaining a measure of ductility at temperatures as low as 4 K. However, PTFE tends to loose dimensional stability, even at low temperatures. To prevent this cold flow, PTFE can be used in a composite. A PTFE matrix provides the composite material with ductility and dielectric properties at low temperatures while a filler, such as glass fibres, adds structural toughness and dimensional stability. When loaded, the glass fibres of such a composite bear most of the load since the filler is stronger and stiffer than the polymer matrix that it supports. By slowing or deflecting the growth of cracks inside the material, the network of fibres ensures that the mode of failure of the composite is energy absorbing and progressive and not brittle as it would be for the bulk polymer alone. As a consequence of the anisotropic nature of the fibrous filler, the load bearing capability of the composite material is strongest in the direction along the fibres and weakest along the orthogonal. To overcome the anisotropy of the mechanical properties, different cross-plying techniques can be employed, however, every layer of fibres which is rotated to strengthen the composite in a new direction, reduces the strength of the material in the former direction [12].

Linear thermal contraction of polymers is about 3–10 times greater than that of most metals in the temperature range between 293 K and 200 K [12]. Fillers can be used to improve this behaviour and to match the contraction and expansion coefficient of the insulator to that of the insulated material.

Failure in a composite generally starts with the initiation of cracks in the matrix, followed by interface failure and subsequent failure of the reinforcements. During this process, the number of cracks increases until failure. The strength of a laminar composite is controlled by the reinforcements and consequently crack initiation is determined by strain and not

stress. The crack density and the point of inception depends on the material used as the composite matrix [13]. Interlaminar shear stress is not supported by the reinforcements in the composite and must be borne by the matrix and the interface between matrix and reinforcements. Consequently it is lower than the tensile or compressive strength. It has been observed that the yield strength of glass fibre reinforced plastic at liquid nitrogen temperature is higher, but that the interlaminar cracks start earlier. Generally the dielectric lifetime is degraded by an applied electric field, even in a cryogenic environment [13].

2.6 Layered versus Bulk Insulation

In a comparative study between polypropylene film and low-density polyethylene film [19], it was found that both polymers performed better in liquid nitrogen (liquid-N_2) than in liquid helium (lHe). Investigation of the surface erosion using a Scanning Electron Microscope (SEM[2]) showed that the films exhibited a mesh like surface pattern after discharge in lHe while the same treatment in liquid-N_2 produced surface uniform erosion. Testing insulation made up of several layers of polymer film showed that under impulse voltage and AC voltages of a magnitude less than the breakdown voltage of liquid-N_2, the layered films performed better. Under AC voltages above the liquid-N_2 breakdown voltage, the single layer sample (same thickness as the multiple layers combined) performed better. This was understood to be due to partial discharges[3] occurring in the liquid-N_2 filled gaps between the layers of the multi-layered samples.

2.7 Synthetic Polymers

Since part of this research is concerned with thermally stimulated current measurements, the following sections provide information on a number of polymers that have often been characterised with TSDC spectrometry.

2.7.1 Polyethylene

Polyethylene (PE) is made up of a large number of macro-molecules (see Figure 2.5b) consisting of the monomer unit shown in Figure 2.5a. As illustrated in Figure 2.5, a PE molecule consists solely of carbon and hydrogen atoms. There exist a number of different types of PE polymers, characterised by their different densities and degree of cross-polymerisation. Table 2.1 lists some of their names and common abbreviations.

[2]Scanning electron microscope: a microscope that uses an electron beam rather than light to image an object.

[3]A partial discharge (PD) is a localised breakdown of a dielectric material under high voltage stress. It does not bridge the insulation system between two conductors completely.

Polyethylene is also a popular choice for polymer blends and serves as a matrix for composite polymers.

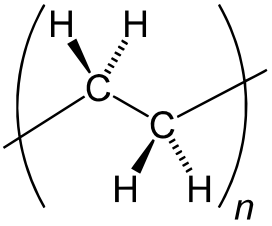

(a) Chemical structure.

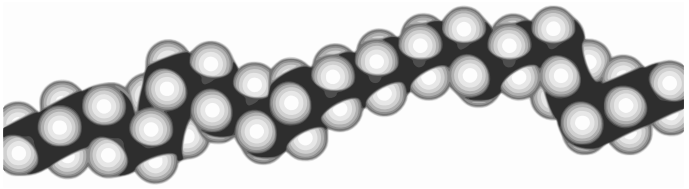

(b) Three-dimensional structure. Carbon atoms are shown in black, hydrogen atoms in grey colour. [17]

FIGURE 2.5: Structure of a polyethylene polymer.

TABLE 2.1: Types of polyethylene.

Name	Abbreviation
Low density polyethylene	LDPE
High density polyethylene	HDPE
Ultra high molecular weight polyethylene	UHMW-PE
Cross-linked polyethylene	XLPE

Table 2.2 lists a number of material characteristics of a polyethylene polymer. However, since most of these properties are affected by a number of parameters, such as the average molecular weight of the polymer, the molecular weight distribution, the degree of polymerisation[4], crystallinity and others; these numbers should only be seen as a general reference.

Polyethylene, specifically LDPE was chosen as the first material of interest for this investigation due to the wealth of information available on it. Commercially and academically, the material has been investigated thoroughly over a wide range of temperatures, including the cryogenic domain [20–27]. The Tony Davies High Voltage Laboratory has previous as well as ongoing research regarding polyethylene blends and composites, and as such it was deemed a good material to test and verify the accurate operation of the new TSDC spectrometer. For further data on the thermal expansion of polyethylene, refer to [28, pp. 1427]

[4]The degree of polymerisation (DP), is the number of repeating units in a larger molecule. For polymers comprised entirely of monomeric units, the number of monomers per polymer is described by the DP.

TABLE 2.2: Reference properties of polyethylene (PE). [29, 30]

Property	Unit	Value
Glass transition temp.	$°C$	-125
Melt temperature	$°C$	$105 - 110$
Volume resistivity	Ωcm	$> 10^{16}$
Surface resistivity	Ω	10^{13}
Dissipation factor ($50 - 10^{16}$Hz)		$2 \cdot 10^{-4}$
Breakdown strength	kV/mm	> 70

2.7.2 Ultra High Molecular Weight Polyethylene

As the name suggests, Ultra High Molecular Weight Polyethylene (UHMW-PE) is a form of polyethylene that exhibits a very high average molecular weight (molecular weight of more than $3 \cdot 10^6$ to $6 \cdot 10^6$) [29]. One of the major problems that faces polymer dielectrics in the cryogenic domain, is their mechanical stability. Thermal contraction of polymers at low temperatures is generally much higher than that of metals. The increased mechanical stress, combined with the polymer's brittle behaviour in its glassy state at low temperatures often leads to stress cracking. Polymer dielectrics are no exception to this phenomenon. In order to overcome this problem, several different methods have been developed. They are:

- Applying the dielectric as laminar tapes/films.
- Removing the dielectric as far away from the cryogenic parts/conductor as possible.
- Avoiding fast thermal gradients.
- Reinforcement of the polymer matrix using fillers e.g. glass fibres.

The most advantageous solution would be a material that can be used in bulk but which is not susceptible to stress cracking at cryogenic properties. One polymer that performs favourably at low temperatures is UHMW-PE. Its general characteristics are enumerated below [31] and reference properties tabulated in Table 2.3.

- Highest resistance to notched impact of any commercially available plastic material.
- Outstanding resistance to abrasion.
- Very low coefficient of friction.
- Self lubricating, non-stick, surface.
- Good chemical resistance.

- Negligible absorption of water (even less of an issue at cryogenic temperatures).
- Very high stress cracking resistance
- Very good absorption of energy and sound dampening properties.
- Excellent dielectric properties.

TABLE 2.3: Reference properties of UHMW-PE. [29, 32]

Property	Unit	Value
Glass transition temp.	$°C$	-160
Melt temperature	$°C$	$125 - 135$
Volume resistivity	Ωcm	$> 10^{16}$
Surface resistivity	Ω	$> 10^{13}$
Dissipation factor $(50 - 10^{16}\text{Hz})$		$3 \cdot 10^{-4}$
Breakdown strength	kV/mm	> 70

In a mechanical test, where the breakdown strength of samples was tested before and after 100 thermal shocks (77K using liquid-N_2), UHMW-PE performed in a superior manner to electrical grade polyethylene tapes, both LDPE and HDPE, as well as HDPE paper. The test results ascribe UHMW-PE an extremely good resistance to cryo-fracture. Tests of tensile strength, treeing initiation voltage and crack inception voltage confirmed that UHMW-PE is superior in performance to both LDPE and XLPE at cryogenic temperatures [26, 27].

2.7.3 Polyethylene terephthalate

Polyethylene terephthalate is a very common engineering plastic and has been studied extensively[24, 33–38]. The polymer is made up of the aromatic monomer unit shown in Figure 2.6 and has general properties tabulated in Table 2.4. It exhibits good mechanical properties (Figure 2.7) and has been used as a polymer in cryogenic settings [25, 34] PET was used as the second reference material to test and verify the operation of the new TSDC spectrometer.

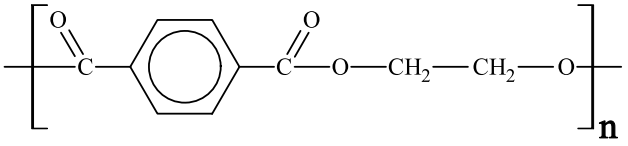

FIGURE 2.6: Polyethylene terephthalate

Tensile test of PET at cryogenic temperatures show that the biaxially oriented and the heat-set variety of the polymer exhibit an increased elastic modulus and are tougher than amorphous PET [25]. The polyethylene terephthalate used in this research is of the biaxially oriented kind.

TABLE 2.4: General properties of polyethylene terephthalate (PET). [29]

Property	Unit	Value
Glass transition temp.	$°C$	98
Melt temperature	$°C$	255
Volume resistivity	Ωcm	$2 \cdot 10^{14}$
Surface resistivity	Ω	$6 \cdot 10^{14}$
Dissipation factor (50Hz)		$2 \cdot 10^{-3}$
Breakdown strength	kV/mm	60

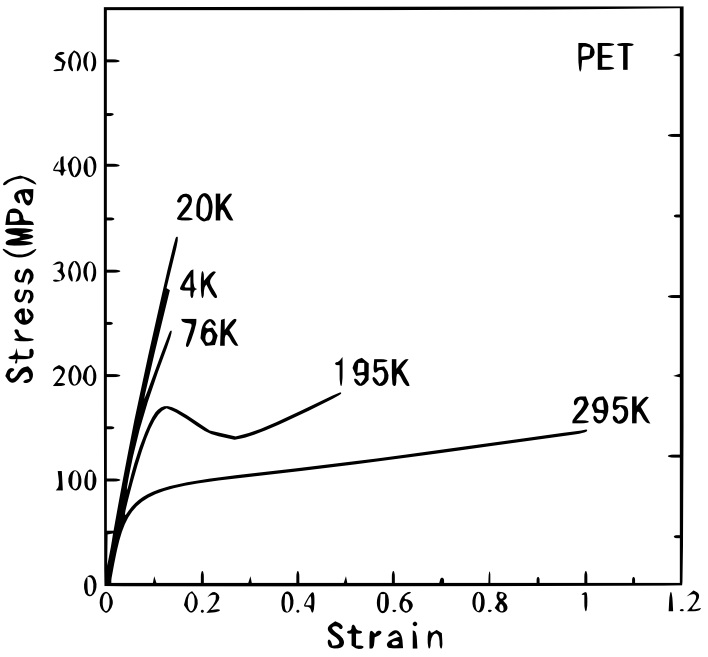

FIGURE 2.7: Stress-strain behaviour of PET at different temperatures. [13]

2.7.4 Polyphenylene sulfide

Poly(p-phenylene sulfide) or PPS for short, is an organic, semi-crystalline macromolecular (Figure 2.8) formed by the linear catenation of aromatic polyphenylene rings with sulphur atoms. It is a thermoplastic with a high crystalline melting point of $T_{melt} = 285°C$ and exhibits excellent thermal, mechanical and chemical resistance. This comparably expensive polymer is commercially available in a cross-linked, and in a linear variety and in a range of molecular weights. The common method of industrial processing is by injection molding and extrusion into mono– and multifilaments, sheets, pipes or solid rods [39].

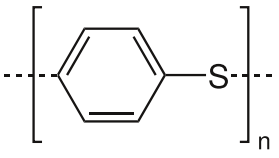

FIGURE 2.8: Poly(p-phenylene sulfide)

The electrical breakdown strength of PPS film is lower under DC than under impulse conditions. The reduction in breakdown strength has been interpreted as influence of space charge on the local field distribution within the sample [40]. Impulse breakdown strength was reported to be almost constant over a temperature range from -60°C to 150°C, but lower for thicker (25 µm) than for thinner (6 µm) samples [41]. This was seen to be indicative of a principally electronic breakdown as supposed to a thermal breakdown process. DC pre-stressing of samples was found to increase the breakdown strength when the pre-stressing and the impulse voltage have the same polarity, and was found to decrease the breakdown strength when of opposing polarity. Again, this has be explained by the reduction of the local electric field due to homo-charge near the electrodes and, inversely, as the increase of the local field by the presence of hetero-charge. For the thin samples (6 μm) the induced homo-charge was found to act as hetero-charge and resulted in a reduction of breakdown strength [40]. Laser induced pressure pulse (LIPP) measurements on biaxially stretched, semi-crystalline PPS film samples has shown that homo charge accumulates near the anode, whereas is was shown to range throughout the sample on amorphous PPS. This difference in impulse breakdown strength has been explained by a higher effective carrier mobility in amorphous PPS due to a lower trap density [40].

2.7.5 Polytetrafluoroethylene

The chemical structure of poly(tetrafluoroethylene) is shown in Figure 2.9. As the name suggests, the polymer is comprised of tetrafluoroethylene monomer units shown in Figure 2.9a.

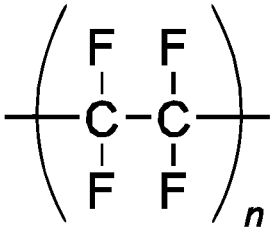

(a) Chemical structure.

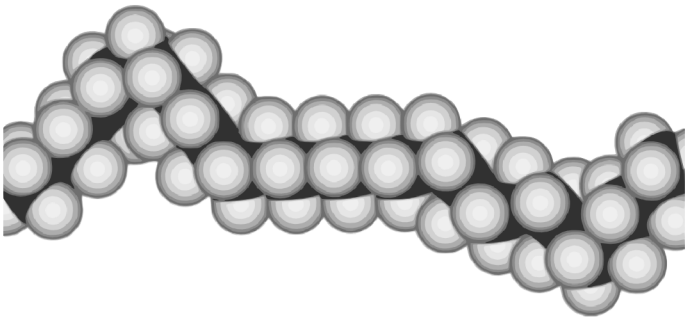

(b) Three-dimensional structure. Carbon atoms are shown in black, hydrogen atoms in grey colour. [17]

FIGURE 2.9: Structure of a polytetrafluoroethylene polymer.

Polytetrafluoroethylene has physical properties as tabulated in Table 2.5 and characteristics as follows: [29]:

- Nearly universal chemical resistance.
- Insoluble in all known solvents under 300°C.

- High thermal stability. Continuous use in temperatures ranging from -270°C to +260°C.
- Outstanding electrical and dielectric properties.
- Resistant against stress cracking and weathering.
- Low mechanical stability and stiffness limits its use for weight bearing parts.

TABLE 2.5: Reference properties of polytetrafluoroethylene. [29]

Property	Unit	Value
Glass transition temp.	$°C$	127
Melt temperature	$°C$	327
Volume resistivity	Ωcm	$> 10^{18}$
Surface resistivity	Ω	10^{17}
Dissipation factor (10^3Hz)		$2 \cdot 10^{-4}$
Breakdown strength	kV/cm	600–800

For data on the thermal expansion of PTFE, refer to [28, Fig.407, p.1444]

2.7.6 Polyimide

Polyimide (PI) is an interesting material because it is the solid dielectric currently used by the American Superconductor Corporation for their high temperature superconducting wire and employed in their current commercial HTS power cables. Their choice of dielectric insulation is a single or multi-layer Kapton® polyimide film applied in a lapped spiral pattern using a silicone adhesive. The temperature dependent stress–strain behaviour of polyimide is shown in Figure 2.10. Polyimide has the following characterising properties [29]:

- High toughness over a wide range of temperatures (-240°C to +370°C).
- High stiffness, hardness and thermal stability.
- Favourable wear and abrasion behaviour.
- Good electrical properties.
- Little out-gassing under vacuum.
- Sufficient chemical resistance.

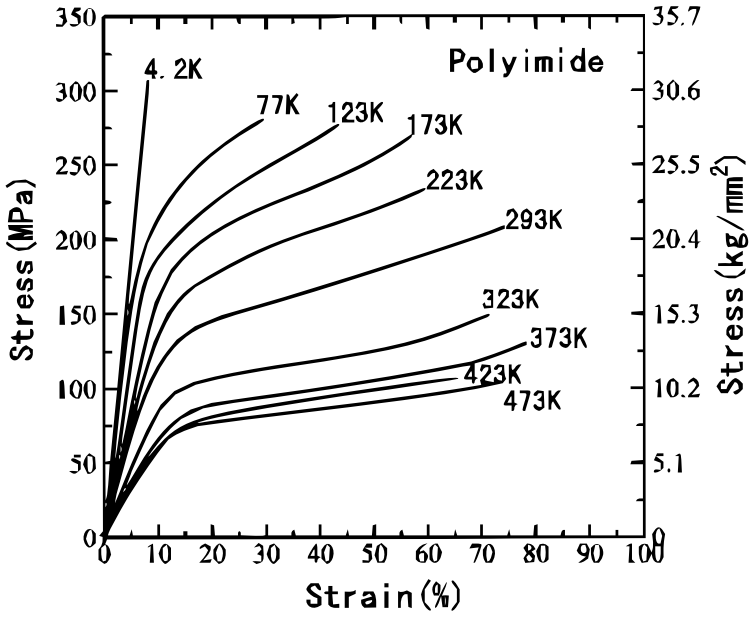

FIGURE 2.10: Stress-strain behaviour of polyimide at different temperatures. [13]

2.8 Natural Polymer - Paper

Paper is made by draining a dilute suspension of cellulose fibres and then pressing and heating the resulting sheet. The fibres of the water suspension are gained by separating wood into its constituent fibres by a mechanical or chemical process. The method of manufacture has an influence on the characteristics of the resultant pulp. Producing pulp mechanically is more economic but results in shorter fibres and retains most of the amorphous hemicellulose and lignin parts in the pulp. Paper made from mechanically produced pulp is called wood-containing. In the chemical process, the fibres are cooked and solubilised which preserves their length and enables the removal of lignin. The resulting fibres are more porous and, due to their length, impart a higher mechanical strength onto the final paper. Paper derived from only chemical pulp is referred to as wood-free or kraft paper [42]. In either case, the fibres that make up the sheet of paper are held together by hydrogen bonds between the hydroxyl groups on the cellulose. Besides wood, many other sources of natural fibres are also in use, for example hemp, horse radish, flax and others. Figure 2.11 illustrates how cellulose derives from natural sources. In addition to natural fibres, artificial fibrous materials such as glass, polymers carbon nanotubes or graphene oxide have also been employed to make paper.

Hemicellulose and lignin, like cellulose, are parts of the cells that make up the wood fibres. Unlike cellulose, hemicellulose is a branched polymer made up of shorter chains of different saccharide monomers (see Figure 2.12). Lignin is an aromatic crosslined polymer and more hydrophobic in nature. Lignin has a tendency to cause the paper to appear yellow, however for electrical applications this is not an issue [44].

Paper is classified according to mass per unit area, also referred to as grammage, and

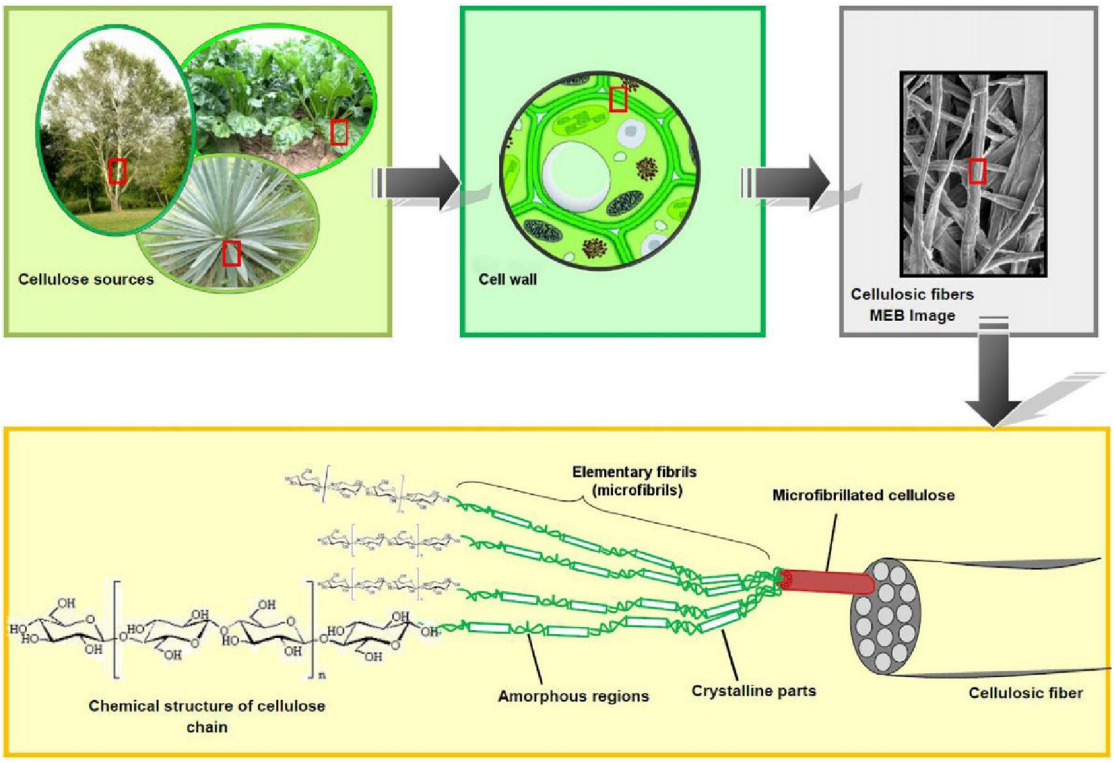

FIGURE 2.11: Depiction of cellulose fibres and their origin. [43]

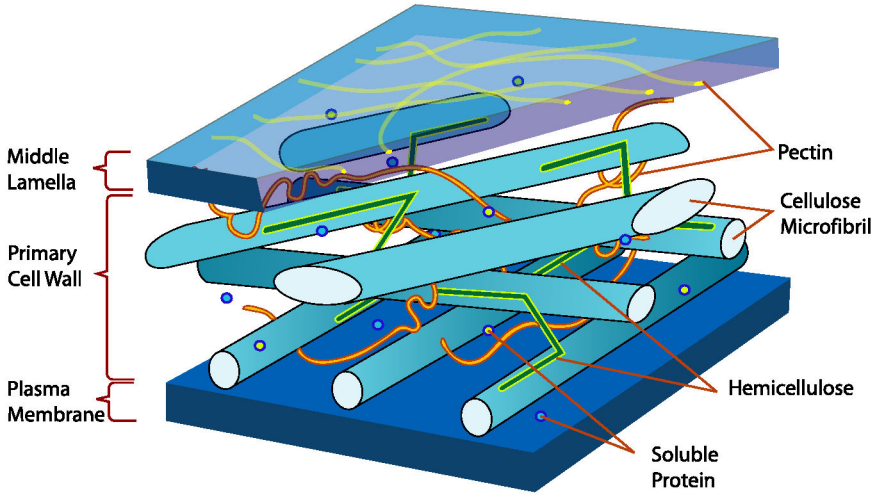

FIGURE 2.12: Hemicellulose and Cellulose fibrils shown in a section of the cell wall of a plant cell. [17]

thickness. Average copy paper has an approximate thickness of 100 µm and a grammage of around $80\,\mathrm{g\,m^{-2}}$. Thicknesses of over 300 µm or grammages exceeding $200\,\mathrm{g\,m^{-2}}$ to $800\,\mathrm{g\,m^{-2}}$ are referred to as cardboard whereas grammages below $30\,\mathrm{g\,m^{-2}}$ usually denote tissue or specialty papers.

There are several ways in which paper may be enhanced. The most common methods are the addition of fillers, chemical additives, calendering, and coating. Fillers are added to the pulp in order to improve certain paper properties. Mineral fillers such as calcium

carbonate ($CaCO_3$), chalk, clays, kaolinite, aluminium oxide or titanium dioxide are employed to increase whiteness, ink absorbency, surface smoothness and opacity [45]. Figure 2.13 shows the paper surface of an unfilled and a filled paper under an Alicona InfinityFocus optical microscope. The white inclusions in Figure 2.13b are the talcum particles. Further additives may be added to increase mechanical strength, such as starches, gums or resins. The difference between the colour of the paper and the information printed on it, is an important property for office papers. To increase contrast, pulp may be bleached and mineral fillers as well as fluorescent whitening agents are employed.

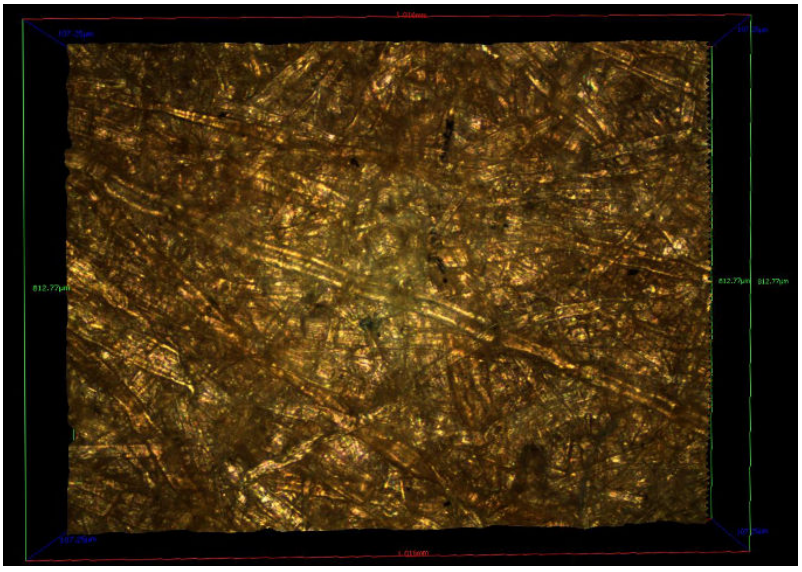

(a) A paper made only from fibre.

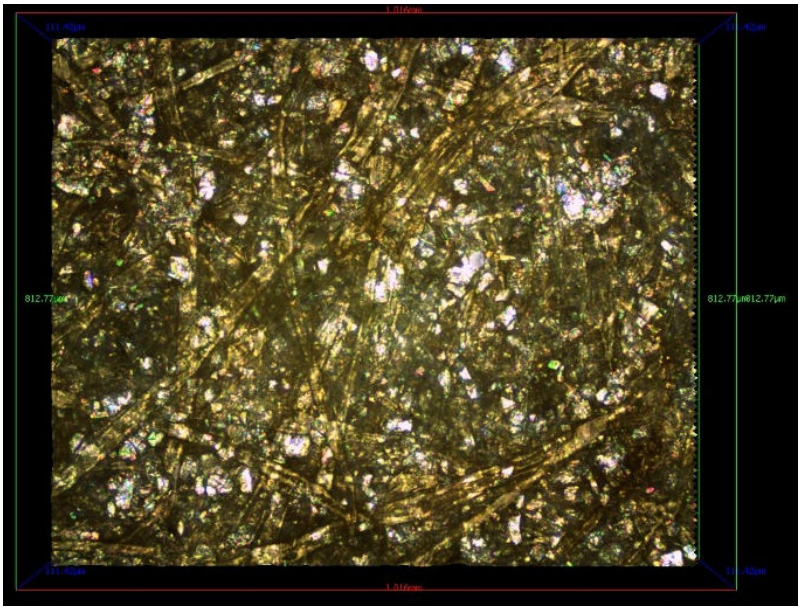

(b) A talcum filled paper (top side). White inclusions are talcum.

FIGURE 2.13: Images of a paper surface observed with an Alicona InfiniteFocus optical microscope. The sample shown in both images is 1.016 mm wide and 812.77 µm high.

Chemical additives may be classified into two groups. The first group of additives is added in order to improve the paper production process. This group includes chemicals such as retention aids, fixing agents and drainage accelerators. The second group of additives adds special properties to the paper. For example colourants, fluorescent whitening agents (FWA), also called optical brightening agents (OBA), dry strength and wet strength agents and sizing agents [46]. In this investigation the main focus was placed on tensile strength increasing additives (dry- and wet-strength agents). Sizing agents are additives that increase the hydrophobicity of the paper surface. In contrast to wet strength agents which increase the number and strength of chemical bonds within the paper, sizing agents attempt to keep the water away from the bulk of the paper. Sizing agents should make the paper more hydrophobic i.e. more lipophilic and therefore facilitate the penetration of an insulation oil into the paper. The penetration of insulation oil into the paper is the most time consuming step in the industrial production of oil-paper insulated electrical apparatus. A combination of higher breakdown resistance, better mechanical strength and increased lipophilic behaviour should result in insulation paper with improved electrical properties as well as improved manufacturing characteristics.

Calendering is a process where the paper is pressed between smooth metal, paper or polymer rolls under high pressure and often elevated temperatures to improve surface smoothness and increase bulk density [44]. Thin paper with higher density tends to show increased electrical breakdown values as calculated relative to thickness in kilo-volt per millimeter ($\mathrm{kV\,mm^{-1}}$). Increased smoothness improves the surface contact between the sample and the measurement electrodes, or in the case of lapped installation, the contact area between the individual paper strips.

Coating of the paper surface with pigments may further reduce the paper porosity and surface roughness. The pigments used for coating tend to contain further chemical additives such as dispersion agents and thickeners. Examples are sodium polyacrylate, caboxymethyl cellulose or starch [46]. Figure 2.14 shows a series of scanning electron microscope images of different coating methods that effectively convey the changes to the paper surface that may be achieved by coating applications. Figure 2.14a shows an uncoated reference image. Figure 2.14b depicts an uncoated paper that is filled with talcum. Figure 2.14c to Figure 2.14e illustrate the paper surface after different coating processes. Figure 2.14f shows a lateral cut of a paper that was coated only on the top side.

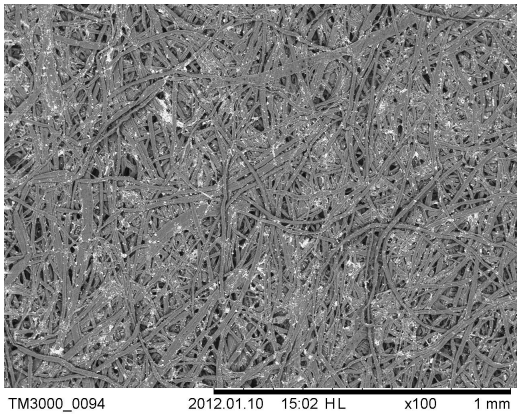

(a) Uncoated and unfilled paper.

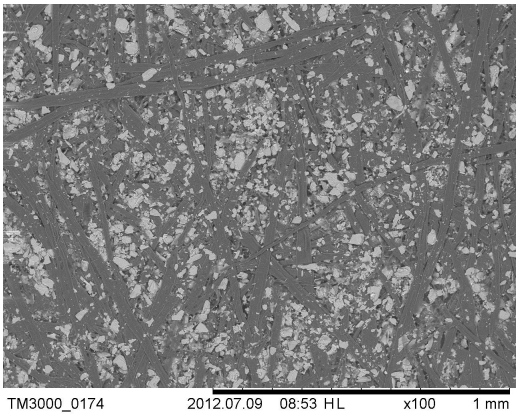

(b) Filled Paper.

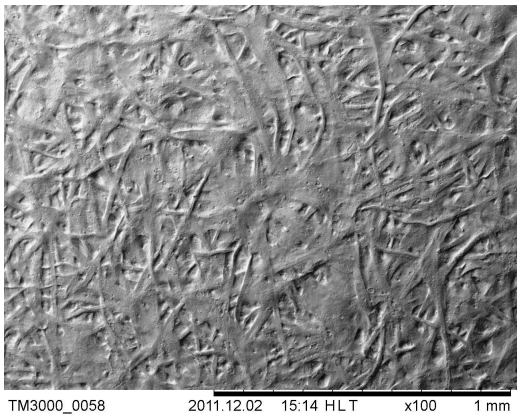

(c) Film press treated paper.

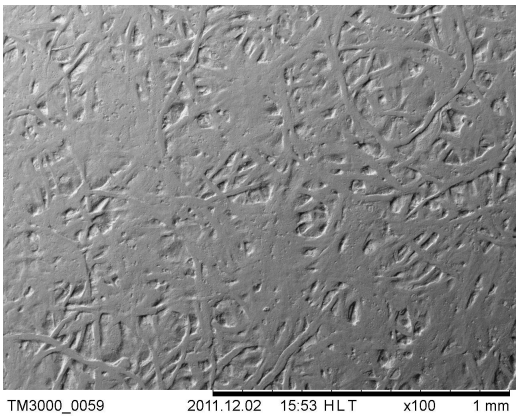

(d) Film press treated and calendered paper.

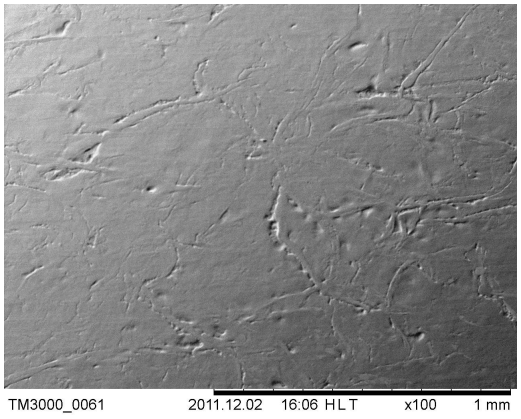

(e) Blade coated paper.

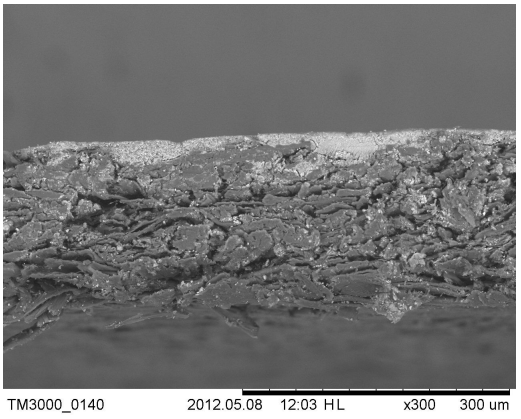

(f) Lateral cut of a paper coated on the top only.

FIGURE 2.14: SEM images of the surface of different papers recorded with a Hitachi TM3000.

2.9 Summary

This chapter provided an overview of solid electrical insulation materials. Solid dielectrics were introduced as the most important form of dielectrics on the basis of their necessity for other forms of insulation. General requirements and desirable properties for dielectrics at room and low temperatures were also listed. The temperature dependence of important physical properties in solid dielectrics, such as electrical breakdown strength and the dissipation factor, were introduced in order to assist the understanding of measurement methods and data analysis in the following chapters. Synthetic polymers were introduced as the dominant material category for solid electrical insulation systems. The differences between thermoplastic and thermosetting polymers, as well as the influence and importance of crystallinity were addressed. Ceramics, glasses and composite materials were briefly discussed, and followed by a review of select synthetic polymeric materials that are frequently investigated with the measurement methods that are introduced in a later chapter. Cellulose paper was presented as an example of a natural polymer that finds application as an insulation material in the electrical industry—most often in conjunction with a liquid impregnating agent. The origin and composition of paper, as well as several standard manufacturing processes and their intended effects were also introduced. This is necessary for the understanding of results presented in Chapters 6 and 7.

The literature review in next chapter provides an overview of the current theories that try to expound and model the mechanisms of charge transport in solid materials. Relevant technical terms and concepts are introduced as perspicuous as possible in a brief and comprehensible fashion, to support the understanding and analysis of data presented in later chapters.

Chapter 3

Charge Transport Mechanisms in Solids

Despite more than fifty years of research into the electrical conduction and breakdown of solid insulation materials, the search for a complete model of the electrical response of materials is ongoing. As of yet, no complete and encompassing theory has been accepted by the scientific community that could explain all the conduction mechanisms at work in ceramics, glasses or amorphous polymers. Concepts from semiconductor physics have been transposed to explain dielectric solids, including polymers, but there is still controversy as to the applicability of semiconductor physics to the cases of amorphous and disordered solids as they are often found in the form of polymers in the field of electrical insulation [47]. There are a number of theories that try to explain, model, and predict the processes involved, and the following overview will cover the traditional energy band model as it is known in semiconductor physics, as well as alternate models on the conduction in amorphous solids.

In general, conduction within a solid material depends on the availability of charge carriers and the speed in which they can move through the material. Charge carriers may take the form of electrons, ions or polar molecules, the density and mobility of which will be specific to a material and its environment. The conductivity (σ) of a material due to a single charge carrier type i, is given by the product of, the concentration of the carriers species n_i, the magnitude of the charge they carry (e_i) and their mobility μ_i.

$$\sigma_i = n_i e_i \mu_i \tag{3.1}$$

Differences in conductivity are then explained as variation in the number of charge carriers and their mobility. Variations in the amount of charge per carrier, as exhibited by highly ionised molecules, are rarely considered since their large electric charge means that they are likely to be held in place and not free to move through the solid. As

such, they cannot directly contribute to charge transportation. However, if present, such ionised species will affect the mobility of other mobile charge carriers. The effect is discussed in Section 3.6.1 [16].

Simple conduction within an ordered solid, i.e. a metal, proceeds by electrons moving balistically through the solid, only hindered in their progress by scattering from defects within the lattice structure and interactions with lattice vibrations. These hindrances explain the finite resistance of metals and their inverse relationship between conductivity and temperature. Within disordered solids such as polymers, conduction is thought to be afforded by the confluence of several conduction mechanisms. In addition, surface phenomena between the electrode and the sample under investigation will also play a role. The next sections will provide a background on charge transport in such materials. Charges within a solid dielectric that is subjected to an external electric field, experience a force and are motivated to move. When discussing such charges, it is helpful to distinguish between *true* or *free* charge, i.e. that which can move; and *bound* or *polarisation* charges, those which are restricted in their position (q.v. Section 3.3). Charge located on the surface of the material is termed *surface charge* and that residing within the bulk of the material is referred to as *space charge* (q.v. Section 3.2). Furthermore, one may want to distinguish charge originally associated with the sample, so called *intrinsic charge*, from *extrinsic charges* that were injected into or onto the sample from an external source.

3.1 Homo-charge and Hetero-charge

Charges at interfaces between two different materials in general, or, more specifically, between a metal electrode and a non-metallic dielectric material, can either show the same or the opposite polarity to that of the adjacent reference material/electrode and they are termed *homo-charge* and *hetero-charge* accordingly (see Figure 3.1 for an illustration). When charge is injected into a sample of solid insulation from a pair of electrodes, then the polarity of the injected charge is the same as that of the injecting electrode and referred to as homo-charge. As a consequence, the magnitude of the electric field within the bulk of the sample is increased, while the field at the electrode-sample interface is weakened. The charge injection process is dependent upon temperature, applied field, surface contact between the electrode and the sample, and the material of the electrodes. The later also dictates whether the injected charge is mono-polar or bipolar. Over time and motivated by the electric field, the charges can migrate through the bulk of the sample and recombine with homo-charges from the opposite electrode. Continued homo-charge injection may lead to a build up of charge within the sample and is discussed further in Section 3.2. The speed and magnitude of this process depends on the relative magnitudes or efficiencies of the charge injection, trapping and recombination processes involved, as well as the mobility of the charge within the material.

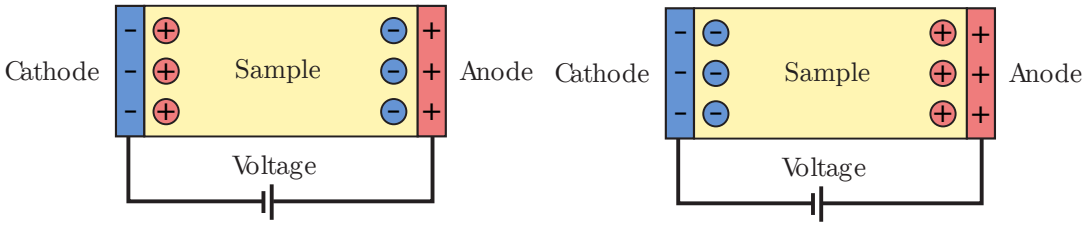

(a) Hetero-charge (b) Homo-charge

FIGURE 3.1: Illustration of hetero-charge and homo-charge. Hetero-charge denotes charge with the opposite polarity to that of the electrode; homo-charge bears the same polarity. [48]

Hetero-charge, i.e. charges of opposite polarity to that of the adjacent electrode, are commonly ions created from impurities within the bulk of the material. Examples of this are polymer additives and leftover byproducts from cross-linking reactions during the manufacturing process. In symmetry to the effects of homo-charge, the accumulation of hetero-charge at an electrode interface will increase the electric field across the interface, but reduce the field within the bulk of the sample.

3.2 Space Charge

Space charge denotes any kind of charge in the bulk of an insulator or semiconductor that is not balanced by an equal concentration of charge with opposite polarity. The result of such charge accumulation is a local field enhancement according to Poisson's equation:

$$\nabla \cdot E = \frac{\rho_c}{\epsilon} \tag{3.2}$$

where ρ_c denotes charge density in Cm^{-3} and ϵ is the permittivity. The unbalanced charges lead to a local change in the electric field that may cause or contribute to a local enhancement of the field stress and overpower the dielectric strength of the material, leading to electrical breakdown and failure of the insulation system. Space charge has been linked to degradation, ageing and premature breakdown of solid dielectric insulation in general, and polymeric dielectrics especially. In Section 3.1 it was mentioned that mobile ions will migrate through the bulk of the dielectric under the influence of an applied electric field and accumulate as hetero-charge at the electrodes. Since, unlike electrons, they cannot penetrate the metal electrodes, such ions will result in the formation of space charge near the electrode interfaces and lead to a local field enhancement across the electrode-dielectric interface.

3.3 Polarisation

One of the effects of applying an external electric field across a solid material, is to polarise it. There are a number of mechanisms by which polarisation occurs and on which the permittivity of a material depends. In alternating fields, the polar species will resonate in response to the changing field polarity. The quickest response in any material is a slight bias in the position of electrons in their orbit around their respective nuclei. Akin to the origin of the London dispersion forces[49], this introduces a weak dipole response and is termed *electronic polarisation*. Similarly, an applied electric field results in the separation of positive and negative charge on an atomic scale. In ions, but also in neutral atoms, the positive and negative charges will tend to separate under the electric field, and such response is called *atomic polarisation*. *Dipolar polarisation* describes the tendency of polar molecules and dipoles to try and align themselves with the direction of the field. This process is disturbed by thermal vibrations. Also, the rotation of large molecules or parts thereof will be restricted by the entanglement with neighbouring molecules and other surrounding field effects. Ions of slow and limited mobility will appear as dipoles whereas mobile ions will diffuse towards the electrode of opposite polarity. Ions that are able to travel to the electrode interface will either be neutralised by opposing charges resident there, or accumulate as hetero-charge at the electrode interface. If only one of the ionic species is neutralised at the interfaces, then the material has effectively captured free charge. All of the above mentioned processes are frequency dependent and can be observed using a Frequency Response Analyser (FRA). The individual responses will only be effective at their characteristic frequency and below. Above that, the change in field polarity is too fast for the process to respond. The fast processes of electronic and atomic polarisation are referred to as 'resonances' due to their undamped nature. The slower processes are heavily damped and termed 'relaxations' [50]. Figure 3.2 illustrates the concept.

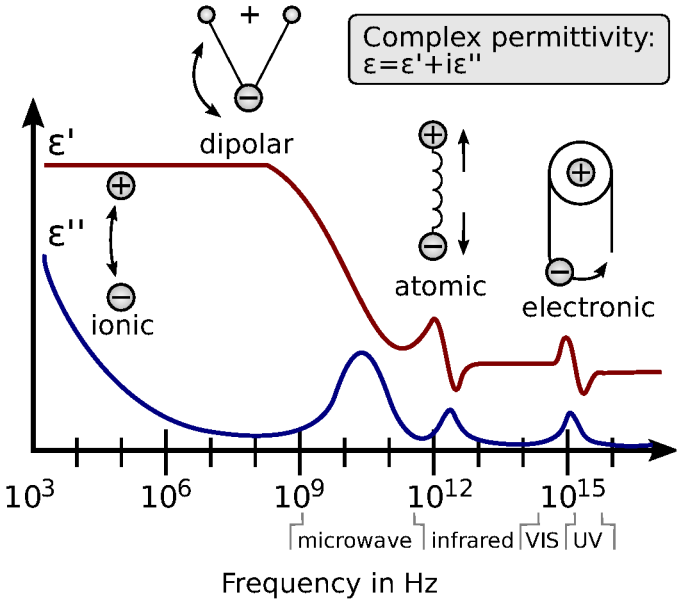

FIGURE 3.2: Frequency spectrum of permittivity: real part (ϵ') and imaginary part (ϵ'') of the complex permittivity (ϵ). Ionic and dipolar relaxation effects at lower frequencies, atomic and electronic resonance effects at higher frequencies. (Reproduced and modified with permission from Dr. Kenneth A. Mauritz)

3.4 Energy Band Theory

Energy band theory, also 'Band Theory of Solids', was originally developed to explain conduction in covalent or ionicly bound crystals and is now used extensively in silicon-based electronics. The use of the concept consequently expanded from semiconductor physics to include semi-crystalline and amorphous solids [16]. Although it is arguable whether the concept can be successfully applied to disordered solids, the energy band theory nevertheless introduces a number of general concepts that merit a brief introduction.

Electrons are fermions, indistinguishable physical particles with half-integer spins that obey the Pauli exclusion principle and Fermi-Dirac statistics [51]. Quantum theory explains how the energy of electrons surrounding the nucleus of an atom is quantised and the Pauli exclusion principle describes how a maximum of two electrons of opposite spin may simultaneously occupy a state of the same energy. When atoms come close together to form a solid or a molecule, the quantum wave functions of their electrons start to interact and electrons of equal energy and spin come into conflict. Such conflicting energetic states are referred to as 'degenerate' [16, 52]. In order to remove the degeneracy, the conflicting energy states sub-divide to accommodate every electron pair with its own distinct energy level, thus removing the degeneracy. When only a few atoms interact, the number of energy levels is small and the difference between them distinct. However, the enormous number of electrons that constitute the average solid material result in numerous energy levels that are so finely divided that they are commonly considered as

'energy bands' instead. This imprecision is permissible because the energetic separation between the levels within an energy band is comparable with the energy that electrons constantly exchange with vibrations in the crystal lattice and is also considered with Heisenberg's uncertainty principle. As a consequence, energy bands are regarded to be continuous and electrons may occupy any free energy level within a certain energy band. Figure 3.3 depicts the concept and illustrates how each such band is centred about the corresponding orbital energy level of the original single electron.

The energy bands are separated by energy gaps, energetic states that are inaccessible to electrons. When considering electrons as quantum waves within a regular crystal lattice, then the forbidden energy gaps may be explained as electron waves that suffer reflection by the crystal lattice (Bragg reflection condition) and consequently cannot exist within the lattice structure [16, 51].

At absolute zero temperature, all electrons occupy the lowest, possible, energy levels. This minimum energy of the system is termed the Fermi energy (E_f) and corresponds to the highest occupied energy level in the energy band diagram at absolute zero temperature. Whether an energy level is actually available at E_f, or solely exists as a reference within the energy gap, depends on the material in question.

For an atom with an even number of valence electrons, the energy level at E_f will be completely occupied at zero Kelvin [16, 53]. At higher temperatures the crystal lattice will be thermally excited and electrons may acquire kinetic energy from electrostatic interactions with vibrations in the crystal lattice. This energy transfer may also be considered in a quantised manner and such quanta of vibrational energy are termed *phonons* and commonly treated like a fictitious quasi-particle. Since electrons are fermions, the probability of an electron occupying a specific energy level ε, at a certain absolute tem-

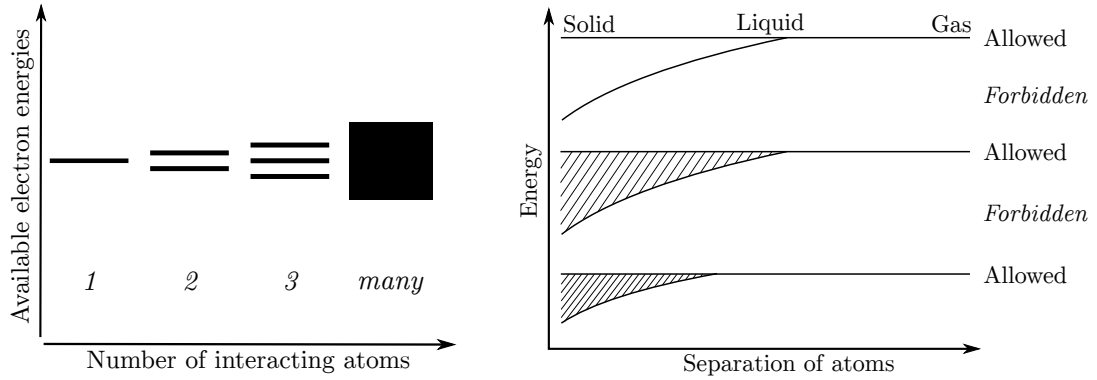

(a) Splitting of degenerate energy levels. [16]

(b) The effect of atomic separation on the availability of electron energy levels. Hatching denotes filled energy bands. [50]

FIGURE 3.3: When atoms are brought into close proximity, the overlapping wave functions result in sub-divided energy levels that, for a large number of atoms, may be regarded as continuous energy bands.

perature T, is governed by the Fermi–Dirac distribution function, P_{FD}; a treatment in statistical mechanics [51]. Letting ε be the energy level under consideration, k_B the Boltzmann constant, and T the absolute temperature, then

$$P_{FD}(\varepsilon) = \left\{1 + \exp\left(\frac{\varepsilon - E_f}{k_B T}\right)\right\}^{-1} \tag{3.3}$$

Theoretically a solid has an infinite number of energy bands, however, most of them lie above the energy that an electron requires to escape from the solid. As such, those energy bands are irrelevant to any conduction mechanism within the solid and will not be considered further. Energy band theory focuses on two energy bands, the valence band (E_{val}) and the conduction band (E_{con}) as well as on the forbidden energy gap separating the two. Most electrons in the valence band are not available for conduction since they are covalently bound within the stereo-specific bond orbitals of the crystal lattice. Electrons in the conduction band on the other hand, possess enough energy to delocalise from individual atoms and to contribute to the conduction process [16].

A popular way to distinguish metals, semi-conductors and insulators in terms of the band theory is by the difference in the magnitude of their band gap at a temperature of zero Kelvin, as illustrated in Figure 3.4. Metals either have a very small band gap of less than 0.2 eV[1] with a half filled valence band, or exhibit overlapping bands with no band gap at all. Semiconductors show band gaps of magnitudes somewhere between 0.2 eV and about 2.0 eV. Materials with bigger band gaps are classified as insulators [16, 51].

Charge transport can only occur if there exists an unoccupied energy level for an electron to move to. In the case of a partially filled valence level or overlapping energy bands this is not a problem. However, if the material is an undoped (i.e. intrinsic) insulator, then it will not only exhibit a large energy gap, but the Fermi energy will lie in the middle of it. This means that all the energy levels in the valence band are occupied, and the conduction band is empty of charge carriers. The only way to achieve conduction in this case is to excite an electron across the energy gap. This results in a conducting electron in the conduction band and an unoccupied state in the valence band. The energy necessary to promote an electron from the valence band to the conduction band, is equal to the difference in energy between the valence level and conduction level.

$$\Delta E = E_{con} - E_{val} \tag{3.4}$$

In order to compare the otherwise relative energies on an energy-band diagram, the *vacuum (energy) level* is introduced as a reference. It is defined as the energy of a free electron at rest. The energy required to move an electron from the material specific

[1]Electron volts. A unit of energy where 1 eV = $1.60217646 \times 10^{-19}$ Joules

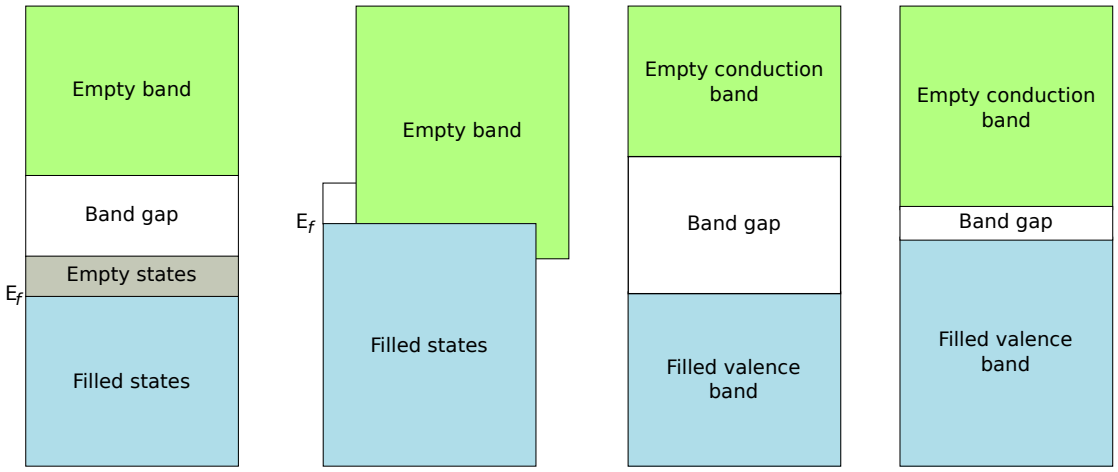

(a) Copper (b) Magnesium (c) Insulator (d) Semiconductor

FIGURE 3.4: Electron energy-band structures of various solids at 0° Kelvin. (a) Electron band structure of copper where energy states are available above and adjacent to filled states. (b) Metals such as Magnesium show overlapping energy bands. (c) Electron energy band structure of an insulator with the characteristically large band gap (> 2 eV). (d) Semiconductors exhibit relative narrow energy band gaps (< 2eV) [54].

Fermi energy to the vacuum level, is termed the *work function*. It describes the minimum energy required to free an electron from within the material at zero absolute temperature. The energy that is required for an electron to escape a negatively charged material, is represented by the electron affinity. Analogously, it also describes the strength with which an additional electron is held by a neutral atom [16]. The concepts are illustrated in Figure 3.5.

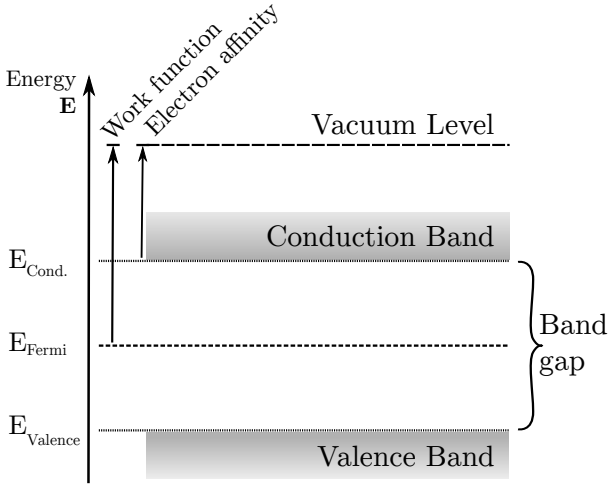

FIGURE 3.5: Illustration of the energy band model of an insulator.

Energy may be imparted to an electron by phonon interaction or by an external electric field. In the concept of the energy band theory, the increase in energy promotes the electron under consideration onto a higher energy level. Whether the electron is able to be motivated this way, depends on the availability of an energetically suitable state

within the energy band. In the case of an ideal solid dielectric, all the energy levels within the valence band are fully occupied and the only free states of higher energy lie beyond the energy gap. Whether the electron is able to bridge the gap and occupy an empty energy level within the conduction band depends on the amount of energy that was transferred to it, and on the magnitude of the specific energy gap.

The electric field acting on any electron within the crystal is the confluence of the externally applied electric field and the internal, periodic, electric field created by the atoms in the crystal lattice. Since electrons on full energy levels are paired with another electron of opposite spin, excitation of a single electron across the band gap results in a half-filled energy level in the top of the valence band. In order to be able to stay within Newtonian physics, the behaviour of the electron in this situation may be described by the semi-classical model of particle transport in crystals, where the response to electric and magnetic fields is treated like that of free particles in vacuum, but with a modified 'effective' mass (m^*). In this consideration, the residual electron in the half filled energy level of the valence band is ascribed a negative effective mass which is also reflected in its kinetic energy (E) and implies that it will be motivated towards the cathode [16], such that

$$E = \frac{1}{2} m^* v^2 \tag{3.5}$$

This behaviour is mimicking a positive charge carrier and consequently solitary electrons on half-filled energy levels are often simply described in terms of fictitious quasi-particles referred to as 'holes', in energy band theory contemplations [51].

3.4.1 Limitations of the Energy Band Model

The common energy band model is based on a number of assumption and simplifications that facilitate analytical solutions. There are two fundamental simplifications that tend to be employed in its consideration:

1. An adiabatic approximation to the crystal lattice that renders the lattice static and allows for the separation of electronic and nuclear effects. This means that electronic state calculations can be done independently from the lattice vibration calculations and then combined at a later stage.

2. A simplification or omission of the interactions between individual electrons, i.e. electron-electron interactions [55, Chapter 2.2.1].

3.4.2 Applicability to Polymers

A polymer is made up of covalently bonded[2], monomer[3] molecules, each of which has its own electronic states. The assembly of the monomers results in degenerate molecular energy states and may form extended energy states that support intra-molecular conduction similar to that described by the energy band model for a periodic one-dimensional crystal. The energy gap between the highest, filled molecular energy-level and the lowest, unfilled molecular energy-level i.e. the degree to which a polymer chain affords conduction along its backbone, will depend on the overlap of the atomic wave-functions between the individual molecules that it is comprised of. The energy gap will be smaller for unsaturated and conjugated[4] polymers and bigger for fully saturated[5] polymers [16].

Real polymer chains are not as rigid, periodic or static, as the energy band model assumes. Polymers with functional or pendant groups are likely to exhibit minimum energy conformations that are non-linear and consequently will not exhibit the ideal one-dimensional crystal structure. Above T_{glass}, the polymer chains are motivated by thermal energy and segmental motion will, at least temporarily, alter the inter-atomic spacing and thus break any symmetry of the periodic chain of monomers. This compromises one of the assumptions on which the formation of continuous energy bands relies, namely a static, periodic lattice.

It follows that, at any instant in time, distinct energy states may exist locally at a point on a polymer chain, yielded by, and restricted to, a molecule and its local environment [56]. The implications of these phenomena introduce irregularities in the distribution of the energy states which affects the edges of the energy bands and renders the magnitude of the energy gap time dependent [16].

Even though in theory idealised linear polymer chains may be regarded as a one-dimensional crystal lattice and treated using the energy band model, unlike metals and inorganic semiconductors, disordered solids do not feature a permeating isotropic crystal lattice. In a real, disordered solid dielectric, the regions of order will be very restricted and embedded within an otherwise highly disordered material. In a polymeric solid this means that the macro-molecular chains are likely to be convoluted and entangled, thus reducing the applicability of the energy band model to regions of local order i.e crystallites, randomly located within an amorphous phase. The extent to which conduction inside the crystalline regions can be explained by the energy band model, is thus influence by the length of the polymer chains, their density, conformation and orientation relative to the applied electric field. Consequently, the use of the band model is limited, by the very basis of its assumptions, to intra-molecular conduction in linear,

[2] A covalent bond is a type of chemical bond between atoms characterised by mutually shared electrons.

[3] A small molecule that, bonded together with other monomers, results in a polymer.

[4] A conjugated system is characterised by alternating single and multiple bonds.

[5] In organic chemistry a saturated compound has no multiple bonds i.e. only single bonds.

periodic macro-molecules and other models ought to be considered in the explanation of inter-molecular conduction within the amorphous regions [56].

3.5 Hetero–junctions and Charge Injection

In order to measure the electric properties of a dielectric, contact often has to be made, and that usually involves a metal-dielectric hetero–junction. It is desirable for the contact between such a sample under investigation, and the electrodes, to be ohmic in nature, in order to minimize any impact on the measurement. The amount of charge being transferred to and from the sample, ought to be equal. However, this is rarely the case. When more charge is being extracted from the sample than can be supplied, the behaviour of the hetero–junction is termed a *blocking contact* or Schottky barrier. When the inverse is the case, i.e. more charge is being transferred to the sample than is being extracted, the behaviour is called *charge injection*. Which type of contact is formed by a hetero–junction, depends on the relative magnitudes of the work functions ϕ of the metal and the insulator respectively. Figure 3.6 schematically illustrates the process of charge injection in the case of a hetero–junction between a metal and a polymer. When two dissimilar materials meet, charges will flow to equalise the chemical potential energy at the junction. This leads to a separation of charge and results in an electric field across the junction which 'bends' the energy bands. Which way they bend, is dependent on the relative magnitude of the work functions of the materials e.g. of a metal and an insulator. For an electron to move from the metal electrode into the dielectric solid, it has to overcome a potential barrier ϕ_0, the magnitude of which depends on the work function of the metal ϕ_{metal} and the electron affinity of the dielectric χ_{dielec}, i.e.

$$\phi_0 = \phi_{metal} - \chi_{dielec} \tag{3.6}$$

Any applied electric field will excite the electrons and reduce the effective barrier height they have to overcome. However, charge can only transfer into the dielectric via the Schottky injection mechanism if it has sufficient energy to overcome the barrier. Since thermal activation or excitation is one of the common ways in which charges can pick up energy, if follows that this process is temperature dependent.

For high applied electric fields, the potential barrier at the interface becomes very thin and charge transport across the potential barrier is possible via the Fowler–Nordheim injection mechanism. The theory is based on the fact that electrons can equally well be described as quantum wave functions, and as such they can tunnel through the thin potential barrier without having the energy that would have been required to pass over it. Section 3.7.2 provides additional information about this phenomenon. [16, 51]

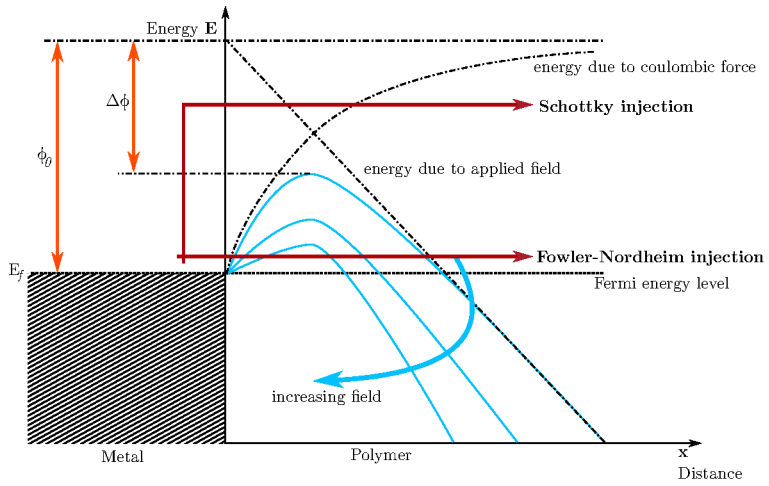

FIGURE 3.6: Schematic illustration of charge injection processes. Schottky injection and Fowler Nordheim tunneling. [57]

3.6 Localisation of Energy States

Section 3.4 introduced the concept that within a solid material, an electron can only exist on individual energies called energy states. If these energy states are restricted in their spatial extension and closely associated with a position inside the solid, then they are referred to as *localised energy states*. When a number of localised states start to overlap, they can form *extended states* where the electron is free to move from one spatial location to another. In crystalline materials these extended states may permeate large parts of the crystal lattice and form the familiar energy levels. As mentioned previously, a large number of tightly packed, energetically similar energy levels, may be treated as energy bands. Figure 3.7 illustrates the equivalent quantum mechanical consideration, where electrons are described by quantum wave functions. The concept of a localised state may then be described as a standing quantum wave with a decaying envelope, whereas an extended state would be able to host a continuous quantum wave [51, p.521].

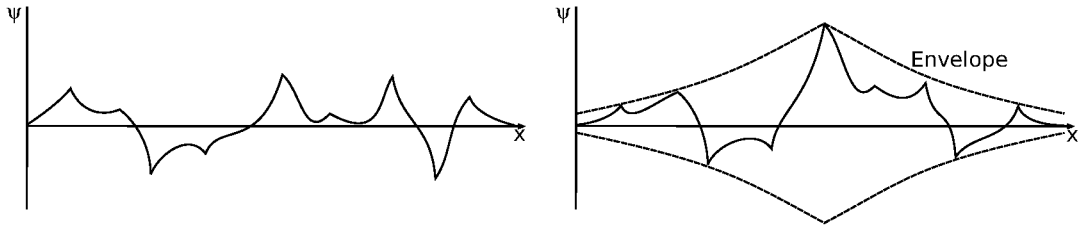

(a) Delocalised quantum wave function.

(b) Weakly localised quantum wave function.

FIGURE 3.7: Schematic representation of the effect of localisation on the quantum wave function, ψ. [58]

Electrons that enter local energy levels may get trapped there and thus effectively become removed from the conduction process. In a crystalline material, localised states may

be classified into electron traps (energetically situated just below the bottom of the conduction band) and traps that localise free energy states in the valence band. In addition there exist *localised states* where the surrounding structure will be altered into a potential well by either species, effectively self-trapping the occupant [16]. The quasi-particle that is formed when considering an electron with its concomitant lattice polarisation is termed a *polaron*. Electrons may be able to delocalise by interaction with random photons or phonons. In other words, if sufficient energy is imparted to the localised charge, it may break out from the trap.

It is worth noting, that in the energy band model where conduction proceeds on extended states or energy levels, phonon interaction is regarded as a limiting influence that scatters the charge carriers and reduces their mobility. In the subsequent models, where charge transportation in localised states is contemplated, the interaction with phonons is one of the enabling processes by which charge transportation is enhanced [59].

3.6.1 The Origin of Disorder

Disorder in condensed matter originates from defects, impurities and distortions in the structure of crystalline and semi-crystalline materials. It can be differentiated by origin between topological and chemical disorder, both of which break the symmetry of the material structure on a molecular scale. Topological disorder generates weak localisation that can momentarily capture charge carriers, thus impeding the flow of charge and effectively reducing the overall mobility. Disorder of chemical origin, however, may permanently bind charge in local defects. As a consequence, the conductivity of disordered solids is greatly affected by the spatial and energetic density of localised states [60].

Topological disorder describes the degree of randomness in the position of atoms in space. It is present in all amorphous materials. In polymeric materials it is fundamentally due to disorder in the macro-molecules that make up the polymer and may take the form of folds, incisions, twists and kinks in the polymer chains.

Compositional disorder describes disorder of a chemical nature, like the presence of intrinsic lattice defects—such as vacancies or interstitials—as well as undesirable impurities or intended doping species. Chemical disorder induces topological disorder due to the inherent randomness of its distribution.

Disordered alloys, mixed crystallites and impure crystals suffer disorder of the topological type, glasses and amorphous materials exhibit the compositional type of disorder. The influence of the impurities on total scattering of the electron wave functions is more pronounced at low temperatures where thermal excitations are reduced. In those circumstances the effect of scattering by polaron interaction does not outweigh the scattering on lattice distortions, as it may be induced by impurities. At high temperatures

the increased lattice vibrations dominate the scattering via electron-phonon interactions [52].

3.6.2 The Effect of Disorder

As previously explored, disorder within ordered crystal structures can be the source of localised energy states. Anderson (1958) was the first to consider disorder educed localisation [61]. The disorder in the case of Anderson localisation is due to a random variation in the potential energy between the individual lattice sites (i.e. vertical disorder) and of sufficient magnitude as to completely localise all charge carriers within an otherwise crystalline material. In this scenario, the wave functions for the E_f are all localised and no conduction is possible at absolute zero temperature because no charge carriers are free to move. Raising the temperature slightly, would enable conduction to proceed via thermally activated hopping as described in Section 3.7.2. Anderson termed this a *Fermi glass* [62].

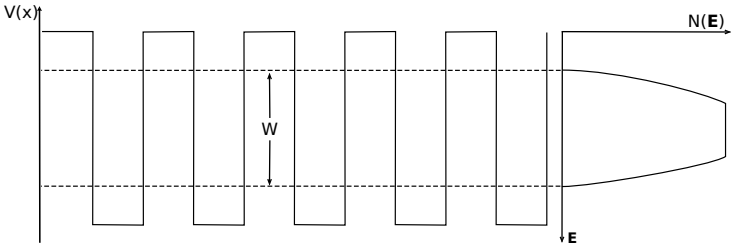

(a) No variation in potential energy, $\Gamma = 0$. W is the band width of the resulting energy band.

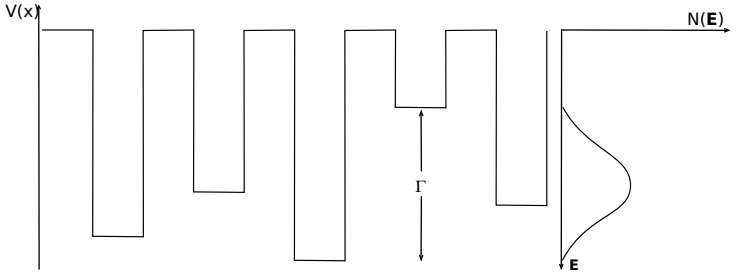

(b) A finite and random variation in potential energy, $\Gamma \neq 0$. The density of states reflects whatever distribution the potential energies take.

FIGURE 3.8: Schematic illustration of the potential energies, $V(x)$, and density of states, $N(E)$, in a disordered system according to the Anderson model. Γ describes the spread in potential energy. [58]

In 1967, Mott pointed out that even if the extent of the disorder is insufficient to localise all energy states, small variations in potential would start to induce localisation on the fringes of energy bands [62]. Figure 3.8 illustrates how a randomised variation in potential across several lattice sites obscures features of the energy band which rely on the perfect order of an ideal crystal structure. The energy bands are broadened and

their edges blurred by the presence of the additional energy states within the formerly inaccessible energy gap [59]. Increased disorder then extends the localisation further into the centre of the energy band. Figure 3.9 illustrates the concept. According to this, a material could posses a certain number of states at E_f, but due to localisation of the charge carriers, would not exhibit any conductivity i.e. behave as an insulator. This may be the case for localised states induced by impurities and situated in the band gap. In this case an increase in temperature may enable charge transport across the localised states by one of the mechanisms explained in Section 3.7.

The effect of injected charges on the material, as may be the case in high voltage applications, is to shift E_f upwards. This may also be achieved by doping of semiconductors. When E_f moves into the region of localised states at the fringe of an energy band, a finite number of charges will be able to exist in the localised states yet unable to conduct via the extended states. In this scenario, the focus shifts from the energy separation between the conduction band and the valence band, to a separation in mobility between the localised, and the extended states. This critical energy has been termed the *mobility edge* (E_c) and separates local states of low mobility from extended states with intrinsically high mobility. Figure 3.9 illustrates the concept and highlights the dependency of mobility on the density of states. The total conductivity of the material is then the combined contribution of conduction via localised and extended states, such that

$$\sigma = en_{ext}\mu_{ext} + en_{hop}\mu_{hop} \tag{3.7}$$

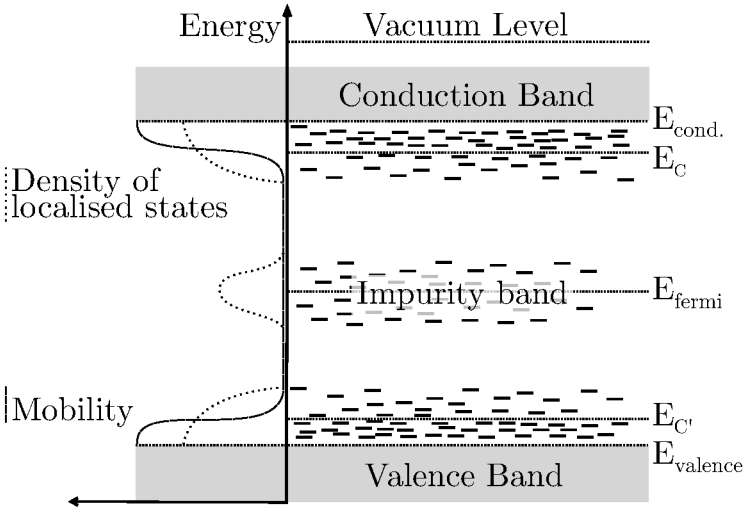

FIGURE 3.9: Impurities may introduce localised states in the energy gap and form an impurity band. E_c, the mobility gap, separates localised states of low mobility, from extended states of high mobility. [16, 60]

3.7 Localised Charge Transport Models

If the case where states at the Fermi energy are localised, two theories explain the transport mechanisms, conduction via multiple trapping or by hopping.

3.7.1 Multiple-Trapping Model

The multiple trapping model is based on the idea that the density of localised states is sufficiently low as to prevent any form of direct charge transfer from one localised state to another. Conduction thus has to proceed via excitation into the extended state [60] for which the required activation energy ΔE is described by the energy difference between the localised energy state (E_{local}) under consideration and any extended states E_{extend} that connect multiple localised states. This means

$$\Delta E = E_{extend} - E_{local} \tag{3.8}$$

This may only be a temporary excitation and does not mean that the charge carrier will stay in the extended state. However, it requires the interaction with an energetic particle to delocalise in the first place. According to this model, the charge transport across the material happens via a series of de-trapping and re-trapping events. The mobility of this conduction model is thus dominated by the average time a charge spends trapped in a localised state.

3.7.2 Hopping Models

Electrons in localised states may proceed directly via the hopping model. In this model, an electron jumps from one localised energy state to another free localised state nearby. This is thought possible if the quantum wave function of the charge under consideration extends far enough beyond the local state, that there is a certain overlap with another localised energy state. Because the location of the electron cannot be specified completely, there exists a finite probability that the particle may exist in any one of the local energy states that overlap with the quantum wave function. Whether such a quantum mechanical tunnelling event can occur depends not only on the presence of a local state within the extent of the localised quantum wave function, but also on the difference in energy between the energy states involved and on the availability of the right phonon activation. Every time the electron moves, it must exchange energy with another particle e.g. a phonon and thus the process is inherently rate determined. Due to the interaction with other particles, the model is also called phonon-assisted hopping model, photon induced hopping or thermally activated hopping model.

If the localisation is very strong, the hopping process tends to involve energy states in the immediate vicinity and is termed nearest–neighbour hopping (also Miller–Abrahams hopping). At low temperatures, however, it may be preferential not to hop to the nearest available local state. Jumping further away increases the choice of energy states and may minimise the total energy spent on the transition. In other words, it may be preferable to jump to a state of matching energy further away rather than to jump to a state nearby with a higher energy. The model is termed variable–range hopping [62].

3.8 Summary

In the energy band model, conduction depended on the availability of free energy states. In the case of an insulator this depends on E_f, on the size of the energy gap and the available excitation energy. Taking into account the localisation of charges makes the charge transportation process more complicated. It introduces dependencies on the density of states, the mobility edge and on available activation energies. The charge carrier density in the extended states mainly depends on the value of the mobility edge E_c. Consequently, more disorder within the material increases the value of the mobility edge and reduces the conduction in extended states. In highly disordered materials, conduction is thus dominated by the mobility of the charge transport in the localised states. If the density of localised states is sufficiently low that no hopping mechanism can take place, then conduction requires the excitation of an electron to extended states. For high densities of localised states, conduction may proceed via the hopping model. An immediate conclusion that can be drawn from this, is that in disordered materials, reduced temperature favours charge transport in extended states and reduces the availability of phonons which facilitate conduction among the localised states via phonon-assisted hopping [52]. At the same time, a decrease in thermal energy will reduce the chance of electrons being thermally excited into higher energy states. For disordered dielectrics this results in an reduction in the density of charge carriers with high mobilities that are available for conduction.

This chapter introduced a number of scientific terms and expressions which are necessary for the understanding of the models and methods that are discussed in the following chapters. Furthermore, the general theories of charge transport in ordered and disordered solid dielectric materials have been discussed to support the interpretation of data in later chapters.

Chapter 4

Space Charge Measurement Methods

The desire to measure the internal charge distribution in materials is not new and over time a panoply of measurement techniques have been developed. Some of the earlier techniques such as the electron beam probing method, the field probe technique or vapour-induced depolarisation current technique [63, 64], are physically all destructive to the sample under investigation. Other techniques rely on optical effects in order to indirectly measure the charge on, or contained within, a material. They have the benefit of being non-destructive and they do not deplete the sample of charge as a byproduct of the measurement. Examples are electro-optic field mapping techniques based on the Pockel or Kerr effect[1][65, 66], and Stark or Raman spectroscopy. The focus of the following review, however, will be on direct measurement techniques for the probing of charge distributions within solid dielectrics. Destructive or indirect methods will not be discussed further, but are reviewed in [67].

The measurement techniques reviewed in this chapter are all direct methods which implies that the charges under investigation are perturbed by the process employed to take the measurement and the signal is generated directly by the charges under observation. The techniques can be classified and distinguished by, and are often named after, the principle that is used to excite the internal charge and polarisation distribution. According to that, there are three families into which these direct measurement techniques may be categorised, namely thermal, pressure, and acoustic methods. Thermal techniques rely on the diffusion of heat, a temperature step or pulse, to perturb the charges accumulated inside the sample. Pressure wave or pulse methods employ a mechanical disturbance at the surface of the sample which travels through the material and acts on

[1]The electro-optic Pockel or Kerr effect is observed as a birefringence in an optical medium under the stress of a varying or constant electric field. When the birefringence is proportional to the electric field, the effect is named the Pockel or Pockels effect; for a quadratic dependence it is called the Kerr effect.

the accumulated charge wherever it is present. Acoustic techniques work in reverse. An electric field pulse is applied across the sample and perturbs the internal charge. The resulting acoustic waves propagate outwards from the charges and may be picked up by transducers which convert them into electrical signals. The following sections provide an introduction to a number of such direct measurement techniques suitable for the observation of space charge inside dielectric materials; a side-by-side comparison being provided by Table 4.3 in the discussion at the end of the chapter.

4.1 The Pulse Electro-Acoustic Method

One of the most popular developments in probing the internal charge distribution of materials is the Pulse Electro-Acoustic (PEA) technique, also sometimes referred to as the electrically stimulated acoustic or elastic, wave technique. Developed in the 1980s, it is the preferred choice in many industrial applications due to the simplicity and robustness of the measurement equipment [68–70]. In the PEA method, a pulsed electric field is applied across a sample which accommodates an unknown amount of charge. The electric field pulses interact with the charge and upset the equilibrium between elastic and electrostatic forces. This results in elastic waves originating from the position of the charges inside the material and propagating outwards at the speed of sound specific to the material.[2] The elastic waves are commonly picked up by piezoelectric transducers attached to the ground electrode of the measurement setup. A schematic of a PEA setup and a typical measurement signal are shown in Figure 4.1 and Figure 4.2 respectively.

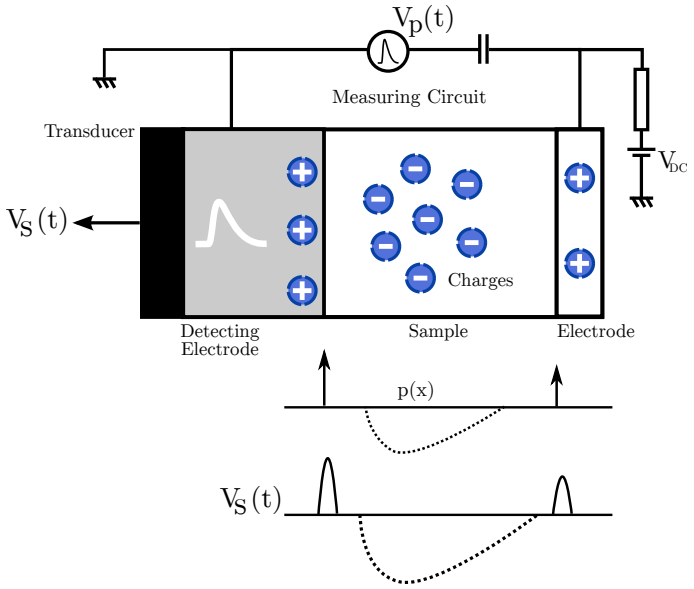

FIGURE 4.1: A schematic illustration of a PEA measurement setup [68].

[2]This refers to the 'speed of sound' in a solid which is specific to the material and not the same as the 'speed of sound' in air.

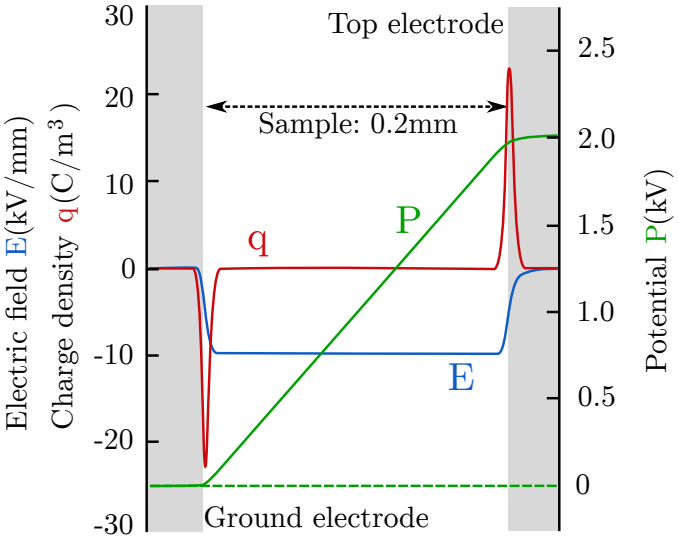

FIGURE 4.2: A typical signal produced by the PEA method under DC conditions by a polystyrene sheet [69]).

The magnitude of the measured PEA signal reveals the amount of charge and the relative time of reception is indicative of the distance to the source of the acoustic wave, i.e. the charge, and the receiving sensor. The measurement method can thus resolve the magnitude as well as the spatial distribution of the charge under observation. All types of charges are observed, including internal charge, induced charges on the electrodes, as well as surface charges in the case where the pulse is applied across an air gap [69, 71].

It is worth noting that any acoustic technique measures the net charge in a given volume as determined by the space and time resolution of the individual measurement system. It follows that no signal will be observed in a unit volume under investigation where at the same time, equal amounts of positive and negative charge exist. It is important to remember in the evaluation that that these 'blind spots' do not necessarily denote places where no charge exists, or that charge has been destroyed, but rather that no net charge was observed at the time of measurement. Fukunaga [69] reports that the signal amplitude strongly depends on the characteristics of the electrode interface. Any acoustic mismatch between the sample and the electrodes attenuates the signal. Evaporated electrodes showed the best transfer of elastic energy and resulted in higher signal amplitudes and better signal-to-noise ratio. For measurements on non-planar samples, the piezoelectric transducers must be arranged on the sample in such a way as to observe the elastic wave in phase [72]. This may be achieved using a waveguide[3]. For further discussion of the PEA signal and its interpretation, refer to Section 4.2.3.

The development of a three-dimensional PEA measurement system on the basis of an acoustic lens has been reported [73]. It enables charge observations in the lateral direction in addition to the usual measurements across the thickness of the sample. Although

[3]A waveguide is a structure/material that transfers and directs waves of different types. They exist for electromagnetic and acoustic waves.

the resolution is not yet high enough to investigate interfacial phenomena around filler particles, it has already provided indicative data on larger fillers in composite materials. In a similar vain, a two-dimensional PEA system with multiple transducers has been developed which is capable of collecting multiple charge profiles simultaneously in order to observe transient space charge phenomena [20]. This multisensors method is not as precise as the acoustic lens technique, but a lot faster and thus affords the capture of transient response profiles [69]. In addition, the PEA setup has been successfully scaled to a portable instrument that may be used on site [74].

4.2 Pressure Wave Propagation Methods

The Pressure Wave Propagation (PWP), or elastic wave methods have been used extensively for more than 30 years to study dielectric materials. It was the first technique that achieved real time measurements under pulsed and 50Hz AC voltages [65]. The PWP technique relies on pressure pulses that are made to travel through the sample under investigation in order to perturb the internal charge accumulation. The pressure pulse enters the sample through one of its interfaces and progresses through it at the speed of sound specific to the solid. When the elastic wave encounters any charges or imperfections, they are displaced mechanically, thus breaking the equilibrium between the elastic and electrostatic forces in the material [75]. This local deformation creates a small variation in the electric field which can be measured on adjacent electrodes as either a small current through a low-impedance measurement circuit, or as a variation in voltage across a circuit of high impedance. A typical PWP signal is shown below in Figure 4.3 for both a sample with, and without, an internal charge distribution. Figure 4.3a shows that the signal exhibits two pronounced peaks at either interface, even when no internal charge is present. These peaks correspond to the capacitive charges which are induced by the applied voltage on both of the electrodes. When internal charges are present, the magnitude of these peaks will change with any variation in the interfacial electric fields [65]. Peaks in the signal between the aforementioned interfacial peaks, as illustrated in Figure 4.3b, correspond directly to positive or negative charge accumulations within the sample. In this way the PWP signal returns a direct but qualitative image of the charge distribution within the material.

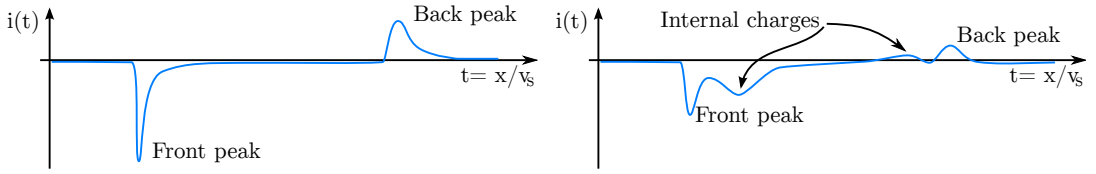

(a) No internal charge present.

(b) Internal charge present

FIGURE 4.3: The shape of a typical PWP signal for a sample under applied voltage with a) no internal charge, and b) with internal charge present [65].

The time of reception of the measured signal and the position of the observed charge are related by the speed of sound inside the material. In order to obtain quantitative results, the attenuation and dispersion of the pressure wave within the sample has to be taken into account [76]. This is especially important when the sample is either very thick or the rise time of the pressure pulse is very short and the concomitant frequency spectrum therefore broad [72]. Spatial resolution depends inversely on the spatial extent of the probing pressure pulse [77] i.e. the shorter the pulse, the higher the resolution of the measurement. Unfortunately, the attenuation coefficient and the signal dispersion increase as the pulse width is reduced. For the best signal resolution and measurement sensitivity, the length of the pressure pulse therefore has to be matched to the thickness of the sample under investigation [65, 76].

PWP is an umbrella term for a set of measurement techniques which all rely on the progression of pressure waves for the perturbation of the internal charge accumulation. The techniques are named after, and distinguished by, the way in which the pressure pulse is generated. Originally the pressure waves were generated by shock tubes or the discharge of capacitors in fluid [76], however, newer methods rely on laser light or piezoelectric transducers for the same effect. Two modern methods are briefly discussed below.

4.2.1 Laser Induced Pressure Pulse Method

In 1981 it was proposed to use laser light pulses in order to generate the pressure waves required for PWP measurements [72]. In the Laser Induced Pressure Pulse (LIPP) technique, the pressure pulse is generated by the impact of short pulses of laser light on the surface of the material sample or, more commonly, on an acoustically coupled or bonded target material. The laser pulse is absorbed by the target, leading to rapid heating and concomitant local expansion of the target material. The resulting elastic wave is transmitted onto the sample under observation by an acoustic coupling agent (e.g. grease) or by directly bonding the target onto the sample. The displacement of the integral charges by the elastic wave induces the variation in the internal electric field which can then be measured by adjacent electrodes. Figure 4.4 illustrates the principle of the LIPP technique. Generally, metal electrodes evaporated onto the sample are to be preferred. They may be used as both the target and the electrode, or in combination with an acoustically coupled target layer [72].

The target for the laser is preferably made of a material that has a high absorption coefficient at the wavelength of the laser employed, low thermal conductivity, and a low heat of vaporisation [65, 72, 76, 79]. For polymeric samples, a highly carbon-doped polymer satisfies the requirements outlined above and also results in a good acoustic match between the target and the sample. The target should be as thin as possible in order to avoid a broadening of the pressure pulse as it propagates through the target [76].

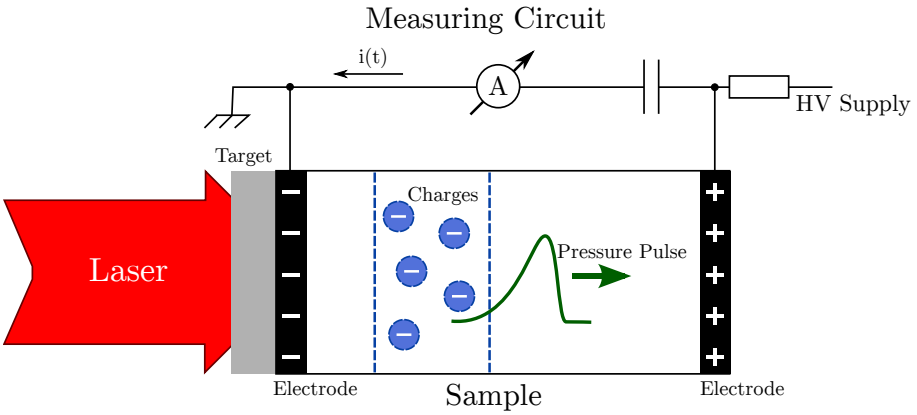

FIGURE 4.4: The principle of the LIPP technique [78].

The choice of the laser is defined by the desired pulse duration and the target material. The laser pulses ought to be sufficiently homogeneous and applied to the entire face of the target in order to create a uniform pressure wave-front. Practical limitations mean that pulse lengths shorter than a few nano-seconds are challenging to implement [76]. This frequency limit is inversely dependent on the thickness of the sample. At the same time, the sample must be sufficiently thick so that even at lower frequencies the signal remains above the noise level and able to distinguish charged from uncharged samples (Section 4.2.3 gives more details). The reduction in pulse length is also not proportional to the improvement in spatial resolution. A mechanical, lower limit is imposed by the penetration depth of the laser in the target layer which is dependent on the wavelength of the laser and the material of the target.

The large speed difference between light and sound waves means, that the LIPP method may also be used on non-planar sample geometries. The small time difference between the arrival of the laser pulses on different parts of the target may be neglected when compared to the speed of the elastic wave inside the sample [72].

4.2.2 Piezoelectrically Induced Pressure Pulse Method

The Piezoelectrically Induced Pressure Pulse Method (PIPP) is in almost all ways identical to the previously described LIPP technique. The two techniques only differ in the way the pressure pulse is generated. The PIPP technique employs piezoelectric transducers to generate the elastic pulse signal at the interface of the sample. This is the the same technology that is used in reverse for the PEA method, where it captures the acoustic waves originating at the internal charges and converts them into electric signals. By using piezoelectric transducers, the PIPP method removes the need for a laser, optics and target. Pressure waves of varying shapes may be generated by feeding different voltage wave-forms to the transducer directly mounted on the sample. The quality of the pressure pulse entering the sample will depend on the characteristics of the trans-

ducer and on the quality of the acoustic coupling or bond between the transducer and the sample [65, 75].

4.2.3 Signal Resolution and Interpretation

When performing PWP measurements on non-uniform or non-planar samples, the signal analysis becomes more complicated and spurious contributions to the measurement signal have to be taken into account. Complications may arise from non-uniform electric fields inside the material or from changes in its acoustic properties; both of which may be caused by the heterogeneous composition of modern insulation materials such as filled polymers or composites. It is worth noting, that the following discussion also applies to the PEA method. Although the PEA method does not employ pressure waves to perturb the internal charges, it nevertheless relies on the propagation of elastic waves from the charges to the piezoelectric transducers for detection. It follows that any discussion of factors that influence the elastic waves inside the material is equally relevant to the PEA method.

The basis of such spurious signal contributions may be found in the physical processes underlying the acoustic or elastic waves on which the PWP and PEA measurements rely. When an elastic wave displaces the charges under observation, it also introduces a small change in the relative permittivity of the material. The elastic wave locally compresses the material and consequently alters the quantity of polarisable molecules per unit volume. This results in a higher density of induced dipoles per unit volume and therefore a higher permittivity. The phenomenon is known as the electrostrictive effect [65]. The electrostrictive effect is responsible for a displacement current which is proportional to the time derivative of the electric field. Since the spatial and time derivative of the electric field inside the material are related by the material's speed of sound, any spatial variation of the electric field will result in a signal contribution due to the electrostrictive effect. In the case of uniform, planar samples, the spatial derivative of the electric field corresponds to the internal charge distribution and consequently the signal contribution by the electrostrictive effect is not different to that produced by the charges themselves. If the spatial derivative of the internal electric field across the thickness of the sample is not proportional to the internal charge distribution, then the divergence in the electric field results in a spurious signal contribution due to the electrostrictive effect. In such situations the internal electric field is no longer sufficiently described by one spatial coordinate and a more complicated measurement setup and experimental protocol are required. Specially designed samples and an iterative approach to signal analysis on the basis of sample-response-models have been suggested in such situations [65].

Modern insulation materials often include fillers or fibres to modify the mechanical, electrical and thermal properties of the host material. If such inclusions are much smaller

than the spatial resolution of the measurement method and randomly as well as uniformly distributed, then the elastic wave experiences a unique equivalent characteristic corresponding to the average of the material under the probing pulse. Larger fillers and fibres, however, can not be considered uniformly distributed and introduce a spatial dependence that has to be taken into account when the signal response is interpreted [65]. Acoustic mismatch between the host and the filler regions introduce reflections and attenuate the elastic wave. Reflections for small, randomly distributed filler particles are in a similar order to that of general signal attenuation and dispersion and may be neglected [76].

Differences in the permittivity and electrostrictive properties between different regions inside the heterogeneous material may create apparent charges with densities proportional to the electric field. Such apparent charge ought not to be confused with trapped charges. The time constant of a charge accumulation due to mismatched conductivities generally ranges from minutes to hours in most dielectric materials and can in that way be distinguished from the quasi-instantaneous appearance of apparent charge due to permittivity mismatch [65]. An additional spurious contribution to the measurement signal is generated by inclusions that carry charges or act piezoelectrically. Piezoelectric inclusions create a signal under the influence of compression by the elastic wave, independently from any applied electric fields. Charged inclusions and their concomitant electric fields, on the other hand, would induce a capacitive charge on the front and back electrodes. It follows, that a short-circuit measurement can discriminate between these two species of heterogeneities [65]. In conclusion it may be said that in the case of non-planar, inhomogeneous samples, the signal interpretation is significantly more complicated and more elaborate experimental procedures and signal analyses are required.

Table 4.1 provides a summary overview of the positive and negative aspects of the PWP methods.

Table 4.1: Positive and negative attributes of the PWP method.

Positive Attributes	*Negative Attributes*
Short measurement duration.	Pulse width has to be matched to the sample thickness.
Signal-to-noise ratio is good for sample thicknesses up to 1 cm.	Divergent electric fields require careful signal analysis for correct interpretation.
Suitable for real time measurements.	High pulse repetitions as required for real-time measurements may lead to electrode degradation or temperature changes.
Signals return immediate useful, qualitative results.	Quantitative results require processing.

4.3 Thermal Diffusion Methods

In a similar manner to the previously described PEA and PWP methods, the Thermal Diffusion Methods (TDM) rely on the perturbation of the equilibrium between the elastic and electrostatic forces in the material under observation. In the case of the TDM, the diffusion of heat through the sample expands the material in a non-uniform fashion and results in a displacement of charges which in turn induces a charge on adjacent electrodes. Thermal diffusion methods offer an alternative to the acoustic methods which are financially attractive and offer a good resolution [80]. TDM are commonly implemented using the absorption of laser light to generate controlled heating in an opaque electrode on one of the sample interfaces (Figure 4.5). Light can be focused very tightly and thus achieve high lateral resolution more easily than other methods [81].

The requirements for the measurement circuitry of the PWP methods and the TDM are identical and any fundamental advantages or disadvantages between the measurement technologies are a result of the difference in the underlying physical process that is used to probe the internal charge distribution. The thermal diffusion methods encompass implementations in the time domain, namely the Thermal Step Method (Section 4.3.1) and the Thermal Pulse Method (Section 4.3.3), and a frequency-domain based technique referred to as the Thermal Wave, or Laser Intensity Modulation Method (Section 4.3.2).

In general, the signal created by the thermal diffusion techniques may be recorded as a voltage across a high impedance measurement circuit, or as a current through a low impedance. The broadband measurement of voltages may, however, be more convenient to undertake, than the measurement of very small currents which are common for this type of measurement [82]. Figure 4.6 visualises the shapes of the excitations and resultant response signals, for the different TDM techniques. It clearly illustrates the transient quality of the TSM and the TPM, and the frequency-based nature of the continuous wave excitation of laser intensity modulation methods.

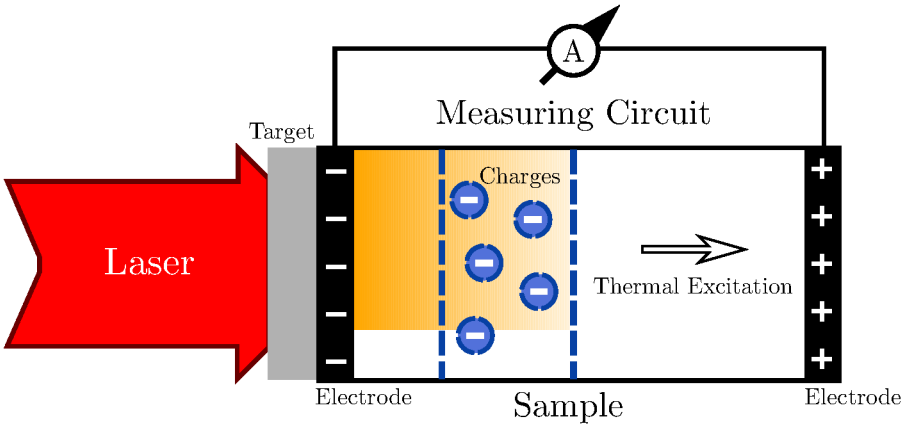

FIGURE 4.5: The principle of thermal diffusion techniques based on excitation by laser light [82].

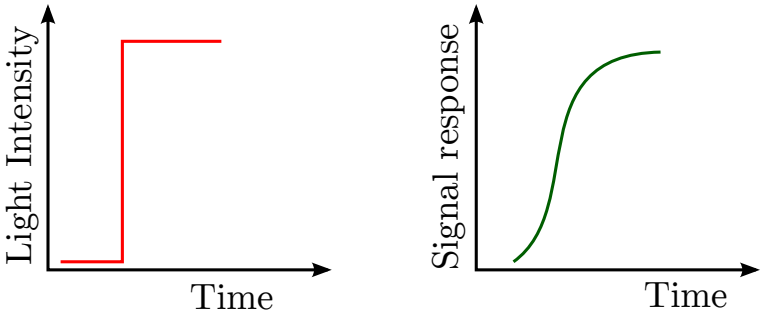

(a) Excitation and response of the thermal step method.

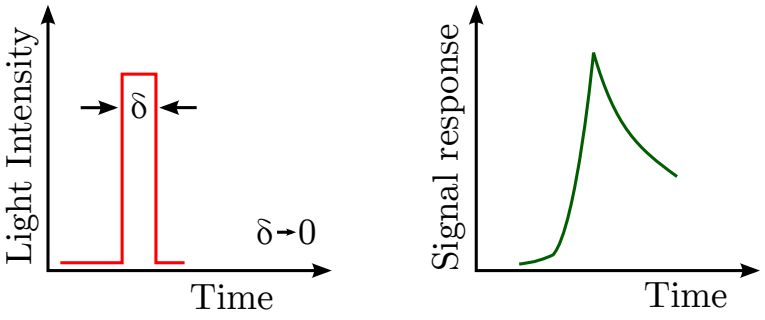

(b) Excitation and response of the thermal pulse method

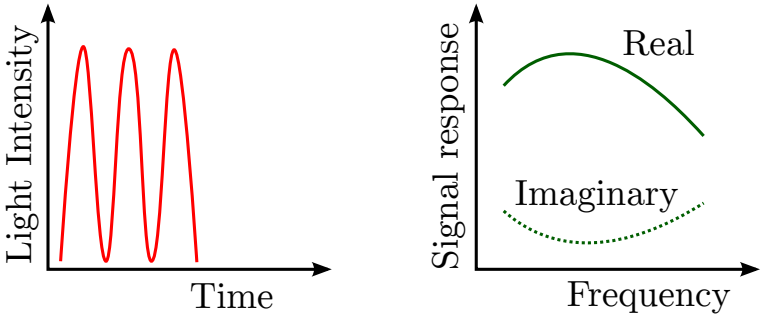

(c) Excitation and response of the LIMM method.

FIGURE 4.6: The shapes of excitation and response signals for different thermal diffusion techniques, based on excitation by laser light. [82]

4.3.1 Thermal Step Method

The Thermal Step Method (TSM) is, as the name suggests, a thermal method in which a rapid change in temperature is employed to disturb the accumulated charge under observation. The thermal step propagates through the sample and induces a capacitive charge on attached electrodes which can be recorded as a capacitive thermal step signal, e.g. as a current (10^{-12} to 10^{-9} A) by a pico-ammeter or current amplifier [83]. The inherently slow speed with which the thermal step is generated, results in a time resolution in the order of fractions of a second and consequently in a low spatial resolution [82]. The TSM is, however, suitable for very thick samples and may be applied to a range of sample types and geometries including flat specimens, short cable pieces or long cable loops. [83].

Two variations of the TSM have been published for cable samples [83], which have been aptly named the 'Inner Heating Technique' and the 'Outer Cooling Technique'. The first method implements the thermal step stimulus by heating the core of the cable, something that may be conveniently achieved by a circulating current. The latter technique achieves a temperature step by cooling the outside of a cable section by passing a coolant through a cylindrical radiator mounted on the outside of the cable. In each case the thermal step current is recorded between the cable core and ground. It has been advocated to employ a double-capacitor configuration for cable testing in order to account for polarisation and conduction currents in the space-charge current profile [83]. An example of the suggested setup is provided in Figure 4.7, and an equivalent electrical circuit diagram is depicted in Figure 4.8.

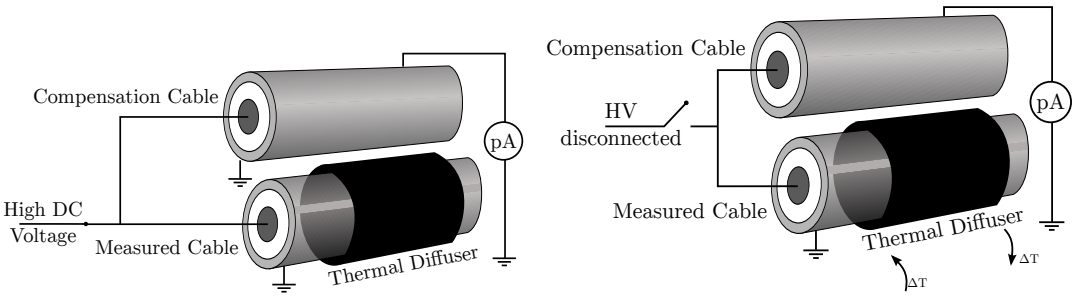

(a) A field is applied to the cables.

(b) Measurements are taken after the source is disconnected.

FIGURE 4.7: The double capacitor configuration for measurements with the Thermal Step Method via the Outer Cooling Technique. a) A high voltage DC field is applied to the cable. b) The HV source is disconnected before a measurement is taken. [83]

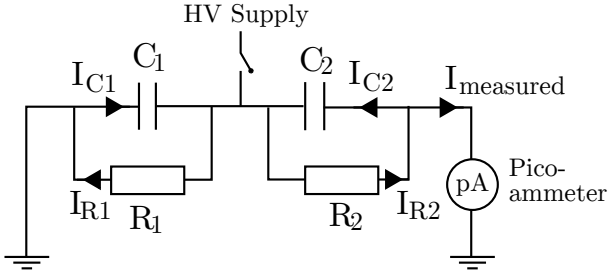

FIGURE 4.8: Circuit diagram of the double capacitor configuration reported [83] for the Outer Cooling Technique – a type of TSM.

4.3.2 Laser Intensity Modulation Method

The Laser Intensity Modulation Method (LIMM) was first published in 1984 [84] and has since been used for a variety of materials including ceramics, polymers and composites [85]. LIMM is based on the idea of modulated surface heating of the sample. One side of the sample, usually coated with an opaque surface layer, is exposed to a sinusoidally modulated laser beam. The absorption of the light results in sinusoidal temperature fluctuations in the absorption layer that propagate as waves into the sample. As the

thermal waves propagate through the sample, they are attenuated and retarded in phase. The effect of attenuation and retardation is less for lower frequencies and increases with probing depth [85]. The result is a time-varying, spatially non-uniform temperature profile across the sample which perturbs the internal charge distribution and gives rise to a sinusoidal pyroelectric current. This current is a unique function of the frequency of modulation and the internal polarisation and charge distribution [67]. Measurements are generally performed at 50 to 100 different, logarithmically spaced frequencies over an appropriate frequency range [85]. A complete measurement is therefore slow and most suited for the observation of slowly evolving phenomena. Data analysis of the LIMM signal requires knowledge of the thermal diffusivity[4] of the material under investigation [85] and mathematical deconvolution is required to compute the polarisation and charge distributions from the frequency motivated current data [67]. A LIMM implementation capable of three-dimensional measurements has also been reported [86].

4.3.3 Thermal Pulse Method

The Thermal Pulse Method (TPM), illustrated in Figure 4.9, provides a quick measurement that achieves sample rates of a few μs for specimen thicknesses in the order of micrometers [82]. It follows that this technique is suitable for the observation of transient charge behaviour and polarisation mechanisms. The thermal pulse method is 20-50 times faster than the LIMM method at similar bandwidth and quality [87]. This is an improvement over the previous implementations where the slow speed of measurement at a single frequency usually resulted in a trade-off between the spatial resolution and the sample area that was investigated [81]. Modern implementations of the thermal pulse method allow for three-dimensional probing of charge and polarisation profiles [81, 87, 88].

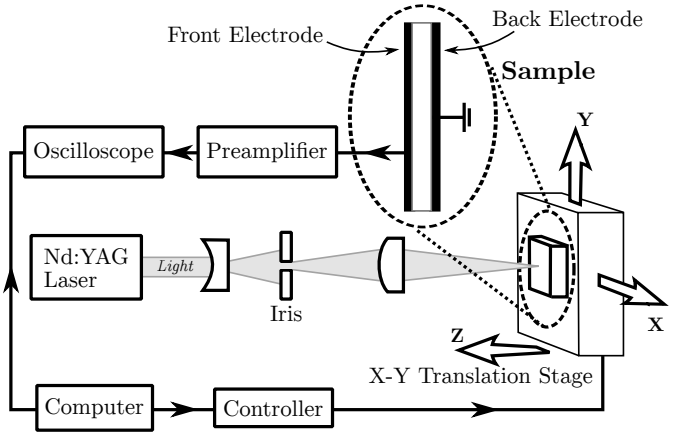

FIGURE 4.9: Setup for a three-dimensional TPM measurement [81].

[4]Thermal diffusivity is the ratio of thermal conductivity to volumetric heat capacity in SI units of $m^2 s^{-1}$.

4.3.4 TDM signals

Many of the challenges associated with the correct interpretation of measurement signal have already been mentioned in Section 4.2.3 for the PWP technique and are equally relevant for the thermal techniques. Further problems, associated with the nature of the thermal diffusion methods are illustrated in Figure 4.10 on the basis of a LIMM signal. Most TDM implementations apply the heat excitation on one side only. This may lead to an asymmetric expansion of the sample and result in deformation. In samples accommodating a non-uniform charge or polarisation distribution this mechanical deformation may give rise to spurious signal contributions due to piezoelectricity. According to Wübbenhorst et al. [80], the resulting resonances are visible as flexural waves on a number of published LIMM spectra. A good mechanical fixation of the sample is recommended to reduce the problem. Heat loss may be present due to drifts in the laser intensity or the degradation of the absorbing target layer. Random, rather than sequential measurements may help to capture such temporal changes in the measurement setup. Finally, the gain/phase characteristics of the measurement electronics also ought to be taken into account and calibrated for, to arrive at a faithful measurement signal [82].

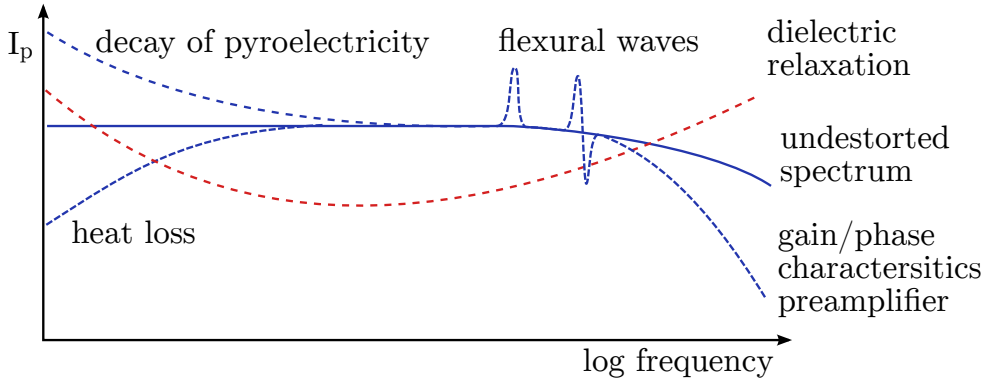

FIGURE 4.10: Possible signal distortions for the thermal diffusion methods exemplified by a LIMM signal [80].

Although the TPM is a time-domain based measurement, the signal analysis is often performed in the frequency domain. The motivation for this conversion is the need to preserve the phase information of the thermal pulse response, which necessitates the removal of the phase shift introduced by the measurement and amplifier electronics. The adjustment is most conveniently performed in the frequency domain [87, 88].

4.4 Thermally Stimulated Current Methods

The Thermally Stimulated Current (TSC) methods, like the previously described PEA, TDM and PWP techniques, are not physically destructive to the sample under investigation. In contrast to the other techniques, however, the TSC methods are depleting

in nature, which means that the sample is discharged of its internal charge distribution in the course of the measurement [89]. TSC is a very mature technique that was first demonstrated in 1936 [90], and has since been used to investigate a range of materials including polymers, semiconductors and dielectrics [91]. TSC measurements have been extensively employed to characterise and monitor thermally activated charge emission and capture in dielectrics and semiconductors with localised energy states [91]. Furthermore, TSC techniques have been used to study charge storage and decay phenomena, dipolar relaxation events, space charge redistribution and the migration of ionic charges [91]. TSC measurements determine the energetic depth and nature of the localised energy states which accommodate the polarisation and charge distribution. Spatial distributions of charge and polarisation, as are supplied by the TDM, PEA and PWP methods, are difficult to obtain [89]. The TSC method thus reveals information about the nature of the charge or polarised species present in the sample and provides insight into the propensity of a material to acquire and store charge. TSC techniques have been reviewed thoroughly [67, 90–93] and a number of different technical setups have been developed by different research institutions [89, 91, 94, 95].

TSC measurement techniques can be distinguished by the way in which they polarise the sample. For Thermally Stimulated Polarisation Current (TSPC) measurements, an unpolarised sample is cooled and then a polarising field is applied during the temperature rise [96]. This way the TSC signals are generated by thermally enabled polarisation of the sample. In other words, the sample is gradually polarised by thermal activation of different polarisation and injection mechanisms. For Thermally Stimulated Depolarisation Current (TSDC) measurements, the sample is polarised before it is cooled down and the thermally activated relaxation of charge is recorded during heating with the poling voltage removed. This is the more popular TSC technique and the one considered here [90]. Generally, an implementation of a TSC measurement device is comprised of a sample sandwiched between a charging electrode and a measurement electrode, all of which is attached to a temperature control element. The later may, for example, be achieved by a combination of heating elements and a cooling coil [95, 97], or by employing a thermoelectric cooler (TEC) [91]. A general schematic of a TSC setup is provided in Figure 4.11. A more detailed TSDC implementation is illustrated in Figure 5.4, in Chapter 5.

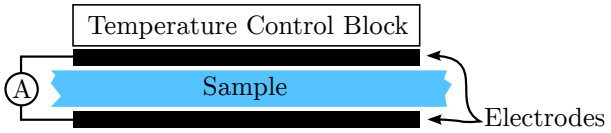

FIGURE 4.11: A simplified schematic of a TSC measurement setup.

To perform a thermally stimulated discharge current measurement, the dielectric is first placed in a non-equilibrium condition by applying an external electric field or excitation, and then quenched to a lower temperature in order to lock-in or freeze the

non-equilibrium state. Finally, the sample is heated in a controlled fashion by which the material acquires sufficient thermal energy to relax back to its equilibrium state [90, 91]. By cooling the sample below glass transition temperature, any charges or polarisation effects caused by the applied electric field, are effectively immobilised due to the reduced thermal motion within the material. A very sensitive ammeter is used during the heating period to record the current signal that is created every time the rising thermal excitation leads to de-trapping of charge or dipole relaxation inside the material. The signal response first rises with temperature and then decays when the liberated charge is depleted. Whether an ammeter, a voltmeter, an electrometer or current amplifier is employed for the measurement, depends on the technical setup. The thermally stimulated or liberated charge induces a change in charge on the measurement electrodes which may be measured with a voltmeter across a high impedance circuit, or via an ammeter in line with a low impedance circuit. TSC is thus a form of thermally stimulated or activated spectroscopy [96], where a material is characterised using thermal stimulation, as opposed to chemical, physical or photo stimuli [92]. A more detailed experimental protocol for a TSDC measurement is discussed in Section 5.6.

4.4.1 Signal Origin and Resolution

There are a number of different charges and polarisation mechanisms that can be investigated using a TSDC measurement, most of which fall into one of the following categories [92]:

Orientational polarisation Molecular or ionic dipoles tend to align themselves with externally applied electric fields. The rotation of large molecules, or parts thereof, will be restricted by the entanglement with neighbouring molecules and other surrounding field effects.

Space charge polarisation Space charge in the material may be electronic or ionic in nature and can be polarised by an external field. Space charge can take the form of homo-charge or hetero-charge (q.v. Section 3.1).

Interfacial polarisation Space charge tends to accumulate at interfaces between regions of different conductivity or permittivity. This effect is especially pronounced in heterogeneous materials like composites, but also occurs around impurities in otherwise homogeneous materials.

It is important to remember that no TSC technique directly measures the charges on or within the sample. Only the charges moving to or from the electrode can be recorded. As the sample relaxes towards its equilibrium state, the compensation charges held on the electrodes by the polarisations and charges accumulated in and on the sample, are released and may move through the electrode and be recorded by the meter. A current

peak will therefore register at any temperature where charge carriers are activated or released from localised energy states. The total polarisation and charge distribution inside a material is usually a combination of individual events with varying activation energies and relaxation times. The TSC response is thus, in principle, a complete temperature-dependent characteristic of the material and large TSC currents reflect major readjustments of the internal charge or polarisation distribution [90]. Not all movement of charge will register on a TSC response. Injected charges may simply move back onto the electrode they originated from and cancel the corresponding compensation charge without ever producing a measurable response. Also, if equal amounts of opposite charge progress to both electrodes at the same time, then no measurable current will flow and the process will go unnoticed on the TSC thermogram [90]. The separation of different processes relies on temperature dependence. It is next to impossible to disentangle two processes that are activated at the same temperature. Both signals will contribute to the magnitude of the same peak on the TSC thermogram. Consequently it may be complicated to correctly interpret the results of a TSC measurement. In order to increase confidence in the results, systematic variations in the measurement parameters (voltage, time and temperature) are advisable. The repeatability of TSDC measurements depends on the measurement system as well as on the material under investigation. A good TSDC spectrometer will always produce identical results for the same observation. However, in practice no two observations or measurement runs are identical, even for two samples of the same batch of material and with the same experimental history. For example it has been reported by several people that the repeatability of the TSDC peak corresponding to space charge in PET "leaves much to be desired" [37]. Since every TSDC measurement comprises a poling step and a thermal cycle, it follows that further physical changes my be induced with each measurement. The repeatability of a TSDC measurement is therefore an empirical value that depends not only on the measurement setup, but also on the sample under investigation.

4.4.2 Signal Deconvolution

The partial heating technique, and the fractional polarisation technique, are two experimental procedures that may help to resolve some of the broader and complex peaks on a TSDC spectrogram. The partial heating technique follows an ordinary TSDC protocol (q.v. Section 5.6) and only differs in the heating stage where the sample is relaxed. After the sample has been cooled to a lower limit T_{low}, the temperature is ramped up to an intermediate temperature T_{part}. At this cut-off temperature the heating ramp is interrupted and the sample is cooled again to a temperature $T_0 \simeq T_{part} - 50°C$. Repeating this process whilst increasing the cut-off temperature T_{part}, generates a series of component signals that may be analysed individually for the activation energy of the underlying process [98].

The fractional polarisation or thermal sampling technique works by limiting the signal contribution of relaxation processes by choosing a small depolarisation window. A specific relaxation, i, may be found by applying the poling field briefly at T_{pol}. The sample is then cooled and short circuited at $T_d = T_{pol} - \Delta T$ where ΔT is the polarisation window. The remaining excitation is then arrested by cooling the sample to $T_0 \simeq T_{pol} - 50°C$ before the temperature is ramped up and the signal recorded according to the usual TSC procedure. By shifting the polarisation window over the temperature range under investigation, a set of elementary peaks can be obtained that are assumed to represent single relaxation processes and thus may help to interpret the overall TSC response [99]. Figure 4.12 illustrates the concept.

If only the dipolar relaxations are to be measured, a thin gap may be inserted between the electrodes and the sample. It blocks ohmic currents that may be created by ionic charges liberated during the heating process and thus removes the ionic conductivity from the measurement results. Neither the polarisation process nor the measurement of the polarisation or depolarisation currents requires a direct contact between the electrodes and the sample. Section 4.4.3 provides more information on the implications of this approach [94].

TSC thermograms of polymeric solids can be compared to results obtained using mechanical or dielectric relaxation techniques. The signals are considered to originate from the same underlying processes. Due to the different technical principles involved in each of the measurements, a direct comparison between the thermograms requires the dielectric or mechanical measurements to be obtained at a TSC-equivalent frequency. It is defined as the frequency at which the temperature of a peak on the TSC thermogram correlates with the corresponding peak on the thermogram of the mechanical or

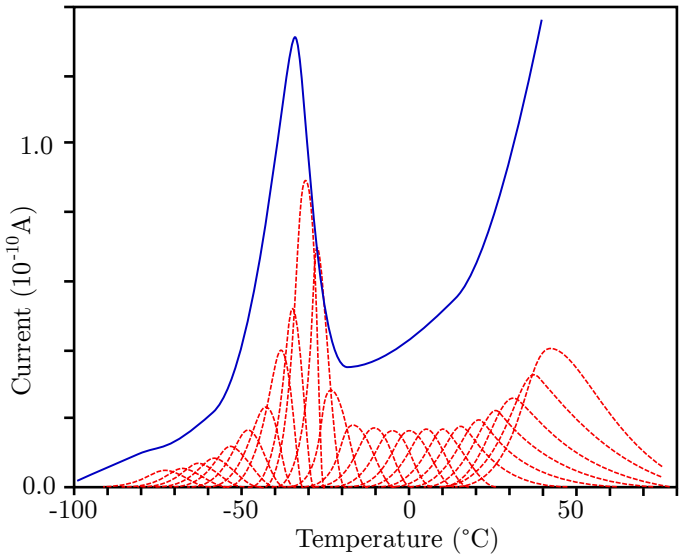

FIGURE 4.12: Fractional polarisation of TSDC data. Complete (solid line) and fractional (dashed line) TSC spectrum of a fluorinated co-polymer P(VDF-TRFE) 75/25 mol%. Polarisation window $\Delta T = 5°C$. [99]

dielectric spectroscopy. The lower effective frequency of the TSC technique tends to provide a better measurement resolution [90, 100]. Measurements of the glass transition temperature (T_{glass}) alone, may also be obtained by Differential Scanning Calorimetry (DSC) or Differential Thermal Analysis (DTA). However, the signal strength of these techniques can not be enhanced to show weak transitions. TSC is an effective tool for the investigation of activation energy and entropy that characterise the glass transition temperature [101]. By increasing the electric field strength, the signal strength can be raised and thus the sensitivity of the measurement increased [94].

4.4.3 Signal Interpretation

Compression and expansion of PET sample films have been found to alter the TSDC spectra, and are said to shift the activation energy and the α–peak on the spectrum that is motivated by dipolar processes, towards a lower or higher temperature respectively [102]. Expansion of a PET sample under a reduced pressure of 1100 mbar reportedly changed the activation energy of the α–peak by 0.016 eV [37]. The phenomenon of compression has been explained by an increase in the overlap of molecular orbitals which eases the charge transport and reduces the activation energy [102]. Adsorption and absorption of gasses may also be intensified with increasing pressure of the gas environment. This can lead to changes in the chemical potential and other chemical reactions on the exposed polymer surface. Pressure also directly affects the free-volume in the polymer. [37, 102]

Generally the measurement of space charge via TSC is constrained by two limits in observability. For materials with a sufficiently high conductivity, an externally applied electric field that is strong enough to inject a detectable charge will also motivate any free charge carriers already present in the material and thus give rise to a current large enough to mask the presence of space charge. On the other hand, a sample with a very small conductivity will challenge the sensitivity of the available technology and measurements will be limited to the smallest currents that can be successfully distinguished from the inevitable leakage currents present within the system.

The signal that is recorded in a TSC measurement is a function of temperature and time, and the peaks on the thermogram are commonly labelled in order of temperature. Figure 4.13 shows a typical TSDC spectrogram. The interpretation of the results will depend on the nature of the presumed mechanism that gave rise to the signal peaks. A dependence between the nature of the TSC results and the electrode metal has been reported [90]. This is to be expected, since the transfer of electrons from the electrode to the sample depends on the metal specific work function (q.v. Section 3.4). A lower work function would increase the amount of injected charge. The magnitude of the peak on the TSDC thermogram that is associated with electron injection is therefore dependent on the work function, while its peak temperature is believed to be independent. This can

help to distinguish charge injection processes from dipolar relaxation or reorientation mechanisms which are independent of the metal work function [90]. Charges present in the material during the poling procedure create a non-uniform field within the sample and afford spatial variances in the remaining polarisation. This effectively introduces a spatial error within the measurement [103]. It has been noted that TSDC measurements are more sensitive to reading dipolar relaxation processes than picking up localised charge [104]. The latter may recombine with charges of opposite polarity within the sample, without yielding a measureable signal current in the TSDC measurement circuit.

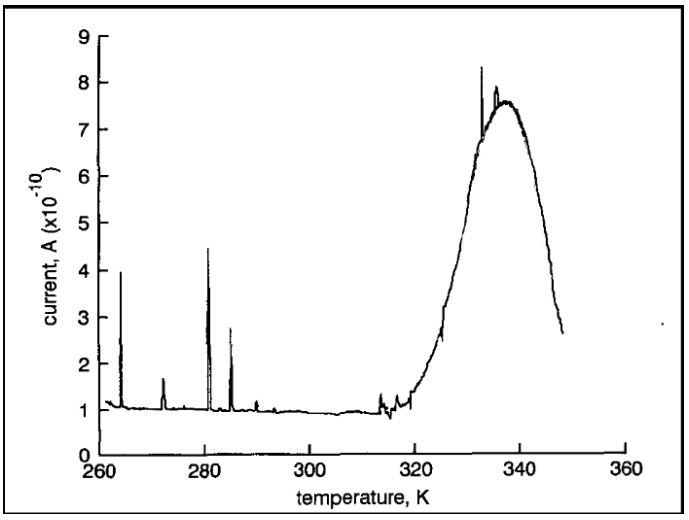

FIGURE 4.13: A TSDC spectrogram of LDPE. [24]

Wang et al. [24] have shown that by matching the experimental data against theoretically simulated results, full use can be made of all available measurement points. This is superior to the older methods like the initial rise method or the asymptotic method where only a subset of the measurement points contributed to interpretation of the results. The characteristics of the TSC thermogram around the glass transition temperature have been modelled [101] and the study showed that unexpected TSDC results around T_{glass} may originate from the misuse of the Arrhenius equation on data sourced from non-stationary experimental conditions.

Fitting TSC thermograms with theoretical models in order to explain the underlying processes, makes explicit the fact that scientific expectations are fitted to observed data. Considering the incomplete knowledge about the charge transfer processes within amorphous dielectric solids, it is questionable whether the theoretical models are comprehensive enough to represent the events within the material, no matter how well they fit the measurement data.

Table 4.2 provides a brief summary of the positive and negative aspects of the TSC methods.

Table 4.2: Positive and negative attributes of the TSC methods.

Positive Attributes	*Negative Attributes*
Signal strength may be improved by increasing the poling field strength.	The sample is discharged during each measurement.
High resolution	Resolution is non-homogeneous and dependent on probing depth.
Low equivalent frequency (10^{-3}–10^{-4} Hz) [99].	Transient effects are hard to capture.

4.5 Discussion

Although the thermal diffusion methods, the electro-acoustic methods and the pressure wave propagation techniques, all rely on different physical processes to perform the measurement, it has been demonstrated that all three types of measurement rely on the perturbation of the equilibrium between elastic and electrostatic forces and consequently all work to measure the same electrical information in a sample [75].

The resolution of measurement methods that rely on the diffusion of heat has been found to decline with probing depth inside the sample, in other words, with distance from the heat source. In contrast to this non-uniform spatial resolution, the resolution of techniques based on the propagation of pressure waves or those relying on electro-acoustic effects, is almost constant with position [77]. It can be concluded that, in terms of their resolution, the three families of measurement techniques, the PEA techniques, the PWP methods and TDM, conveniently complement one another [82]. PEA and PWP methods ought to be the preferred choice for the investigation into thicker samples, while the TDM provides higher resolution for smaller probing depths and is more suited to thinner samples [23]. Finally, thermally stimulated spectroscopy measurements, such as the thermally stimulated discharge/depolarisation current (TSDC) method, provide additional information on the nature of the localised states which accommodate the polarisation and charges under investigation. In this way, the confluence of data collected by the different techniques may form a more complete picture of the state of the material and consequently lead to more informed models and concepts about the behaviour of charge in solid dielectrics. Table 4.3 provides an overview and summary of the previously discussed measurement technologies.

This chapter provided an overview of physically non-destructive measurement methods for the investigation of space charge in solid dielectric materials. Some of their individual strengths and weaknesses were presented, and the complementary nature of the TSDC method was highlighted. The introduction and general discussion of the thermally stimulated discharge current method supports the next chapter, which presents the design and construction of a custom TSDC Spectrometer. Furthermore, it is also facilitates the discussion of TSDC measurement results in Chapter 6.

[5]The presented data (next page) is, in parts, an update on similar work by Gerhard-Multhaupt (1987)[93] and Ahmed and Srinivas (1997)[67].

TABLE 4.3: Comparison of selected space charge measurement technologies [5].

Method Name	Abbrv.	Excitation	Scanning Mechanism	Detection	Resolution	Deconvolution	Refs.
Laser Intensity Modulation Method	LIMM	Absorption of modulated laser light at the front electrode.	Time-dependent, spatially non-uniform temperature profile.	Current induced on adjacent electrodes.	$\geq 2\mu m$	Required	[67, 81, 85]
Laser Induced Pressure Pulse	LIPP	Absorption of short laser-light pulse(s) in front electrode.	Pressure pulse propagates with longitudinal sound velocity.	Current induced on adjacent electrodes.	$1\mu m$	Not required	[67, 93]
Pulse Electro-Acoustic	PEA	Electric field pulse(s) generate acoustic wave(s).	Pressure pulse propagates with longitudinal sound velocity.	Piezoelectric transducer at sample electrode.	$\sim 2\mu m^a$; $\sim 100\mu m^b$	Required	[67, 69, 70, 73, 74, 105, 106]
Thermally Stimulated Current	TSC	Rising thermal profile.	Relaxation of charge as a function of temperature.	Current flowing between the sample electrodes.	5×10^{-17} A	Not required, but possible.	[90],[95]
Thermal Pulse Method	TPM	Absorption of laser-light pulse(s) in opaque layer.	Time-dependent, spatially inhomogeneous temperature profile.	Charge induced on adjacent electrodes.	$\leq 0.5\mu m$ (near surface)	Required.	[77, 88]
Thermal Step Method	TSM	Temperature step excites trapped charges.	Time-dependent, spatially inhomogeneous temperature profile.	Charge induced on adjacent electrodes.	$1 \times 10^{-3}\,\mathrm{C\,m^{-3}}$	Required.	[83, 107]

[a] Resolution in the field direction (thickness).
[b] Resolution in the lateral direction.

Chapter 5

Design and Construction of a TSDC Spectrometer

The general principles of Thermally Stimulated Discharge Current (TSDC) measurements have been introduced in Section 4.4. This chapter presents details on the implementation of a TSDC spectrometer. The TSDC instrument complements and extends the existing measurement and research capabilities of the Tony Davies High Voltage Laboratory, which has already a strong interest in both dielectrics in general, and their behaviour at low temperatures in particular [108].

5.1 General Design

In the present configuration, the TSDC Spectrometer is designed for the investigation of solid dielectric films or papers. It was designed around an existing but inoperable cryostat vessel and electrode system which was recycled and refurbished for this purpose. The system was cleaned and completely rewired, but the electrode assembly was retained as it was previously. Figure 5.1 illustrates the state of the electrodes prior to reconditioning. It shows the brittle and broken nature of the old dielectric film separating the heater disk from the guard ring and signal electrode. The drill holes seat insulating screws that hold the electrode assembly together. For technical drawings of the cryostat vessel and the electrodes, please refer to Griffiths et al. [97]. Figure 5.2 shows a detailed schematic of the electrodes and temperature control elements. In order to perform a measurement, the sample under investigation is placed between the low voltage electrode (LV-electrode) and a sprung high voltage electrode (HV-electrode). The LV-electrode is surrounded by a guard ring in order to capture leakage currents and improve measurement accuracy by removing edge effects. Temperature control is achieved using a digital temperature controller and a combination of electric heating and cooling by liquid nitrogen (liquid-N_2). The electric heater cartridges are embedded in

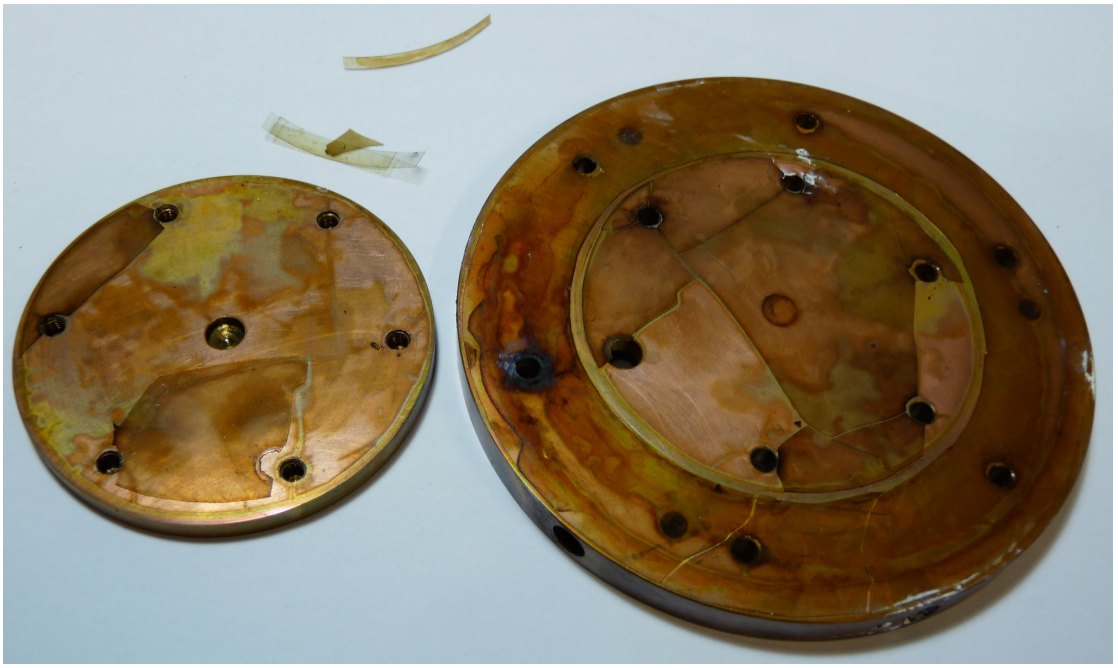

FIGURE 5.1: State of the electrodes prior to refurbishment. Signal electrode inverted on the left, (heated) copper disk on the right.

a copper disc and bonded with heat conducting paste. The cooling coil through which the liquid-N_2 is fed, is situated below the copper disc and also bonded to the former with heat conducting paste. Together, the cooling coil and the heated copper disc make up the temperature control unit. The LV-electrode and the guard ring are separated by a small gap and attached to the temperature control unit with insulating screws. Electrical separation between the electrode, the guard ring and the temperature control unit is achieved by a thin mask of Polyimide film. Using a solid electrical insulator at this point improves thermal conduction and control. Temperature measurements are taken both in the copper disc and in the guard ring using platinum pt-100 temperature sensors. The complete assembly is suspended from the lid of a double-walled stainless steel cryostat by three metal tubes. The cryostat provides thermal insulation and electromagnetic shielding for the measurement, as well as protection for the operator from the high voltages present during the poling process.

For practical reasons, the TSDC spectrometer only provides and controls the temperature on one side of the sample. The explicit assumption is made, that the temperature is homogenous in the plane of the sample, and the temperature gradient across the sample is negligibly small. This assumption is further supported by the disparate mass and heat capacities of the two electrodes. The unheated electrode is smaller in size and hollow, whereas the heated copper block has a mass and area that is approximately ten times larger than its counter electrode. In addition, the sprung electrode was loaded with a weight to improve electrical and thermal contact.

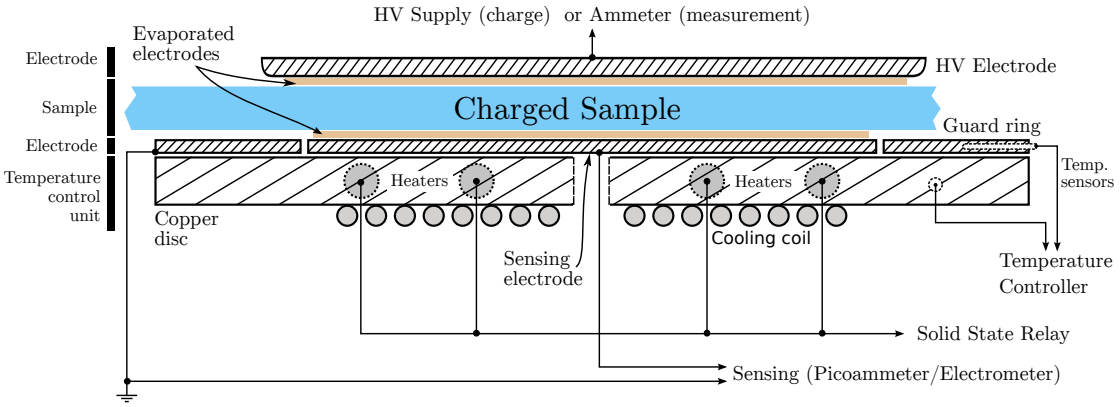

FIGURE 5.2: Diagram of the TSDC Spectrometer electrode assembly.

In summary, the TSDC spectrometer consists of the following major components:

- Cryostat
- Liquid nitrogen
- Temperature controller
- High voltage supply
- Electrometer or picoammeter
- Computer for data acquisition and control.
- Vacuum pump system and/or insulating gas for environment control

The measurement process is computer controlled using a custom LabVIEW[1] programme. The program interacts with a Eurotherm 3508 temperature controller via serial communication (RS-232) to monitor and record the temperature. The temperature profile which the controller follows, may be independently defined and written to the memory of the controller using the Eurotherm iTools software. Cooling is controlled manually using a valve on the liquid-N_2 vessel. Once the heating ramp starts, the valve is closed and the remainder of the process is fully automated. The signal current is measured using either an electrometer (Keithley 6514) or a picoammeter (Keithley 486). Either instrument is controlled from LabVIEW via GPIB[2]. The HV-supply can also be computer controlled in either a current limiting or voltage limiting mode. A USB–powered data acquisition device (DAQ) from National Instruments forms the interface between the digital and analogue domain. The 8 analogue inputs have a resolution of 14 bits and a maximum sampling rate of 48 kS/s, whereas the 2 analogue outputs have a resolution of 12 bits and an output rate of 150 Hz. Signal data are thus captured in near

[1]Laboratory Virtual Instrumentation Engineering Workbench (LabVIEW), a proprietary platform and development environment for a visual programming language from National Instruments.
[2]General Purpose Interface Bus, also often referred as IEEE-488.

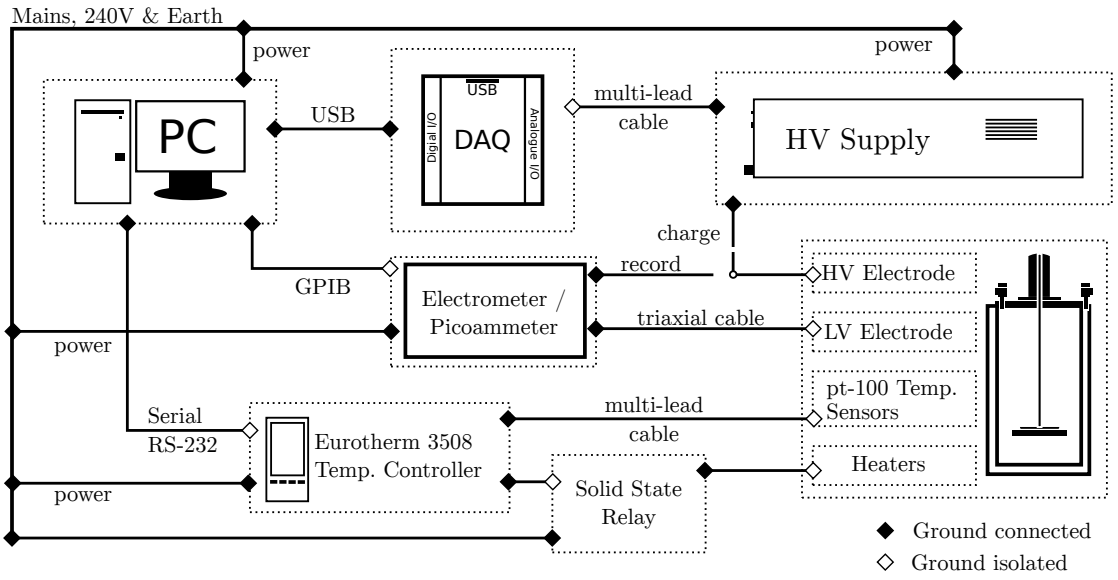

FIGURE 5.3: The TSDC Spectrometer setup.

real–time, displayed for the operator and saved to disc for subsequent processing. Figure 5.3 illustrates the interconnections between the individual components and Table 5.1 summarises the hardware.

TABLE 5.1: Hardware of the TSDC Spectrometer.

Item	Model / Description	Manufacturer
HV Supply	PS/ML60P05.0F22	Glassman High Voltage Inc.
Temperature Controller	3508	Eurotherm
Temperature Sensor	pt100 (platinum)	TC Direct (UK)
Computer Input (14 bit)	6009 (USB)	National Instruments
Computer Output (12 bit)	6009 (USB)	National Instruments
GPIB Communication	PCI–GPIB	National Instruments
Control Software	LabVIEW	National Instruments
Electrometer/Picoammeter	6514/486	Keithley

Figure 5.4 shows the open rack-enclosure that houses the measurement system as well as an upside down view of the electrode assembly. The tubular cryostat (blue) is mounted inside a steel frame and guided by two precision linear rails. The cryostat vessel is actuated from below and moves downwards when opened. The lid of the cryostat is attached to a horizontal steel plate at eye-level. The frame itself is attached to the rack-enclosure by screws and may be removed if necessary. The guide rails guarantee that the vessel and the lid meet correctly upon closure. Nevertheless, in order to reduce stress and wear on the screws that seal the cryostat, the lid was suspended on nylon bolts which allow it to rest supported on top of the vessel when it is closed. This way, the lid is screwed onto the vessel, instead of the heavy vessel being attached to the lid. All connections to the cryostat are made via the lid of the vessel. By moving the vessel bottom instead of the lid, the signal and coolant connections are not disturbed and could be shortened in length. Furthermore, the cryostat may be opened immediately after a

measurement run without having to wait for the coolant connections to warm up to prevent brittle-fractures in the leads. Removing this delay can reduce the time it takes to run a consecutive measurement on a different sample by several hours. In addition– and for the same reasons–measurement noise may be reduced since triboelectric currents which are caused by moving the triaxial measurement lead, are minimised in this design. Figure 5.5 provides a closer look at the electrode assembly and the internal cable routing through the lid of the cryostat.

A risk assessment was performed and precautionary safety measures undertaken to prevent forseeable mishaps. As a consequence, the enclosure is interlocked to safeguard the operator from high-voltage shock or injury from the moving actuator while the cryostat is opened or closed. The rack-enclosure has three removable side panels and a door, all of which have to be closed for the the high-voltage supply and the actuator to be operable. Two buttons on the outside of the enclosure control the opening and closing of the cryostat vessel. The bottom end of the stroke i.e. cryostat fully open, is set by the internal limit switch of the actuator. The closed position of the cryostat is set by an external limit switch which replaces the internal limit switch in the fully extended position. Figure C.1 in the appendix shows the internal wiring of the actuator used in the opening mechanism of the Southampton TSDC Spectrometer. The transformer in the power supply had to be replaced and re-wired according to the diagram provided. On that occasion the external limit switch was included at the upper end of the stroke path.

The current signals created in a TSDC measurement are very small and in order to increase the resolution of the TSDC measurement, it is desirable to record the smallest signal response possible. To achieve this, external influences on the measurement and the resultant current signal have to be reduced as much as possible. Electromagnetic shielding, correct ground connections for all the components, clean electrodes and a noiseless and central earthing point are important. Influences on the response signal are curtailed by shielding the signal carrying conductor and by capturing leakage currents at the point of measurement so that they may be taken into account by the measurement instrument. The Keithley picoammeter and electrometer devices are equipped with a three-slot[3] bayonet mounting connector at the input, intended for the termination of triaxial (TRX) cables. For generic current observations, the ammeter is connected to the sample or device-under-test (DUT) with the central lead (HI) carrying the measurement signal, and the inner shield conductor (LO) either floating or connected to ground (GND). Figure 5.6 shows the signal allocation on the triaxial cable. The sensitive measurement signal is carried on the centre conductor (HI) and is surrounded by two shields. The inner shield carries the leakage signal (LO) from the point of measurement and the outer shield is grounded in order to provide electromagnetic shielding. The measurement circuit of the TSDC Spectrometer is shown in Figure 5.7.

[3]The three slots on the TRX plugs are a more recent development and are intended to prevent the

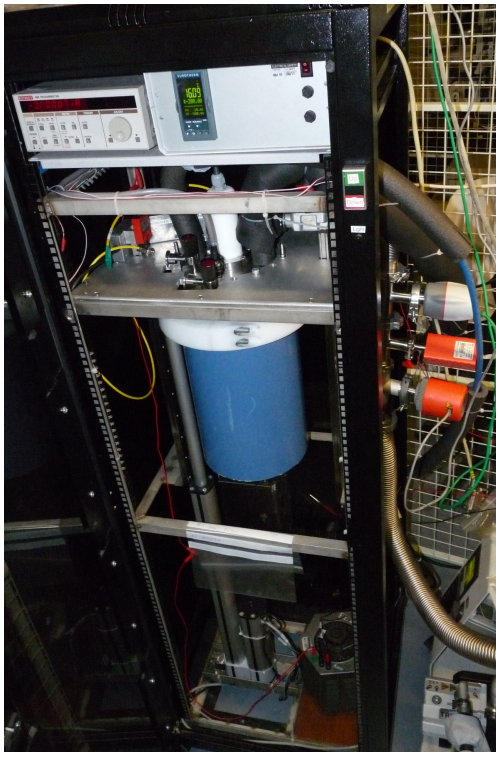

(a) The complete TSDC system.

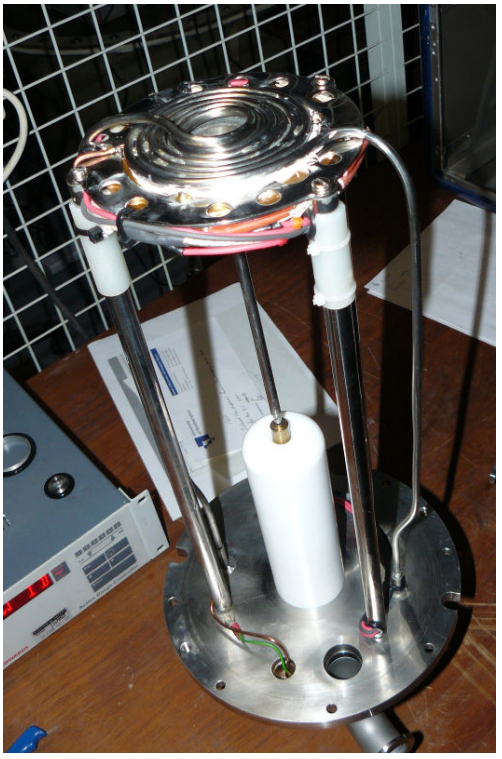

(b) The electrode assembly upside down.

FIGURE 5.4: The complete TSDC Spectrometer and electrode assembly. (a) Shows the instruments in the enclosure. (b) A closer look at the cooling spiral on the underside of the electrode assembly.

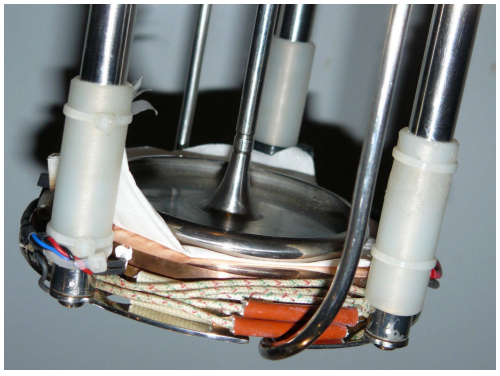

(a) The TSDC electrode.

(b) Internal connections.

FIGURE 5.5: The TSCS electrode assembly after refurbishment. (a) The white wires power the heater cartridges. Plastic insulation around the support rods improves the insulation of the top (HV) electrode. The thin stainless tube feeds the cooling spiral at the back of the bottom electrode. A white tissue is seen clamped between the top and bottom electrodes. (b) The signal wire is routed through a different support rod from the heater power. The high voltage is connected through the white central pillar.

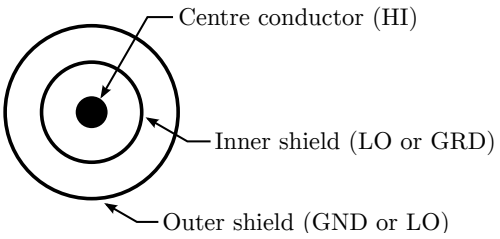

FIGURE 5.6: Triaxial plugs and cables. An outer shield surrounds and protects an inner shield and the signal carrying core conductor (HI). The inner shield may be used to carry leakage currents (LO), or for guarded measurements (GRD). If the later case, LO is carried on the outer shield instead of ground (GND).

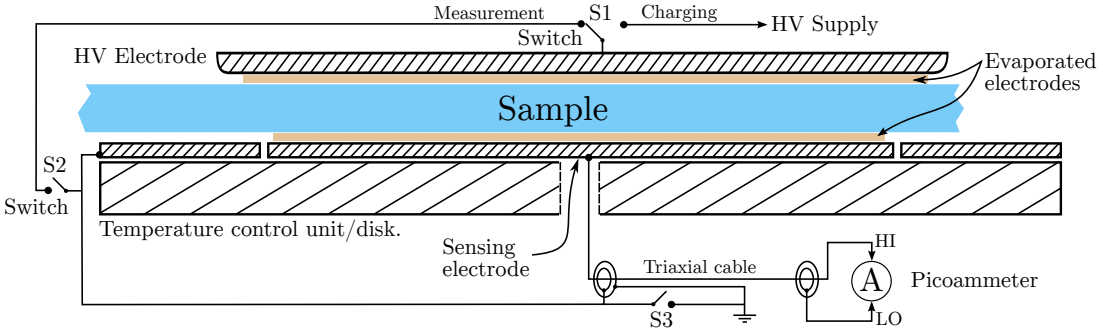

FIGURE 5.7: The equivalent measurement circuit of the TSDC Spectrometer. The switches illustrate the different possible circuit configurations.

With a LV-electrode diameter of 700mm and a total electrode diameter (incl. guard ring) of 1100mm, the design of the TSDC Spectrometer is able to observe a sample area many times larger than any other TSDC instrument detailed in the literature [91, 94, 95]. The bigger test area is expected to yield better signal strengths for low charging voltages, and results that are more representative of the average material characteristics. The latter is especially useful for materials that have larger morphological features such as for example oil impregnated paper. There are also disadvantages to the large electrode area. The sourcing and handling of samples in the appropriate size may be a problem, especially if samples are produced in the laboratory and not manufactured industrially. The assumption of homogeneity of the samples in the plane i.e. perpendicular to the measurement direction, tends to be stronger for smaller sample areas. During the charging stage, the chance of electrical breakdown through defects or impurities in the sample increases with the size of the electrode area. Furthermore, the temperature distribution of smaller electrodes and sample areas is more easily controlled. However, the behaviour of charge in dielectrics often exhibits a dependency on the strength of the applied electric field. For instance the distribution of space charge in XLPE has been reported to show differences for different field strength. Fields of about $0.23 MV/cm$ showed hetero-charges which stabilise through saturation, whereas measurements with field strengths $> 1 MV/cm$ displayed dynamic behaviour including charge injection and charge drift [109]. The TSDC Spectrometer aims to accommodate high electric field

damage that may be caused when accidentally mating triaxial and biaxial (BNC) connectors.

magnitudes and measurements over a wide range of electric field strengths and sample thicknesses, with the intention to observe results that are comparable to real-world HV applications and apparatus.

5.2 Samples

Each sample that was tested, has been assigned a unique sample identification (SID) number to track it through its lifetime. In this way, every sample is connected to logbook entries and measurement data sets, effectively carrying a history of relevant notes and details.

Synthetic polymer samples had electrodes applied to them in order to improve the electrical contact between the sample surface and the electrodes. This was achieved using an Emitech K 550X cold sputter coater, set to 25 mA for 210 s to 240 s. Most samples were furnished with electrodes on either side. The different electrode patterns are illustrated in Figure 5.8. Pattern A has been used for both the HV and the LV face. Pattern B was used on some samples for the LV face. The motivation for pattern B is to improve the contact between the guard ring and the sample so as to better safeguard against surface leakage currents.

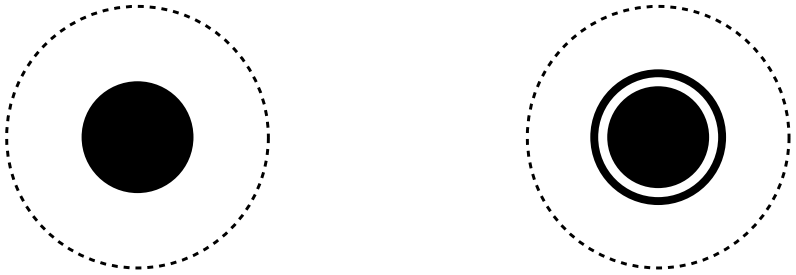

(a) Pattern A (b) Pattern B

FIGURE 5.8: Evaporated electrode patterns. Pattern A is a single disc electrode ($\phi = 68mm$). Pattern B is a disc electrode ($\phi = 64mm$) with a concentric ring electrode ($width = 5mm$). The dashed line denotes the sample border.

5.3 Temperature Control

For improved thermal control, temperature measurements are taken at two places, at the point of interest and at the point where the control action is taking place i.e. the copper disc that houses the heaters. The desired measurement point for the temperature-of-interest would be the low voltage centre electrode, however, since that is the point of measurement, the temperature sensor is placed in the guard ring. This is a good approximation because the guard ring is made from the same material and the gap

between the guard ring and the heated copper disk is equal to that between the LV centre electrode and the copper disk.

An initial implementation of the temperature control with two single-loop Eurotherm controllers (Eurotherm 2408 and Eurotherm 808) was replaced with a modern dual-loop Eurotherm 3508 controller. With this upgrade, the lower range measurement limit on both control loops now extends to -200°C. Furthermore, the new 3500 series offers more advanced computer control features and also allows for the implementation of cascade control within a single device. Cascade control is a technique that compensates for the time lag that is introduced into the control loop by the physical distance between the point of interest (guard ring) and the point of control (heated copper disk). For a cascade control scheme, a master control loop monitors the temperature at the point of interest and feeds a set point to the slave loop that monitors and controls the temperature at the point of control. The performance of the Eurotherm 3508 dual–loop heating system was tested to find the maximum temperature ramp rate that still results in a linear temperature ramp–response. Figure 5.9 shows an arbitrary linear heating ramp demand signal of $10.10\,^{\circ}\,\mathrm{min}^{-1}$ which lies above the capability of the heating system. As the demand temperature rises beyond room temperature, more heating is required and the ramp response falls further below the temperature demand. The test thus revealed a ceiling to the system performance of $\approx 7.22\,^{\circ}\,\mathrm{min}^{-1}$, which was subsequently avoided by assuming a maximum linear temperature ramp rate of $7.14\,^{\circ}\,\mathrm{min}^{-1}$. At that setting the system provides a linear temperature response of $7.07\,^{\circ}\,\mathrm{min}^{-1} \pm 1.03 \times 10^{-3}\,^{\circ}\,\mathrm{min}^{-1}$ with a straight-line fit of $R^2 = 0.999$[4]. The limiting factor in the heating system is the current rating of the connector in the lid of the cryostat (max. 2 A), which may be replaced if deemed necessary. Figure 5.10 shows the result of a common linear ramp temperature demand of $3.10\,\mathrm{K\,min}^{-1}$ as measured in the guard ring of the TSDC electrode assembly. The straight-line fit is excellent ($R^2 = 0.999$) and shows a response ramp-rate of $3.10\,\mathrm{K\,min}^{-1} \pm 3.875 \times 10^{-5}\,\mathrm{K\,min}^{-1}$. The fit was performed with QtiPlot (Version: 0.9.8.8 svn 2255).

This smoothness of the linear ramp can mainly be attributed to the dual–loop 'proportional control' scheme to which the Eurotherm 3508 was set during the measurement run. Under proportional control, the solid–state relay (SSR) is driven by a pulse-width modulated (PWM) square wave that allows for more fine-grained control of the power dissipated in the heaters than is otherwise possible under an On-Off control setting. All TSDC experiments in this thesis were performed under direct–current heating, i.e. the cartridge heaters in the copper disk were DC powered from a pair of TENMA Switching Mode Power Supplies[5] (Output: 1–36V_{DC}, 0–3A) in series. This configuration allows the operator to set and limit the maximum current that is flowing through the heater circuit and thus operating it safely at the rated limit of the components.

[4]The coefficient of determination (R^2) provides a measure of the goodness of fit e.g. how well the linear regression line fits the real data points.

[5]Distributor: Premier Farnell UK Limited, Model: 72–8345.

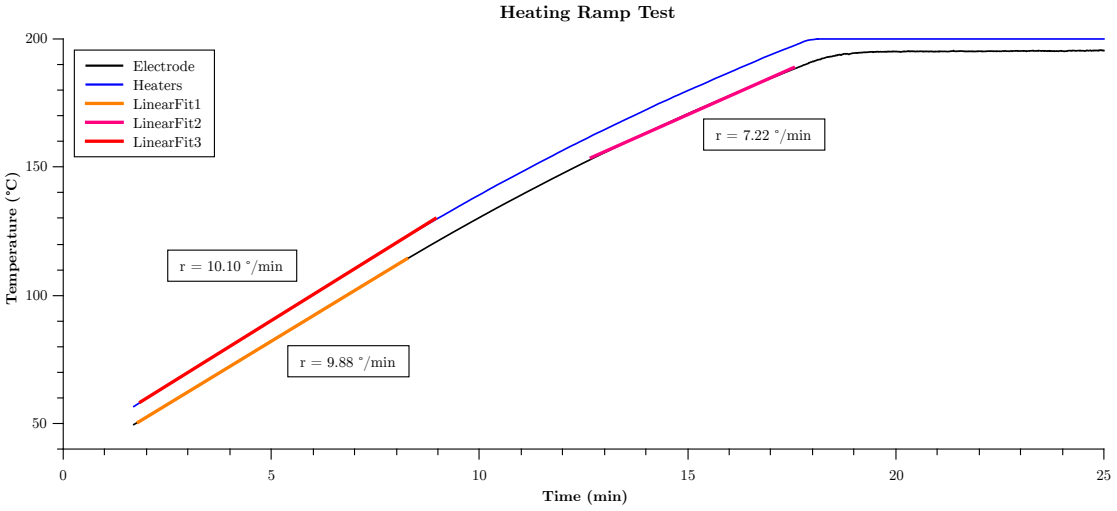

FIGURE 5.9: Test of the maximum heating ramp. A linear temperature ramp rate demand–signal of 10.10 °/min was set. The highest possible linear temperature ramp response was found to be 7.22°/min.

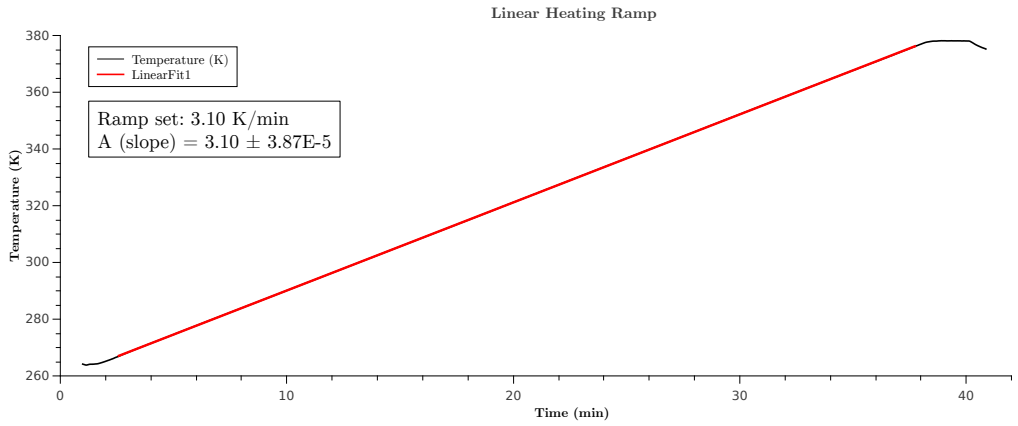

FIGURE 5.10: A commond heating ramp of the TSDC experiment. Red part denotes region of linear fit.

5.4 Control Software

The control software is written in LabVIEW and provides a single graphical user interface (GUI) for the control of all the automated components. The main purpose is to capture process data from the temperature controller and the ammeter and to display them to the operator before saving them to disc. The decision was made not to include any data analysis in the operating software of the TSDC spectrometer. Not only would this consume unnecessary time, but it would make it more difficult for future operators to understand and modify the control software. Figure 5.11 depicts the graphical user interface and controls of the programme. The underlying graphical programme code is provided in Appendix C.2.

The LabVIEW control programme essentially consists of two independent processes. When the programme starts, various parameters that may be controlled by the operator are set to their default values and the presence of the devices that are to be controlled, is checked for. Should some of the devices not respond, their (error) status is pointed out to the operator in a set of red indicators. Inside this loop are two separate elements, each of which control, poll and record one of the main instruments that make up the TSDC experiment. One serves the temperature controller and one handles the ammeter. The two loops start simultaneously and each observe the number of seconds (or fractions thereof) that passed since the start of the experiment. Whenever one of the loops records a datum, it also records the elapsed time. Keeping the two loops independently has the advantage that it makes it possible to record temperature and current with separate measurement intervals. The speed of the temperature readings is fixed, but that of the ammeter changes with the chosen operator settings, such as power line integration cycles, internal averaging filters and others. The elapsed time in the two data sets is then used later in the data processing to match current and time values together.

The following options have been implemented and are set in the software at the beginning of each recording. Apart from the file output path, which the software prompts for at the start, all other parameters may be set, changed or unset at any time during the experiment.

- The path of the folder into which the results of the measurement are to be written in a tab-separated text file format.
- The range on the ammeter (as set by the control software). The auto-range feature of the ammeter may be selected instead.
- The number of power-line cycles (NPLC) over which the ammeter should integrate the readings before recording a datum. This settings determines the reading rate as well as the amount of reading noise. Depending on the mains power frequency, one power line cycle equates to 16.67 ms for 60 Hz and 20 ms for 50 Hz [110].

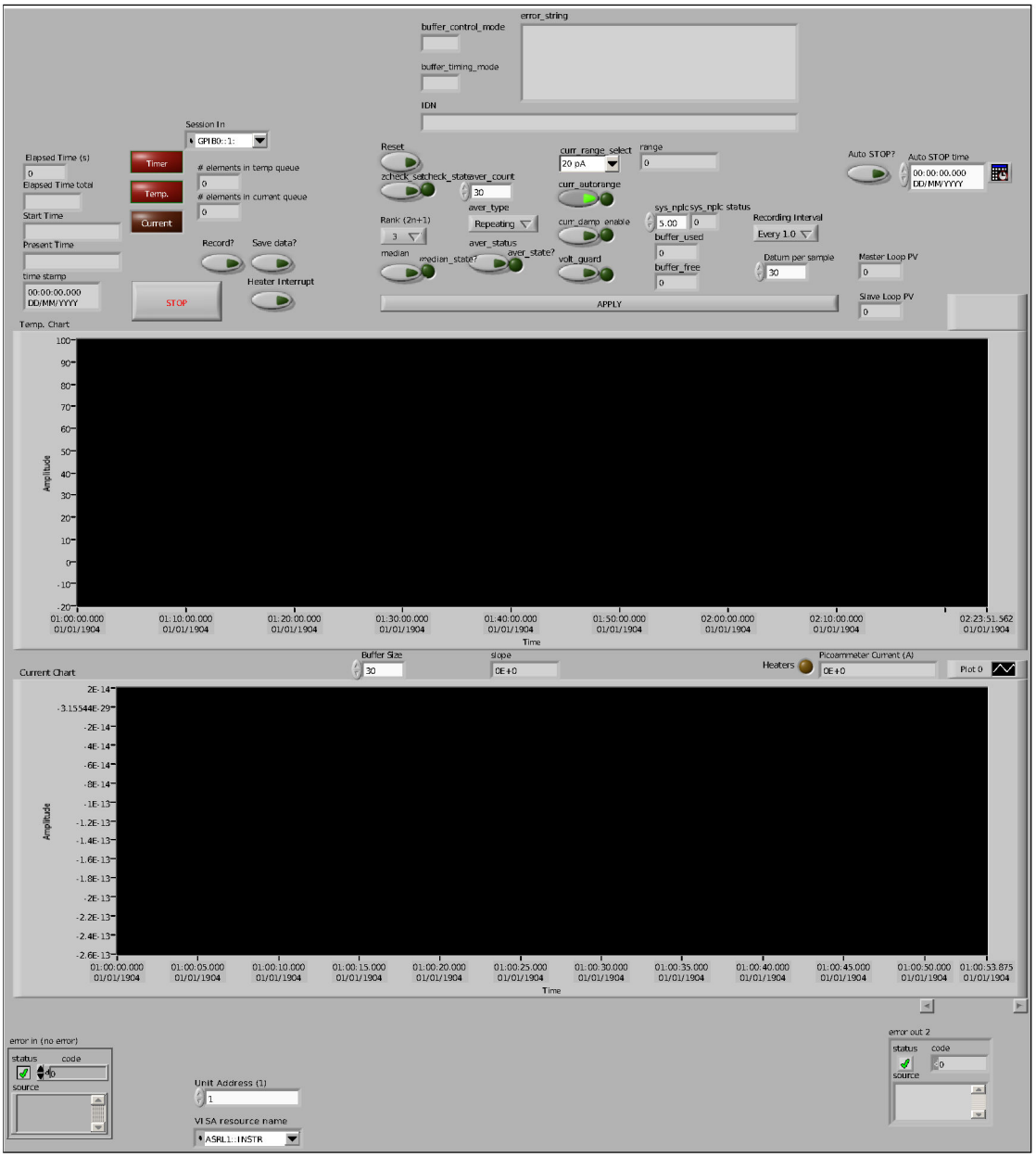

FIGURE 5.11: The graphical user interface of the LabVIEW control programme for the TSDC Spectrometer

- Control for average or median filters available on the ammeter itself have been implemented in the software and may be set or unset at any time.

- The ammeter offers a damping feature that reduces the capacitance in the measurement circuit. This may be set/unset from the control software.

- An interrupt feature was implemented that, if selected, turns off the heaters in regular user-defined intervals and also records the current during that time in a separate column. A side effect of this setting is that the temperature ramp becomes less linear and the current is only recorded every full degree (or different user defined increment) of temperature.

- A timer allows the software to stop all recordings and terminate itself at an operator set time (and date).

The timer feature allows for a recording to finish in the absence of an operator. Since the liquid-N_2 cooling and the HV supply are turned off at the beginning of the TSDC recording, only the heating and the PC remain to be controlled for a safe shutdown. The heating elements are contained in a stainless steel pressure vessel and controlled by an independent programme on the temperature controller that is set to cut power to the heaters at the end of the linear heating ramp. This way, the heating is disabled even in the case of a LabVIEW software glitch or other computer malfunction.

The following values are being displayed online in the control software in either a numerical and/or graphical fashion:

- Temperature: The current temperature is displayed numerically, and a graph shows the trend over time.
- Current is displayed in real time, numerically and graphically.
- The current time, as well as the start time of the current recording. This is of interest, as the start time of the recording forms part of the automatically generated output file name. By generating the file name automatically from the current date, day and recording start time, a sensible and continued naming convention is guaranteed.
- All of the ammeter controls are implemented with visual feedback that allows the operator to read their status.

Several of the parameters that are set in the software are also written to the output file. Examples are the measurement range setting on the ammeter, which may be changed during the course of the experiment, or any error events that may occur during the measurement. Table 5.2 and Table 5.3 present the file format of the two text files that, for each experimental run, hold the current data and the temperature data respectively. The simple clear-text format of the files allows for direct error-checking and control by the human operator and facilitates the import of the data in other programmes. This is a consequence of the decision to perform as much of the data analysis as possible, outside of the measurement and control software. The two text files also reflect the independence of the recording loops that observe the ammeter and the temperature controller. Evidently, the two data sets have to be merged and synchronized in order to arrive at a current-temperature plot, as is customary for TSDC spectrographs. This processing step is performed by another custom Python script and detailed in Section 6.1.

TABLE 5.2: File format of the text file that records the TSDC current data.

Elapsed Time (s)	Current (A)	Measurement Range	Error Status	Interrupt Current(A)
30.812500	-6.869211E-11	2.100000E-10	0,"No error"	-
31.500000	-6.760976E-11	2.100000E-10	0,"No error"	-
32.187500	-3.763705E-11	2.100000E-10	0,"No error"	-
⋮	⋮	⋮	⋮	⋮
175.468750	-3.830089E-09	2.100000E-08	0,"No error"	-
176.140625	-4.241357E-09	2.100000E-08	0,"No error"	-
176.828125	-4.303025E-09	2.100000E-08	0,"No error"	-
⋮	⋮	⋮	⋮	⋮

TABLE 5.3: File format of the text file that records the TSDC temperature data.

	Loop 1	Loop 2	
Elapsed Time (s)	Temperature (°C)	Temperature (°C)	Date-Time Stamp
30.640625	-43.070000E+0	-40.470000E+0	07/04/2012 18:20:36
31.015625	-43.090000E+0	-40.460000E+0	07/04/2012 18:20:36
31.390625	-43.070000E+0	-40.460000E+0	07/04/2012 18:20:37
⋮	⋮	⋮	⋮
175.093750	-41.530000E+0	-38.770000E+0	07/04/2012 18:23:00
175.484375	-41.490000E+0	-38.750000E+0	07/04/2012 18:23:01
175.859375	-41.450000E+0	-38.720000E+0	07/04/2012 18:23:01
176.234375	-41.420000E+0	-38.710000E+0	07/04/2012 18:23:01
176.609375	-41.410000E+0	-38.690000E+0	07/04/2012 18:23:02
176.984375	-41.420000E+0	-38.670000E+0	07/04/2012 18:23:02
⋮	⋮	⋮	⋮

5.5 Vacuum

While it is generally possible to undertake TSDC measurements in any atmosphere, the measurements in this thesis were all performed in an insulating dry nitrogen atmosphere to suppress discharges inside the cryostat. The gas used initially was an industrial oxygen free compressed nitrogen gas[6] which was later switched for a purer grade of Nitrogen 5 0 by Linde Gas (Purity $\geq$ 99.999% incl. noble gases). After a new sample has been placed into the cryostat, vacuum is applied and then backfilled with the insulating gas until atmospheric pressure is once again reached. The cryostat is fitted with an sprung valve that prevents dangerous overpressure in the vessel. Pressures of 70 mPa were regularly set for the removal of air and moisture. The vacuum system is a combination of an Edwards RV5[7] roughing pump and a Pfeiffer Vacuum HiPace 80 turbo pump. The latter is controlled via a Pfeiffer Vacuum TC110[8] module, by a Pfeiffer Vacuum DCU 110 controller[9]. A Pfeiffer Vacuum compact full range gauge[10] is attached to the controller and enables it to display online pressure values. The nominally dry industrial gas that is employed for backfilling is further dried and filtered by four columns (diameter:20 mm; length: 200 mm) filled with oven dried molecular sieve 3 Å[11] which are placed in line with the dry gas feed.

5.6 General Experimental Protocol

The experimental protocol for a Thermally Stimulated Discharge Current measurement follows the general steps outline below and illustrated in Figure 5.12. The status of the different switches refers to Figure 5.7. The experimental parameters have the following ranges or limits: the voltage magnitudes (V_{pol}, V_{bias}), may be zero or higher and are only limited by the capabilities of the voltage source, the electrical breakdown strength of the sample under test or by the testing equipment e.g. ionisation of the insulating gas or discharge to the walls of the testing chamber; the time settings (e.g. t_{pol}) are umbound, values may be zero or any amount of time; the temperature settings (T_{pol}, T_{low}) may be any temperature below the melting point of the sample material and above the lowest temperature the equipment is capable to cool down to.

1. A sample is prepared and placed between the electrodes (sputtered metal surface contacts on the samples are preferable). For experiments in environments other than air, a vacuum is then established in the cryostat to remove air and moisture.

[6] Distributor: BOC; Compressed nitrogen gas: UN1066, EEC No. 2317839
[7] Manufacturer: Edwards; Model: RV5; Code No.: A653–01–903
[8] Manufacturer: Pfeiffer Vacuum; Model: TC110; Mod.–Nr.: PM C01 790 A
[9] Manufacturer: Pfeiffer Vacuum; Model: DCU 110; Mod.–Nr.: PM C01 820
[10] Manufacturer: Pfeiffer Vacuum; Model: PKR 251; No.: PTR26000
[11] Manufacturer: Carl Roth GmbH & Co.KG.; Product nr.: P729.2; 0.3 nm, Type 562 X, beaded

If experiments in vacuum are not desired, it may be backfilled with a different gas e.g. dry nitrogen gas.

2. The sample is polarised under a constant DC voltage, V_{pol} for a chosen time t_{pol}, at a starting temperature T_{pol}.

3. The sample is then cooled to a low temperature T_{low}, usually below T_{glass}, at constant polarising voltage V_{pol}.

4. The temperature is held at T_{low} and with constant voltage V_{pol} in order to remove any transient effects.

5. The polarising voltage is then changed to V_{bias}, at constant temperature T_{low} (Switch S1 in measurement mode, S2 & S3 closed).

6. A measurement device for small signals (voltage or current) is set to record the data. The TSDC Spectrometer employs either a Keithley 6514 Electrometer or a Keithley 486 Picoammeter to observe the signal current.

7. The temperature is raised linearly, while measurements are recorded.

8. When the intended temperature range has been covered, the measurement can either be terminated or, optionally, the temperature may be changed back to T_{pol} in order to run another measurement.

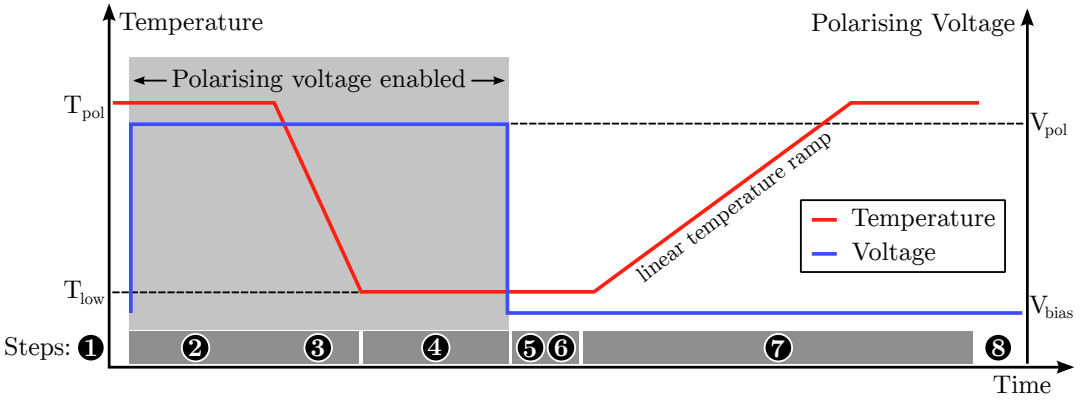

FIGURE 5.12: Illustration of the TSDC experimental procedure.

5.7 Performance Check and Validation

In order to test the correct operation and accuracy of the ammeter, a test was conducted in which a known current was observed in the system. To this end, a $800 M\Omega$ resistance was placed in line with the high voltage input to generate an ohmic current. The resistor chain was situated outside of the cryostat, and the electrodes were short-circuited using aluminium foil. This was necessary, because the HV-electrode is larger than the opposing

measurement electrode (LV-electrode), which is surrounded by a guard ring (refer to Figure 5.2 for an illustration of the electrode setup). A connection between the poling electrode and the guard ring would divert the current to ground and lead to inaccurate results. The measurement was conducted at room temperature and atmosphere, with the cryostat closed. The ohmic current was observed and recorded using the same equipment and configuration that would record thermally stimulated discharge currents. The results of the ohmic test were exported to an external software package for analysis and graphing. Figure 5.13a shows a plot of both the actual current readings as well as the expected ohmic current. It shows that the two agree very well. Figure 5.14 presents the average currents shown in Figure 5.13a with their predicted average ohmic currents. For a better resolution, Figure 5.14b shows an enlarged section of Figure 5.14a. It illustrates the accurate operation of the measurement circuit and of the ammeter in observing small Ohmic currents.

Figure 5.13b illustrates the voltage demand signal that was driving the HV supply and the monitor signal returned from it. It can be seen clearly that the voltage supply is more accurate in tracking the demand as the voltage increases. This is most likely due to the supply having a maximum voltage rating of 60kV, and being less precise in the lower

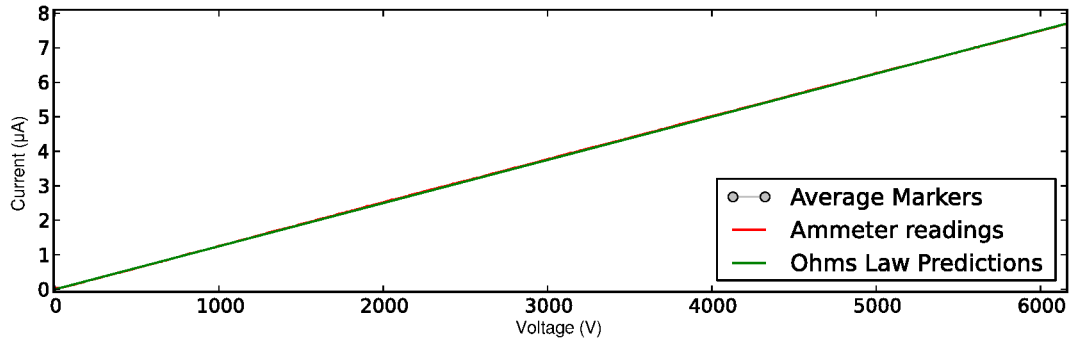

(a) Currents measured by the ammeter and current values predicted by Ohm's law. The grey border denotes the average currents markers, which at this resolution are too numerous to be distinguished.

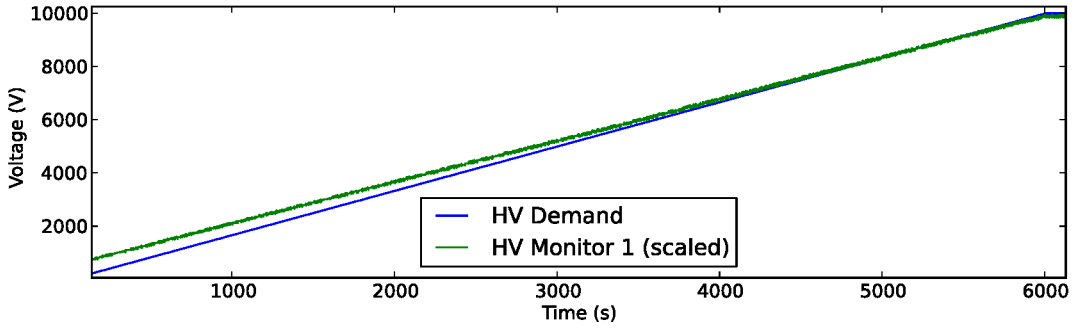

(b) Voltage demand signal to the HV supply and HV supply monitor signal (1-10V signal, 10V ≡ 60kV

FIGURE 5.13: Test of the measurement circuit. An aluminium foil sample connects the HV electrode and the measurement electrode, and a 800MOhm test-resistance was placed in line with the HV input path. Ammeter set to the 2mA scale.

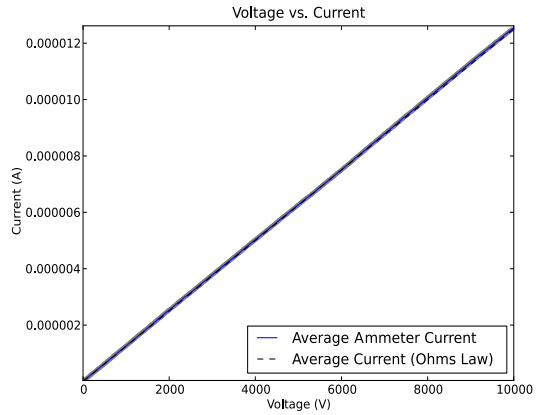

(a) Average of ammeter current measured, and currents predicted by Ohm's law.

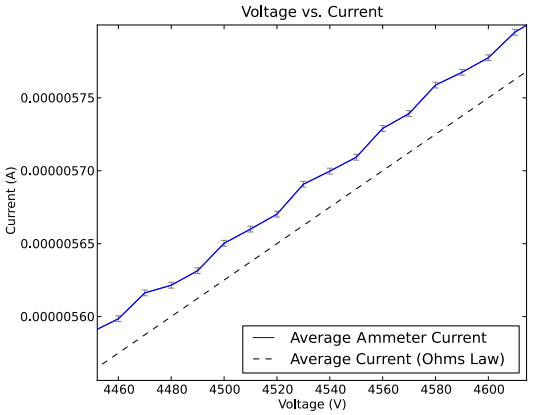

(b) Enlarged section of Figure 5.14a

FIGURE 5.14: Test of the measurement circuit. An aluminium foil sample connects the HV electrode and the measurement electrode, and a 800MOhm test-resistance was placed in line with the HV input path. Ammeter set to the 2mA scale. Error bars on Figure 5.14b denote the ammeter measurement error on that range, according to the manufacturer's data sheet.

part of its operating window. The HV monitor signal is denoted as a scaled signal since it is measured using a voltage divider circuit. The demand signal appears perfectly linear since it was recorded in numeric form before its conversion to an equivalent analogue drive signal.

The signal–to–noise ratio (SNR) of the TSDC measurement system was calculated for the interval during which the system is actively recording i.e. while the heaters are on but the cooling is off. A SNR_{dB} of 21 dB has been calculated from the current peak of the dataset shown in Figure 6.1 in Chapter 6. The noise floor of the TSDC system was recorded with the input lead disconnected and found to have a peak maximum current of 1.5×10^{-15} A. It has been noted that the noise is visibly increased when liquid nitrogen is flowing through the cooling coil prior to a TSDC recordings.

5.8 Summary

A measurement system was designed and constructed to observe thermally stimulated currents in solid dielectric film specimens. A cryostat shields an electrode assembly from external electrical and thermal noise and allows for measurements in different atmospheres. The measurement electrode has a large area and is equipped with a guard ring. The opening and closing of the heavy cryostat has been motorised and linear guide rails assure the repeatable mating of the vessel and the lid. The entire apparatus is enclosed in an interlocked rack that provides further shielding for the measurement system as well as protection for the operator. External button controls allow for the safe operation of the actuator inside. A combined cooling and heating system with

associated dual-loop temperature controller provides for precise temperature control. A custom computer control programme permits the setting of experimental parameters and the collection of results from the ammeter, the temperature controller and the high-voltage supply. The operation of the measurement system was verified by observing currents through a known ohmic resistance, and the linearity of the temperature ramp was determined by fitting a linear line to the recorded data in an external analysis and graphing software.

This chapter introduced and discussed the design and construction of a custom built TSDC spectrometer for the observation of charge in solid dielectric materials. The next chapter makes use of this information and presents a number of scientific results that were gathered with this measurement system.

Chapter 6

Thermally Stimulated Discharge Measurements of Synthetic and Natural Polymers

The long and distinguished history of the TSDC measurement has already been mentioned in Section 4.4, and the particulars of the instrument implementation and operation developed as part of this research were detailed in Chapter 5. Furthermore, the synthetic polymeric materials that are being investigated in this chapter were introduced in Section 2.7. The following sections present and discuss the obtained results of measurements and resulting analyses.

6.1 Data Processing

As detailed in Section 5.4, the control software of the TSDC Spectrometer stores the relevant temperature and current data in two separate files in order to retain independence between the two main control loops. Before these results may be further processed, they need to be combined and synchronized into a single time-current-temperature table. The task is performed by a custom python script, that works as follows:

When called, the programme checks for any files with the file ending '.tab' in the local directory. It uses the fixed file naming convention that is adhered to by the LabVIEW control programme (file names always have the following format: YYYY-MM-DD_ {Mon-Sun}_hhss_ {current/temp}.tab, e.g. '2012-04-07_Sat_1542_current.tab') to pair the current and temperature files for each experiment. It then offers the user a choice of which experiment to process, and asks whether a plot of the data is desired. Error checking at various stages in the process tries to avoid obvious complications, such as for example an uneven number of eligible data files. The programme then reads the

selected current and temperature data with their associated timing data into list structures in memory. Finally, it steps through the list of current data, and for each datum does the following: It converts the textual representation of the number into a numeric format and checks whether it is smaller than $1 \times 10^{+37}$. If not, it rejects the datum as an obvious out-of-range value. If the datum is valid, the programme runs through the list of times associated with the temperature readings, until it finds the first time datum that is larger than the time associated with the present current datum. It then chooses the temperature measurement of the previous time datum, i.e. not the one that is larger, to associate with the actual current datum. It does that for every datum in the current file. Depending on the settings of the ammeter, this matches one of two-to-three temperature readings per second, to one of the current readings.

After the temperature and current data sets have been combined, further processing may be performed, such as the application of a filter. The recorded datasets contain noise that may be alleviated with an appropriate filter. The following filters were considered:

- Butterworth (6th order, low pass, zero–phase)
- Chebychev (6th order, low pass, zero–phase)
- FFT smoothing (window size: 30 pts)
- Savitzky–Golay smoothing (window size: 30 pts)
- Butterworth (3rd order, low pass, zero–phase, cut–off frequency: 0.01)

The Chebychev and Butterworth filter were at first implemented separately in the LabVIEW graphical programming environment. Using the internal filter functions of LabVIEW made it possible to quickly implement both filters for a comparison. In both the preliminary LabVIEW code as well as the final python programme, the Butterworth and Chebychev filters were always applied as zero-phase filters. Since the data processing was performed 'off-line', this was readily achieved by applying the linear-phase filter a second time on an inverted dataset in order to cancel out any phase shift that was introduced in the first run. Figure 6.1 illustrates the concept. The noisy raw data is plotted in blue. The dashed red line represents the first application of the linear infinite impulse response (IIR) filter (3rd order Butterworth filter, cut-off frequency: 0.01), and the solid red line represents the second. The use of the filter clearly introduces a cumulative phase shift. When the filter is applied once forward, and once backwards, the phase shift cancels out and a zero-phase filter response is obtained as shown by the solid black line.

The FFT and the Savitzky–Golay smoothing filters were standard smoothing functions available as part of Origin 8.6, a data analysis and graphing software application by OriginLab Corporation. The different filters were all tested with different filter parameters and applied to the same data for a visual comparison. Figure 6.2 shows an enlarged

section around the peak of a TSDC dataset that was processed with these filters. Both, the FFT and the Savitzky–Golay smoothing filter were set to a window size of 30 points. As illustrated, the Butterworth filter appears to track the data best.

Filtering of the measurement data should be avoided if possible, since it may cause information loss. However, since the activation energy calculations rely on a well defined peak current value, the post–processing of the datasets was found to be necessary. Smoothing filters work on all the data within their processing window. Outliers may thus significantly effect their result. Low–pass filters may be used for smoothing if the high frequency components of the signal do not carry relevant information. Due to the nature of the thermally stimulated current response, all high frequency components may be suppressed by a low–pass filter without causing a loss of relevant TSDC information. The decision to employ a Butterworth filter was based on an empirical judgement of the different filter performances (see Figure 6.2), as well as on the fact that the frequency response of the Butterworth filter is maximally flat in the pass band. The good empirical performance of the filter in its phase–shift compensated (zero–phase) application supports the assumption that no information that is relevant to the TSDC analysis, is lost or distorted in the filtering process. After the decision was made to employ a Butterworth filter for the cleaning of all TSDC datasets prior to further analysis, an implementation of a Butterworth filter in the Python programming language was adapted for this purpose (cf. SciPy.org:Cookbook/FiltFilt [111]).

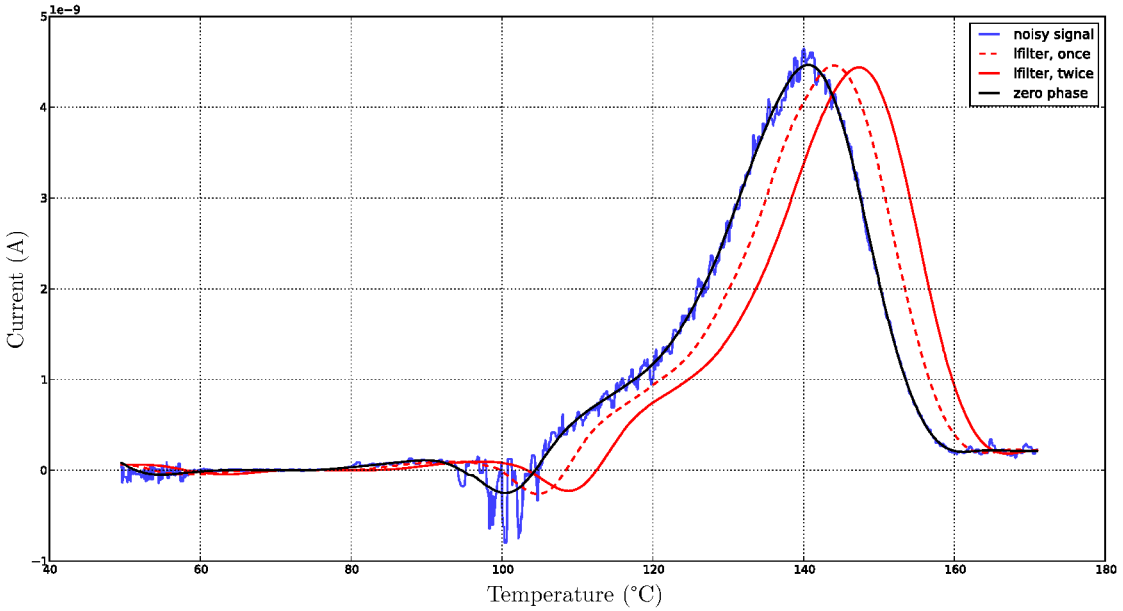

FIGURE 6.1: A TSDC measurement of PET processed with the python Butterworth filter programme. Third-order Butterworth filter with a cut-off at 0.01. The dashed line represents the first application of the IIR filter and illustrates the concomitant phase shift. The solid line shifted further to the right, denotes the second application of the same filter. The solid line tracking the raw data, represents the filter applied in a zero-phase fashion.

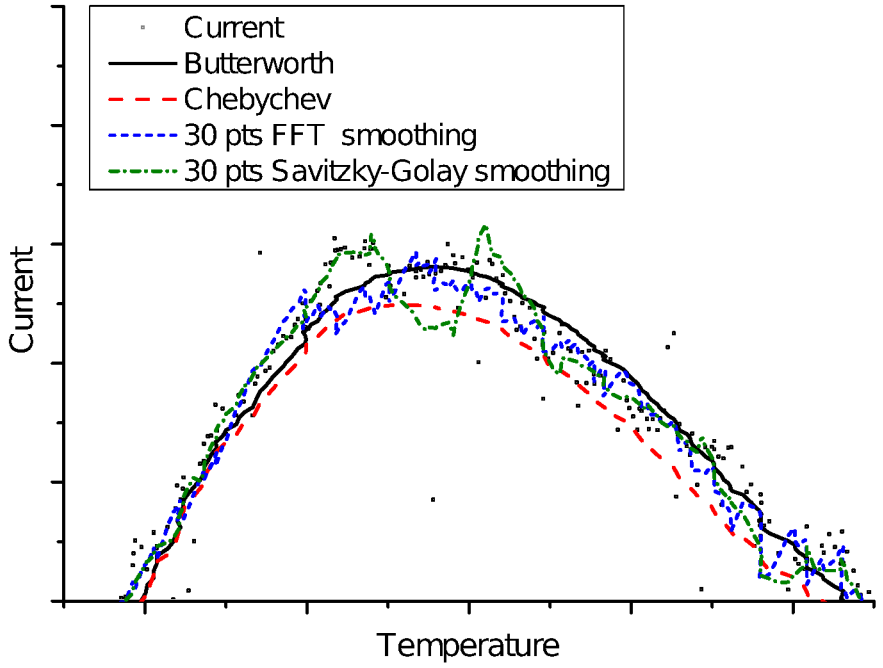

FIGURE 6.2: An exemplary TSDC dataset processed with different filters for comparison. Only the top of the peak shown. Chebychev and Butterworth filters implemented as zero-phase filters.

6.2 Activation Energy Calculations

The asymptotic activation energy calculation requires knowledge of the peak data (T_{peak}, I_{peak}) and one further arbitrary datum (T_j, I_j) where T_j is less than T_{peak}. It follows, that the method may be applied multiple times to the same set of data and thus an average value may be obtained for the trap depth. The trapping level E(eV) is defined as follows [24, 112]:

$$E = A\frac{kT_{peak}T_j}{T_{peak} - T_j} \tag{6.1}$$

with A determined to satisfy the following equation:

$$A = -ln\frac{I_j}{I_{peak}} + \sum_{n=0}^{N}(-1)^n \cdot \frac{(n+1)!}{A^n} \cdot \left(\frac{T_{peak} - T_j}{T_j}\right)^n \cdot \left\{1 - \left(\frac{T_j}{T_{peak}}\right)^{n+2} \cdot e^{-A}\right\} \tag{6.2}$$

An implementation of the asymptotic method in the Python programming language was used to calculate the activation energies from the sets of data that were recorded on the TSDC Spectrometer. The iterative estimation of a value for A that satisfies Equation 6.2 is performed with precision to 10 decimal points. A detailed description of the mathematical derivation may be found in the original publication by Maeta and Sakaguchi [112]. In order to validate the correct operation of the programme, it was run against a set of published data for a simulated TSDC curve of LDPE [24], the data of which are tabulated in Table 6.1.

Table 6.1: Validation of the asymptotic method calculation.

	Data by Wang et.al. (2000) [24]			
Nr.	Temperature (K)	Current (A)	Trapping level (eV)	Trapping level (eV)
10	337	7.50×10^{-10}	peak current	peak current
9	336	7.43×10^{-10}	1.341	1.3395
8	335	7.26×10^{-10}	1.270	1.2683
7	334	7.01×10^{-10}	1.241	1.2393
6	333	6.69×10^{-10}	1.231	1.2297
5	332	6.33×10^{-10}	1.219	1.2181
4	331	5.96×10^{-10}	1.200	1.1992
3	330	5.54×10^{-10}	1.200	1.1995
2	329	5.11×10^{-10}	1.201	1.2004
1	328	4.68×10^{-10}	1.203	1.2018
0	327	4.26×10^{-10}	1.204	1.2031

If the results of the python programme are rounded to the same decimal point as the published values, then there remain small differences in the third decimal point between the published values and the values returned from the python programme. These differences are thought to be due to rounding errors in the estimation of A. As mentioned in the publication by Wang et al. [24], the activation energy values increase as the difference between the chosen datum (T_j, I_j) and the peak gets smaller. Figure 6.3 illustrates

the trend for the published values. After the fourth datum, the values visibly increase. If only the first four data points are counted towards the average activation energy, then the value of the average activation energy returns as 1.20 eV in the case of both the published data by Wang et al. and the data calculated by the present implementation of the asymptotic method. Figure 6.4 shows the equivalent representation for a PET sample measured with the TSDC Spectrometer. Similarly, only data in the horizontal region are counted towards the calculation of the average asymptotic activation energy.

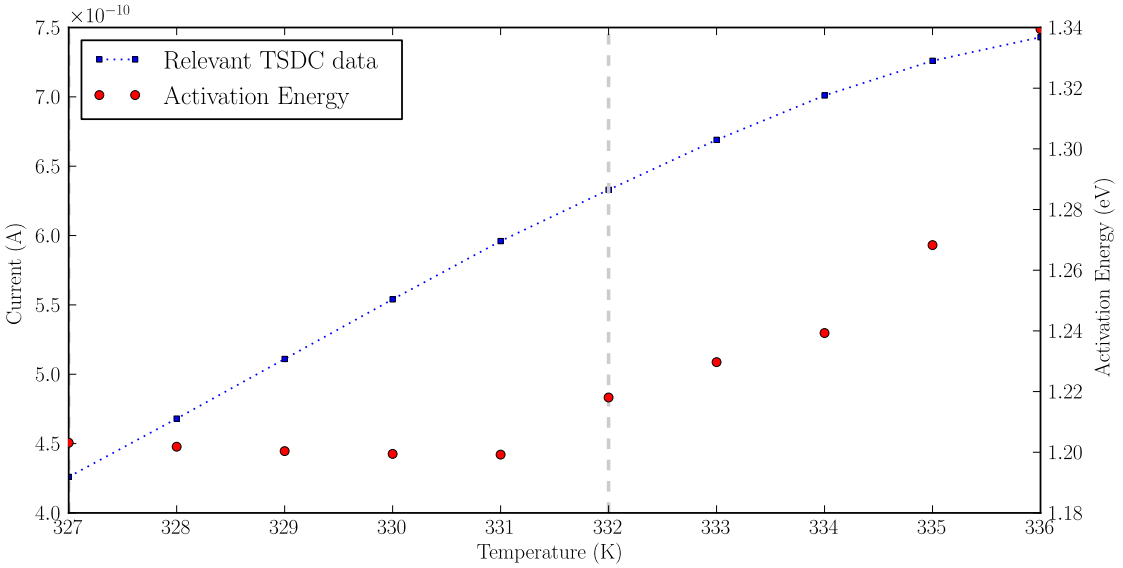

FIGURE 6.3: Plot of activation energies in Table 6.1. The dashed vertical line denotes the upper limit below which data are counted towards the computation of the average activation energy.

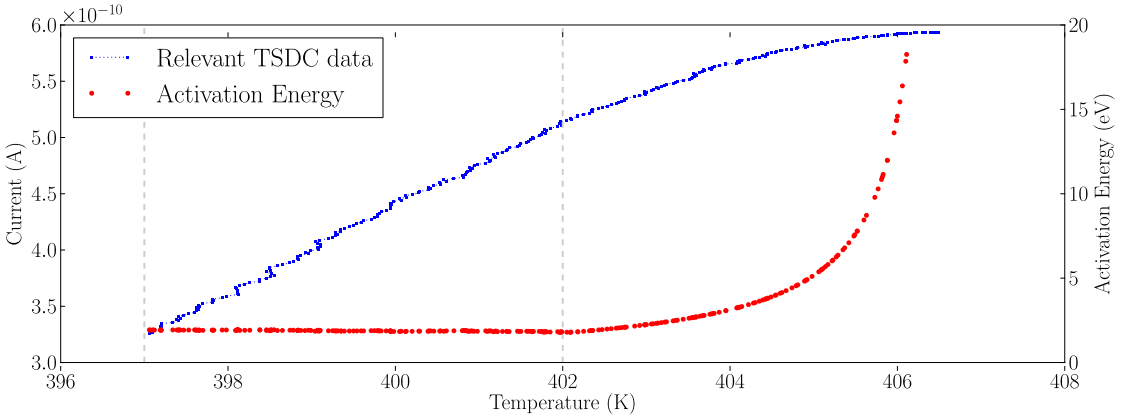

FIGURE 6.4: Plot of a TSDC peak of PET and the corresponding activation energies. The vertical lines mark the upper and lower limits between which the data are counted towards the calculation of the average activation energy.

Next, the asymptotic activation energy calculation is employed on thermally stimulated discharge current spectra observed with the TSDC Spectrometer in order to verify its correct operation.

6.3 Low–Density Polyethylene

Low–density polyethylene (LDPE) is a well characterised synthetic polymer for which there exists a good deal of previous practical experience at the Tony Davies High Voltage Laboratory. It was thus chosen as a material to verify the performance of the TSDC instrument. A reel of commercial additive free LDPE film with a nominal thickness of 0.1 mm was sourced from Goodfellow Cambridge Ltd.[1]. All LDPE samples feature sputtered gold electrodes in pattern A (see Figure 5.8) on both sides.

In order to avoid the electrical breakdown of the sample during the charging period of the TSDC measurement, preliminary direct current electrical breakdown tests were performed to gauge the approximate point of failure for the LDPE polymer film material that was to be investigated. The DC measurement setup is essentially identical to the apparatus used in the alternating current electrical breakdown strength measurements described Section 7.1.3, illustrated in Figure 7.2 and depicted in Figure 7.1. Instead of the sinusoidal signal generator, amplifier and transformer, the test made use of a direct current Spellman SL150 high–voltage power supply which had the negative module fitted and was directly connected to the electrodes. The ramp rate was set to $100\,\mathrm{V\,s^{-1}}$.

Figure 6.5 shows a Weibull analysis of the electrical breakdown strength measurements. A Weibull analysis is a statistical method that allows to predict the life-time of a population by fitting a statistical distribution to a representational data sample. In this way the mean life and failure rate of a class of materials may be estimated. The Weibull distribution is further explained in Section 7.2.1. Due to previous work by Green [113], on the suitability of different regression methods for the analysis of electrical breakdown strength measurements, the fit parameters were calculated by the least-squares X-Y approach. The correlation coefficient for the fitted line of 0.976 is sufficiently high, and all the data points are found to lie within the envelope of the two-sided 95% confidence interval. The Weibull scale parameter of $490\,\mathrm{kV\,mm^{-1}}$ was therefore accepted as an approximate upper limit on the field strength that should not be approached too closely in the charging stage of the TSDC experiment.

Figure 6.6 show the TSDC spectra observed for low–density polyethylene film samples using the TSDC Spectrometer. The measurements followed the general experimental protocol introduced in Section 5.6. The Glassman power supply and the Keithley 6514 electrometer (see Section 5.1) were used. A field stress of $100\,\mathrm{kV\,mm^{-1}}$ was applied for 30 min and a linear heating ramp of $7\,\mathrm{K\,min^{-1}}$ was set for all samples. Charging temperatures and times are tabulated individually with the peak values and activation energy calculation results in Table 6.2. LDPE 1 and LDPE 2 are typical observations for a well conditioned LDPE sample. The two curves exhibit good repeatability and similarity in the important features i.e. the peak parameters and the rise leading up to

[1] Goodfellow Cambridge Ltd.,Ermine Business Park, Huntingdon, England, PE29 6WR

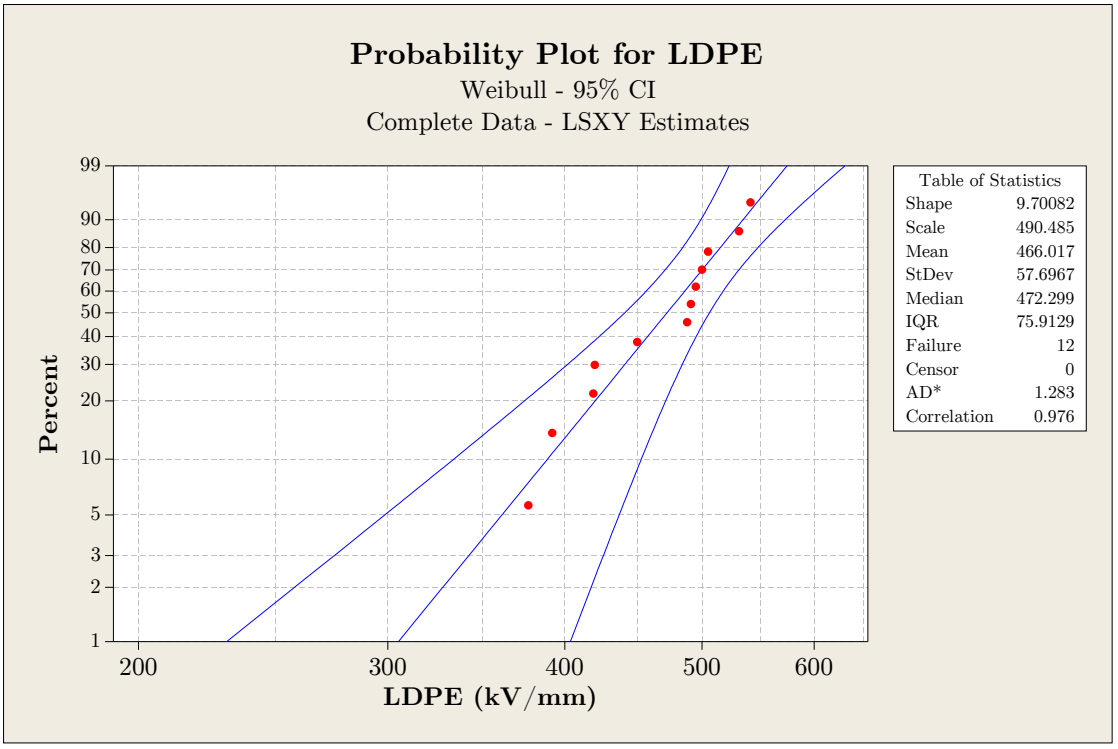

FIGURE 6.5: DC electrical breakdown strength of 0.1 mm LDPE film.

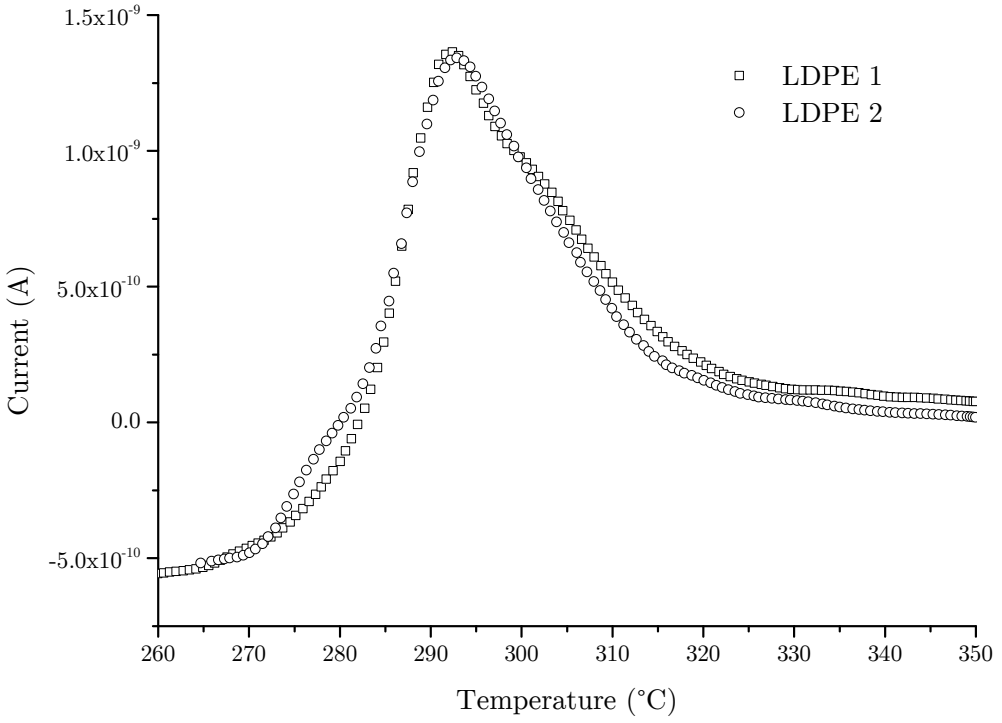

FIGURE 6.6: Experimental TSDC data for a well conditioned LDPE film of 0.1 mm thickness in the temperature range of 260 K to 350 K in a dry N_2 gas atmosphere. Polarisation field strength: 100 kV mm^{-1}; heating rate: 7 K min^{-1}; temperature of polarisation: 303 K; ammeter NPLC: 5.

it. The small differences between the two curves are believed to be due to differences in the experimental history of the samples. Published TSDC spectra for LDPE note between one and two peaks, depending on the range of temperatures. A single peak at 337 K [24] or two peaks at 323 K and 358 K [114] have been reported, and respective activation energies of approximately 1.19 eV to 1.30 eV for the first peak, and 1.5 eV to 1.7 eV for the second peak, have been calculated under the slow retrapping mechanism. This compares to an activation energy of 1.7 eV for a peak at 292 K as recorded by the TSDC spectra for LDPE. Since polymer characteristics are contingent on the synthesis of the polymer and may vary widely, a direct comparison of material parameters is only possible to a certain extent. In case of the spectra returned by the TSDC Spectrometer, the temperature region of the LDPE current peak deviates slightly from that published elsewhere, the calculated activation energy, however, agrees very well with published findings [114]. To further verify the operation of the TSDC Spectrometer, measurements with polyethylene terephthalate were also performed.

Table 6.2: Results for LDPE film

		Peak		Activation Energy (eV)	
LDPE	Charge Temp. (K	Current (A)	Temp. (K)	Mean	Stdev.
1	303	1.364×10^{-9}	292.24	1.76	0.034
2	303	1.342×10^{-9}	292.79	1.66	0.093

6.4 Polyethylene terephthalate

A commercial biaxially oriented polyethylene terephthalate (PET) film was investigated. Circular samples of 110 mm diameter or larger, were cut from a reel of 0.1 mm thick film material which was sourced from Goodfellow Cambridge Ltd.[2]. The samples were furnished with sputtered gold electrodes in pattern A on both sides (see Figure 5.8). As with the LDPE samples, the direct current electrical breakdown strength of the PET polymer film was measured in order to gauge the maximum field stress that may be employed in the charging stage of the TSDC experiment. Figure 6.7 depicts the results of the Weibull probability plot, and states the Weibull shape and scale parameters. With a correlation coefficient of 0.986, the data is judged to be fitted well. Furthermore, the Weibull shape parameter of 12.8 indicates that the spread of the breakdown values is clustered well, and better than that of the LDPE polymer samples. Similar to LDPE, the Weibull scale parameter provides an approximate upper limit for the field strength that may be employed in the charging stage of the TSDC measurement of PET, i.e. 466 kV mm^{-1}.

PET has been studied extensively in the past, also using thermally stimulated discharge current spectroscopy [24, 34, 37, 115–120]. According to the literature, a typical TSDC

[2]Goodfellow Cambridge Ltd.,Ermine Business Park, Huntingdon, England, PE29 6WR

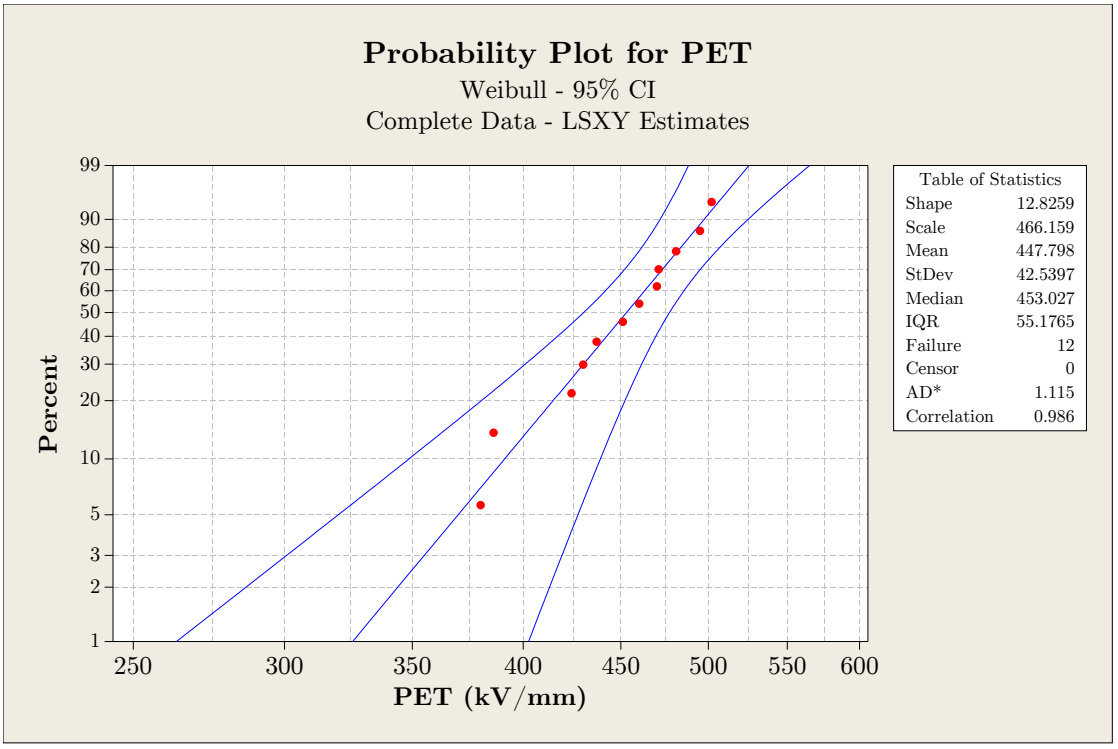

FIGURE 6.7: DC electrical breakdown strength of 0.1 mm PET film.

spectrograph of PET shows two peaks at approximately 80 °C and 125 °C or 350 K and 400 K respectively [37, 119]. Conventionally, the two peaks are labelled from high to low temperature as ρ–peak and α–peak respectively, with a third β–peak sometimes recorded at a lower temperature of around 120 K to 210 K. The effect of variation in the polarisation parameters such as time, temperature or polarisation field, show that of the three, only the charging field strength has a direct influence on the maximum current magnitude of the α–peak. This indicates, that the α–peak is caused by dipole polarisation, and may be related to the conformational changes happening in the polymer as it undergoes glass transition. The ρ–peak is situated above the glass transition temperature (T_{glass}) of PET. It is independent of charging time, but dependent on charging temperature and charging field strength. The ρ–peak is thought to be due to space charge [119].

The TSDC measurements of PET were conducted in a dry nitrogen atmosphere, and the high temperature spectra in the temperature range of 340 K to 445 K are presented in Figure 6.8. Two current peaks may be distinguished at 350 K and 405 K, which agrees well with the published information for the α–peak and ρ–peak [37, 119, 121]. The TSDC parameters of PET 1 to PET 3 are tabulated in Table 6.3.

All three experiments were set to the same polarisation field strength ($E_{pol} = 101\,\mathrm{kV\,mm^{-1}}$) and the same heating rate ($\tau_{heat} = 3\,\mathrm{K\,min^{-1}}$), however the polarisation temperature differed significantly. For PET 1, the lower temperature was set to the polarisation temperature, i.e. $T_{low} = T_{pol} = 298\,\mathrm{K}$. For PET 3, the polarisation temperature was set to

TABLE 6.3: Experimental parameters of the PET TSDC spectra.

PET	V_{pol} (kV)	t_{pol} (min)	T_{pol} (K)	T_{low} (K)
1	10.1	12	298	298
2	10.1	12	298	233
3	10.1	12	233	233

the lower temperature, i.e. $T_{pol} = T_{low} = 233\,\mathrm{K}$. PET 2 was recorded with 'traditional' TSDC settings, where $T_{pol} = 298\,\mathrm{K}$ and $T_{low} = 233\,\mathrm{K}$, i.e. $T_{low} < T_{pol}$. The difference in peak magnitude between PET 3 and PET 1 or 2, may therefore be ascribed to the difference in polarisation temperature. This provides further corroboration that the major peak is the ρ–peak and indicative of space charge. Similarly, the independence of the peak magnitude at 350 K from this same change in polarisation temperature, supports its classification as the α–peak. The results of the activation energy calculations by the asymptotic method are tabulated in Table 6.4.

The good agreement between published and recorded results of the thermally stimulated discharge current spectroscopy measurements of PET, confirms again the correct operation of the TSDC Spectrometer.

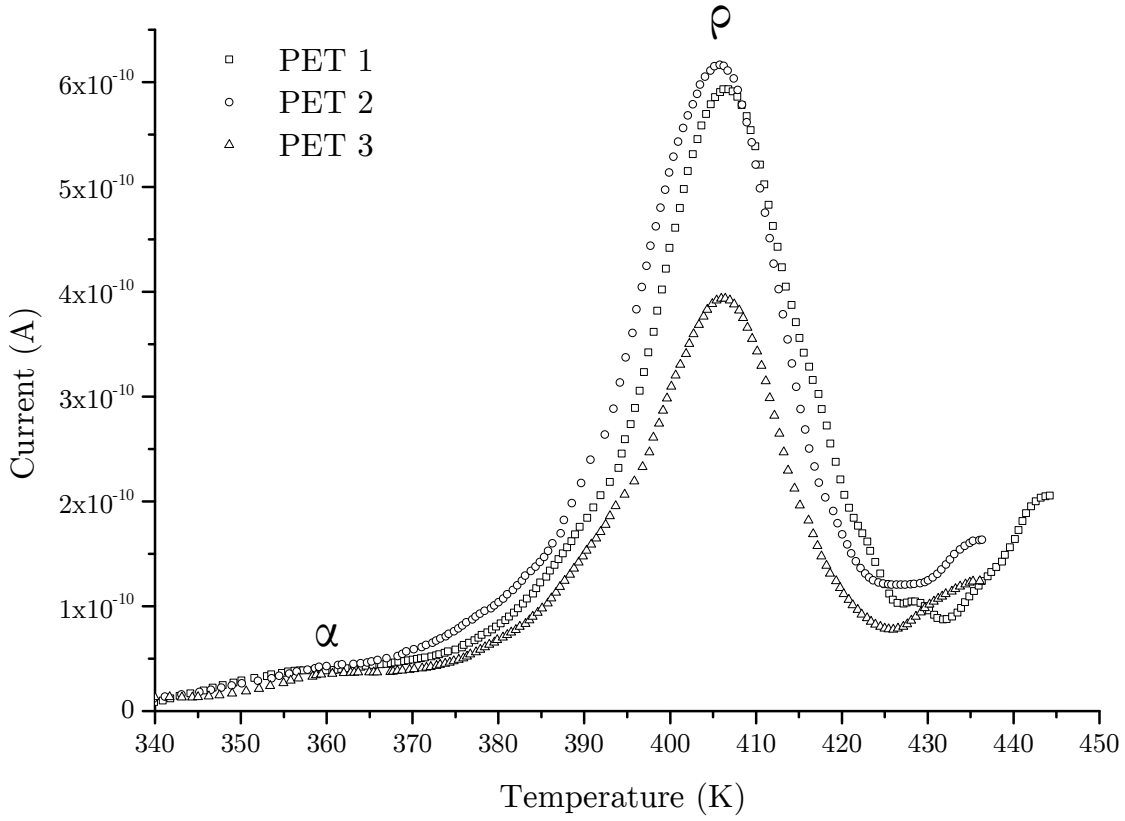

FIGURE 6.8: TSDC spectra of biaxially oriented PET film of 0.1 mm thickness in the temperature range of 340 K to 445 K in an inert and dry N_2 gas atmosphere. Polarisation field strength: $100\,\mathrm{kV\,mm^{-1}}$; heating rate: $3\,\mathrm{K\,min^{-1}}$; temperature of polarisation for PET 1 to 3: 298 K, 298 K and 233 K; ammeter NPLC: 10.

Table 6.4: Results for PET film

PET	Charge Temp. (K	Peak Current (A)	Peak Temp. (K)	Activation Energy (eV) Mean	Activation Energy (eV) Stdev.
1	298	5.94×10^{-10}	406.55	1.90	0.027
2	298	6.17×10^{-10}	405.84	1.60	0.047
3	233	3.94×10^{-10}	406.14	1.83	0.024

6.5 Electrical Insulation Paper

The major constituent of most papers is fibre pulp, which consists almost entirely of cellulose and, in the case of unbleached pulp, of hemicellulose and lignin. All three constituents are natural polymers, and thus it seems normal to apply tests and theories for synthetic polymers to such natural polymeric materials. One material parameter that is of special interest for TSDC spectroscopy, is the glass transition temperature (T_{glass}). At T_{glass}, previously trapped charge tends to be released by an increase in molecular motion. Both synthetic and natural polymers may possess crystalline and amorphous regions or states. The amorphous phase may occur in two states: rubbery, above the glass transition temperature; and exhibiting hardness, stiffness or brittle behaviour similar to an inorganic glass at temperatures below T_{glass}. The crystalline phase has an associated melting point. For cellulose, however, that temperature lies beyond the point of decomposition. The change in behaviour around the glass transition temperature may be explained in terms of free volume, i.e. the volume not occupied by polymer molecules. Free volume is near constant up to T_{glass}, and then expands. Expressed as a fraction of the total volume, the actual value of the free volume is of the order of 0.025 at the glass transition temperature, and doesn't differ greatly between polymers [122].

In order to attain relevant results that are close to the real industrial application of electrical insulation paper, the samples that were measured in the thermally stimulated discharge spectrometer were dried and immersed in transformer oil prior to testing. To date there are no published results of TSDC spectrometry for oil impregnated cellulose composite insulation systems.

Figure 6.9 shows the high–temperature TSDC spectra of a talcum filled paper made of unbleached kraft pulp in the temperature range of 260 K to 380 K. The upper temperature limit was chosen to prevent irreversible changes in the available hydrogen bonding areas of cellulose. The sample contains 17.5% talcum, 1.5% starch, 1% PVA and 1.5% wet strength agent. The dried paper samples were soaked in Nynas Libra mineral oil for 30 min, the ammeter was set to NPLC = 10 and the charging temperature was 296 K.

Two peaks are evident around 332 K with significantly different maximum discharge current maxima. The solid line shows the first measurement of this sample, and has peak values of $T_{peak} = 3.547\,74 \times 10^{-8}$ A at $I_{peak} = 331.97$ K. The dashed line denotes the

second measurement with the peak at $T_{peak} = 331.72\,\mathrm{K}$ and $I_{peak} = 8.383\,23 \times 10^{-8}\,\mathrm{A}$. The difference in peak current magnitude of $4.835\,49 \times 10^{-8}\,\mathrm{A}$ may be explained by the thermal conditioning of the sample. The activation energies for the two peaks were determined by the asymptotic method to be 0.57 eV and 0.77 eV for the first and second measurement respectively. A related investigation on semi–crystalline and amorphous cassava starch [123] found a dependence of the highest temperature peak around 300 K, on humidity. The peak which they termed β–peak, was found to shift upwards in temperature and down in magnitude, as the sample was dried. These results from starch (poly α–anhydroglucose), a very similar polysaccharide to cellulose (poly β–anhydroglucose), suggest that a re–wetting process may have occurred in the filled paper sample in which moisture in the gaseous environment or the oil impregnating agent, moved back into the bulk of the paper after the heating cycle was complete. On the other hand, an increase in peak height is commonly observed with conditioning of the sample.

In order to address this effect, and to gain better control over the moisture level in the paper sample, a system was devised that emulates the industrial manufacturing process of oil impregnated paper insulation. The laboratory setup shown in Figure 6.10 allows for the paper samples to be dried and oil impregnated under vacuum and elevated temperature. Single handsheets of dried paper were prepared according to the procedure

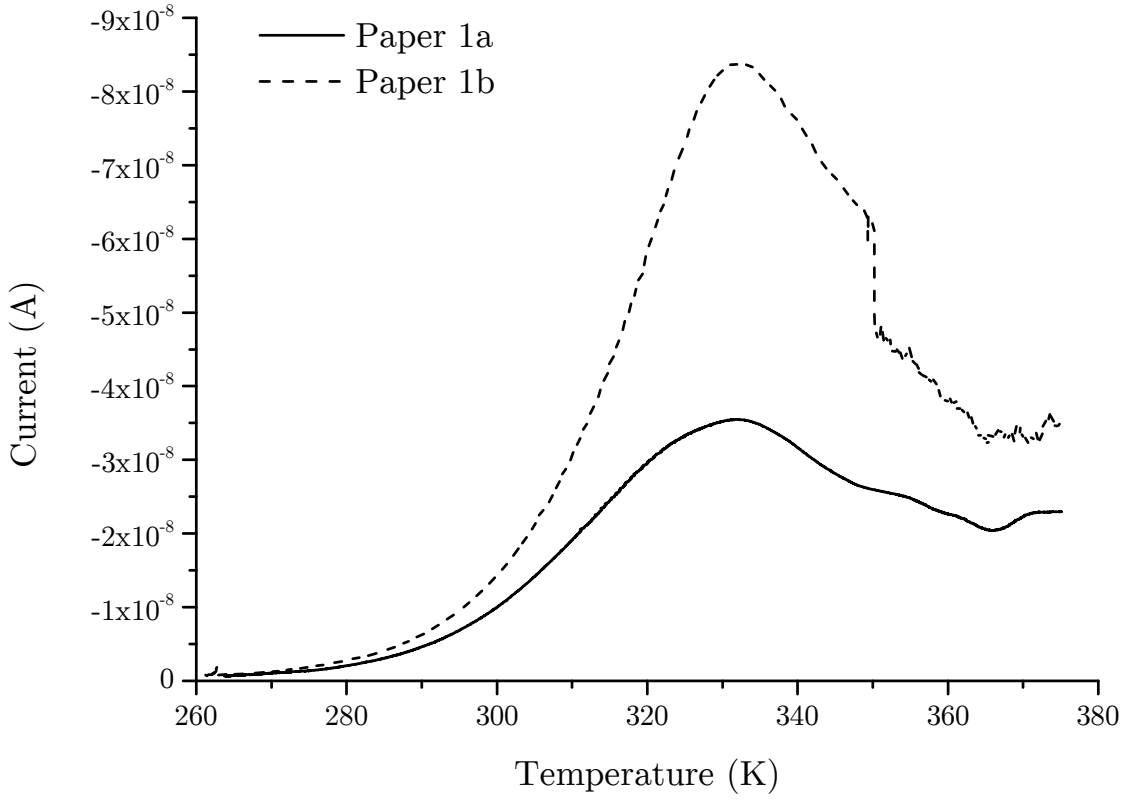

FIGURE 6.9: TSDC spectra of dried and oil soaked kraft paper (17.5 % talcum, 1.5 % starch, 1 % PVA and 1.5 % wet strength agent) in an dry N_2 gas atmosphere. Polarisation voltage: 1.1 kV; heating rate: $3\,\mathrm{K\,min^{-1}}$; temperature of polarisation: 296 K; NPLC: 10.

described in Section 7.1.10 and consequently dried further by storage in a desiccator over activated silica gel for at least 24 hours at room temperature. The samples were cut to fit the TSDC spectrometer and then transferred into an evacuated desiccator and further dried for 16 h over activated silica gel at 67 °C and a vacuum of 3×10^{-2} mbar. Nynas Libra mineral oil at room temperature was employed to impregnate the papers under vacuum. The oil itself was part of the drying process and therefore in a degassed and dry state prior to impregnation. More information on the mineral oil is provided in Section 7.1.9.

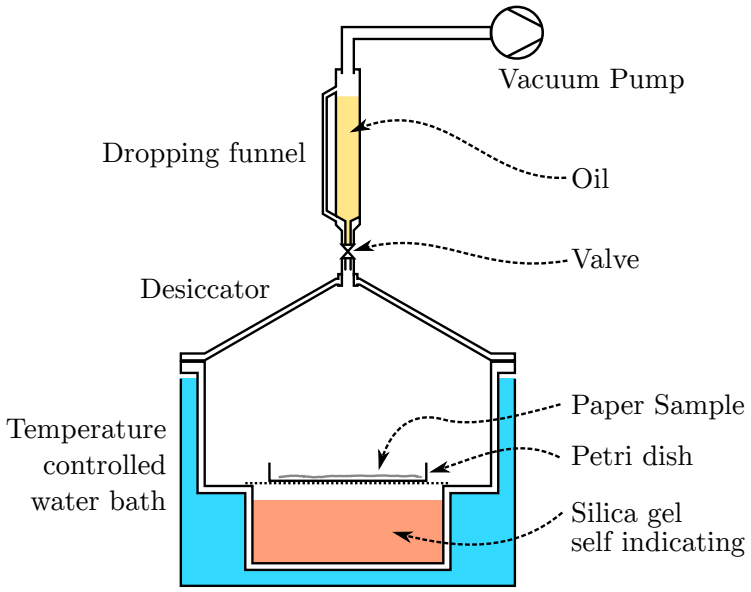

FIGURE 6.10: The laboratory setup employed to dry and oil impregnate the paper samples under vacuum.

The impregnation procedure is carried out as follows: The paper samples were placed in a petri dish inside a desiccator and directly underneath an oil filled dropping funnel. Once the whole system was evacuated and dried, the valve on the dropping funnel was opened and the oil allowed to fill the petri dish containing the paper samples. Vacuum was maintained until all bubbles were removed from the oil and samples. An oil impregnated sample was then removed from the desiccator, wiped down to remove excess oil and placed between the electrodes of the TSDC Spectrometer. Vacuum was applied to remove moisture from the measurement chamber, and the cryostat then backfilled again with dry nitrogen gas as detailed in Section 5.5.

Paper samples that were prepared according to this new vacuum oil impregnation procedure, show markedly different TSDC spectra from those simply dried and soaked in oil. Figure 6.11 exhibits the response of an unmodified paper sample made from unbleached kraft pulp i.e. containing no filler or chemical additives. The first measurement run (Paper 2a) provides a first indication of the shape of the TSDC response, but mainly conditions the sample. The second measurement (Paper 2b) shows the trend affected by

the conditioning of the sample. The third spectrum is a measurement run (Paper 2c). The TSDC spectra of the vacuum oil impregnated paper sample show an unpredicted change in polarity with strong features on both the positive and negative side. A reference measurement was performed (Paper 2d) for which the sample was not charged. The linear response of the reference test supports the conclusion that the features of the previous spectra are not due to a systematic measurement error, but are in fact the response of the sample under test. It follows, that the observed signal is a consequence of the high–field treatment and that it is motivated by the increasing thermal excitation.

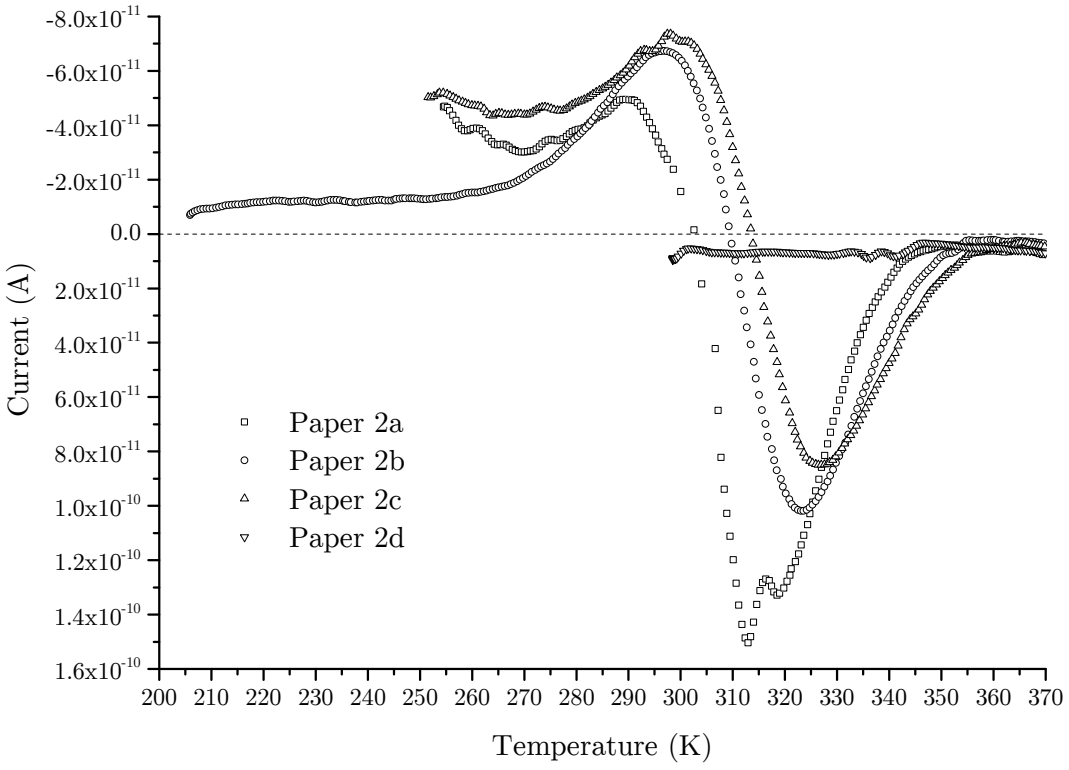

FIGURE 6.11: TSDC spectra of an unmodified oil impregnated kraft paper in an dry N_2 gas atmosphere. Polarisation voltage: 1 kV; heating rate: 3 K min^{-1}; temperature of polarisation: 313 K; ammeter NPLC: 5.

In order to determine, whether the influence of the talcum filler may be observed using TSDC spectrometry, a 35% talcum filled and vacuum oil impregnated paper sample (Paper 3) was prepared in the same way as Paper 2, and tested under identical conditions. Figure 6.12 presents the recorded TSDC spectra for the filled paper sample, and Figure 6.13 plots the last two measurements of the unmodified and modified papers together for comparison.

It is immediately obvious from Figure 6.11 and Figure 6.12, that the spectra of the talcum filled sample (Paper 3), look similar in shape to the unmodified vacuum oil impregnated (Paper 2) samples. However, on the unmodified paper, the larger peaks were on the positive half of the spectrum, whereas on the talcum filled samples the larger peaks appear on the negative side. Furthermore, Figure 6.13 highlights a shift between

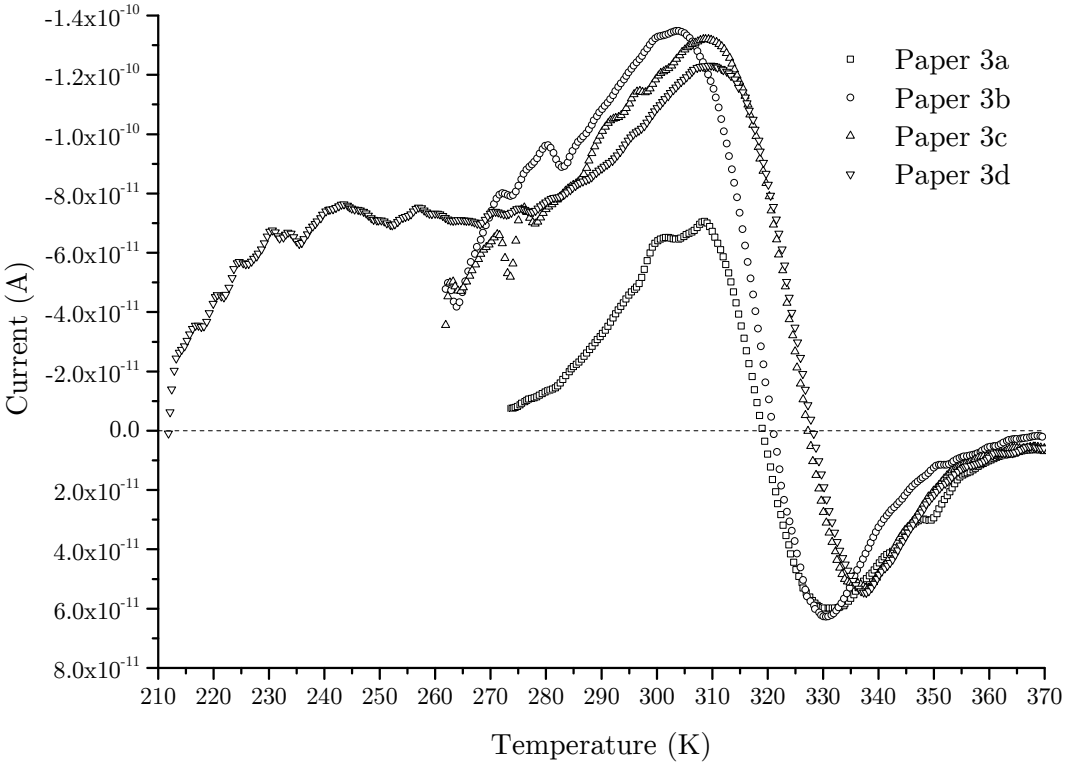

FIGURE 6.12: TSDC spectra of oil impregnated kraft paper containing 35 % talcum filler. Recorded in an dry N_2 gas atmosphere. Polarisation voltage: 1 kV; heating rate: 3 K min^{-1}; temperature of polarisation: 313 K; ammeter NPLC: 5.

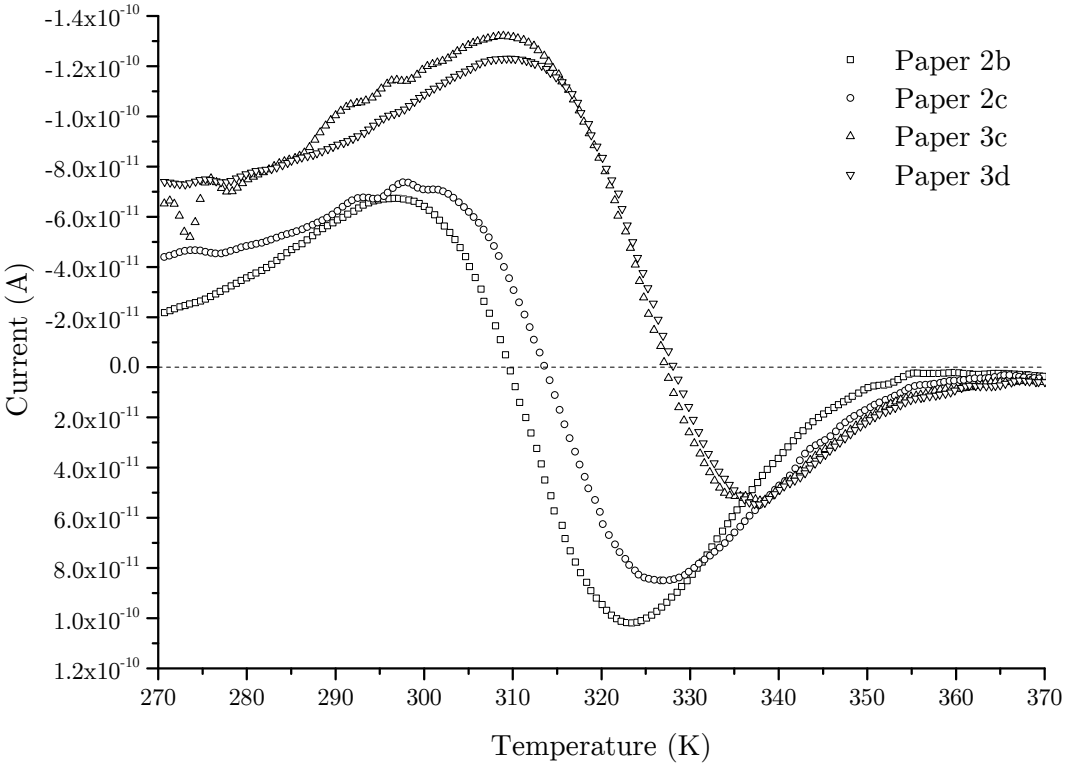

FIGURE 6.13: TSDC spectra of unmodified and talcum filled oil impregnated kraft papers. Paper 2 is unmodified, paper 3 contains 35% talcum filler.

the unmodified and filled samples. The significant features of the talcum filled sample, e.g. peak position and point of zero–crossing, are shifted towards higher temperatures.

For both the filled and unfilled sample, the differences between the first and second measurement run show a clear and immediate conditioning effect. For the unmodified Paper 2 in Figure 6.11, the conditioning effect shifts the entire curve towards higher temperatures and more negative currents. The change in peak magnitude is more pronounced on the positive peaks than on the negative peaks and thus results in an almost symmetrical curve on the third run (Paper 2c). This is in contrast to the conditioning effect for the talcum filled Paper 3 sample, which starts out with an almost symmetrical response curve of and then shifts further towards the negative domain. The negative peak on the first response (Paper 3a) for the talcum filled Paper 3, shows a 'double hump'. The first one is aligned with the negative peak on the second run (Paper 3b), whereas the second 'hump' and overall peak is aligned with the peaks of the last two curves (Paper 3c-d). Only the first run shows the 'double hump' feature, which suggests that it is an artefact of the conditioning process.

The comparative plot in Figure 6.13, shows two small 'humps' on the rise towards the first peak on the curves of Paper 2c and Paper 3c. The features are co–located at the same temperature, and only present on the third measurement run on either paper compositions. The second runs (Paper 2b, Paper 3b) do not have this feature. The fourth measurement run for Paper 2 is a validation run (Paper 2d), but the curve of Paper 3d does not exhibit this feature. Since this feature is present on the independent measurement spectra of the unfilled paper sample as well as on the filled paper sample, it may be concluded that the feature is an intermittent conditioning effect that arises from either the cellulose paper, the insulation oil, or an associated effect. If the cause were independent of the paper–oil sample, one would have expected it to also be present on other measurement responses e.g. the spectra of the oil soaked paper shown in Figure 6.9.

Figure 6.13 also illustrates that while the two paper compositions may differ greatly in their negative peaks, they both exhibit the same trend on the decline from the positive peak (trough on the graph) on the upper end of the temperature scale. It appears that as the temperature increases ($Temperature > 340\,\mathrm{K}$), the response of the paper compositions converges. The similarities seem to increase with the degree of conditioning, since Paper 2c and Papers 3c+d are more alike than they are to Paper 2b. It is conceivable, that as the temperature increases, the effect of the liquid component in the paper–oil composite starts to play a more dominant role in the overall material response. The same overall shape of a peak followed by a trough, has been reported elsewhere for thermally stimulated current spectra of mineral oil impregnated (electrical grade biaxially–oriented) polypropylene films [124]. This would suggest that the general shape of the TSDC response is caused by the mineral oil or the solid–oil interface.

The peculiar shape of the TSDC response for the vacuum oil impregnated paper samples suggests more complex processes and makes interpreting the spectra difficult. The zero–crossing may be due to polarisation/depolarisation processes in combination with charge recovery or redistribution between the liquid oil and the solid fibre matrix of the paper. The oil impregnated cellulose sample constitutes a solid–liquid composite that is further complicated by thin layers of oil between the paper and the metal electrodes, making it a multi–layer composite system. The response of both the modified and unmodified samples is sufficiently alike and similar in shape to TSDC spectra reported elsewhere for a solid–liquid composite comprising mineral oil, to conclude that they represent valid measurements. Further work is required to differentiate the processes that give rise to the observed TSDC response.

6.6 Summary

Low–density polyethylene, polyethylene terephthalate and oil impregnated cellulose papers were measured using a thermally stimulated discharge current spectrometer. Low-density polyethylene (LDPE), a well characterised polymer, was used as the first candidate to test the performance of the new TSDC instrument. In order to avoid the electrical breakdown of the sample during the TSDC charging period, DC electrical breakdown strength measurements were conducted. The Weibull scale parameter of $490\,\mathrm{kV\,mm^{-1}}$ was accepted as an approximate upper limit on the field strength. The TSDC spectra of LDPE was measured at a charging temperature of 303 K and resulted in an activation energy of 1.66 eV to 1.76 eV. The standard deviations of these calculations were 0.034 and 0.093. This correlates very well with the published activation energy of LDPE at 1.7 eV.

Biaxially oriented polyethylene terephtalate (PET), another very well characterised polymer, was used as the second candidate for the test of the TSDC instrument. The measurement of the DC breakdown strength resulted in a Weibull scale parameter of $466\,\mathrm{kV\,mm^{-1}}$. The measurements of PET conducted with the TSDC spectrometer show two peaks at 405 K and 350 K, which agrees very well with the published information for the ρ–peak and α–peak. All measurements were performed at the same polarisation voltage and the same heating rate, but with different polarisation voltages. An independence of the α–peak, and a dependence of the ρ–peak on polarisation temperature was shown and confirmed with data from literature. It indicates that the peak at 350 K is caused by dipole polarisation and may be related to conformational changes in the glass transition temperature range. Similarly, the peak at 400 K was shown to be due to space charge. The TSDC spectra as well as the dependency of the peak magnitude on polarisation voltage show very good correlation to the published data, and therefore prove again the correct operation of the TSDC.

TSDC spectroscopy measurements of a natural polymer dielectric were undertaken. TSDC spectra were presented for the composite dielectric system that is oil impregnated cellulose paper. Initial measurements of a dried and oil soaked paper (Paper 1) containing 17.5% talcum filler, 1.5% starch, 1%PVA and 1.5% wet strength agent, showed a broad and pronounced peak around 332 K. Consecutive measurements showed that the peak magnitude increased on subsequent observations which is in agreement with normal conditioning effects. Activation energies of 0.57 eV and 0.77 eV were calculated for Paper 1a and 1b respectively.

First measurements of vacuum oil impregnated samples of unmodified and talcum filled papers resulted in spectra that showed peaks for both positive and negative current. The peculiar but reproducible TSDC response of the vacuum oil impregnated paper samples is not readily explained. The similarities between the spectra of the unmodified and the talcum filled samples supports the conclusion that this is due to the basic nature of the paper–oil composite, and not solely an effect of the filler component. Other research on solid–liquid composite materials suggests that the overall shape of the TSDC response is motivated by the mineral oil and dependent on the type of oil used [124].

The results that were presented in this chapter inevitably give rise to a new set of questions and generate further directions in which this research may be pursued. The future work section (Section 8.1) in Chapter 8 picks up on this and discusses a number of possible next steps.

It has been reported elsewhere, that the properties of electrical insulation paper before oil impregnation play a significant role in determining the behaviour of the final paper–oil cable insulation [125, 126]. In order to gain a better understanding of the basic paper parameters that influence the thermally stimulated discharge current response, or more generally, the electrical performance of modified papers, a series of constructive trials with different fillers and chemical additives was undertaken next. The findings are presented in the next chapter.

Chapter 7

Modified Electrical Insulation Papers

In the electrical industry, paper is an economical insulation material with a long history. Impregnated with oil, it is used to insulate high voltage cables, bushings and transformers. Hundreds of thousands of paper-oil insulated transformers of various types and ratings are in continuous use and every year thousands of tons of cellulose are processed for insulation in the electrical industry [127]. Advances in the understanding of cellulose and paper insulation are therefore very relevant in today's paper manufacturing industry. Paper is an economic and sustainable resource and has been used for the production of electrical insulation materials for over a century [128]. Despite the rising insulation requirements modern electrical insulation paper has adequate mechanical, thermal and electrical strength for power applications with a wide range of operating voltages. A plethora of fibres, fillers and impregnating agents have been explored in the past [129, 130], however, today's insulation paper is made almost exclusively from pure virgin unbleached kraft pulp and impregnated with mineral oil [131]. It may also be chemically upgraded to extend its life-time and raise its thermal operating temperature [132]. The intention of this research is to investigate the feasibility of improving the electrical performance of oil-paper insulation systems by applied modern paper technology.

This chapter examines changes in the electrical and mechanical performance of insulation paper as a result of changes to its structure and surface properties. The base paper, the effects of fibre type, fillers and the role of paper additives are investigated. In addition, variations in filler content, density, thickness, smoothness and porosity were considered in terms of their impact on the electrical breakdown strength of oil-paper insulation.

7.1 Materials and Measurement Methods

A number of different materials were used in the production and during testing of the paper samples. The following sections provide information on the individual products as well as the measurement systems that were employed.

7.1.1 Tensile Strength Measurements

A universal testing device by 'Zwick/Roell´ was used to determine the tensile strength of the insulation paper with and without oil. The samples were prepared and tested according to the EN ISO 1924-2 standard. Since there is no machine-direction (MD) and cross-direction (CD) for laboratory handsheets, the samples were tested in one direction only. The samples were cut into 15mm wide strips and clamped down with a test span of 100mm separation. For the oil-impregnated tests, the paper was soaked in Nitro Libra oil for 30 minutes, then wiped down and dried to remove excess oil and to prevent any slippage. Tensile strength, tensile index, elongation and other values are automatically calculated by the Zwick Roell test software testXpert® II.

7.1.2 Measures of Porosity and Surface Smoothness

Surface smoothness was tested according to the ISO 8791-4 standard of Parker Print-Surf (PPS) roughness, and porosity according to Bendtsen (ISO 5636-3).

Bendtson Procedure (ISO 5636-3): A test object is clamped between a circular gasket and a flat annular surface of known dimensions. The absolute air pressure on one side of the test area of the sample is maintained at atmospheric pressure, and the difference in pressure between the two sides is maintained at a small and constant value during the test. The Bendtson value is then the mean air flow rate, in millilitres per minute, passing through the test area of $1000\,\mathrm{mm}^2$ at a rated pressure of $1.47\,\mathrm{kPa}$ in the measuring head.

PPS Prodecure (TAPPI T555om-04): The measuring head, which features a circular metal measurement surface surrounded by concentric guard surfaces, is pressed against the specimen, which in turn is supported by a resilient backing surface designed to simulate backing materials used in printing processes. Air is fed under pressure into the gap between one of the guard surfaces and the measurement surface, and the rate of flow between the edge of the measurement surface and the specimen is recorded.

7.1.3 Electrical Breakdown Strength Measurements

Electrical breakdown strength (BDS) is a measure of how much electric potential a material can withstand before it electrically fails and enables current to flow from one electrode to the other, through the sample. It is different for direct current (DC) and alternating current (AC) systems. Electrical breakdown is not only a stochastic, material dependent process, it is also affected by the rate of rise and frequency of the voltage, sample thickness and area, electrode material and geometry, configuration and method of attachment as well as temperature and humidity. Consequently, only relative conclusions should be drawn between samples with the same experimental history and measured with the same measurement system. There are two common methods in which electrical breakdown strength is determined, either under constant stress, or using a progressive stress method. In the former, all samples in a trial are subjected to the same experimental conditions, often simultaneously, and the time to failure is recorded. Times to breakdown may vary by as much as two orders of magnitude. In the progressive stress test, an increasing voltage is applied to the sample(s) under test, and the voltage at breakdown is recorded. The progression of the voltage magnitude may be a linear ramp, or a series of steps. The distribution of results for this method may be as low as 2% [133]. In this investigation, BDS measurements were performed as progressive stress tests. Due to availability, two different measurement instruments were used: a custom built system at the Tony Davies High Voltage Laboratory, and a PGO-S3 testing device from BAUR at the Institute for Paper Technology. Samples were prepared in 'trials', where a set of samples of different paper compositions were compared and relative conclusions drawn on a per-trial basis.

The custom designed measurement apparatus at the University of Southampton is based upon the general considerations laid down in the ASTM standard D149-87 [134]. The system is depicted in Figure 7.1 and an equivalent schematic representation is shown in Figure 7.2. Two vertical ball-bearing electrodes (6.3 mm diameter) pin the sample in place inside an oil bath. A 50g weight on the top electrode applies a constant and repeatable pressure. The insulating oil reduces the chance of surface flash-over where the discharge occurs on the surface and around the sample, rather than through it. A signal generator, depicted by the combination of a ramp- and function generator in Figure 7.2, provides a steady 50Hz sinusoidal signal with a linearly increasing magnitude. The signal is amplified into the high-voltage domain by a power amplifier and a transformer. A test starts with a very small amplitude and linearly ramps up the voltage magnitude by 50V/s until the sample breaks down and the system trips. The highest voltage that occurred before the system tripped is then recorded. Since electrical breakdown is a stochastic process, the test was performed 10-20 times for every sample in order to capture the variation in measurement. All samples were tested as single layers of material and the insulating oil used for all measurements on this system was silicone oil as specified in Section 7.1.7.

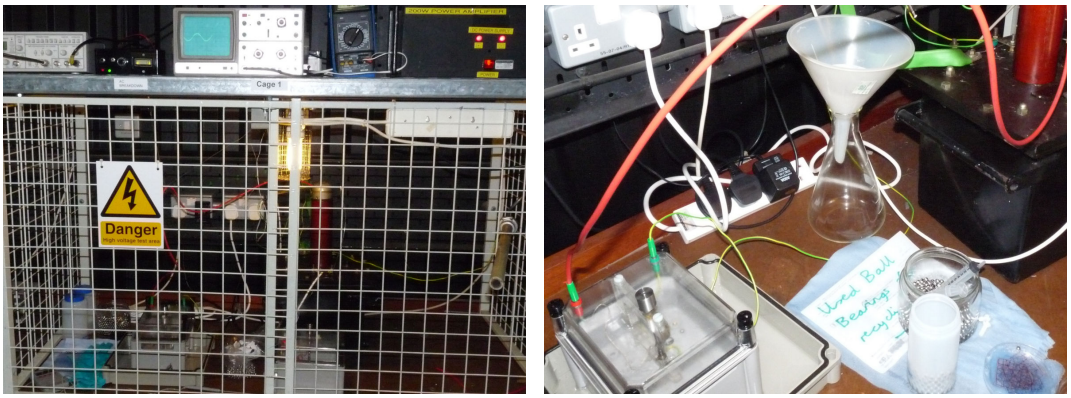

(a) Outside the safety cage. (b) Inside the safety cage.

FIGURE 7.1: The electrical breakdown strength measurement system at the University of Southampton. 7.1a Signal generator, automation and power amplifier on top of the cage. 7.1b The HV transformer on the right, the box containing the oil-immersed vertical electrodes on the left.

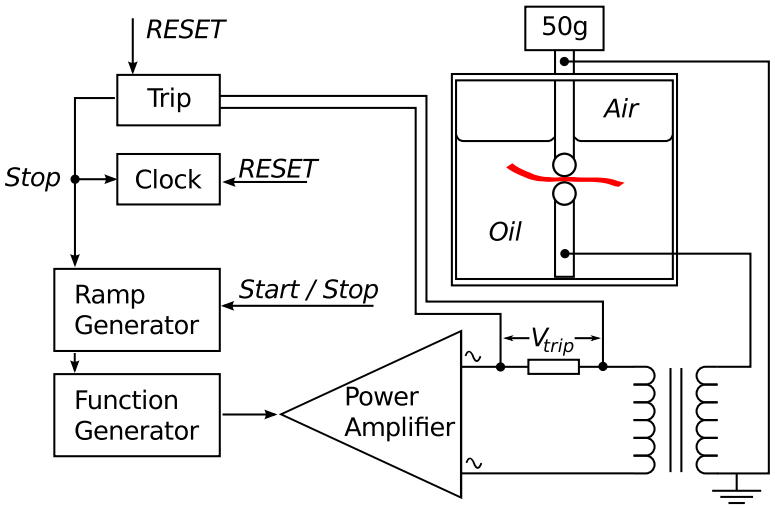

FIGURE 7.2: Schematic of the AC electrical breakdown strength measurement device at the Tony Davies High Voltage Laboratory.

The BAUR PGO-S3 measurement system was set to perform the rapid-rise test as specified in BS EN/IEC 60243-1:1998 with a rate-of-rise of 500V/s at power frequency. The paper samples were placed between the electrodes such that the plane of the paper was parallel to the plane of the electrodes. Since the dominant orientation of the cellulose fibre structure is in the plane, the electrode system was oriented normal to the dominant fibre directions, as specified for laminated materials in section 4.1 of BS EN/IEC 60243-1:1998. The electrode system employed, consisted of unequal electrodes with diameters of 20mm and 60mm, for the top and bottom electrode respectively. The electrode system and its dimensions are shown in Figure 7.3. All measurements on the BAUR PSO-S3 were performed in transformer oil (q.v. Section 7.1.7 for details) meeting IEC 60296 specifications as set out in Section 6.2 of the BS EN/IEC 60243-1:1998 standard. All of the samples tested on the PGO-S3 system were dried in a dessecator prior to testing

and their moisture content determined using a moisture analyser (q.v. Section 7.1.4). The PGO S-3 tester only reliably arrested on breakdown voltages over approximately 7kV, which meant that all samples that were tested on the PGO S-3 system were folded into multiple layers. Due to the size of the electrodes relative to the samples, only six electrical breakdown strength values were recorded per sample. In order to compensate, multiple samples of the same paper type were tested. However, since only one electrical breakdown sample could be cut from a single handsheet, this inevitably introduced the variation of laboratory handsheet production into the measurement. Section 7.2 provides more information on how this was taken into account in the analysis of the data.

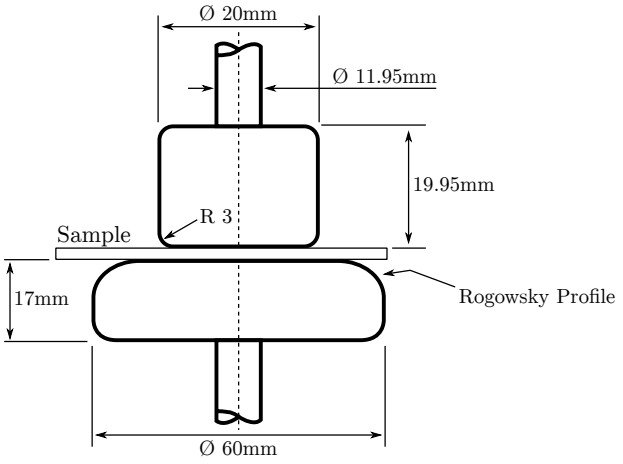

FIGURE 7.3: Diagram of the electrode system used with the BAUR PSO-S3 measurement system.

7.1.4 Dielectric Spectroscopy

The response of a material to alternating currents that vary across a wide spectrum of frequencies may be obtained by Dielectric Spectroscopy, also called Frequency Domain Spectroscopy. The measurement reveals the energy storage and dissipation properties of the material under test. The material response is commonly analysed in the dimensionless terms of relative permittivity and dissipation factor i.e. loss tangent. The first term denotes the impact of the material on the electric field in comparison to vacuum as a medium, and the second describes the inherent electromagnetic energy loss within the material. Both parameters are commonly used to characterise dielectric materials in electrical engineering. For a material to be a good electrical insulator, both parameters are desired to be small. A Solartron SI 1260 Impedance/gain-phase analyzer in combination with a Solartron dielectric interface 1296 was used to take dielectric spectroscopy measurements of selected paper samples (see Figure 7.4).

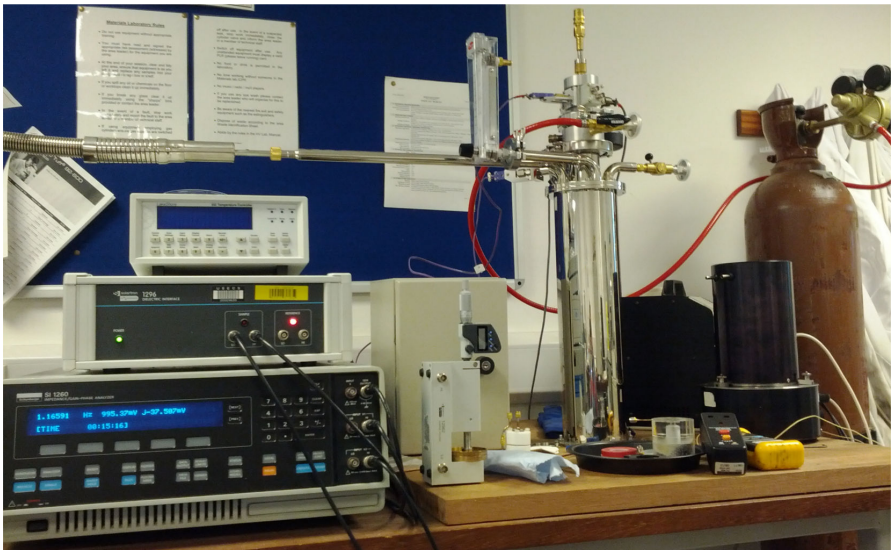

FIGURE 7.4: The Solartron SI 1260 Impedance/gain-phase analyzer and Solartron dielectric interface 1296.

7.1.5 Moisture Control Measures

Moisture has a significant effect on the performance of paper [135, 136], electrically as well as mechanically. All handsheets were stored in a desiccator over activated silica gel for 24 hours or longer, prior to any electrical testing. Since not all of the handsheet was used for electrical testing, some of the trimmed parts could be used with a Precisa EM 120 moisture analyser to determine the dry content of the sample sheets prior to electrical breakdown testing. Any paper strips that were cut from the handsheets for mechanical tensile testing were placed in a climatised room for 24 hours or longer at standardised conditions (23°C and 50% humidity).

7.1.6 Pulp Refinement

Pulp is refined to increase fibrillation; to open up and activate the surfaces which increases the number of available hydrogen bonding sites. This in turn leads to an improved mechanical strength and formation of the paper [45]. In the paper industry, the grade of refinement is commonly stated in the Schopper Riegler (SR) value. It is a measure of the fibres' or pulp's ability to retain water [42]. The more refined the pulp, the longer it takes the water to leave the suspension. Untreated fibres have a SR of around 10 to 15, medium refined fibres show SR values of 30–40, and highly refined pulp may have SR > 70.

7.1.7 Fibres and Fillers

Three types of pulp were compared. The hardwood pulp is never-dried Eucalyptus (Aracruz) pulp, refined to a Schopper Riegler value of 32°SR. The bleached softwood pine-spruce ECF[1] pulp, with an initial Schopper Riegler of 13°SR, is refined to a Schopper Riegler of 34°SR with a lab ball mill. The unbleached kraft pulp with an initial Schopper Riegler value of 15°SR, is refined with a lab ball mill to a Schopper Riegler of 32-34°SR. De-ionised water was used for disintegration and refining, but standard tap water was used for the formation of the papers to obtain samples that more closely resemble commercial paper produced in paper mills.

Three different commercial electrical insulating papers were tested for comparison. All three candidate papers are unfilled, uncalendered and made from unbleached softwood kraft pulp.

Two very different fillers were chosen to illuminate the effect of fillers in general, and those materials in particular. Talcum or talc, is a magnesium–rich phylosilicate mineral that may be found as a gangue component in base metal sulfide ore deposits. The talcum silicate mineral is layered and comprised of octahedral magnesium hydroxide structures that are sandwiched between silicon–oxygen tetrahedra. Cohesion of the layered talcum sheets is provided by weak van der Waals forces [137, 138].

The talcum filler used in these experiments is a hydrophobic mineral with a high aspect ratio, packed bulk density (ISO 787/11) of 1.05 g/cm^3 and moisture content (ISO 787/2) of 0.2%. The particle size distribution of the powdered talcum filler employed in this research was determined with a Mastersizer 2000, and the two measurements are shown in Figure 7.5. The complete report may be found in Appendix C.3.

Bentonite is already known in the electrical industry where it is being used in the treatment process of aged transformer oil to improve its breakdown strength [139]. In comparison to talcum, the montmorillonite bentonite filler is highly hydrophilic. For the preparation of the filler slurry, a calculated amount of filler was soaked and wetted with de-ionized water for approximately 10 minutes until a homogeneous colloidal slurry was obtained. The slurry may then be added to the pulp to produce filled papers.

[1] Elementary Chlorine Free (ECF).

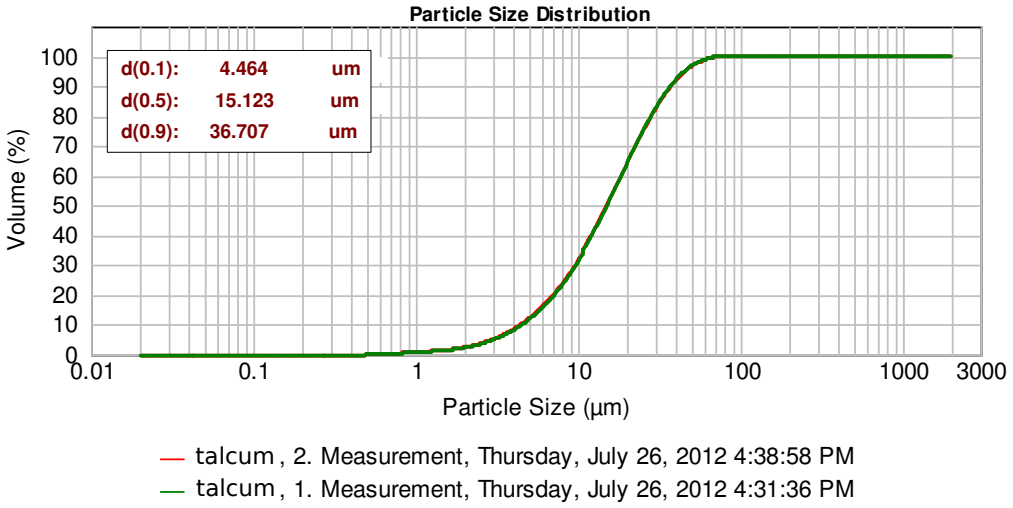

FIGURE 7.5: Particle distribution of the talcum filler as determined by a Malvern Instruments Ltd. Mastersizer 2000 particle size analyser. Two observations shown (curves overlap).

7.1.8 Chemical Additives

The starch used as dry strength agent is a cationised potato starch. It is a cold water (40-50°C) soluble starch for wet end purposes. Polyvinyl alcohol (PVA) is a water–soluble polymer manufactured by the alcoholysis of polyvinyl acetate. Polyvinyl alcohols are industrially used for many purposes such as for example in the production of paper adhesives, as protective colloid in emulsion polymerisation and as raw material for the production of sizes and textile finishes, as binder in the surface finishing of paper as well as for regulating the processing characteristics of all types of coatings. PVA possesses interesting barrier properties and shows excellent mechanical strength properties on paper or paperboard. PVA is a good insulating material with low conductivity, for which it is highly regarded in the electronic industry and also finds use in composite polymer films [140, 141]. The fully hydrolysed polyvinyl alcohol employed in the trial investigating the combined and separate effects of starch and polyvinyl alcohol, is of high molecular weight with viscosity (DIN 53015) 56.0 ± 4.0 mPa·s and degree of hydrolysis 98.4 mol-% ± 0.4 mol-%. This type of PVA is notable for its good bonding strength and pigment binding capacity which made it feasible to formulate papers with a high amount of talcum filler.

7.1.9 Insulating oils

Nynas Nytro Libra mineral oil with naphthenic characteristics was used for the mechanical tensile tests in oil, as well as for the electrical breakdown tests on the Baur PSO-S3 testing device. Nytro Libra is a standard grade uninhibited insulating oil, meeting IEC 60296 general specifications. The oil is a light yellow liquid with a boiling point in excess of 250 °C, a melting point at −54 °C and a relative density of 0.89 g cm^{-3} at 15 °C [142].

Breakdown strength measurements that were performed on the BDS measurement system of the University of Southampton, were performed in silicone oil XIAMETER® PMX-200 Silicone Fluid, 5-20 CS by Dow Corning.

7.1.10 Sample Preparation

The laboratory handsheets were produced on a Rapid-Köthen sheet former, which is shown in Figure 7.6. A handsheet is formed by draining the pulp from the transparent cylindrical stock container (shown in the open position, hinged back from the forming wire) through a copper wire screen into a suction chamber (gray column in front). Once the wet sheet has been removed from the wire, it is then dried in one of the four drying pans. The drying units work with a combination of heat, pressure and vacuum, to remove the water from the paper sheet. The handsheets were manufactured in accordance with the considerations in the DIN-ISO 5269-2 procedure. Actual timer settings are quoted in brackets.

1. Pulp suspension is added at 4 litres of filled volume.
2. Fill time set to the desired volume e.g. 7 litres. (Set: 22 sec.)
3. Set bubble time to appropriate level to agitate the pulp suspension. (Set: 22 sec.)
4. Rest period. (Set 5 sec.)
5. Time for solution to fall through the forming wire. (Set: 10 sec.)
6. Time for vacuum set such that it overruns for 10 sec. (Set 20 sec. total time.)
7. Drainage. (Set: 20 sec.)

The standard procedure is devised for the production of 'normal' paper using pulp with a higher Schopper Riegler value. The unbleached softwood kraft pulp from which the electrical insulation paper samples were made, is more challenging to work with. By increasing the volume of the solution and the time of agitation, an improved formation of the handsheets is achieved.

FIGURE 7.6: Rapid-Köthen Sheet Former by FRANK Prüfgeräte GmbH.

7.2 Statistical Data Analysis

Results from electrical breakdown strength (BDS) measurements may be readily processed using statistical analysis and this section provides details and justifications for the methods employed. The stochastic electrical breakdown characteristic of individual material samples may be analysed using descriptive statistics and measures of spread i.e. the arithmetic mean, median, standard deviation and range. However, in the electrical industry it is common to employ statistical Weibull life-data analysis in an attempt to deduce the electrical breakdown strength of the class of materials for which the sample is representative. Life data analysis attempts to predict important life characteristics for a population, i.e. a class of materials, by fitting a statistical distribution to the life data from a 'representational sample' of said material, i.e. a selection of tests of the material. The Weibull distribution is briefly introduced in Section 7.2.1.

In the case of the handsheets that were produced in the laboratory for the paper trials, the circumstances are different. In most cases, several different types of paper were tested for comparative analysis and the premier goal was not to deduce the breakdown strength for every type of paper composition, but to see whether the BDS of the compositions

differed significantly, i.e. whether the changes made to the paper resulted in a real difference. As electrical breakdown testing is a destructive measurement, it follows that only a limited number of measurements can be performed per sample—the number of which depends on the sample area and voltage magnitude. Furthermore, the sample size is limited by the measurement equipment to one that is practical to handle inside the confines of the oil bath. In order to gain a measure of the measurement variance, each sample was measured multiple times and more than one sample was tested for each paper composition. In the case of the PVA screening trial for example, 8 different paper compositions were compared, 4 handsheets were produced for each paper type, and each handsheet was tested 6 times. The resulting data are represented for visual inspection in the form of a boxplot in Figure 7.7 (see Section 7.5.3 for more analysis of the PVA trial data). A boxplot or box-and-whisker plot represent and summarises a set of data through the descriptive statistics of the five most important percentiles: the minimum and maximum, the lower and upper quartile (25^{th} and 75^{th} percentile), and the median (50^{th} percentile). The whiskers extend to the smallest and largest value, the ends of the box mark the lower and upper quartiles, and the median is denoted by the vertical line splitting the box.

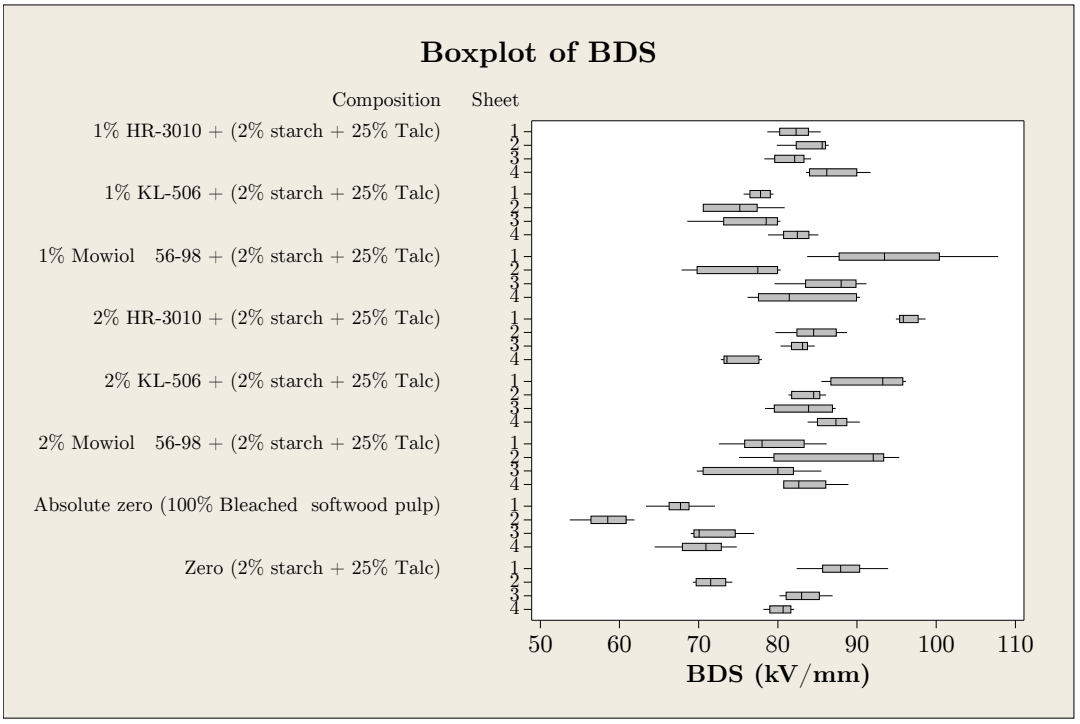

FIGURE 7.7: Boxplot of the PVA data.

It illustrates how the measurement variance of each paper type is a confluence of the variation between the six measurements, and the differences among the handsheets. The former is due to measurement inaccuracy and repeatability as well as the inhomogeneity of the paper sample. The latter is an unavoidable consequence of the laboratory envi-

ronment where each sheet is produced individually and exact reproducibility is nearly impossible. The variance per handsheet is much smaller than it would appear to be if the data of the individual handsheets were pooled and analysis performed on a per paper-type basis. This is in contrast to data gained from measurements of a single batch of industrially produced material, such as polymer film samples cut from a single roll, where inter-sample variation is small and data from several samples with the same history may be pooled without great penalty. In the case of the paper handsheets, the experiment design is more complex. Figure 7.8 illustrates the problem. Every sample was tested n times; every sample is derived from a single handsheet and there are multiple sheets that were tested for each paper type i.e. composition. The data gathered for the handsheets is nested within the paper types, and the analytical approach should take that into consideration. Where the dataset was balanced, nested Analysis of Variance (ANOVA) was used, and where the dataset was unbalanced, the method of the general linear model ANOVA was employed (see Section 7.2.2 for more information).

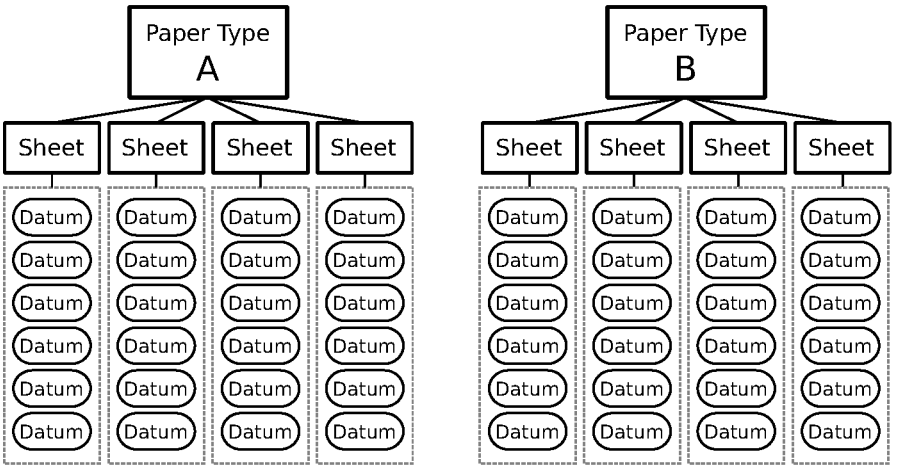

FIGURE 7.8: The electrical breakdown data of the paper trials is nested in nature. Four multiple handsheets were made and tested for every paper type or composition. Every tested handsheet was measured multiple times.

7.2.1 The Weibull Distribution

The cumulative density function for the two-parameter Weibull function is provided in Equation 7.1 below. It describes the probability of failure $F(t)$, which is zero at $F(t = 0)$, and rises continually with increasing time or voltage until it approaches certainty at infinity i.e. $F(t = \infty) = 1$. The scale parameter α denotes the time or voltage for which the probability of failure is 0.632 (i.e. 63.2%) and as such may be thought of as the analogue of the mean on the standard distribution. The units of α are the same as for t. The shape parameter β is a measure of the range of the failure points. A larger value of β denotes a smaller spread of the breakdown values. This is analogous to the inverse of the standard deviation of the normal distribution.

$$F(t;\alpha,\beta) = 1 - exp\left\{-\left(\frac{t}{\alpha}\right)^{\beta}\right\} \tag{7.1}$$

where t is the time to breakdown or the breakdown voltage, $F(t)$ denotes the probability of failure at a time or voltage less than or equal to t, α is the positive scale parameter, and β is the positive shape parameter.

7.2.2 Analysis of Variance

In the trials that were conducted to compare different paper compositions, care was taken to always take the same number of measurements per sample. This being the case, a balanced Analysis Of Variance (ANOVA) approach was selected for analysis whenever possible. The prerequisite of a balanced design are an equal number of observations for each combination of the treatment levels; in this case, the same number of data for each paper compositions in a trial. Some of the earlier trials, however, consist of unequal numbers of observations per sample. This is mostly due to the operator taking additional measurements when samples appeared to exhibit a pronounced stochastic response or when the operator judged a datum to be an outlier at the time of measurement. One possible approach would be to take the first n number of measurements from each sample; where n would be the smallest number of measurements available for all samples in the comparison. However, this would discard a number of measurements from the analysis. Instead, it was chosen to leverage the more general ANOVA method of General Linear Model (GLM) analysis that can cope with unbalanced designs in order to make use of all available data for the analysis.

The statistical methods of the ANOVA presume the following assumptions:

1. Independence of observations – dependent on the statistical model employed.
2. Normality – residuals are normally distributed.
3. Homoscedasticity – equal variance for data in groups.

Residual plots may be used to assess whether the underlying statistical assumptions have been violated. None of the measures and plots discussed next should show a trend, as this would be an indication of dependence. On a normal probability plot, the residuals should be randomly scattered along a straight line. Figure 7.9–top left, shows this to be the case for the data resulting from the PVA trial. Datasets with less than 50 observations may show some curvature in the tails, even if the data is normally distributed. If in doubt, a separate statistical test for normality may be performed (e.g. Anderson–Darling statistic). A scatter plot of the residuals provides information on the error variance. In the case of a good regression, the residuals are disordered and form a

band with a parallel envelope around the horizontal zero line (see Figure 7.9–top right). An increasing or decreasing spread of the residuals suggest an increasing or respectively decreasing trend of the error variance with the independent variable. A drift in the variance may be checked by plotting the residuals against the order of the data. A drift in the variance would be visible as a trend whereas a random distribution of the residual suggests a lack thereof (see Figure 7.9–bottom right). The normal distribution of the variance may be checked by plotting a histogram of the residuals. A symmetric bell-shaped histogram with an even distribution around zero indicates that the assumption of normality is likely to be true. In a case where the histogram suggests a non-normal distribution of the random error, a violation of the underlying statistical assumptions my be assumed. While the distribution of the residuals doesn't have to be an exact fit with the normal distribution for the ANOVA method to work, their near normality is important since computation of the p-values in F or t statistics depend on residuals and not the original values.

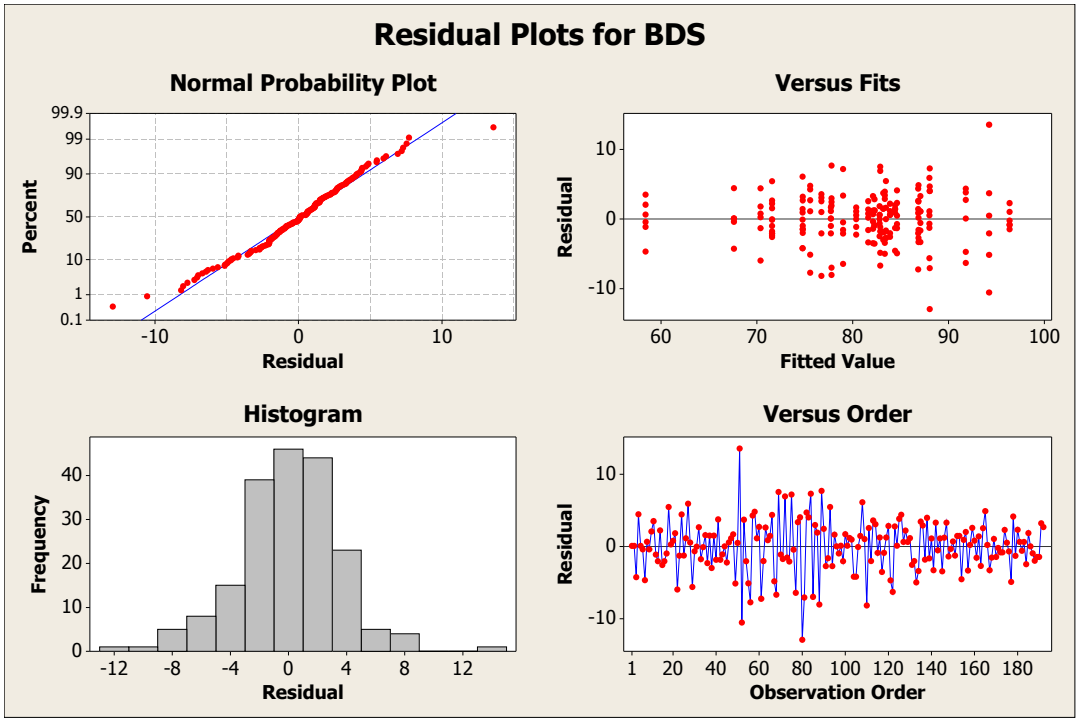

FIGURE 7.9: Residual analysis of the PVA trial.

In conclusion it should be noted, that despite the thoroughness and validity of the statistical analysis that may be performed on electrical breakdown strength data, the parameters that are obtained from such techniques are only estimates of randomly distributed measurements from a given failure mechanism.

7.3 Fibres and Fillers Trial

Three types of pulp were examined with regard to their effect on the electrical breakdown strength of oil-impregnated paper insulation: hardwood pulp (never-dried), bleached softwood and unbleached softwood kraft pulp. Their electrical and mechanical performance is depicted in Figure 7.10. The paper samples made from hardwood pulp displayed a lower electrical breakdown strength and mechanical tensile strength than the softwood samples or the commercial reference papers. The mechanical and electrical strength of the softwood papers were found to be slightly higher than that of the commercial papers, with the unbleached variety performing best overall. This may be ascribed to the refining process and the concomitant densification. In summary these findings confirm the established industry practice of employing softwood kraft pulp for manufacture of electrical paper insulation.

Two very dissimilar fillers were selected to illuminate the effects of fillers on the performance of insulation paper; bentonite, a powdered hydrophilic montmorillonite clay, and talcum, a hydrophobic mineral powder. As illustrated in Figure 7.11, the talcum filled samples outperformed all other paper samples with regard to electrical breakdown strength. The bentonite filled samples performed badly. Electrically this may be explained by the hydrophilic nature of the bentonite filler which also tends to absorb water and swell; high moisture content, ionic charges and impurities associated with such a clay are generally understood to degrade electrical breakdown strength in a material.

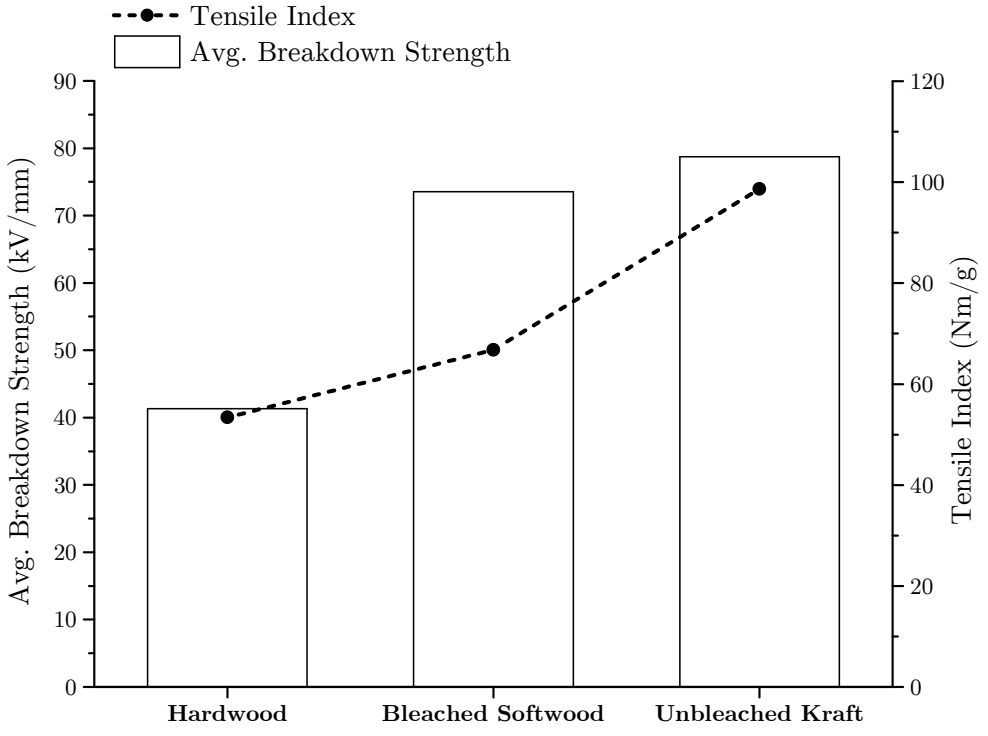

FIGURE 7.10: Tensile index and breakdown strength for different fibre types.

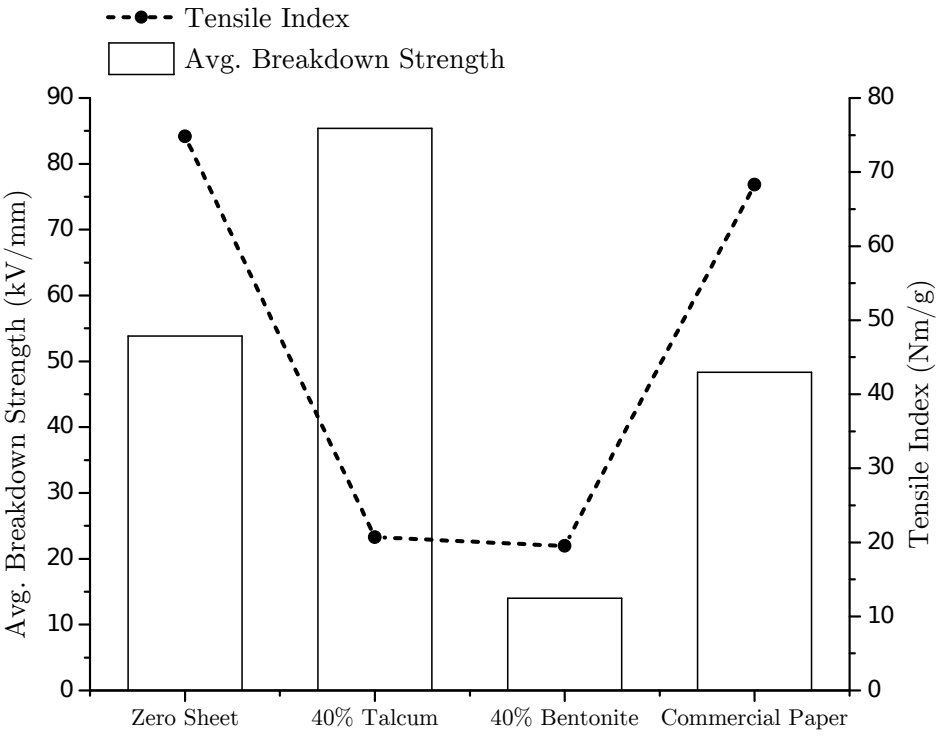

FIGURE 7.11: Tensile index and breakdown strength for different fillers.

An optimisation trial was conducted with varying quantity of the talcum filler to find the best compromise between enhanced BDS and loss of mechanical strength. Figure 7.12 suggests there is no linear relationship between the talcum filler content and electrical breakdown strength. It may be inferred that a sufficient improvement in BDS may be obtained without a significant loss of mechanical strength for talcum contents of 25-30%.

In order to evaluate whether this initial optimisation of insulation paper for electrical properties also improved the dielectric characteristics of the material, the most promising samples underwent dielectric spectroscopy measurements to ascertain their frequency response. The resulting comparison between commercial papers and a set of talcum filled samples with varying degrees of filler content is depicted in Figure 7.13. Since a small real relative permittivity and dissipation factor is desired, it can be seen that the greater electrical breakdown strength of the talcum filled papers is balanced by a reduction in dielectric performance. The data suggest a linear trend and an inverse relationship between the amount of filler and dielectric performance. On that basis it is not surprising that the unfilled commercial papers show the best dielectric results. However, it is noteworthy that the commercial paper designated number three, has a real relative permittivity that is comparable to the filled sample papers around mains frequency.

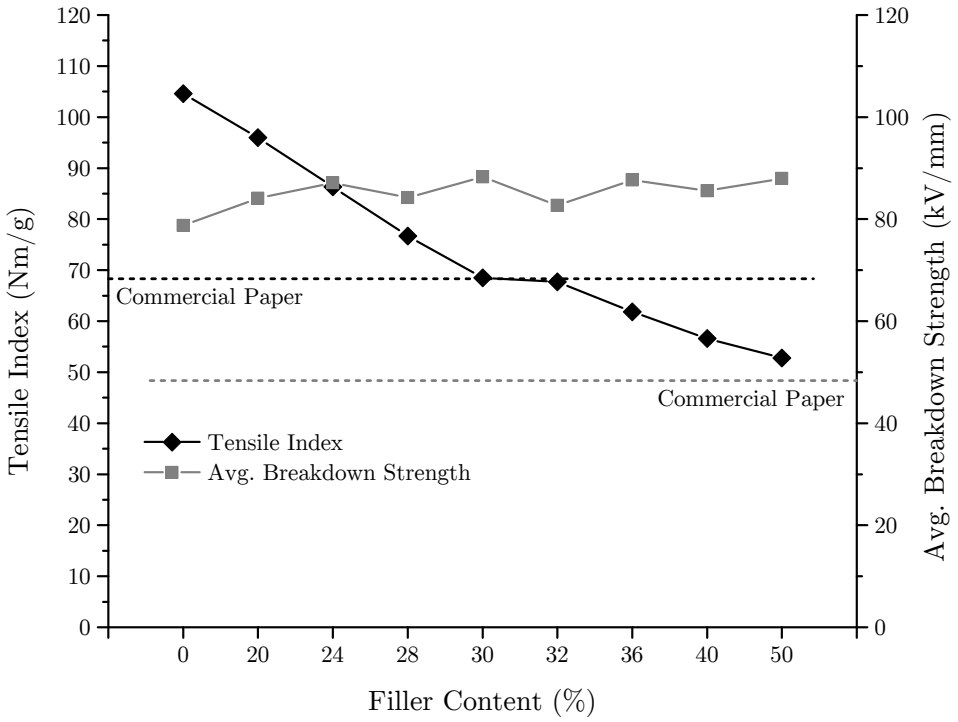

FIGURE 7.12: Optimisation of talcum content for high electrical breakdown strength with minimal loss of mechanical strength.

Figure 7.14 presents the data in Figure 7.13 in an bar chart form for mains frequency only. The real relative permittivity values range from 1.7 to 2.5, with the commercial paper 2 showing the smallest and the 32% talcum filled paper the largest permittivity value. The dissipation factor values range from 3.8×10^{-2} to 1.2×10^{-1}, with commercial paper 3 showing the smallest, and 36% talcum filled paper showing the largest dissipation factor values. While commercial paper 3 showed the smallest dissipation factor value in this trial, its real relative permittivity value is equal to that of the 32% talcum filled paper. The data corresponds well to general values stated in literature [8].

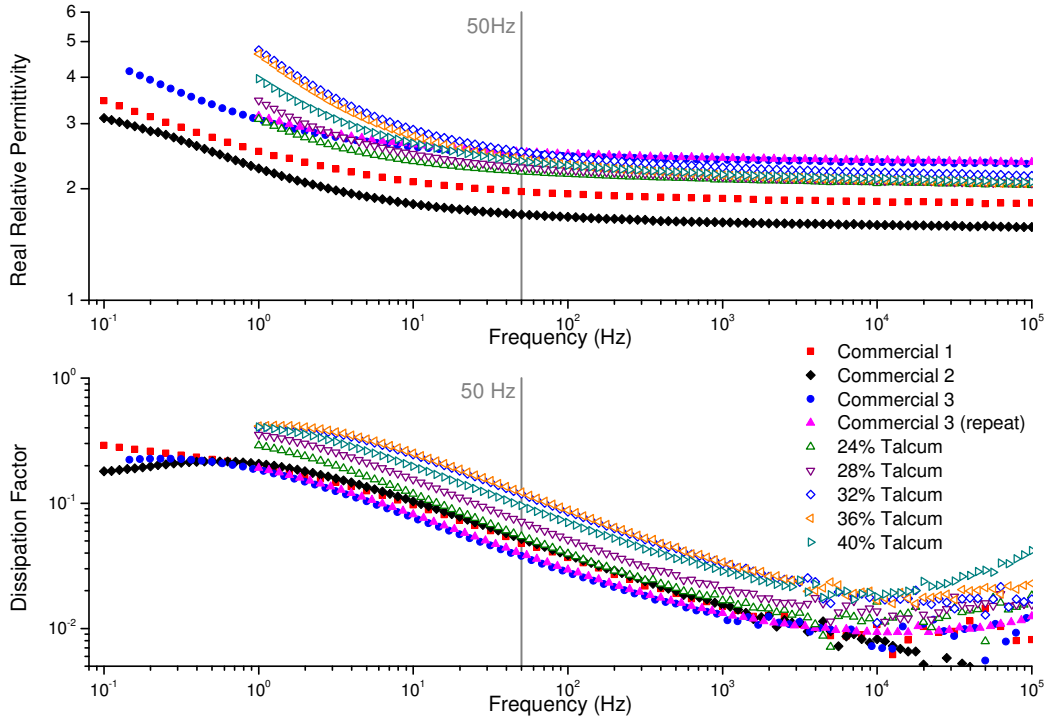

FIGURE 7.13: Influence of various levels of talcum filler-content on the permittivity and dissipation factor of paper in comparison to commercial test papers.

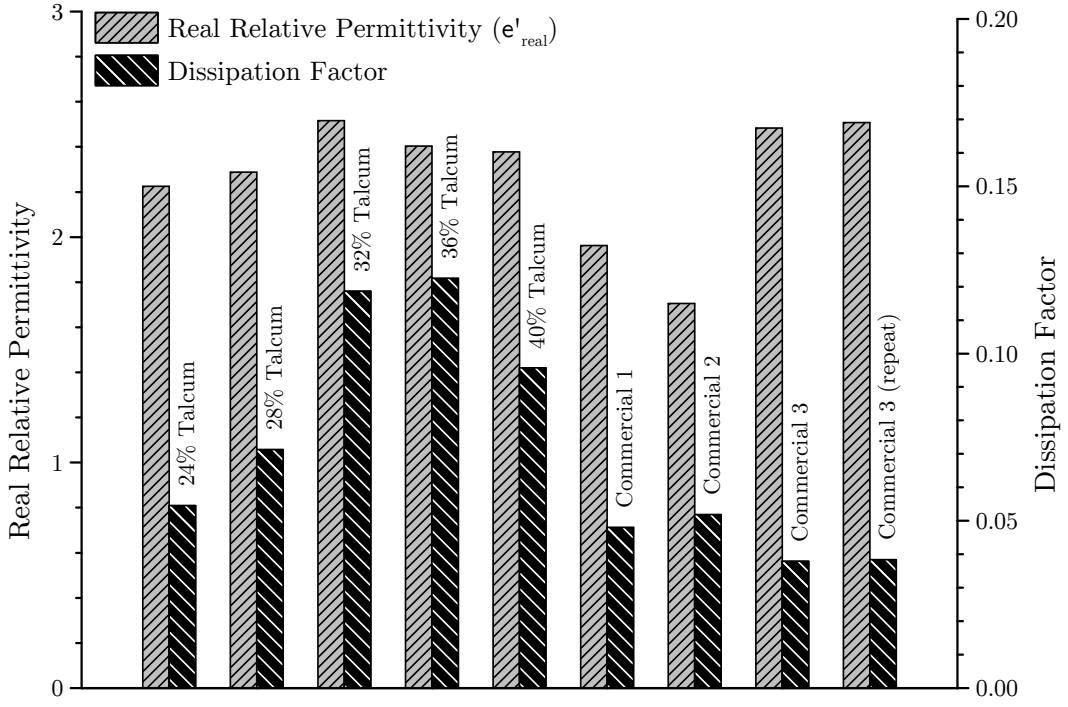

FIGURE 7.14: Permittivity and dissipation factor values of the papers in the talcum filler-content optimisation trial at 50Hz.

7.4 Calendering Trial

As previously explained in Section 2.8, calendering is a processing step in the manufacture of paper wherein the sheet is pressed between rollers to improve its surface properties. An unbleached kraft paper with a filler content of 40% talcum, 3% starch and 1% PVA was used in a comparative trial to assess the effect of calendering on the performance of insulation paper. The samples were calendered with 4 different settings of the hard roll gap laboratory calender (steel on steel) and a constant roll surface temperature of 110 °C. The pressure was set to either 20N or 35N and applied once or thrice. This is representative of one or three presses with two different pressure settings. Figure 7.15 presents the results of the trial and shows how increasing degrees of calendering pressure raises the breakdown strength. The highest electrical breakdown strength value was achieved by the paper that was calendered the most, and the lowest by the reference paper that was not calendered at all. Furthermore, the data suggests that it is the magnitude of the applied pressure rather than the number of calendering steps that is significant. Taking the standard deviation of the measurement data (error bars) into account, the gain between the uncalendered and the '35N $\times$ 3' calendered paper is still 7% in the worst case scenario. As discussed in Section 7.2, the unique nature of the samples introduces additional spread in the electrical breakdown strength values and blurs the evidence in the data, however, the effect of calendering is still recognisable.

Calendering reduces porosity and increases the surface smoothness of the paper. It is inferred, that the local electric field at the electrode-paper interface is reduced by the increased effective contact area and that the reduced surface roughness also decreases the likelihood of local field enhancement and therefore discharges in cavities at the interface [143]. Combined with the increased apparent paper density caused by the reduction in paper thickness, this may explain the increase in electrical breakdown strength of the calendered papers.

The influence of calendering on the dielectric response of paper was also investigated and is depicted in Figure 7.16. The earlier illustrated positive effect on the electrical breakdown strength of paper appears to be achieved at the expense of dielectric performance. It is suspected that the increase in apparent bulk density and smoothness also increased the number of polarisation processes per unit volume, and thus raised the dielectric response parameters.

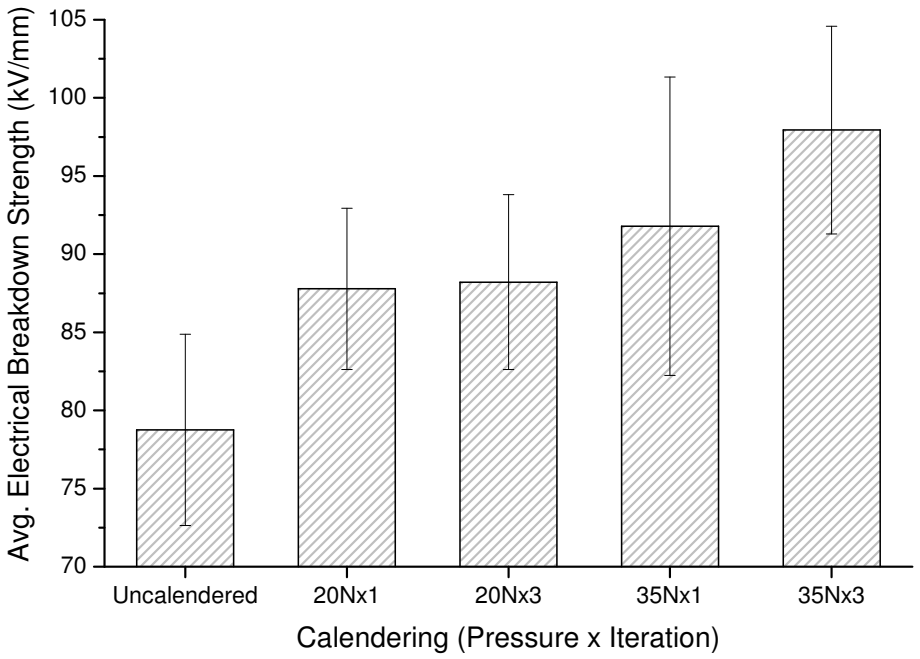

FIGURE 7.15: Impact of calendering on the electrical breakdown strength of paper.

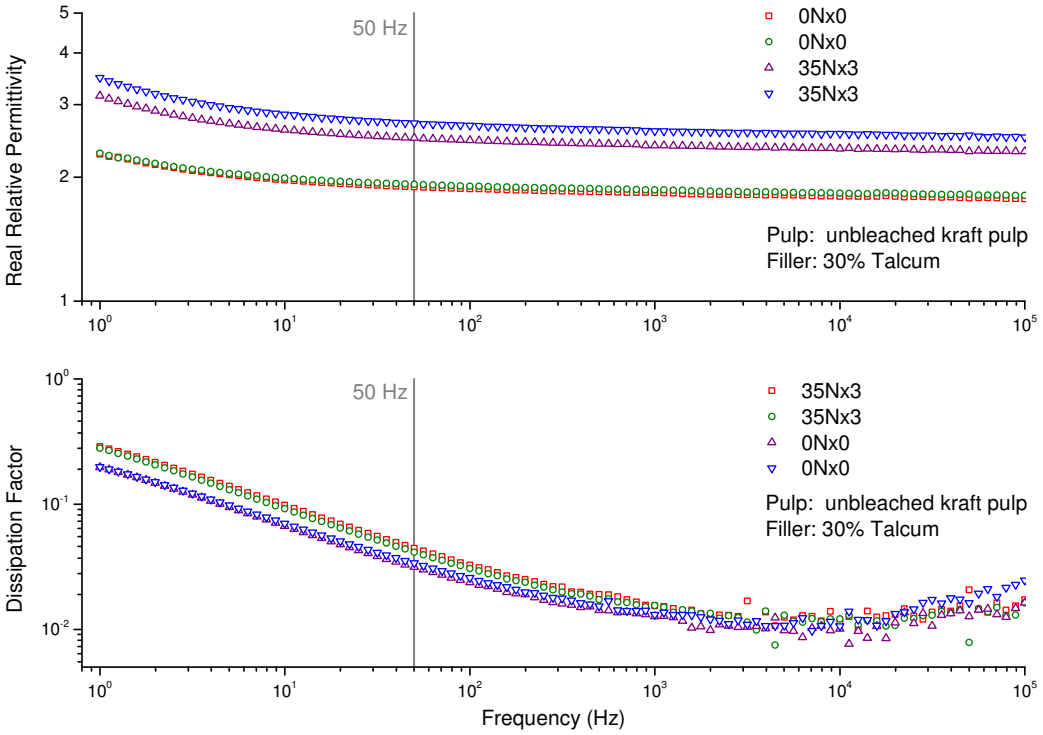

FIGURE 7.16: Influence of calendering on the permittivity and dissipation factor of paper.

7.5 Trials of Chemical Additives

Mechanically, the filled materials presented in Figure 7.11 show a significant reduction in tensile strength compared to the unfilled zero sheet or the unfilled commercial papers. This is not surprising and directly related to the amount of filler—with 40% filler content the samples are considered to be highly filled. In order to amend mechanical performance by means other than reducing filler content, additives were trialled.

7.5.1 Starch and Polyvinyl Alcohol Trial

The strength agent starch and the water soluble co-binder polyvinyl alcohol were added to the filled papers. Starch is a natural additive that increases the hydrogen bonds between the fibres and thus adds to the mechanical strength of the paper. PVA improves the wetting and dispersion of the hydrophobic talcum powder in water and reduced inhomogeneity and two-sidedness of the resulting paper. Figure 7.17 shows the effect of the two additives separately and in combination. It suggests that not only do they have the desired effect on the mechanical performance, approximately doubling the tensile strength of the sample papers, but they even positively contribute to the BDS of the paper. The dotted horizontal lines denote the average value of the three commercial papers with $48.36\,\mathrm{kV\,mm^{-1}}$ and $68.3\,\mathrm{N\,m\,g^{-1}}$ for BDS and tensile index respectively. Compared to the commercial reference, the tensile strength of these highly filled papers is still slightly reduced.

To further study the effect of the additives on the dielectric performance of the paper, a dielectric spectroscopy trial was conducted for papers containing PVA and/or starch. The papers that comprise this study were all filled with 40% talcum and made from unbleached kraft pulp. The results in Figure 7.18 show clearly that the addition of the cationic starch, though successful in raising mechanical strength in the paper, has a detrimental effect on the overall dielectric response. The addition of PVA appears to alleviates this to some degree. Since dielectric spectroscopy is a measure of a material's absorption and dissipation of electromagnetic energy through polarisation processes, this result confirms the expectation that the addition of a polar compound would negatively affect the dielectric response of the material.

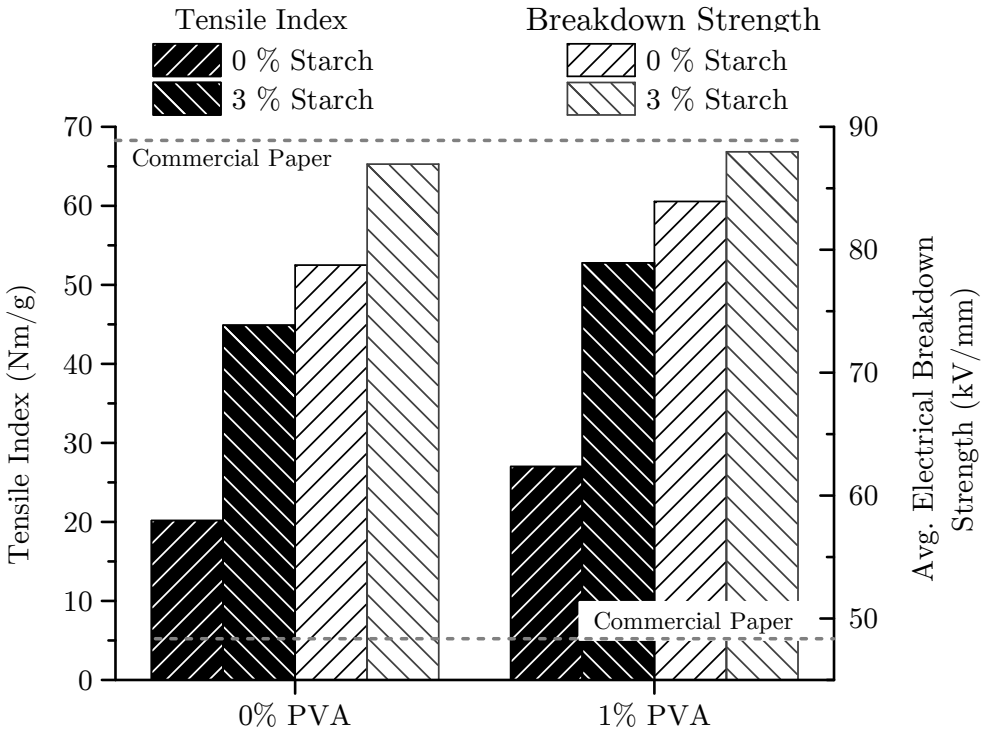

FIGURE 7.17: The effect of starch and polyvinyl alcohol on the electrical breakdown strength and tensile index of 40% talcum-filled unbleached kraft paper. Dashed horizontal lines show average value of commercial reference papers.

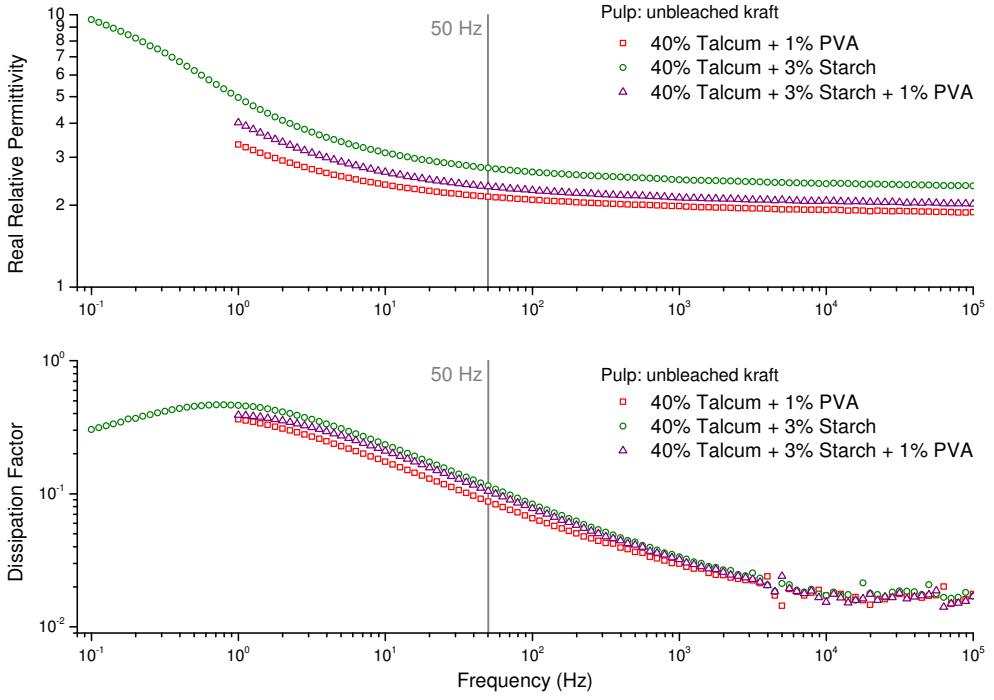

FIGURE 7.18: Impact of starch and polyvinyl alcohol on the permittivity and the loss factor of paper.

7.5.2 Sizing Trial

A trial was conducted to investigate the influence of sizing on the electrical breakdown strength. Handsheets surface sized with Alkenyl Succinic Anhydride (ASA) and Alkyl Ketene Dimer (AKD) sizing agents were produced in the laboratory and tested on the BAUR PGO-S3 apparatus in comparison with zero sheets containing neither. All the sheets in this trial were made of bleached softwood kraft pulp and filled with 25% talcum. Since the relative performance of the papers is of interest, the use of bleached kraft pulp instead of the unbleached variety is permissible. The choice was made due to issues in the availability of the unbleached variety. Visual inspection of the results on the basis of descriptive statistics is provided by a boxplot and a dotplot in Figure 7.19 and Figure 7.20 respectively. Without further analysis, it can be seen that the three sheets containing the ASA sizing agent did not perform as well as the AKD sized papers or the zero sheets. It is also possible to see that there is a variation in both the median of the sheets, as well as their spread of breakdown strengths.

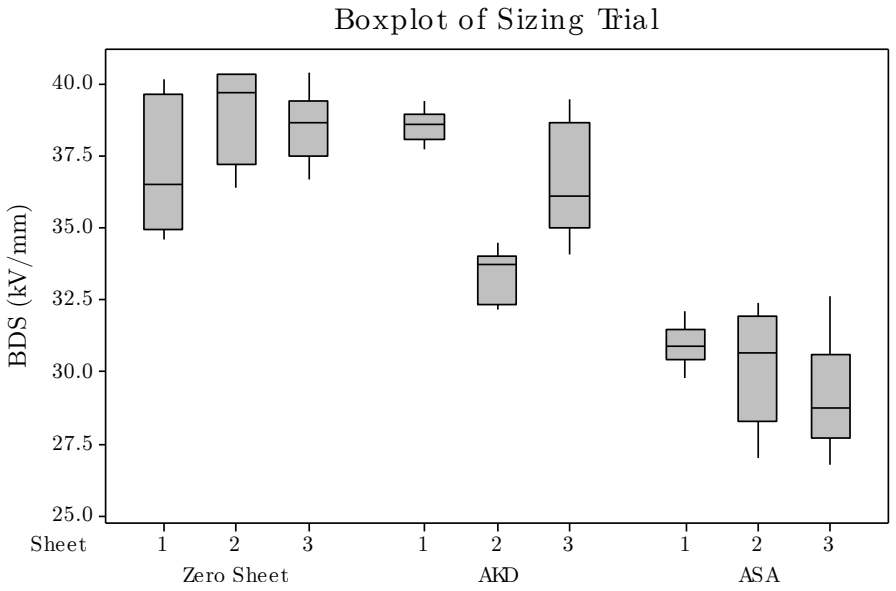

FIGURE 7.19: Boxplot of the sizing trial data showing the effect of AKD and ASA sizing on electrical breakdown strength.

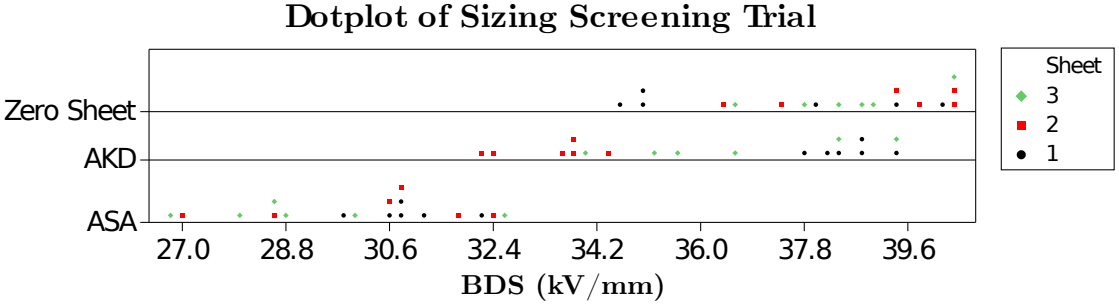

FIGURE 7.20: Dotplot of the sizing trial data.

A comparison of the electrical breakdown strengths of the individual sheets as well as of the overall paper compositions is provided in form of a bar graph in Figure 7.21. The three bold values along the top vertical axes denote the mean electrical breakdown strength of the compositions. The height of the bars show the BDS of the individual sheets, and associated standard error of means are plotted as error bars.

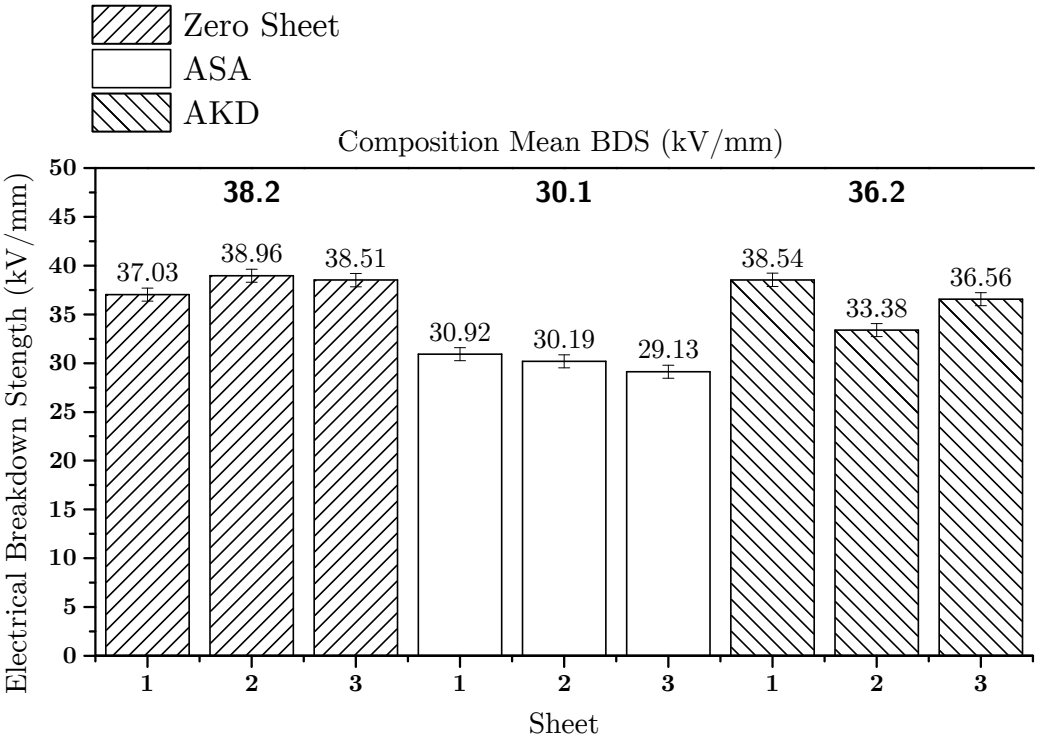

FIGURE 7.21: Mean electrical breakdown strength of the paper compositions in the sizing trial. Error bars denote the standard error of the mean.

Further analysis of the electrical breakdown events by nested ANOVA provides variance components which show that 76.60 % of the total variance is due to the difference in the paper compositions, compared to 11.06 % and 12.34 % for the variation in the individual handsheets and error respectively. This suggests that the differences due to the paper modifications are indeed the main contributor to the differences in electrical breakdown strength. Tukey Pairwise comparison among the paper compositions at a confidence level of 95 % shows not only that the two paper modifications are significantly different from the zero–sheet type, but also that they are significantly different from each other. Figure 7.22 provides the results of an analysis of the residuals, suggesting that the underlying assumptions of independence of observations and normal distribution have not been violated. It may therefore be concluded, that modifying paper by applying AKD or ASA sizing does not lead to a significant ($\alpha = 0.05$) improvement in electrical breakdown strength of paper.

As mentioned previously in Section 7.2, the Weibull analytical method is a common way

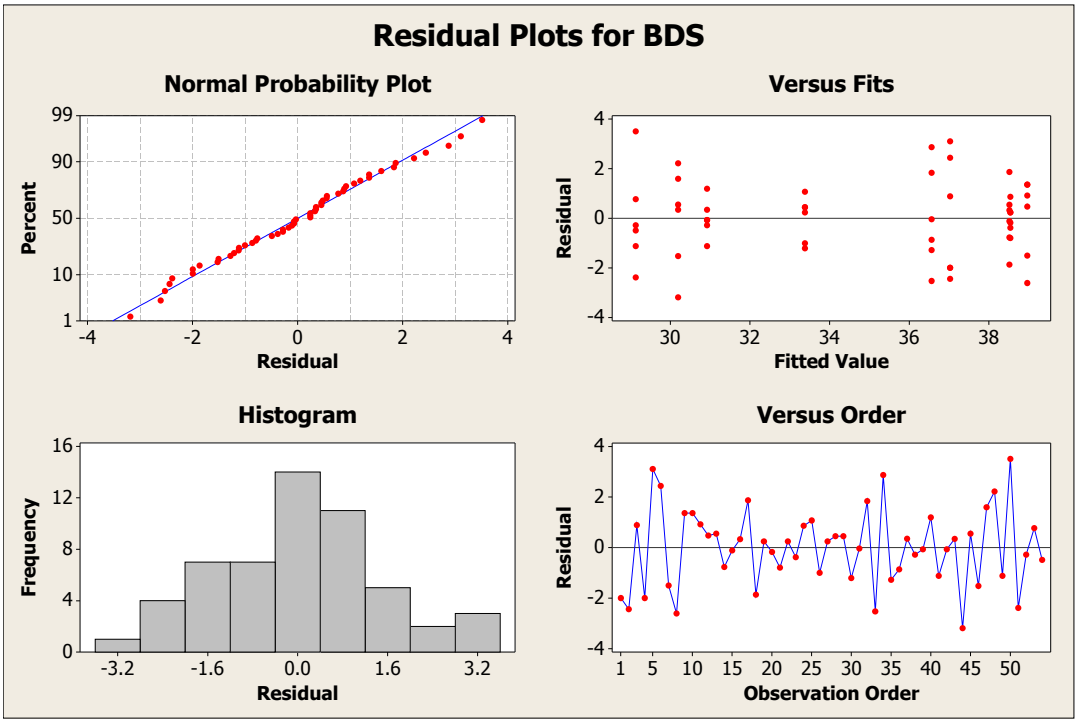

FIGURE 7.22: Residual analysis of the sizing trial.

to interpret breakdown data in the electrical industry. Figure 7.23 shows the Weibull plots of the individual sized paper compositions and their associated parameters. The measures of fit stated inset in the graph show that the chosen 2–parameter Weibull distribution is an acceptable fit for all but the AKD samples, at a confidence level of 95 %. The divergent performance of the individual sheets that were tested for the AKD composition was illustrated in the boxplot previously, and reduces the fit of the otherwise applicable probability distribution for this composition.

The statistical analysis shows clearly, that the samples containing the ASA sizing agent did not perform as well as the AKD sized papers. Whether this is due to the semi–ester, or, more likely due to the hydrolysed product (substituted succinic acid) or due to the cationic starch necessary for the dispersion of ASA, can not be concluded from these measurements. However, the overall effect of ASA results in decreased electrical breakdown strength. Similarly, but not as pronounced as with ASA, the addition of the sizing agent AKD also reduces the electrical breakdown strength. Again, it is impossible to differentiate in this trial, whether the effect is due to the sizing agent AKD, due to the hydrolysed by-product (Ketone) or due to the added starch emulsion agent. In summary, none of the trialled sizing agents had a positive effect on the electrical breakdown strength of paper.

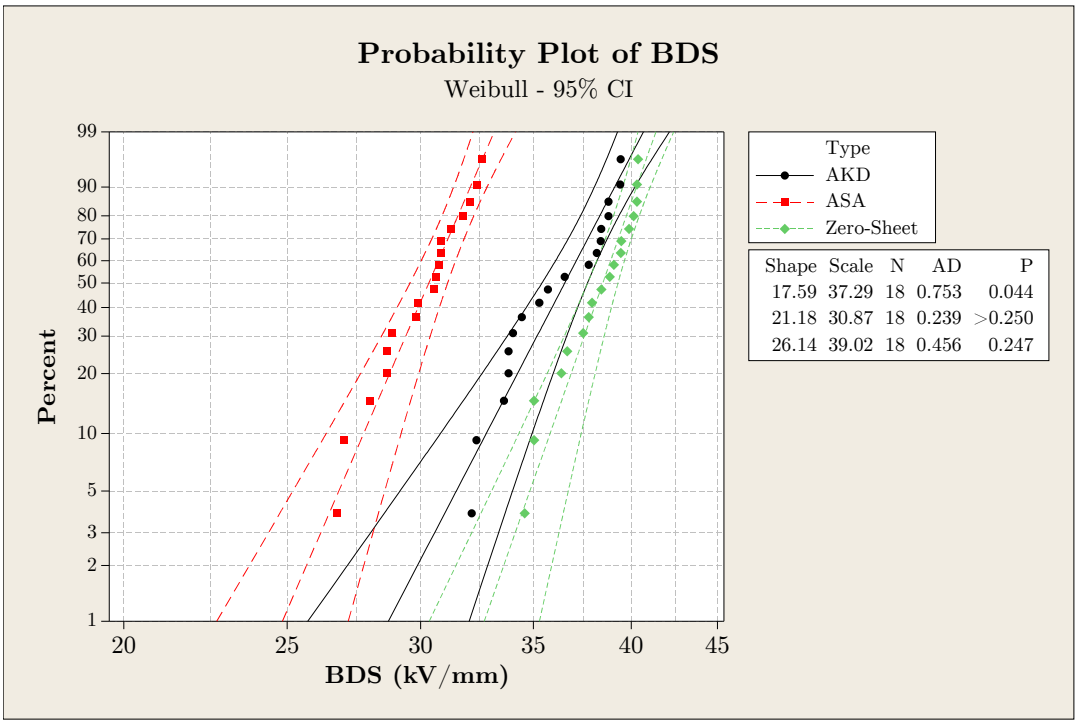

FIGURE 7.23: Weibull probability plot of all the paper compositions in the sizing trial.

7.5.3 Polyvinyl Alcohol Trial

Polyvinyl alcohols are employed in the paper industry because they impart good cohesion and adhesion to fibers, fillers and pigments. PVA has been introduced in Section 7.1.8 and results were presented in Section 7.5 for an exploratory trial where PVA was used with starch. The apparent positive effect motivated a more detailed further study in order to verify previous findings and to see whether different grades of polyvinyl alcohols would have different effects. The following grades of PVA were selected for the trial:

Mowiol 56-98 an example for a highly-viscous and fully hydrolysed polymer that forms a film which is resistant to cold water. This has applications in for example the production of special paper laminates or and sealing materials for packaging.

Kuraray KL-506 a carboxylated polymer that, at the same degree of hydrolysis, shows stronger hydrophilic properties than conventional PVA and therefore dissolves in water more easily.

Kuraray HR-3010 a super hydrolysed PVA with close to 100% hydrolysis. It is understood that fully hydrolysed polyvinyl alcohols show higher water resistance due to their higher degree of crystallinity, than do partially hydrolysed polyvinyl alcohols. Super hydrolysed polyvinyl alcohol allows high levels of filler such as talcum, to be added to the paper formulation.

The following Table 7.1 provides some further information on the three PVA products that are compared in the following PVA trial:

Table 7.1: Grades in the PVA Trial

PVA Grade	Viscosity [mPa s] as 4% aqueous solution at 20°C	Degree of hydrolysis [mol-%]	Max ash content [%]
Mowiol 56-98	56 ± 4,0	98,4 ± 0,4	1
Kuraray KL-506	5,2-6,2	74-80	1.5
Kuraray HR-3010	12.0 - 16.0	99.0 - 99.4	0.4

Figure 7.24 presents the data of the PVA trial in a dotplot for a visual inspection. The legend of the graph clarifies the structure of the trial. Paper compositions containing 1% or 2% of the different grades of PVA in combination with 2% starch and 25% talcum, were trialled against a zero sheet containing only starch and talcum as well as against a control paper containing only pulp. The corresponding boxplot (Figure 7.7) was already provided in Section 7.2 as part of the introduction of the statistical methods. The dotplot and boxplot provide the immediate impression that differences among the grades of PVA, as well as between the zero sheet and the PVA modified papers, are only very small. Furthermore, it shows that in the absolute zero composition i.e. the pure pulp paper, there is an outlier to the left, i.e. a handsheet that performed poorer than the other sheets in that composition. Similarly, there is a sheet with a large spread of data in the 1% Mowiol 56-98 + (2% starch + 25% Talc) composition, that ranges to the right, i.e. shows breakdown strength values that are much higher than others in its composition. The interquartile range of the different papers also provides a visual impression of the homogeneity, i.e. formation, of the individual handsheets. It appears that the handsheets that entail Mowiol 56-98, show a less defined breakdown point than the other compositions.

The variance components computed as part of a nested ANOVA reveal the challenges in the dataset. The variation in the data is to only 39.32 % due to the differences in the paper compositions, to 19.39 % due to error, and principally (41.28 %) due to a variation between the individual handsheets. In other words, because the homogeneity in the handsheets was limited by the laboratory conditions, the results of the trial are obscured by the variation in the handsheets. A rigorous statistical analysis is required, to prevent inaccurate conclusions. Nevertheless, significant results may be obtained from this difficult dataset. The situation may be clarified by the grouping information provided by the Tukey method (at 95% confidence). Table 7.2 tabulates the results for the individual paper compositions. All the compositions that share the same grouping letter have means that are not significantly different from each other at a confidence of 95 %. The results show that the unmodified paper performed significantly poorer than any of the talcum filled papers. The composition containing 1% KL-506, performed better than the unmodified paper, but not significantly better than the zero sheet, i.e. the composition containing only talcum. Two other compositions performed insignif-

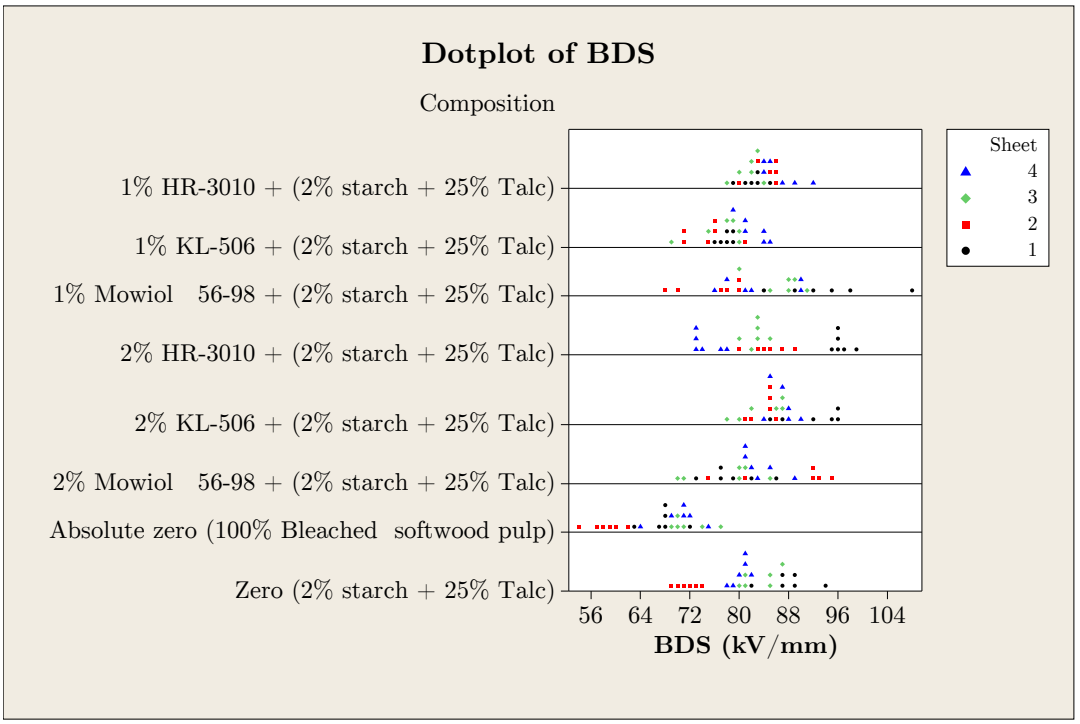

FIGURE 7.24: Dotplot of the PVA data.

icantly better than the zero sheet, namely those containing 2% Mowiol 56-98 or 1% HR-3010. The compositions containing Mowiol 56-98 could not be distinguished significantly from those containing HR-3010, at either concentration. The top four paper compositions contained 2% KL-506, 1% Mowiol 56-98 or HR-3010 performed equally well at the chosen confidence level. In summary, only the top three compositions i.e. 2% KL-506, 1% Mowiol 56-98 and 2% HR-3010, performed significantly better than the zero sheet. The composition that performed best and worst, is that containing PVA KL-506. This grade is different in that, unlike the other polyvinyl alcohols, the KL-506 grade is a partially carboxylated polymer. At the pH–values of normal paper production, the carboxyl groups i.e. organic acids, appear as salts and therefore tend to increase conductivity. The superior performance of the KL-506 PVA grade may therefore be a result of increased conductivity, and not in fact an increase in insulating quality.

The analysis of the residuals for the PVA trials was presented in Figure 7.9 as part of Section 7.2 and shows no violation of the statistical presumptions.

A Weibull analysis of the same results is shown in Figure 7.25 in a single graph, and separate Weibull plots are presented, one per composition, in Figure 7.24 (a) to (e). The plot with the smallest Weibull scale parameter is that of the absolute zero sheet which contains no talcum filler. All other compositions are clustered closely, as expected from the statistical analysis. Figure 7.25 shows that all papers containing talcum exhibit, as expected, a higher electrical breakdown strength than the reference sheet without tal-

Table 7.2: Tukey method grouping information on the PVA paper compositions with a confidence of 95%.

Paper Composition	N	Mean	Grouping				
2% KL-506 + (2% starch + 25% Talc)	24	86.52	A				
1% Mowiol 56-98 + (2% starch + 25% Talc)	24	84.88	A	B			
2% HR-3010 + (2% starch + 25% Talc)	24	84.64	A	B			
1% HR-3010 + (2% starch + 25% Talc)	24	83.75	A	B	C		
2% Mowiol 56-98 + (2% starch + 25% Talc)	24	82.07		B	C		
Zero (2% starch + 25% Talc)	24	80.78			C	D	
1% KL-506 + (2% starch + 25% Talc)	24	77.87				D	
Absolute zero (100% Bleached softwood pulp)	24	66.99					E

cum. The addition of different amounts (1% or 2%) of PVA does not significantly effect the breakdown strength of the paper samples. However, the addition of PVA showed an improvement in the dielectric spectroscopy measurements (Figure 7.18). Nevertheless, the addition of PVA has a supporting influence on the dispersion of the talcum filler, and increases the mechanical strength of the paper. It is therefore an advantageous chemical additive from a paper making perspective.

Separate Weibull probability plots for one of each of the individual paper compositions are shown in Figure 7.24. The individual polyvinyl alcohols were selected on the basis of their different molecular weight and degree of hydrolysis. The measures of fit show that the data of some of the compositions may not be fitted well by the 2–parameter Weibull distribution. The very good fit of some of the papers, combined with the experience in the other paper trials, suggests that this is primarily due to a variation in the formation of the handsheet, and not a characteristic of the electrical breakdown process.

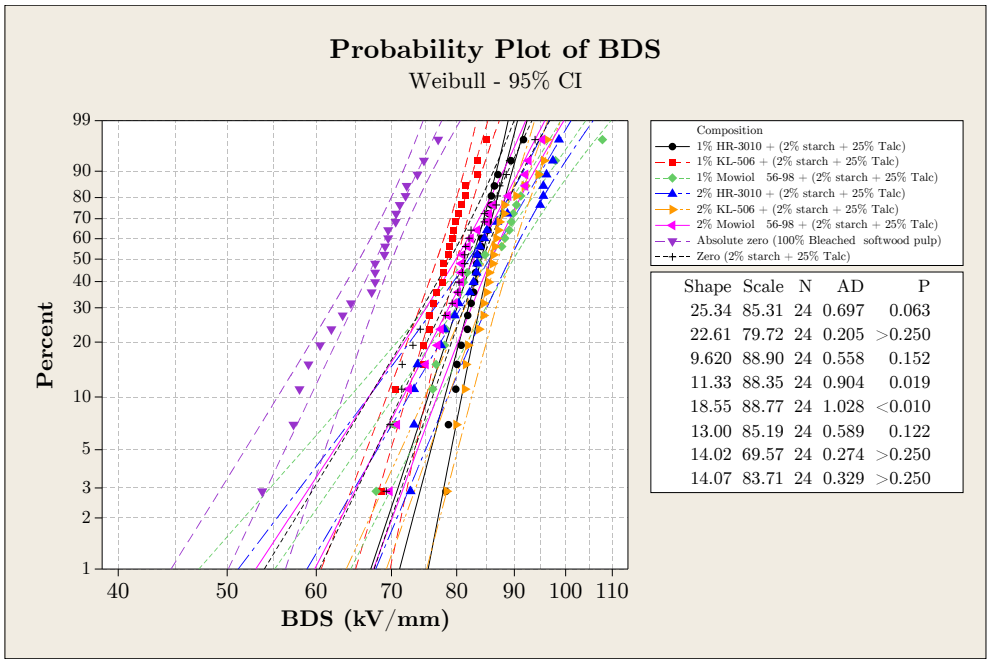

FIGURE 7.25: Weibull probability plot of all the PVA trial paper compositions.

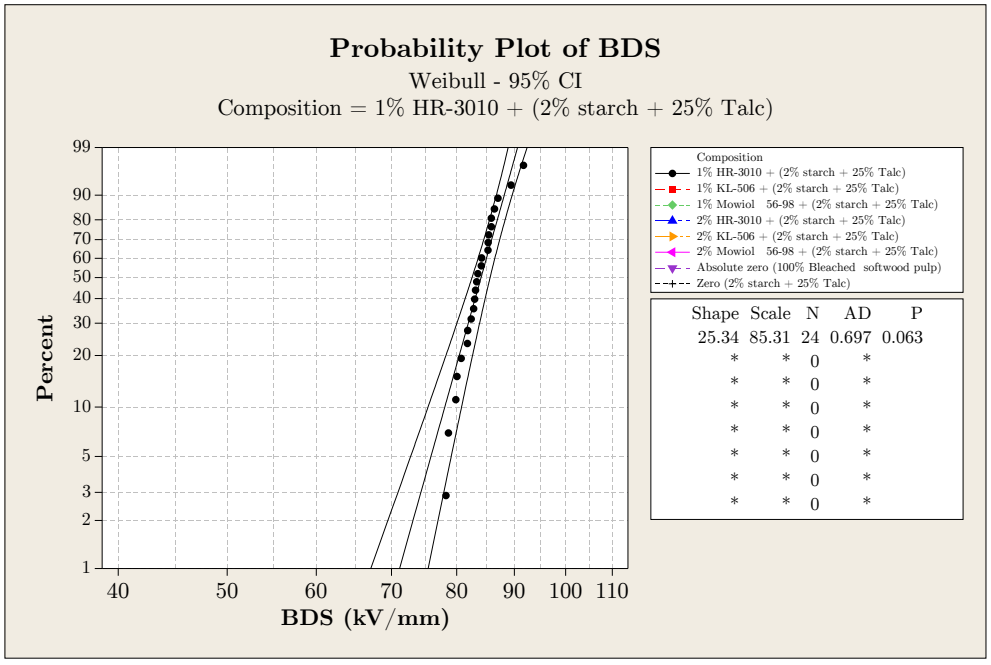

(a) Weibull probability plot of 1% HR-3010 + (2% starch + 25% Talc)

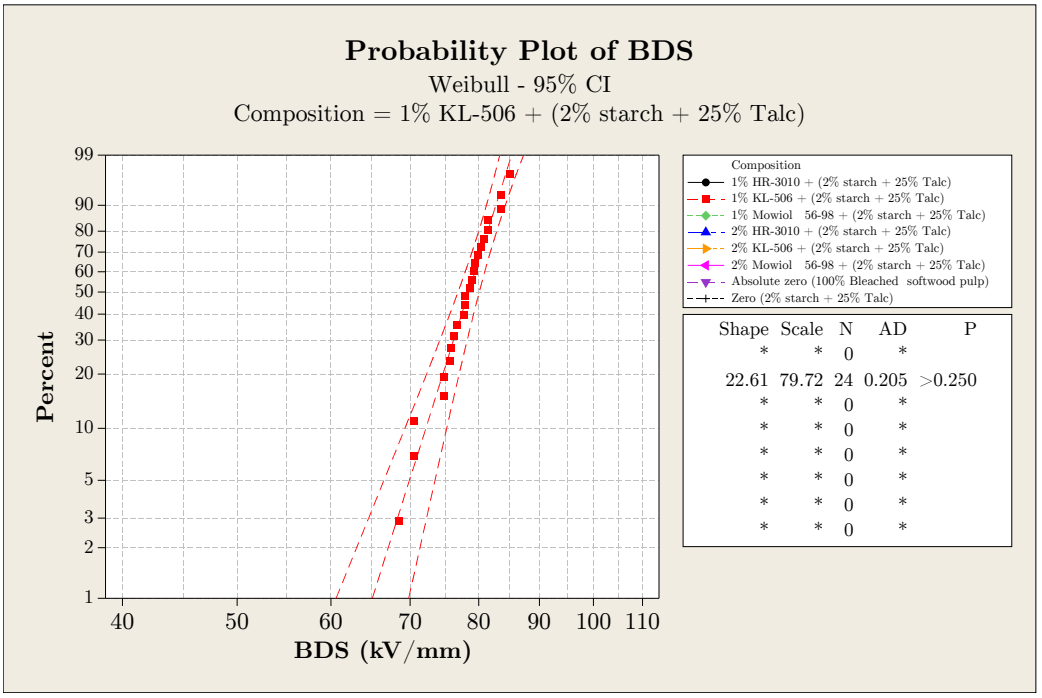

(b) Weibull probability plot of 1% KL-506 + (2% starch + 25% Talc)

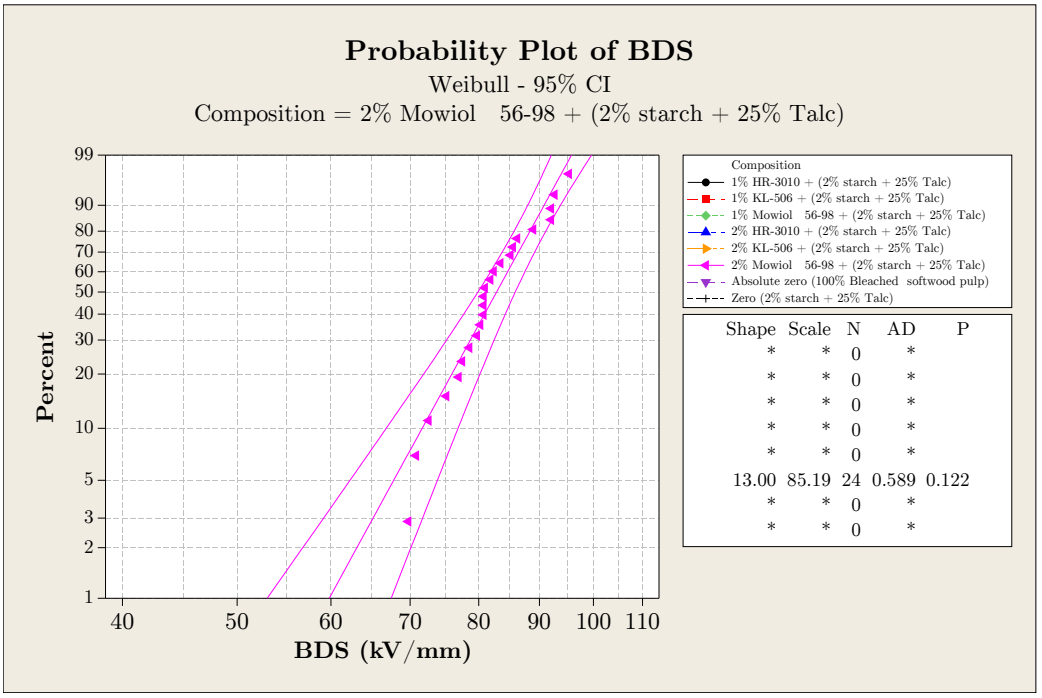

(c) Weibull probability plot of 2% Mowiol 56-98 + (2% starch + 25% Talc)

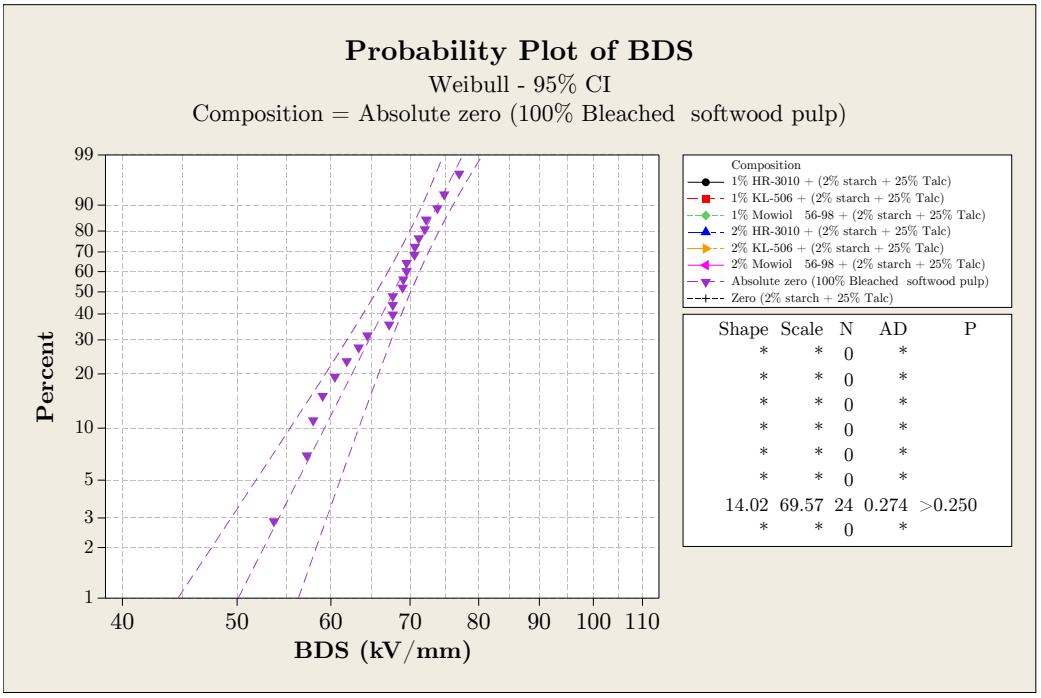

(d) Weibull probability plot of the absolute zero sheet (only bleached softwood pulp)

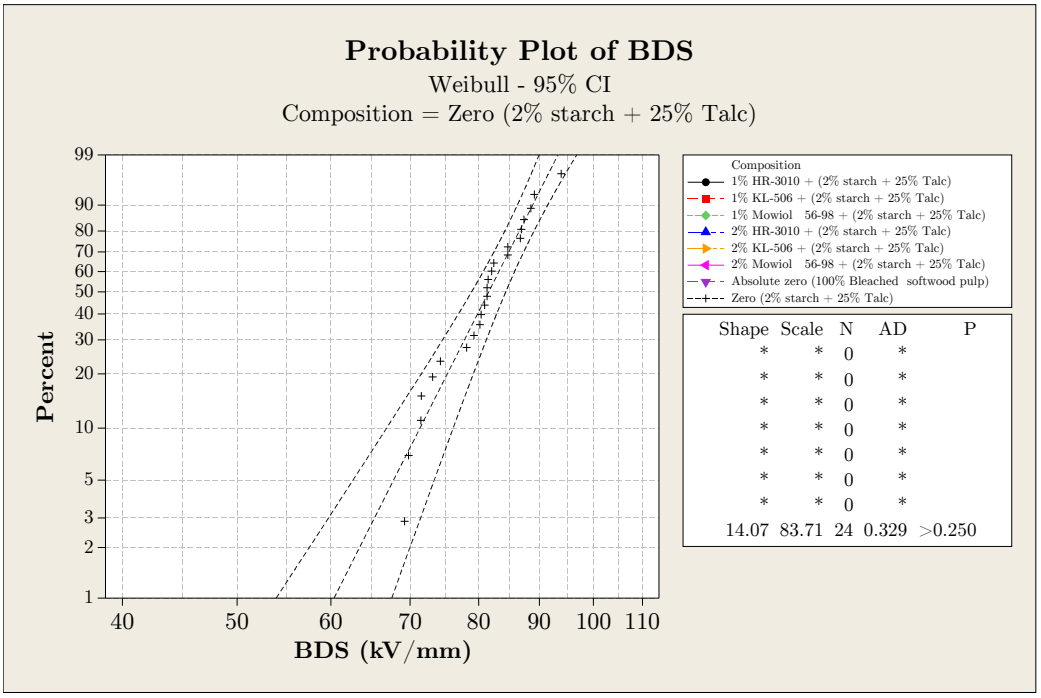

(e) Weibull probability plot of the zero sheet (2% starch + 25% Talc)

FIGURE 7.24: Separate Weibull probability plots for one of each of the paper compositions in the PVA trial.

7.5.4 Guar Gum and Starch Trial

Guar, also called guar gum, consists of D-mannose in the form of the polysaccharide galactomannan. It is primarily harvested from guar beans and typically produced as a pale, coarse to fine powder. Guar is employed in the paper industry to provide a denser surface to the paper, which in turn improves writing properties, bonding strength and surface hardness [144]. In the electrical industry it has been suggested as a water–blocking compound for the application in polymer power cables to prevent water–treeing [145]. In view of its addition to electrical insulation papers, guar gum is of interest because it has qualities that add to the mechanical breaking and folding strength of the paper[146, 147]. Due to its comparably high price, guar is only used in the paper industry in small amounts and usually in the presence of starch [45].

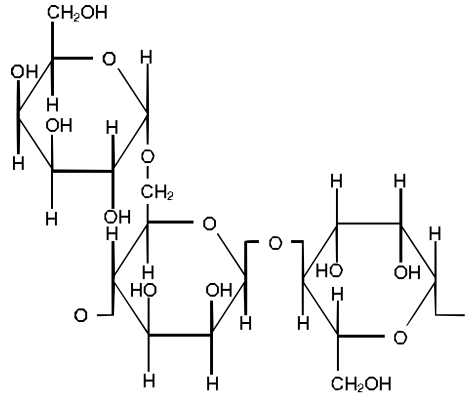

FIGURE 7.25: Chemical structure of guar gum. [145]

Similar to the talcum powder, the guar gum was mixed in water to form a slurry and then added to the pulp before it was poured into the sheet former. Figure 7.27a presents the guar gum and starch trial data in a Weibull probability plot. The measures of fit highlight the fact that the composition consisting of 25% talcum and 3% cationic starch, is not fitted well. From the dotplot and boxplot in Figure 7.26a and Figure 7.26b respectively, it may be concluded that this is primarily due to the fourth handsheet that was tested in this composition. When excluded, the remaining data fits the 2–parameter Weibull distribution very well (Figure 7.27b). The Weibull plot illustrates that all of the paper samples that were modified with guar gum or starch, are enclosed by the data of the absolute zero sheet (pulp only) on the lower end of the breakdown scale, and by the zero sheet (25% talcum, no additives) on the upper end of the scale. It follows that none of the modifications tested in this trial, actually improve the electrical breakdown strength of paper.

This conclusion is further validated and illustrated by a contour plot (Figure 7.28) showing different combinations of the additives in this trial. Electrical breakdown strength only increases for treatment combinations including talcum. The addition of talcum is shown in the top row, going from left to right. All other treatments have either none, or a detrimental effect on the electrical breakdown strength.

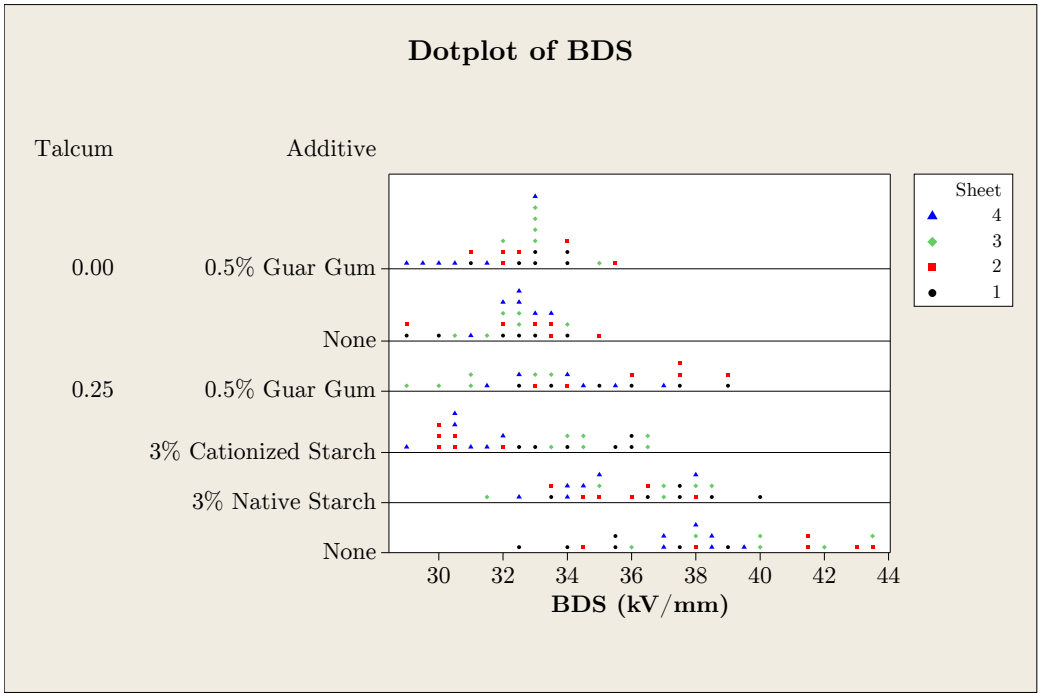

(a) Dotplot of the guar gum and starch trial data.

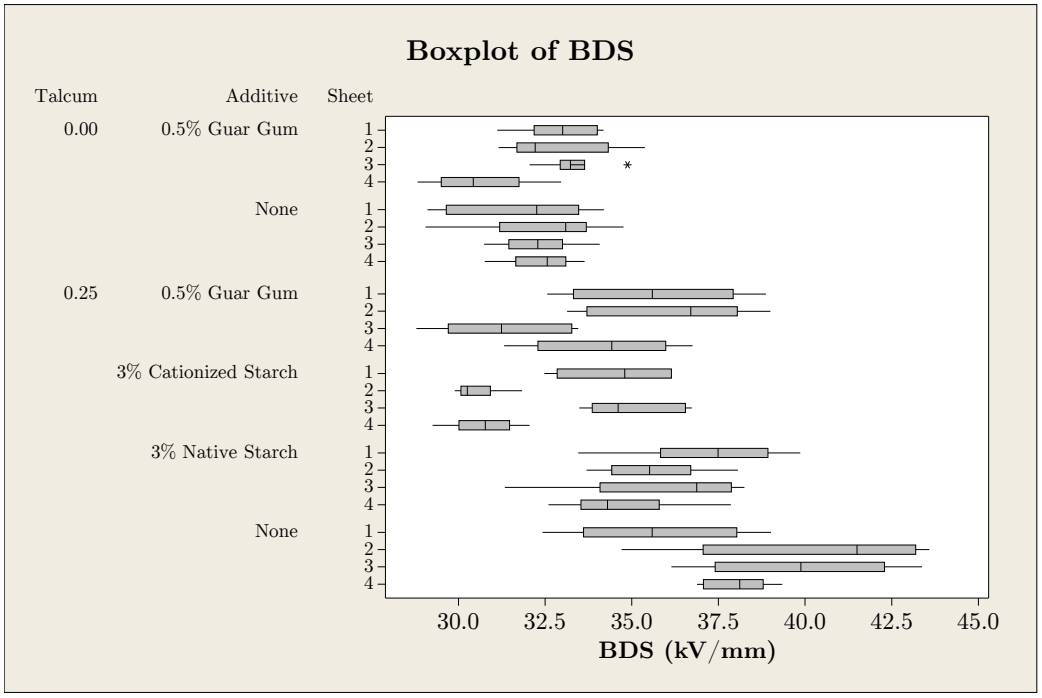

(b) Boxplot of the guar gum and starch trial data.

FIGURE 7.26: Dotplot and boxplot of the guar gum and starch trial data.

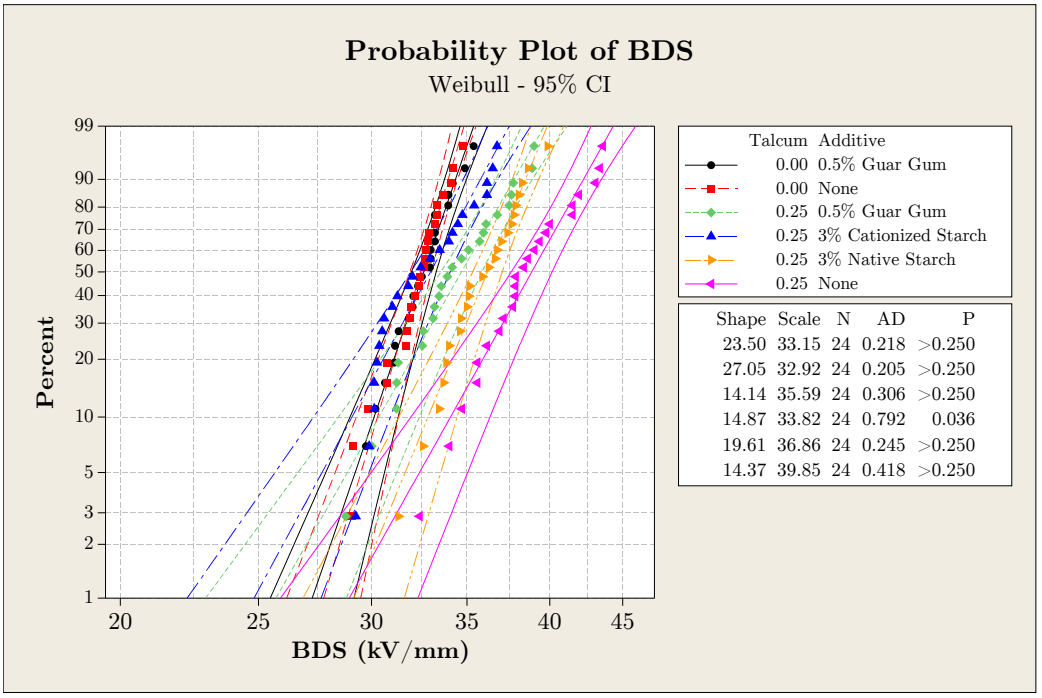

(a) Weibull probability plot of the paper compositions in the guar gum and starch trial.

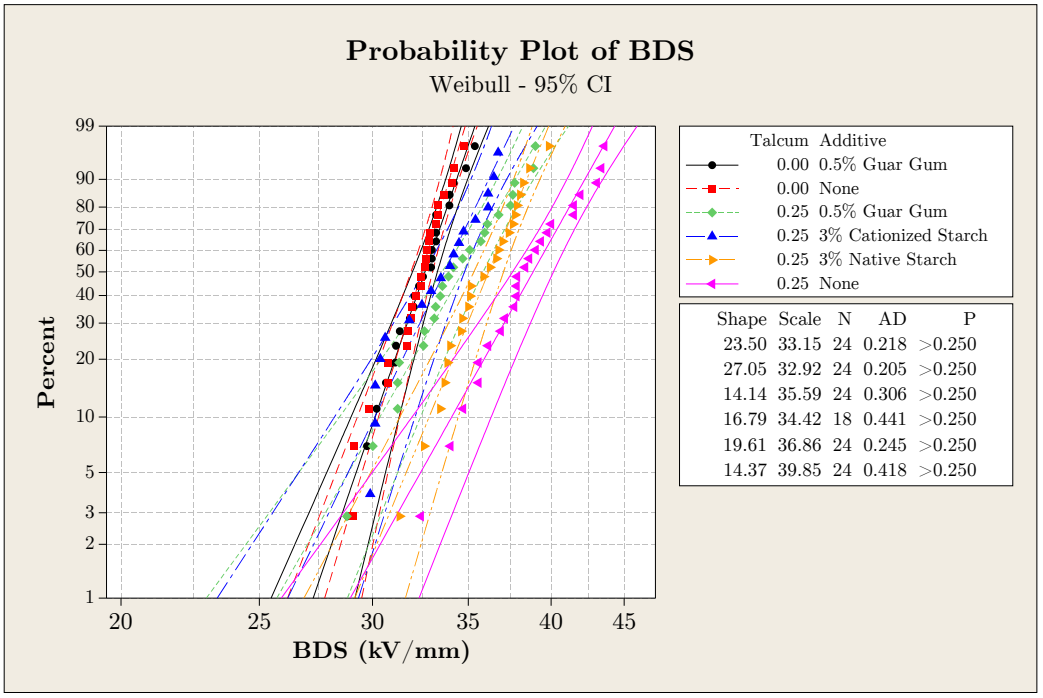

(b) Corrected Weibull probability plot of the paper compositions in the guar gum and starch trial.

FIGURE 7.27: Weibull probability plot of the paper compositions in the guar gum and starch trial.

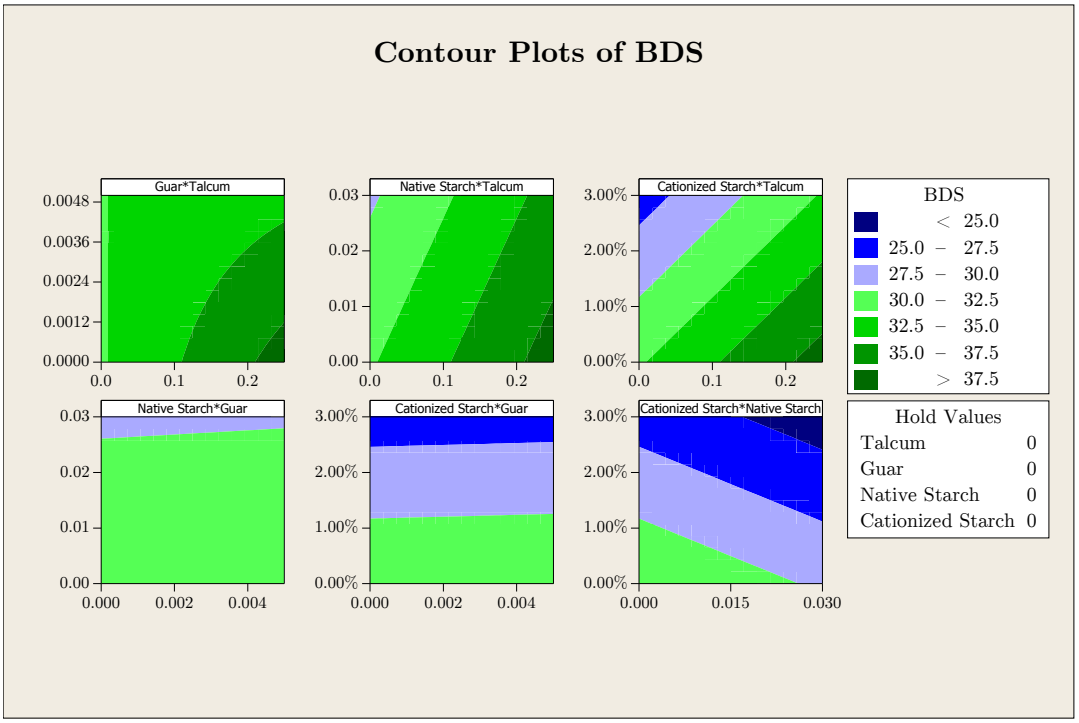

FIGURE 7.28: Contour plots of the effect of guar gum and different grades of starch on electrical breakdown strength of paper.

7.5.5 Polymer Sizing, Dry– and Wet–Strength Agents Trial

The following polymer sizing, dry– and wet–strength agents were investigated in this trial:

Basoplast 400 DS (0.4%) is a polystyrene-acrylate-dispersion commonly used as a polymer sizing agent in paper production. Due to the acrylate groups, the overall charge of the compound is slightly anionic, but still hydrophobic. Polymer sizing agents turn the surface of hydrophilic cellulose fibres more hydrophobic by coating the fibres with a hydrophobic polymer film.

Giluton DSK (1%) is a cationic polyvinylamine dry–strength agent. It acts by creating strong hydrogen bonds between polyvinylamine and closely located cellulose fibres.

EKA WS 505 (2%) is a typical wet–strength agent based on poylamidoamine–epichlorohydrin (PAAE) resin. The wet–strength is a result of the formation of new covalent bonds between the PAAE resin and adjacent amino groups or hydroxyl groups of the cellulose.

A general linear model analysis of the trial data provides grouping information using the Tukey method at 95% confidence. Table 7.3 tabulates the results and confirms

that the talcum filled papers all performed better than the unfilled and unmodified reference composition. However, the composition consisting of 25% talcum and 1% dry–strength agent, did not perform significantly better at the chosen confidence of 95%. The paper compositions containing the wet–strength agent as well as the polymer sized papers, performed significantly better than the unmodified but talcum filled reference sheet. The same Tukey method (see Section B.4) also shows that there is a significant difference between the unfilled and the talcum filled samples across the entire trial.

TABLE 7.3: Tukey method grouping information of the polymer sizing, dry– and wet–strength agents trial with a confidence of 95%

Filler	Additive	N	Mean	Grouping		
25% Talc	0.4% Polymer Surface sizing	24	44.56	A		
25% Talc	2% Wet–strength Additive	24	43.57	A		
25% Talc	None	24	39.25		B	
25% Talc	1% Dry–strength Additive	24	37.38			C
None	None	24	35.03			C

The action and mechanism of these chemical paper additives is not fully understood, thus it is not possible to draw direct conclusions between the chemical formula and the electrical breakdown strength. The superior performance of the polymer sizing agent may be the result of comparably low charge and the tendency to fill in voids in the surface of the paper.

The Weibull analysis in Figure 7.29a shows the same result as the ANOVA statistics in Table 7.3. The addition of 0.4% polymer sizing agent to the 25% talcum filled paper, yielded the highest electrical breakdown strength. This is followed by the paper containing 2% wet–strength agent and 25% talcum. Paper containing 1% dry–strength agent shows lower electrical breakdown strength than paper only filled with talcum i.e. this type of dry–strength agent reduces the positive effect of the talcum filler on the electrical breakdown strength. The Weibull analysis of the data is shown in Figure 7.29a. The measures of fit suggest that the data of the zero sheet (25% talcum) and the composition containing 2% wet–strength agent, are not fitted well. When the problematic sample in each composition is excluded, a very good fit may be achieved (see Figure 7.29b).

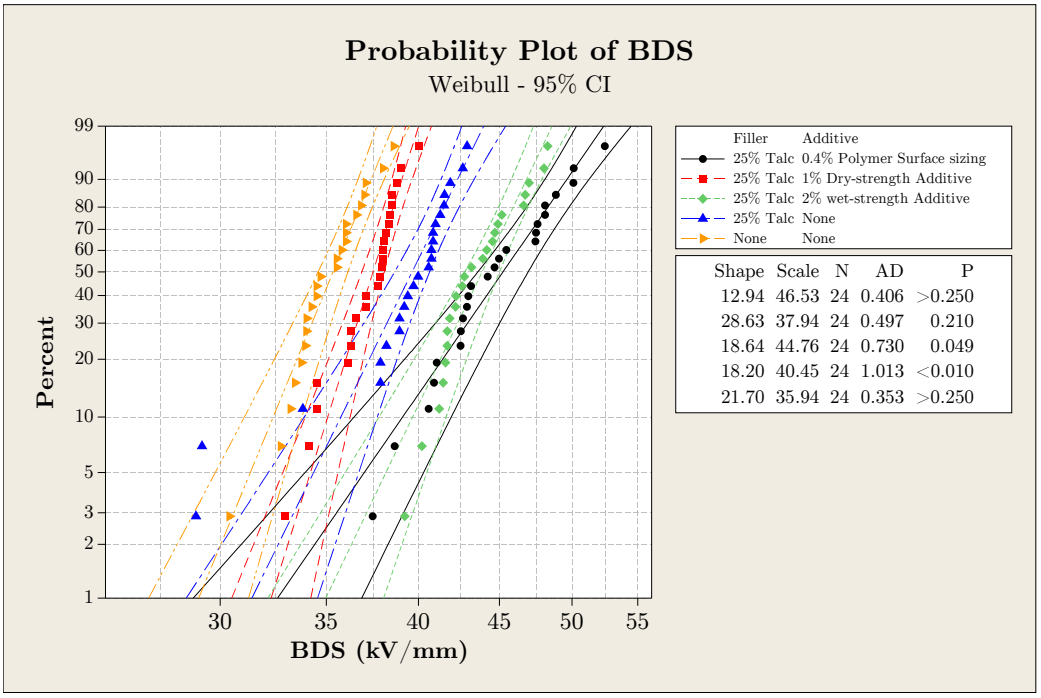

(a) Weibull probability plot of the paper compositions in the polymer sizing trial.

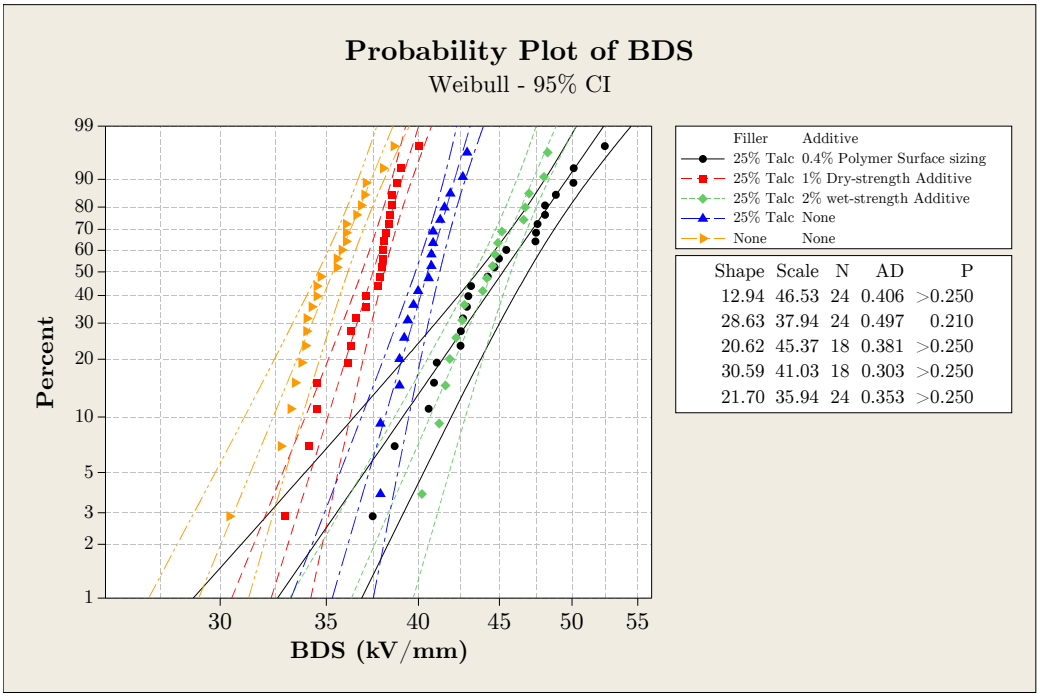

(b) Corrected Weibull probability plot of the paper compositions in the polymer sizing trial.

FIGURE 7.29: Weibull probability plot of the paper compositions in the polymer sizing trial.

7.6 Discussion

The industry standard unbleached softwood kraft pulp outperforms bleached softwood and hardwood pulp in terms of electrical breakdown strength. In comparison to unfilled papers, hydrophilic bentonite filler has been found to degrade the electrical performance of the paper while the hydrophobic talcum filler clearly improves it. Highly filled papers suffered from a reduction in mechanical strength and additives were trialled to address this effect. PVA and starch both increased mechanical as well as electrical strength. The dielectric performance, however, was reduced significantly by the addition of the cationic starch and only remedied slightly by the PVA. Calendering increased the electrical and mechanical strength of the paper but reduced dielectric performance.

Calendered electrical insulation papers with talcum filler and strength agent additives such as starch and polyvinyl alcohol have shown to yield good mechanical performance and significant enhancements in electrical breakdown strength. Due to the reduction in tensile strength with increasing filler content, an application specific balance may be achieved between these paper properties. Dielectric performance as measured by dielectric spectroscopy was impacted by the cationic additives and also dependent on filler content.

The significantly different performance of the ASA sized papers in comparison to both the zero sheets as well as the AKD sized papers may be due to the fact that the ASA sizing agent is, for practical reasons, prepared and applied in a 3% starch emulsion. However, previous trials with starch and PVA suggest that starch has a positive influence on the breakdown strength of paper. Further experimental verification of the negative effect of ASA sizing on the electrical breakdown strength of paper should be obtained before it is permanently ruled out as a chemical additive in electrical papers. For the purpose of this work, however, the statistically significant differences in the performance of the sized papers are sufficient to discard AKD and ASA sizing as treatments for electrical papers. From an industrial perspective, sizing is an additional manufacturing step that has to be sustained by an improvement in performance of the product. This does not seem to be the case for electrical applications.

The comparative trial of different polyvinyl alcohols with varying degrees of hydrolysis, viscosity and ash content explored their effects on electrical breakdown strength and found that no decisive statistical difference could be ascertained between the different compounds. A similar comparison of dry–strength agents, specifically cationized starch, native starch and guar gum, showed no positive effect on the breakdown strength compared to paper filled only with talcum powder. The positive effect of talcum filler on electrical breakdown strength was demonstrated again by a comparison with unfilled paper.

Further experiments with a dry–strength agent, a wet–strength agent and a polymer siz-

ing agent were conducted. The results were analysed by ANOVA and Weibull statistics and show that the polymer sizing and wet–strength agents further increase the breakdown strength, whereas the addition of a dry–strength agent decreased the electrical breakdown strength. On the basis of these finding, further experiments in paper technology may be undertaken to find an optimum between tensile strength, and electrical insulation properties.

The 2 parameter Weibull analysis provides a pair of parameters to summarise the electrical breakdown behaviour of a material. The Weibull scale parameter provides a measure of the breakdown strength, similar to the mean value, and the Weibull shape parameter provides additional information about the spread of the data. Figure 7.30 shows an annotated scatter plot of the Weibull parameters of the different sets of data which provides a good overview and summary of the initial results. The desire is to find data points in the top- right corner of the graph denoting a high breakdown strength and a very narrow data spread representative of a distinct failure point. The talcum filled and calendered samples are found at the top of the graph. The samples with the lowest breakdown strength overall, are the bentonite filled samples. The lowest breakdown values for the talcum data and calendering data are the unfilled and uncalendered (zero) samples. The data series of the talcum and calendering trial are located at the top of the graph, whereas the bleached hardwood pulp papers show a smaller Weibul scale value i.e. breakdown value. The commercial papers show an interesting outlier to the left. That commercial paper (commercial 3) showed a comparably large spread in breakdown values which suggests an inhomogeneous formation of the paper sheet.

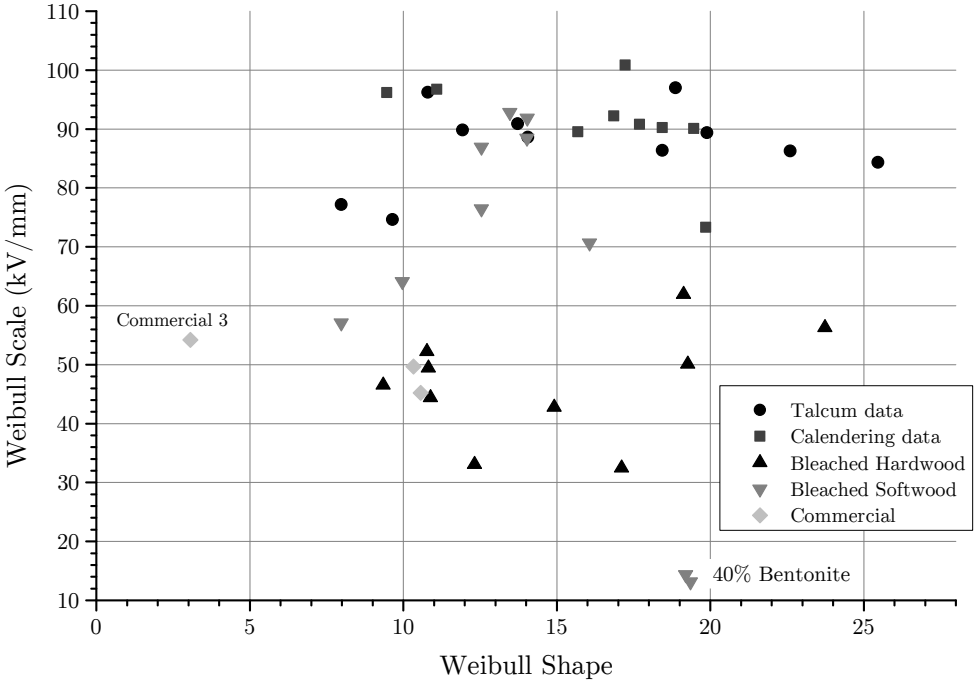

FIGURE 7.30: Summary of initial trials by means of a scatter plot of the Weibull parameters.

Figure 7.31 shows scanning electron microscope (SEM) images of two electrical breakdown sites in oil soaked, talcum filled paper samples at magnifications of ×400 and ×1000. The white talcum filler particles are clearly visible. The location of the breakdown holes indicates that the breakdown path avoided the fibres and progressed along the fibre–filler/oil interface. It has been suggested that the electrical breakdown in the paper–oil composite may be caused by internal partial discharges in voids or imperfections in the oil–filler matrix among the cellulose fibre reinforcements which may in turn lead to mechanical stress, local warming and erosion that would finally result in thermo–electric breakdown of the composite along a matrix–reinforcement interface [131].

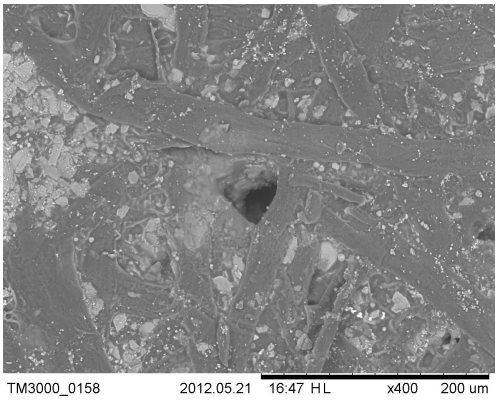

(a) Breakdown Site A

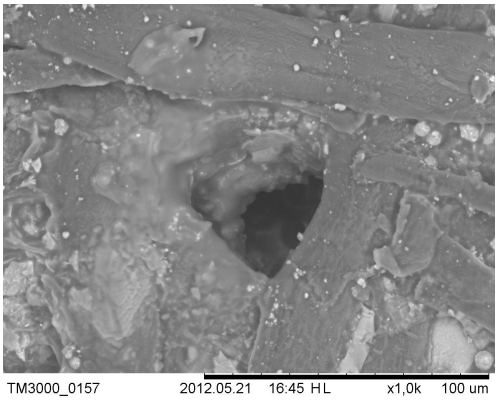

(b) Breakdown Site A

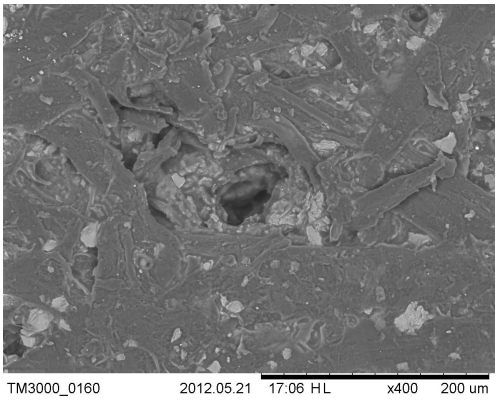

(c) Breakdown Site B

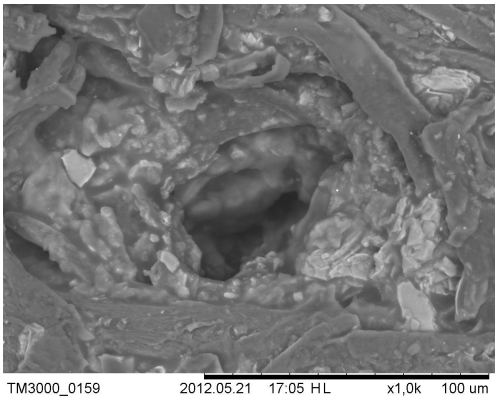

(d) Breakdown Site B

FIGURE 7.31: SEM images of a two breakdown sites in a 32% talcum filled paper made from unbleached kraft pulp and calendered once with 20 Newton.

Together with the last chapter, this chapter forms the heart of the thesis. The results of a series of constructive trials have been presented and discussed, with the aim to explore different modifications of paper and to investigate whether they would improve the mechanical, electrical and dielectric performance of paper in paper–oil composite insulation systems. The next chapter summarises and concludes the thesis.

Chapter 8

Conclusions

A general introduction of solid dielectric systems was expanded by a consideration of the behaviour of solid dielectrics at low temperature. A categorical overview of polymers, ceramics and glasses, as well as polymer composites was then followed by a closer look at a number of synthetic and natural materials that are commonly characterised by thermally stimulated current measurements.

Direct measurement techniques for the investigation of electrical processes in solid dielectrics have been reviewed. It was shown that electro–acoustic, thermal and pressure wave propagation methods all rely on the perturbation of the equilibrium between elastic and electrostatic forces and consequently all work to measure the same electrical information in a sample. Their respective strengths and weaknesses have been discussed and the complementary nature of thermally stimulated current spectroscopy has been highlighted. An overview of the aforementioned measurement technologies has been provided and a summary drawn based on their excitation, scanning mechanism, detection, resolution and deconvolution. Due to the objectives of this research, the Thermally Stimulated Discharge Current method is of special interest. Like PEA, TDM and PWP techniques, TSDC is a physically non-destructive method. This make it possible to measure the same sample several times and thus to observe time and temperature dependant relaxation processes. TSDC allows the study of charge storage, dipolar relaxation events, space charge redistribution, decay phenomena and the migration of ionic charges. It thus reveals information about the nature of the charge or polarised species present in the sample and provides insight into the propensity of a material to acquire and store charge.

The design and construction of a TSDC Spectrometer has been completed successfully. The TSDC contains an electrode with a large area and is equipped with a guard ring on the measurement side. A computer driven automation has been implemented and proven to work. Control of the temperature within the testing environment has been implemented and verified to work with the latest hardware and software. A combined cooling

and heating system with associated dual-loop temperature controller allows for precise temperature control. A custom LabVIEW programme provides a modern user interface for the instrument control. This permits the settings of experimental parameters and automatically protocols the results from the ammeter, the temperature controller and the high-voltage supply. Apart from the file output path, which the software prompts for at the start, all other parameters may be set, changed or unset at any time during the experiment. A built-in timer feature allows for a recording to finish in the absence of an operator. Besides the software design, the new instrument design includes several other security features to protect the operator or the TSDC instrument from harm. The opening and closing of the heavy cryostat as been motorised and linear guide rails assure the repeatable mating of the vessel and the lid. The entire apparatus is enclosed in an interlocked rack that provides further shielding for the measurement system as well as protection for the operator. While it is generally possible to undertake TSDC measurements in any atmosphere, all measurements in this thesis were performed in an insulating dry nitrogen atmosphere to suppress discharges inside the cryostat. Extremely pure and separately dried nitrogen gas was used. The correct function of the TSDC has been proven with the two common and well characterised synthetic polymers; LDPE (low density polyethylene) and PET (polyethylene terephtalate). LDPE as a well characterised polymer was used as the first candidate to test the performance of the new TSDC instrument. The Weibull scale parameter of a direct current electrical breakdown test was found to be $490\,\mathrm{kV\,mm^{-1}}$ with a shape factor of 9.7 and was accepted as an approximate upper limit on the non-critical field strength.

The peak on the TSDC measurement of LDPE was found to be at 292 K and an activation energy of 1.7 eV was calculated using the asymptotic method. The LDPE spectra returned by the TSDC spectrometer deviate slightly from those published elsewhere in terms of the temperature of the current peak, the calculated activation energy, however, agrees very well with published findings. To further verify the operation of the TSDC Spectrometer, measurements with biaxially oriented PET, a another very well characterised polymer, were performed. The measurement of breakdown strength resulted in a Weibull scale parameter of $466\,\mathrm{kV\,mm^{-1}}$ and a shape factor of 13. The measurements of PET conducted with the TSDC instrument showed two peaks at 405 K and 350 K, which agrees very well with the published information for the ρ–peak and α–peak of PET. Lower polarisation voltages reduced the magnitude of the ρ–peak and thus confirms the results from literature. The independence of the α–peak from temperature indicated that this peak is caused by dipole polarisation and may be related to conformational changes within the glass transition temperature range. The TSDC spectra as well as the dependency of the peak magnitude on polarisation voltage showed very good correlations to the published data, and therefore proved the correct operation of the TSDC Spectrometer.

For measurements of a natural polymer, first TSDC spectroscopy measurements of an

oil immersed cellulose paper were undertaken. The samples were vacuum dried and oil soaked paper containing 17.5% talcum filler, 1.5% starch, 1% PVA and 1.5% wet–strength agent. They exhibited a broad and pronounced peak around 332 K. Consecutive measurements showed that the peak magnitude increased on subsequent observations which is in agreement with normal conditioning effects. Activation energies of 0.57 eV and 0.77 eV were calculated. First measurements of vacuum oil impregnated samples of unmodified and talcum filled papers resulted in spectra that showed peaks for both positive and negative current. The peculiar but reproducible TSDC response of the vacuum oil impregnated paper samples is not readily explained. The similarities between the spectra of the unmodified and the talcum filled samples, supports the conclusion that this is due to the basic nature of the paper–oil composite, and not solely an effect of the filler component. TSC spectra of mineral oil impregnated polypropylene have been reported to have a similar overall shape, and suggest a strong influence of the mineral oil on the overall response of the solid–liquid composite. In order to gain a better understanding of the basic paper parameters that influence the thermally stimulated discharge current response, or more generally, the electrical performance of modified papers, a series of constructive trials with different fillers and chemical additives was undertaken.

A series of investigations have been performed to find an insulation paper with higher electrical breakdown strength at comparable or improved dielectric performance. All BDS measurements were performed as progressive stress tests on paper samples in insulation oil. The response of the samples to alternating currents across a wide spectrum of frequencies was obtained by dielectric spectroscopy. Measurements of the various modified papers were performed and contrasted in self–contained scientific trials. Conclusions were drawn on the basis of rigorous statistical analysis. For the first time, an insulation paper was measured with BDS, DS and TSDC that contained a high amount of filler. A hydrophilic and a hydrophobic filler material were contrasted in the form of papers filled with bentonite or talcum respectively. Bentonite was found to reduce breakdown strength, but the talcum filled papers yielded remarkably high breakdown strength values. The resulting comparison between commercial papers and a set of talcum filled samples with varying degrees of filler content revealed that the greater electrical breakdown strength of the talcum filled papers is balanced by a small reduction in dielectric performance. The data suggest a linear trend and an inverse relationship between the amount of filler and dielectric performance. A calendering trial was performed to investigate the effect of such a mechanical processing step on the electrical breakdown strength and dielectric properties of paper–oil insulation systems. Results showed that electrical breakdown strength is increased, but dielectric characteristics are reduced by calendering. The pressure magnitude rather than the number of applications appears to be the deciding factor.

Additional trials were performed with chemical additives in order to investigate the pos-

sibilities to further enhance electrical and mechanical paper properties. Trials were run with PVA, starch, sizing agents, guar gum as well as a dry and wet strength agent. The trials with starch as well as polyvinyl alcohol showed positive effects on mechanical tensile strength and electrical breakdown strength, but at the expense of real relative permittivity and the dissipation factor values. A further trial compared polyvinyl alcohols with different degrees of hydrolysis, viscosity and ash content for their effects on electrical breakdown strength and found that no decisive statistical difference could be ascertained between the different compounds. The popular sizing agents Alkenyl Succinic Anhydride (ASA) and Alkyl Ketene Dimer (AKD) were investigated for their effect on the electrical breakdown strength of electrical paper–oil insulation. Neither compound was found to have statistically significant beneficial effects. A comparative trial of dry–strength agents, specifically cationized starch, native starch and guar gum, also showed no positive effect on the breakdown strength in comparison to paper filled only with talcum powder. The positive effect of talcum filler on electrical breakdown strength was, however, demonstrated again by a comparison with unfilled pulp–only paper. An examination of talcum filled papers that were modified by either a polymer sizing agent, a cationic dry–strength agent or a wet–strength agent was presented. Results showed that the dry–strength agent had a statistically significant negative effect on the electrical breakdown strength of the paper–oil insulation, whereas both the wet–strength additive as well as the polymer sizing agent had a statistically significant positive result.

In conclusion, this thesis investigated a number of different mechanical and chemical modifications for their impact on the mechanical, electrical and dielectric characteristics of paper for electrical applications. The results suggest that the use of talcum as a filler in electrical paper–oil insulation may yield technical advantages.

8.1 Future Work

The work that is presented in this thesis is likely to give rise to further questions and to generate new ideas for other research work that may build on the results presented here. This section on 'future work' recognizes the fact that there are always outstanding questions that were not answered, and possible research avenues that could not be explored, within the context of this research thesis. The following items address some of these.

- In order to get a more complete picture, the modified electrical papers that were investigated in this work, should also be tested with one or more of the other non–destructive space charge measurement methods that were introduced in Chapter 4.
- Additional TSDC experiments with different types of metal electrodes and interfaces may be undertaken to determine their influence on the TSDC response. This

may be achieved by sputter coating or by methods of plasma coating. Specifically, the question may be if or how a metal coating on the dielectric introduces a further interface i.e. metal_electrode–metal_coating–sample, and how different materials effect the TSDC response.

- Investigations into other filler materials and additives should be undertaken to further explore possible improvements to electrical insulation papers. Based on the results presented in this thesis, other hydrophobic minerals appear to be most promising. Filler materials with extremely small particle sizes may also lead to interesting and possibly unexpected results.

- Electrical testing of fillers and their effects on bulk conductivity and surface resistivity of filled and otherwise modified papers may be of interest to complement the data presented in this thesis.

- Oil impregnation time plays an important role in the industrial application of electrical papers. Standard tests for the penetration speed of water in the paper industry may be used to determine the oil penetration of different electrical papers. Tailoring of the paper surface and bulk properties for increased oil impregnation is also conceivable.

- Further research into the ageing of the filled and otherwise modified papers that were presented in this thesis, appears to be a necessary step to validate the use of talcum filled papers for industrial applications. Procedures for the rapid ageing and testing of paper samples already exist in the paper as well as the electrical industry.

- Investigation into the upgrading of paper i.e. life–time extension measures or increasing operating temperatures. Particularly of interest are basic additives for the capture of acidic compounds as they are already being used in the electrical industry to date.

- Further research into the long–term effects of the talcum filler and chemical additives on insulation oil and its performance in the electrical domain are also of interest. What happens to the filler particles once the cellulose reinforcements start to age? What are the effects of free filler particles on the electrical breakdown strength of the transformer oil?

The results that are presented in this thesis have demonstrated that it is worthwhile to re-examine the established ideas with regard to paper–oil composite insulation systems. The findings in the body of this thesis as well as the ideas in this future work section outline the direction in which research has to proceed in order to verify, and to further improve upon, this new class of modified electrical insulation papers.

Appendix A

Publications

Parts of this thesis have already been published. With permission of the publisher, the journal publications are reproduced in the following pages.

Table A.1: Table of publications.

Title	Publication	Language
Professional Papermaking	Paper & Power: Modifying Electrical Insulation Paper	English
Wochenblatt für Papierfabrikation	Paper & Power: Optimierung von Isolationspapieren	German

Paper & Power: Modifying Electrical Insulation Paper

Abstract

Paper is employed in conjunction with oil in the electrical industry to insulate high voltage cables and transformers. This research examines changes in the electrical performance of insulation paper as a result of changes to its structure and surface properties. In addition to the electrical properties of the base paper, the effects of fibre type, fillers and the role of paper additives were investigated. Variations in filler content, density, thickness, smoothness and porosity were also considered for their impact on the dielectric breakdown strength of oil-paper insulation.

Of the three fibre types that were tested, the industry standard unbleached kraft pulp performed best electrically. Of the two fillers that were tried, the hydrophobic talcum filler clearly outperformed the hydrophilic bentonite filler. In comparison to the unfilled samples, the latter severely degraded the electrical breakdown strength of the paper, whereas the talcum filled samples displayed improved electrical performance. The high amount of filler employed in the trials reduced the mechanical strength of the papers and lead to the trial of additives to address this effect. The addition of both cationic starch and polyvinyl alcohol (PVA) increased the mechanical strength of the paper and showed positive results in the electrical breakdown tests. The dielectric spectroscopy measurements, however, revealed a marked increase in permittivity and dielectric loss for the samples containing the cationic starch. The use of PVA appeared to alleviate this effect. In a similar vein, calendering as a surface treatment showed positive results for the electrical breakdown strength, but a negative influence on the dielectric performance.

Introduction

Thousands of tons of cellulose are used every year for the insulation of oil-filled high-voltage power cables, condenser bushings and power transformers. At the same time, hundreds of thousands of paper-oil insulated power transformers of various types and power ratings are still in use today. [1]

This assures that advances in our understanding of paper and cellulose insulation materials remain relevant today. Paper is a sustainable, low-cost resource, and a familiar insulation material with a long history in the electrical industry. Its limitations with regard to degradation and aging are an established area of research. [2] In the early days of "paper" insulation, various other kinds of fibres, fillers and liquids were explored: cotton rag, silk, jute, asbestos or hemp in resin, varnished or boiled in oil. [3,4]

Despite ever increasing insulation requirements, modern electrical insulation paper has adequate mechanical, thermal and electrical strength for applications that range from line voltage to mega-volts. Today, insulation paper is made almost exclusively from unbleached virgin kraft pulp, and where necessary, chemically upgraded to withstand higher temperatures and remain viable for a longer life-time. [5] It is used, most often in conjunction with mineral oil, as a solid insulation material for spacers and as the main insulation on cable conductors and transformer windings.

It is the intention of this research to explore, whether advances in paper technology may be transferred to the field of power engineering and lead to improvements in the performance of paper-oil insulation systems.

Authors: T. A. Kleemann and P. L. Lewin (University of Southampton, UK); S. J. Badakh and S. G. Kleemann (Munich University of Applied Sciences, Germany) – presented at the IMPS 2012 in Munich, Germany

Materials

Pulps: The hardwood pulp is never-dried hardwood eucalyptus (Aracruz), refined to a Schopper Riegler value of 32°SR. The bleached softwood pulp is softwood-pine-spruce ECF, with an initial Schopper Riegler of 13°SR. The bleached softwood pulp was refined with a lab Jokro mill to a Schopper Riegler of 34°SR. The unbleached kraft pulp had an initial Schopper Riegler value of 15°SR, and was refined with a lab Jokro mill to a Schopper Riegler of 32–34°SR. De-ionised water was used for disintegration and refining.

Fillers: The talcum filler used, was a hydrophobic mineral with a high aspect ratio, packed bulk density (ISO 787/11) of 1.05 g/cm^3 and moisture content (ISO 787/2) of 0.2 %. In comparison to the talcum, the montmorillonite bentonite clay is highly hydrophilic. [6] For the preparation of the filler slurry, a calculated amount of filler was soaked and wetted with de-ionized water for approx. 10 min until a homogeneous colloidal slurry was obtained.

Additives: The starch used as dry strength agent is a cationised potato starch. It is a cold water (40–50 °C) soluble starch for wet end purposes. The polyvinyl alcohol (PVA) used for the experiments is a water-soluble polymer manufactured by the alcoholysis of polyvinyl acetate. The fully hydrolyzed polyvinyl alcohol (PVA) of high molecular weight with viscosity (DIN 53015) 56.0 ± 4.0 mPa·s has a degree of hydrolysis (saponification) of 98.4 ± 0.4 mol.-%. PVA imparts good cohesion and adhesion to fibers, fillers and pigments. This type of PVA is notable for its good bonding strength and pigment binding capacity which made it feasible to formulate papers with a high amount of talcum filler.

Insulating oils: The insulating oil used for the tensile strength test was Nytro Libra (mineral oil) naphthenic characteristics by Nynas. Nytro Libra is an uninhibited insulating oil, meeting IEC 60296 (03) general specifications. For the breakdown strength testing silicone oil XIAMETER® PMX-200 Silicone Fluid, 5–20 CS by Dow Corning was used.

Commercial reference papers: A set of three different commercial electrical insulating papers was tested and compared to the sample papers. To the authors' knowledge, all three papers are made of unbleached softwood kraft pulp, are unfilled, and uncalendered.

Measurement Procedures

Paper Testing

The tensile strength of the insulation paper with and without oil impregnation was determined with a 'Zwick/Roell' universal testing device. For tensile experiments samples were prepared and tested according to the

EN ISO 1924-2 standard in one direction (as MD and CD fiber orientation are absent for hand sheets). For performing paper tensile tests, samples of 15 mm width were cut, with 100 mm as the test span in between the clamps. To evaluate the influence of oil on paper tensile strength, the paper was soaked with Nitro Libra oil.

The duration of oil impregnation was constant for all samples with 30 mins. After impregnation the samples were wiped and dried to remove excess oil on the surface in order to avoid any slippage between the clamps. The tensile strength, tensile index, elongation etc. values are calculated automatically and displayed in both tabular and graphical fashion by the Zwick Roell test software testXpert® II. [7]

Porosity was measured according to Bendtsen (ISO 5636-3) and surface smoothness according to the Parker Print Surf roughness measurement (ISO 8791-4) .

Electrical Breakdown Strength Test

Electrical breakdown strength (abbr.: BDS) is the maximum voltage a sample can withstand before it breaks down and current flows from one electrode to the other, through the sample. It is important to note, that electrode geometry and the setup itself have an effect on the results and thus only relative conclusions should be drawn for samples measured with the same measurement setup.

The testing procedure [8] is based upon the general considerations laid down in the ASTM standard D149-87 and an equivalent schematic representation is shown in *Fig 1*. The samples were pinned between two vertical ball-bearing electrodes of 6.3 mm diameter, and put under pressure by a 50 g weight on the top electrode. Similar to the real-world application, the sample (highlighted in red) and the electrodes are immersed in oil. This is done to prevent surface flash-over where the discharge occurs on the surface and around the sample, rather than through it. A signal generator, here depicted by the combination of a ramp- and function generator, provides a steady 50 Hz sinusoidal signal with a linearly increasing magnitude.

The signal is connected to the electrodes through a power amplifier and a transformer in order to amplify it into the high voltage domain. A normal test starts with zero or a very small amplitude, and linearly ramps up the voltage to the point where the sample breaks down. The system then trips on the short-circuit, disables the drive-signal and records the highest voltage that occurred before the sample failed. Electrical breakdown is a stochastic process and therefore the test was performed 10–20 times for every paper sample in order to capture the variation in measurement. All data were obtained with a ramp rate of 50 V/s.

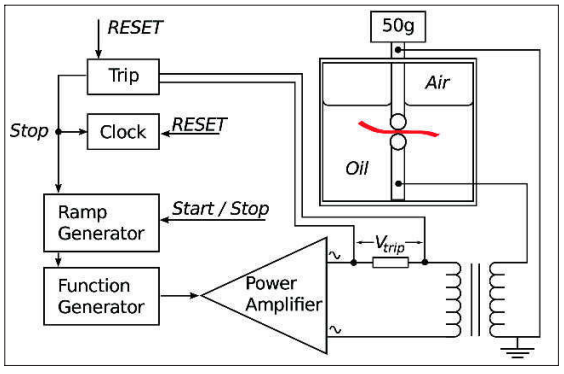

Fig. 1: Schematic representation of the AC electrical breakdown tester

Dielectric Spectroscopy

Dielectric Spectroscopy measures the dielectric characteristics of a medium as a function of frequency. The frequency response of the system reveals the energy storage and dissipation properties of the material under test. The results are analysed in the dimensionless terms of relative permittivity and the dissipation factor. The former parameter describes the influence of the medium on the electric field relative to that of vacuum, and the later is a measure that quantifies the inherent loss of electromagnetic energy within the material. Both parameters are commonly employed to describe dielectric materials in electrical engineering. For classical insulation applications both parameters are desired to be small.

Influence of Paper Properties on Electrical Performance

For a preliminary analysis of the effect of fibre type on electrical breakdown strength of oil-paper insulation systems, three types of pulps were examined: never-dried hardwood pulp, bleached softwood and unbleached softwood kraft pulp. The results of the electrical and mechanical tests are shown in *Fig. 2* (top). The hardwood sample papers displayed a reduced tensile strength and electrical BDS in comparison to both, the other two types of pulp, and the commercial paper samples.

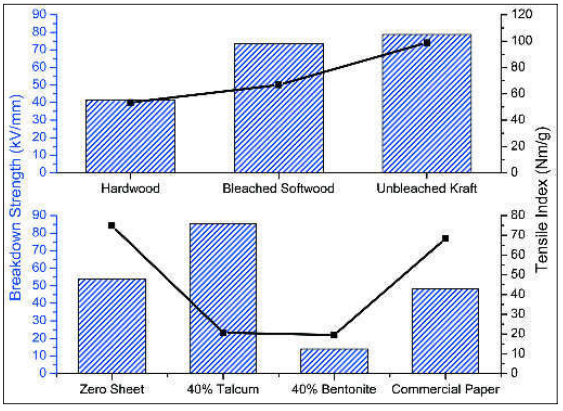

Fig. 2: Influence of fibre and filler type on the performance of insulation paper

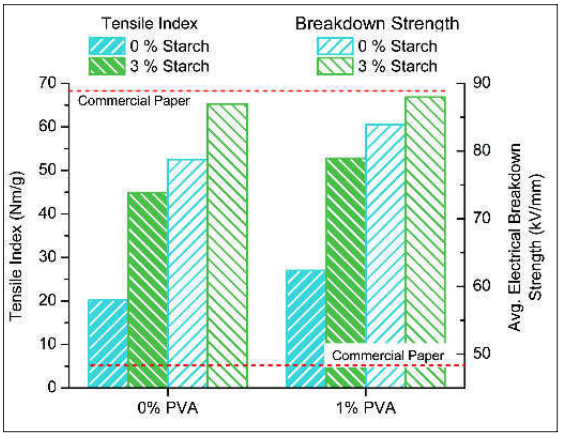

Fig. 3: The effect of starch and PVA on the electrical breakdown strength and tensile index of 40 % talcum-filled unbleached kraft paper. Red horizontal lines show values of commercial reference papers

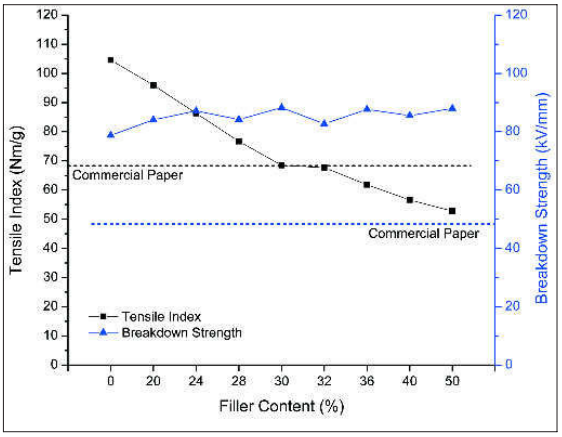

Fig. 4: Optimisation of the talcum filler content with regard to mechanical and electrical strength

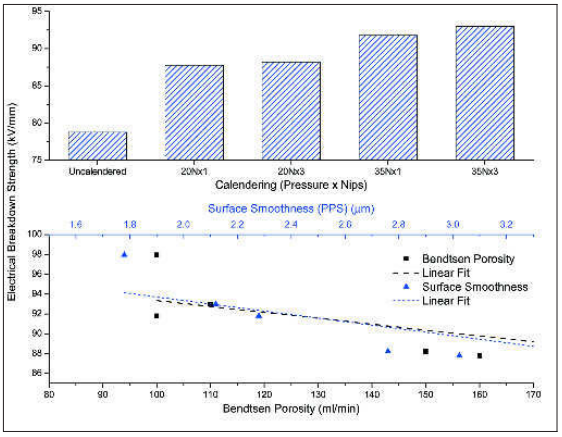

Fig. 5: Influence of calendering and concomitant changes in surface smoothness and structural porosity on the electrical breakdown strength

The softwood pulps showed increased tensile strength, with unbleached kraft papers performing slightly better than the bleached grade. The electrical BDS of both softwood sample paper types proved to be higher than the commercial papers. The improved electrical BDS may be ascribed to the refining process and the concomitant densification. The results confirm the established industry practice of using softwood kraft pulp for electrical insulation paper.[1]

The effects of fillers were also examined. Two very dissimilar fillers were selected: bentonite, a hydrophilic clay, and talcum, a hydrophobic mineral. The results are presented in Fig. 2 (bottom) and show that the talcum filled samples out-performed all other samples in regard to their breakdown strength. The bentonite filler, due to its hydrophilic nature, is known to absorb moisture and swell. High moisture content, ionic charges and impurities associated with such a clay are understood to reduce the breakdown strength of the insulation paper and may explain the inferior electrical performance of the bentonite filler.

With a filler content of 40 %, the sample papers are considered to be highly filled, and mechanical testing revealed an accompanying significant reduction in tensile strength when compared to the unfilled zero-sheet and commercial papers. In order to address this issue, starch – a dry strength agent – was tested as an additive. Furthermore, the wetting and dispersion of the hydrophobic talcum filler in water proved to be challenging and the resulting paper demonstrated inhomogeneity and two-sidedness. Polyvinyl alcohol (abbr.: PVA) which is usually used as a water soluble co-binder in coating formulation, was incorporated as a wet-end additive to enhance the performance of the talcum filler.

Fig. 3 illustrates the increased mechanical strength properties that were achieved by employing these additives and suggests that their use even has a positive effect on the electrical breakdown strength. Values for the commercial reference papers are provided by the red horizontal lines at 48.36 kV/mm and 68.3 Nm/g for BDS and tensile index respectively. Due to the 40 % talcum content, the BDS of the test papers is higher, but their tensile strength is still noticeably reduced.

In order to find the best compromise between enhanced electrical BDS and loss in mechanical tensile strength, an optimisation trial was conducted with varying quantities of the talcum filler. *Fig. 4* shows that there seems to be no linear relationship between talcum content and BDS. It may be inferred that 20–30 % of talcum filler is sufficient to improve the electrical BDS without incurring a significant loss in mechanical strength.

The impact of calendering on the breakdown strength is presented in *Fig. 5*. The laboratory calender that was used for these trials features a hard nip (steel on steel) and was set to a constant roll surface temperature of 110 °C. The papers were calendered to four different settings: with 20N or 35N and for up to three times. This is representative of one to three nips with different pressures. It shows how the increasing degree of calendering leads to a smoother and less porous paper which in turn raises the breakdown strength. It is inferred that the reduction in surface roughness increases the effective contact area between the insulation material and the electrode and thus reduces the local electric field stress at the interface.

Also, the increased surface smoothness reduces the likelihood of cavities at the interface where local field enhancement may initiate electrical discharges and lead to premature breakdown.[9] A further result of calendering was a reduction in paper thickness and an accompanying increase in apparent paper density. The combination of these effects may explain how calendering proved to be such an effective measure in raising the electrical breakdown strength of the test papers.

Dielectric Paper Characteristics

On the basis of the numerous AC breakdown measurements, it was decided to concentrate on the performance of unbleached kraft papers filled with talcum for the dielectric spectroscopy measurements. *Fig. 6* presents the results for filled samples in comparison to the commercial test papers. It shows that the greater electrical breakdown strength of the filled papers is accompanied by a reduction in dielectric performance as illustrated by the real relative permittivity and dissipation factor values. A linear trend may be observed in both figures that shows that the dielectric performance decreases with increasing filler content.

The influence of the two additives on the dielectric performance of paper was also investigated. *Fig. 7* illustrates the results. All the papers used in the comparison were made from unbleached kraft paper and filled with 40 % of talcum. It shows clearly that the addition of cationic starch degraded the dielectric performance, while the addition of PVA improved it. The positive influence of (cationic) starch on the mechanical strength of the papers is thus achieved at the expense of its dielectric suitability. Since dielectric spectroscopy measures the absorption and

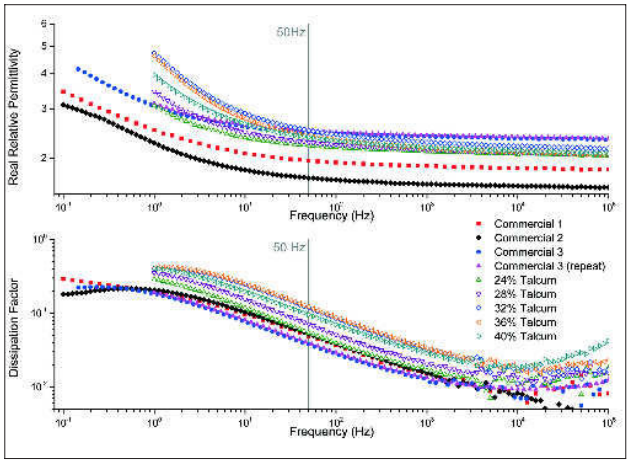

Fig. 6: Influence of fillers on the permittivity and dissipation factor of paper in comparison to commercial test papers

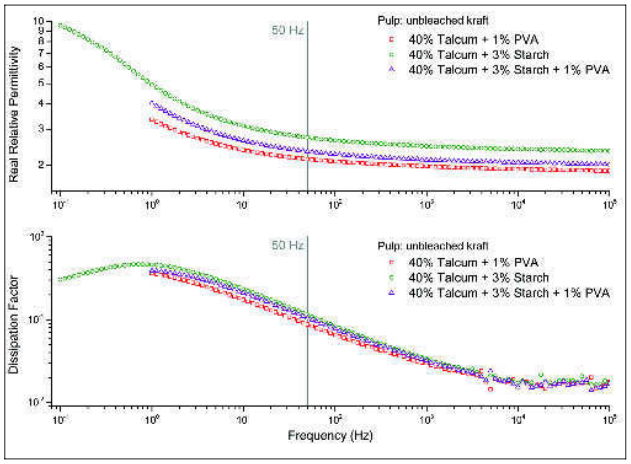

Fig. 7: The effect of starch and PVA additives on the permittivity and dissipation factor

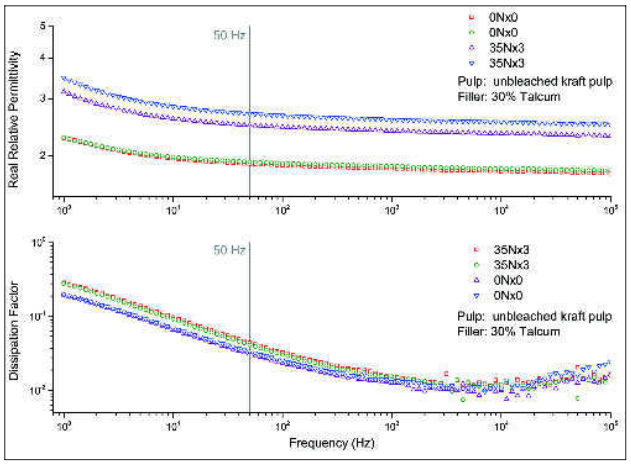

Fig. 8: The impact of calendering on the permittivity and dissipation factor of paper

dissipation of electromagnetic energy by polarisation processes, these results confirm expectations that a polar additive would negatively affect the dielectric performance of the filled material.

The positive effect of calendering on the electrical breakdown strength of oil-paper insulation systems was shown earlier. The real relative permittivity and loss tangent results for the calendered papers are shown in *Fig. 8*. It appears that the increase in apparent density and smoothness of the paper also increased the permittivity and electromagnetic loss of the paper. The defining factor here is most likely the increased density of polarisation processes per volume i.e. the increase in apparent density.

Conclusion

Employing talcum as a filler for electrical insulation paper promises not only considerable cost savings, but also increases the electrical breakdown strength of the paper. The insulation paper likely to exhibit the highest electrical breakdown strength with the modifications presented here, appears to be a talcum filled paper with 20–30 % filler content, calendered to exhibit a smooth surface with reduced porosity, lower thickness and higher apparent bulk density. Polyvinyl alcohol and starch may be employed successfully to raise mechanical strength, but ionic charges should be minimised due to a negative influence on the dielectric response.

Of the many parameters that influence the overall performance of paper as a dielectric medium, the initial findings presented here investigated a select few. They were chosen as a starting point to find and confirm general trends and tendencies. The research intention is to explore, whether recent advances in paper technology may be transferred to the field of power engineering and lead to improvements in the overall performance of paper-oil insulation systems.

References

1 T. A. Prevost and T. V. Oommen, "Cellulose Insulation in Oil-Filled Power Transformers: Part I – History and Development," IEEE Elect. Insul. Mag., vol. 22, no. 1, pp. 28-35, 2006.

2 T. V. Oommen and T. A. Prevost, "Cellulose Insulation in Oil-Filled Power Transformers: Part II – Maintainging Insulation Integrity and Life," IEEE Electrical Insulation Magazine, vol. 22, no. 2, pp. 5-14, 2006.

3 M. Schaible, "Electrical Insulation Papers – An Overview," IEEE Elect. Insul. Mag., vol. 3, no. 1, pp. 8-12, 1987.

4 H. Sheppard, "A century of progress in electrical insulation," IEEE Elect. Insul. Mag., vol. 2, no. 5, pp. 20-30, 1986.

5 S. J. Ferrito and R. L. Stegehuis, "High Temperature Reinforced Cellulose Insulation for Use in Electrical Applications," in Transmission and Distribution Conference and Exposition, 2001.

6 S. & B. I. M. GmbH, "Altonit- Bentonite Products for the paper industry," Dec 2005. [Online]. Available: http://www.ikominerals.de/fileadmin/pdf/sb_spezialbentonite_pdfs_german/ALTONIT_Produktinfo_allgemein_deutsch_neu_13.03.2006.pdf.

7 "testXpert® II – Prüfsoftware für alle Anwendungen," Zwick/Roell, 10 04 2012. [Online]. Available: http://www.zwick.de/de/produkte/pruefsoftware/pruefsoftware-fuer-statische-pruefungen.html. [Accessed 19 04 2012].

8 I. L. Hosier, A. S. Vaughan and S. G. Swingler, "Structure-property relationships in polyethylene blends: the effect of morphology on electrical breakdown strength," Journal of Materials Science, vol. 32, pp. 4523-4531, 1997.

9 E. I. A. N. Seyed Majid Hasheminezhad, "Breakdown Strength of Solid-Solid Interface," in 2010 International Conference on Solid Dielectrics, Potsdam, Germany, 2010.

Paper & Power: Optimierung von Isolationspapieren

Abstract

Der Einfluss von Oberflächen- und Strukturveränderungen auf die elektrische und mechanische Festigkeit sowie auf die dielektrische Systemantwort im Frequenzbereich werden untersucht. Unterschiedliche Zellstofftypen, Füllstoffe und die Rolle von Additiven werden betrachtet, ebenso wie die Auswirkung von Füllstoffgehalt, Papierdichte, Papierdicke, Oberflächenrauigkeit und Porosität. Der industriell verwendete ungebleichte Langfaser Kraftzellstoff erzielt höhere Festigkeitswerte als Papier aus gebleichtem Langfaser Zellstoff oder Laubholz Zellstoff. Im Vergleich zu den ungefüllten Papieren verschlechtert der Zusatz von hydrophilem Bentonit die elektrischen Eigenschaften der Papiere, wohingegen das hydrophobe Talkum diese klar verbessert. Die hochgefüllten Papiere weisen reduzierte mechanische Festigkeiten auf. Um dem entgegen zu wirken, werden verschiedene chemische Additive eingesetzt.
Polyvinylalkohol (PVA) und Stärke verbessern beide die mechanische Festigkeit und die elektrische Durchschlagsfestigkeit. Die dielektrischen Eigenschaften werden durch den Zusatz der kationischen Stärke jedoch signifikant verschlechtert und durch die Gegenwart von PVA leicht verbessert. Das Kalandrieren der Papiere verbessert die elektrischen und mechanischen Eigenschaften der Papiere, reduziert jedoch deren dielektrische Eigenschaften.

Einleitung

Zellulose und Papier sind ein ökonomisches und nachhaltiges Isolationsmaterial, das seit über einem Jahrhundert in der Elektroindustrie Verwendung findet.[1] Ölimprägniertes Papier wird unter anderem für die Isolation von Hochspannungskabeln, Transformatordurchführungen und Wicklungen eingesetzt. Viele tausend Transformatoren mit ölimprägnierter Papierisolation sind noch immer in Betrieb und werden in dieser Art auch immer noch hergestellt.[2] Fortschritte im Verständniss von Isolationspapieren und ihrem Verhalten sind daher auch heutzutage noch relevant. Obwohl die Isolationsanforderungen stetig gewachsen sind, zeigt modernes Isolationspapier hinreichend elektrische, mechanische und thermische Festigkeit, um in der Elektroindustrie in einer Vielzahl von Anwendung mit unterschiedlichen Leistungen und Spannungen Verwendung zu finden. In der Vergangenheit wurden unterschiedlichste Fasern, Füllstoffe und Imprägniermittel erkundet.[1,2,3] Heutzutage wird Isolationspapier fast ausschließlich aus reinem[4] Langfaser Kraftzellstoff hergestellt und in Kombination mit Mineralöl verwendet. Moderne industrielle Verfahren erlauben es, die thermische Festigkeit und damit auch die Langlebigkeit dieser Papiere weiter zu verbessern.[5,6]
Der Zweck dieser Untersuchung ist es zu sehen, ob und inwieweit Fortschritte in der Papierherstellung auf das Gebiet der Elektroindustrie übertragen werden können und dadurch zu besseren und preiswerteren Isolationspapieren führen.

Autoren: T. A. Kleemann (tak07r@ecs.soton.ac.uk), P. L. Lewin (pll@ecs.soton.ac.uk) (University of Southampton); S. J. Badakh (badakh@hm.edu), S. G. Kleemann (kleemann@hm.edu), Hochschule für angewandte Wissenschaften München – Auszugsweise vorgetragen beim IMPS 2012 in München

Rohstoffe und Methoden

Zellstoff: 1) Nie getrockneter Eucalyptus Zellstoff (Aracruz), gemahlen auf einen Schopper Riegler Wert von 32°SR. 2) Gebleichter Langfaser Fichte/Kiefer ECF Zellstoff, mit Hilfe einer Jokro Mühle auf einen Schopper Riegler Wert von 34°SR gemahlen. 3) Ungebleichter Langfaser Kraft Zellstoff, der mit einer Jokro Mühle auf einen Schopper Riegler Wert von 32–34°SR gemahlen wurde. Zum Aufschlagen und zur Mahlung wurde deionisiertes Wasser eingesetzt.

Füllstoffe: Das eingesetzte Talkum ist ein hydrophobes Mineral mit einem hohen Aspekt Ratio und einer Dichte nach ISO 787/11 von 1,05 g/cm³ sowie einem Feuchtegehalt (ISO 787/2) von 0,2 %. Im Vergleich zum Talkum ist das verwendete Bentonit deutlich hydrophiler.[7] Für die Herstellung der Füllstoff-Slurry wurde der berechnete Anteil an Füllstoff mit deionisiertem Wasser benetzt und darin für ca. 10 min bis zum Erhalt einer homogenen Slurry gerührt.

Additive: Als Trockenverfestiger kam eine kationische Kartoffelstärke in Form einer kaltwasserlöslichen (40–50 °C) Stärke zum Einsatz. Der Polyvinylalkohol (Abk.: PVA) ist ein wasserlösliches Polymer, welches durch Hydrolyse von Polyvinylacetat erhalten wird. Der vollhydrolysierte PVA war hochmolekular mit einer Viskosität (DIN 53015) von 56,0 ± 4,0 mPa·s und einem Hydrolyseanteil von 98,4 ± 0,4 Mol-%.

Isolieröle: Nynas Nytro Libra Mineral Öl wurde als Test Öl für die Festigkeitsmessungen verwendet. Nytro Libra ist ein Isolieröl nach den Spezifikationen der IEC 60296 (03). Die Durchschlagsfestigkeitsmessungen wurden in Silikonöl XIAMETER® PMX-200 Silicone Fluid, 5–20 CS von Dow Corning durchgeführt.

Industrielle Referenzpapiere: Drei unterschiedliche Isolationspapiere wurden zu Vergleichszwecken getestet. Nach Kenntnis der Autoren bestehen alle drei Papiere aus ungefülltem, unkalandriertem und ungebleichtem Langfaser Kraftzellstoff.

Papier Testmethoden

Ein universelles Testgerät von Zwick Roell wurde für die Bestimmung der Zugfestigkeit verwendet. Das Papier wurde mit und ohne Öl gemessen. Die Proben wurden dem EN ISO 1924-2 Standard nach erstellt und nur in einer Richtung gemessen, da bei Laborblättern keine MD (Engl.: machine-direction) oder CD (Engl.: cross-direction) besteht. Papierstreifen mit 15 mm Breite wurden mit einer Testabstand von 100 mm in das Gerät eingespannt. Für die ölimprägnierten Tests wurde das Papier für 30 min in Nitro Libra Öl getränkt und dann abgewischt und getrocknet, um überschüssiges Öl zu entfernen und das Rutschen des Probestreifens zu verhindern. Zugfestigkeit, Dehnung und andere Werte werden automatisch von der Zwick Roell Testsoftware testXpert® II[8] errechnet und angezeigt.

Porosität und Rauigkeit

Rauigkeit wurde nach dem Parker Print Surf Verfahren (ISO 8791-4) gemessen, die Porosität nach Bendtsen (ISO 5636-3).

Elektrische Durchschlagfeldstärke Messung

Elektrische Durchschlagfeldstärkemessung ist ein Maß davon, wie viel elektrisches Potenzial an einem Material angelegt werden kann, bevor das elektrische Feld so stark ist, dass es zu einem Durchschlag kommt. Elektrischer Durchschlag ist ein stochastischer Prozess und wird von der Elektrodengeometrie und dem Messaufbau beeinflusst. Aus diesem Grund sollten nur relative Schlüsse gezogen werden zwischen Materialien, die auf dem gleichen Messgerät und unter gleichen Bedingungen getestet wurden. Alle Messungen wurden 10–20 Mal durchgeführt, um Messungenauigkeiten zu erfassen. Die Resultate können z. B. in einem Weibullnetz aufgetragen und verglichen werden.

Die Proben werden nach den generellen Überlegungen des ASTM Standards D149-87 getestet.[9] Ein entsprechender Schaltkreis ist in *Abb. 1* zu sehen. Die Probe wird zwischen zwei vertikalen Kugellagerelektroden (6,3 mm Durchmesser) in einem Ölbad gehalten. Ein 50 g schweres Gewicht auf der oberen Elektrode erzeugt einen konstanten Anpressdruck. Das Ölbad verhindert Oberflächenentladungen. Ein Signalgeber, hier als Kombination von einem Rampen- und Funktionsgenerator dargestellt, erzeugt ein gleichmäßiges 50 Hz Sinussignal mit einer linear ansteigenden Amplitude. Ein Verstärker und ein Transformator verstärken das Signal in den Hochspannungsbereich. Für eine Durchschlagfeldstärkemessung wird ein ölgetränktes Papier zwischen die Elektroden gespannt und die Amplitude des Signals mit 50 V/s von nahe Null gesteigert. Wenn die Durchschlagfeldstärke erreicht ist und das Material nachgibt, entsteht ein Kurzschluss im Schaltkreis, das Messgerät schaltet sich ab und die maximale erreichte Spannung wird notiert.

Dielektrische Messung

Die dielektrische Systemantwort der Materialien wurde mit der Frequenzbereichsspektroskopie (Abk.: FDS, Engl.: Frequency Domain Spectroscopy) gemessen. Die Resultate sind u. a. ein Maß für die Absorption und den Verlust von elektrischer oder elektromagnetischer Energie durch Polarisationsprozesse im gemessenen Medium. Die dimensionslosen Kenngrößen der relativen Permittivität und des Verlustfaktors können von diesen Ergebnissen abgeleitet werden. Ersteres beschreibt den Einfluss des Materials auf das elektrische Feld im Vergleich zu Vakuum, und letzteres den elektromagnetischen Energieverlust im Material. Beides sind Faktoren, die allgemein zur Beschreibung von Materialien in der Elektrotechnik Verwendung finden.

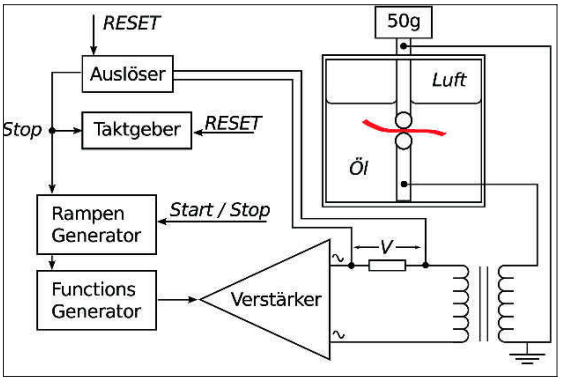

Abb. 1: Schematische Darstellung des elektrischen Durchschlagfeldstärke-Messgerätes

Resultate und Diskussionen

Drei Arten von Zellstofffasern wurden auf ihre elektrische und mechanische Festigkeit in Form von Isolationspapieren überprüft. Nie-getrockneter Kurzfaserzellstoff, gebleichter Langfaser Kraftzellstoff und ungebleichter Langfaser Kraftzellstoff. Die Elektrische Durchschlagfeldstärke und Bruchfestigkeit sind in *Abb. 2* (oben) aufgezeigt. Die Papierproben aus Kurzfaserzellstoff zeigen eine niedrigere Durchschlagfeldstärke und mechanische Festigkeit als die Langfaserzellstoffe oder die kommerziellen Referenzpapiere. Von den beiden Langfaserzellstoffen schneidet die ungebleichte Variante besser ab als die gebleichte, und beide sind besser als die kommerziellen Papiere. Letzteres kann auch an der Mahlung des Zellstoffes und der damit verbundenen Verdichtung des Papieres liegen. Diese Ergebnisse bestätigen die übliche Verwendung des ungebleichten Langfaser Kraftzellstoffes für Isolationspapiere in der Elektroindustrie.

Zwei sehr unterschiedliche Füllstoffe wurden gewählt, um deren Einfluss auf die elektrischen und mechanischen Papiereigenschaften zu erleuchten. Bentonit, ein hydrophiler Füllstoff, und Talkum, ein hydrophobes Mineral. Abb. 2 (unten) zeigt, dass die talkumgefüllten Papiere elektrisch besser abschneiden als die ungefüllten Papierproben, die kommerziellen Vergleichspapiere mit inbegriffen. Im Gegensatz dazu, weist der Bentonitfüllstoff wesentlich schlechtere elektrische und mechanische Eigenschaften auf als alle anderen

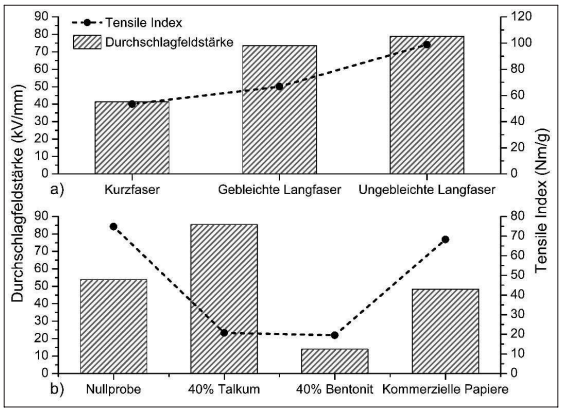

Abb. 2: Einfluss von Faser- und Füllstofftyp auf die elektrischen und mechanischen Eigenschaften

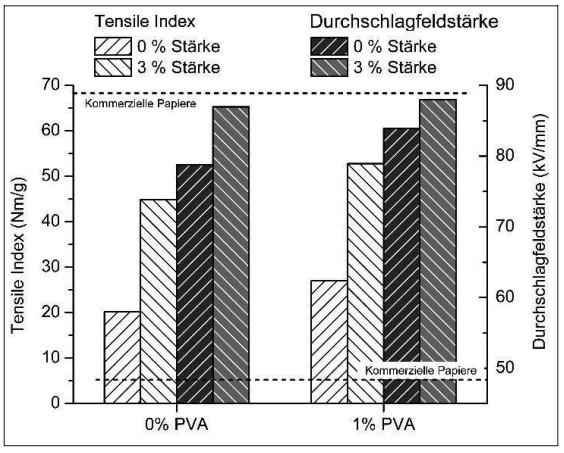

Abb. 3: Die Auswirkungen von Stärke und Polyvinylalkohol (PVA) auf mechanische und elektrische Eigenschaften

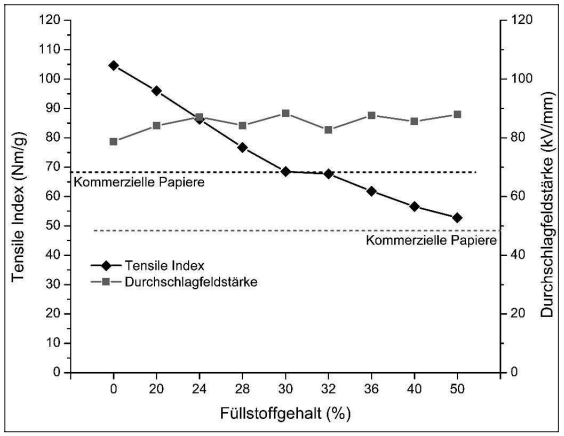

Abb. 4: Optimierung des Füllstoffgehalts (Talkum)

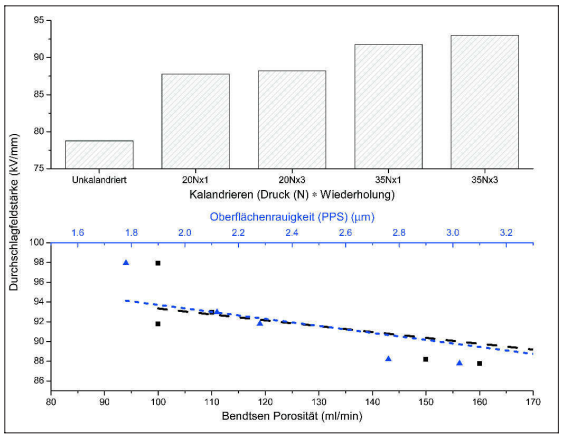

Abb. 5: Einfluss des Kalandrierens auf Durchschlagfeldstärke, Porosität und Oberflächenrauigkeit

gemessenen Papierproben. Dies kann mit der hydrophilen Natur von Bentonit erklärt werden, welches dazu neigt, Wasser einzulagern und zu schwellen. Die damit verbundenen hohen Feuchtigkeitsgehalte, ionische Ladungen und Verunreinigungen führen zu einer Verschlechterung der materialeigenen elektrischen Durchschlagfeldstärke.

Mechanisch gesehen, haben die gefüllten Papiere signifikant geringere Festigkeitswerte als die ungefüllten Papiere oder die kommerziellen Vergleichspapiere. Dies ist nicht überraschend, da die Papierproben mit 40 % Füllstoffgehalt als hoch gefüllt gelten und eine weitgehend lineare Abhängigkeit zwischen Füllstoffgehalt und mechanischer Festigkeit zu erwarten ist, und in der Tat besteht. *(Abb. 4)*

Um die mechanische Zugfestigkeit zu erhöhen, ohne den Füllstoffgehalt zu senken, wurden chemische Additive erprobt. Stärke und der wasserlösliche Cobinder Polyvinylalkohol (PVA) wurden den hochgefüllten Papieren hinzugegeben. PVA bewirkt eine gute Kohäsion und Adhäsion mit Fasern, Füllstoffen und Pigmenten. Der verwendete PVA Typ ist bekannt für eine gute Bindungsstärke und Bindungskapazität. Letzteres hilft außerdem bei der Benetzung und Dispergierung des hydrophoben Talkumpulvers in Wasser und führt dadurch zu einer besseren Homogenität und geringeren Zweiseitigkeit des Papieres.

Die Resultate sind in *Abb. 3* zu sehen und zeigen die Einwirkung der beiden Additive separat und in Kombination. Beide Additive haben demnach nicht nur einen positiven Einfluss auf die mechanische Festigkeit, sondern auch auf die elektrische Durchschlagfeldstärke. Die gestrichelten horizontalen Linien kennzeichnen den Durchschnittswert der drei kommerziellen Referenzpapiere für die Durchschlagfeldstärke und Zugfestigkeit mit respektive 48 kV/mm und 68 Nm/g. Es ist deutlich zu sehen, dass der Zusatz von Stärke die Zugfestigkeit mehr als verdoppelt, die Papierproben jedoch immer noch geringere Absolutwerte zeigen als die kommerziellen Papiere. Im Gegensatz dazu, liegen die elektrischen Durchschlagfeldstärken der gefüllten Papierproben jedoch weit über den kommerziellen Papieren.

Ein Optimisierungsversuch wurde gestartet, um zu sehen, ob und wo der beste Kompromiss zwischen elektrischer Durchschlagfeldstärke und Füllstoffgehalt gefunden werden kann. Den Ergebnissen in Abb. 4 nach existiert kein direkter Zusammenhang zwischen den beiden Größen und eine Steigerung der elektrische Festigkeit kann bereits mit 20–30 % Talkumgehalt erreicht werden, ohne dabei die mechanische Festigkeit bedeutsam zu mindern.

Eine weitere Untersuchung wurde unternommen, um den Einfluss der Kalandrierung auf diese Papiere zu untersuchen. Vier unterschiedliche Kalandereinstellungen wurden verglichen: 20 Newton (N) oder 35 N Druck bei einmaliger oder dreimaliger Anwendung. Der Walzennip ist Stahl-auf-Stahl und die Rollentemperatur konstant 110 °C. Die Resultate sind in *Abb. 5* dargelegt und zeigen, dass erhöhtes Kalandrieren zu einer Steigerung der elektrischen Durchschlagfeldstärke führt und mit einer Reduzierung der Porosität und Oberflächenrauigkeit einher geht. Letzteres läßt darauf schließen, dass die effektive Kontaktfläche zwischen Probe und Elektrode durch die Kalandrierung erhöht wird und lokale Feldverstärkungen sowie mögliche Teilentladungen an der Grenzfläche reduziert werden. Im Zusammenschluss mit einer erhöhten Dichte, welche durch die Reduzierung der Papierdicke hervorgerufen wird, mag dies die Verbesserung der Durchschlagfeldstärke erklären. Es ist beachtenswert, dass der absolute Druck bei der Kalandrierung mehr Auswirkung zeigt, als die Anzahl der Anwendungen.

Die Analyse der elektrischen Durchschlagfeldstärke der unterschiedlichen Papierproben lässt sich mit der 2-parametrigen Weibull Lebensdauerstatistik in einem Weibullnetz darstellen und vergleichen. Hier entspricht der Parameter der charakteristischen Lebensdauer (63,2 % Ausfallwahrscheinlichkeit) in etwa dem Durchschnittswert der elektrischen Durchschlagfeldstärke und der Formparameter (Steigung der linearen Ausgleichsgeraden aus dem Weibullnetz) ist ein Kennwert für die Streuung der Lebensdauerwerte. Er sagt somit zusätzlich etwas darüber aus, wie prägnant der Durchbruchpunkt der einzelnen Materialien ist.

Statt einem Weibullnetz zeigt *Abb. 6* ein normales x-y Diagramm, in dem die Weibull Parameter und nicht die einzelnen Lebensdauerdaten aufgetragen sind. Auf diese Weise ist zusammenfassend ersichtlich, wie gut und wie präzise die einzelnen Papierproben abgeschnitten haben. Bentonit ist, wie bereits erklärt, ganz unten auf der Skala der charakteristischen Lebensdauer zu finden. Der Weibull-Formparameter deutet jedoch auf einen recht prägnanten und wiederholbaren Fehlpunkt. Die Datenserien der talkumgefüllten und kalandrierten Papiere ist am oberen Ende der Lebensdauerskala angesiedelt. Die tiefliegenden Ausreißer dieser Testserien sind jeweils die ungefüllten oder unkalandrierten Papierproben. Die kommerziellen Papiere sind im Mittelfeld um die 50 kV/mm zu finden und zeigen einen bemerkenswerten Ausreißer mit sehr kleinem Formparameter. Dieser zeugt von einer weiten Streuung der Lebensdauerdaten und deutet auf eine Mehrzahl von Entladungsprozessen bzw. auf eine inhomogene Formation des Papieres hin.

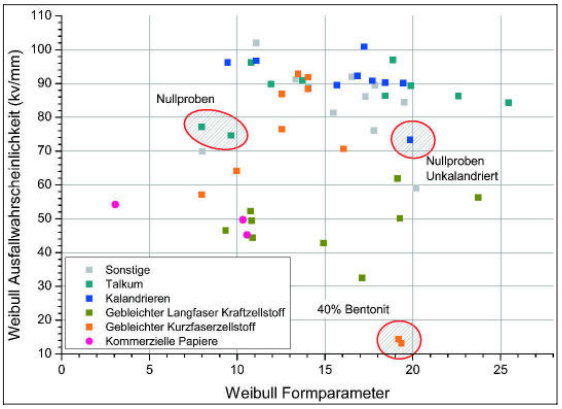

Abb. 6: Zusammenfassung der Weibull Lebensdauerstatistik; die besten Proben erreichen hohe Ausfallwahrscheinlichkeits- und Formparameter-Werte

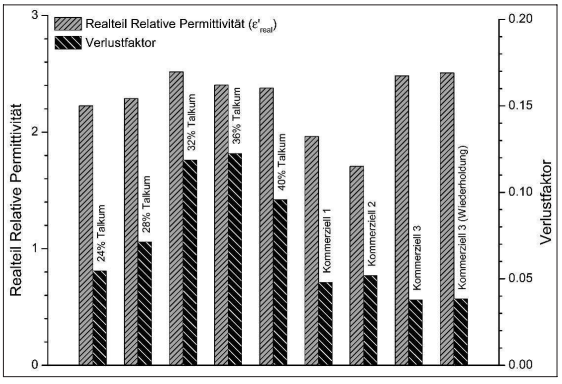

Abb. 7: Dielektrische Systemantwort der talkumgefüllten Papiere

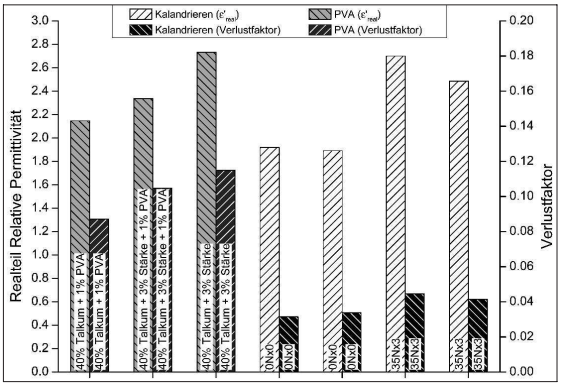

Abb. 8: Einfluss von chemischen Additiven und Kalandrieren auf die dielektrischen Papiereigenschaften

Um zu sehen, ob die elektrische Verbesserung der Isolationspapiere auch eine Verbesserung der dielektrischen Eigenschaften mit sich bringt, wurden die aussichtsreichsten Papierproben einer Frequenzbereichsspektroskopie (FDS) unterzogen, um deren frequenzabhängige dielektrische Systemantwort zu gewinnen. Der Vergleich zwischen den Ergebnissen der talkumgefüllten Proben und den kommerziellen Papieren ist in *Abb. 7* aufgezeigt. Für eine Verwendung als Isolationsmaterial ist ein möglichst kleiner Wert für die relative Permittivität und den Verlustfaktor erwünscht. Es ist zu sehen, dass die erhöhte elektrische Festigkeit der talkumgefüllten Papiere mit einer leichten Verschlechterung der dielektrischen Eigenschaften einhergeht. Die ungefüllten kommerziellen Papiere zeigen hier teilweise etwas geringere Werte. Das Industriemuster Nummer 3 weist jedoch eine vergleichbare relative Permittivität wie die talkumgefüllten Papiere auf. Der Einfluss der Additive auf die dielektrischen Eigenschaften wurde ebenfalls untersucht. In dieser Testserie bestanden alle Papierproben aus ungebleichtem Langfaser Kraftzellstoff und waren zu 40 % mit Talkum gefüllt. Die FDS Ergebnisse für PVA und Stärke sind in *Abb. 8* zu sehen. Der Einsatz von kationischer Stärke, welche so erfolgreich die mechanische Festigkeit erhöht, hat negative Konsequenzen für die dielektrische Systemantwort. Die Zugabe von PVA scheint dies etwas zu mildern. Da FDS die materialabhängige Absorption und den Verlust von Energie in Polarisationsmechanismen misst, ist es nicht verwunderlich, dass die Beigabe von ionisierten Additiven einen nachteiligen Einfluss auf die dielektrischen Eigenschaften hat.

Die Auswirkung des Kalandrierens zeigt sich in ähnlicher Weise. Ein kurzer Punktvergleich (Abb. 8) zeigt, dass auch hier die Verbesserung der elektrischen Festigkeit mit einer Verschlechterung der dielektrischen Eigenschaften einhergeht. Es wird angenommen, dass die erhöhte Dichte des Papieres auch zu einer Erhöhung der Polarisationsmechanismen per Volumeneinheit führt, und so zu einer Steigerung der dielektrischen Werte beiträgt.

Zusammenfassung

Eine Anzahl von Fasern, Füllstoffen und Additiven wurden auf ihre elektrischen, mechanischen und dielektrischen Einflüsse hin überprüft, um zu sehen, inwieweit Fortschritte in der Papiertechnik zu Verbesserungen von Isolationspapier in der Elektroindustrie führen können. Kalandrierte Langfaser Kraftpapiere mit Talkumfüllung und den chemischen Additiven Stärke und Polyvinylalkohol zeigen erfolgsversprechende elektrische und mechanische Eigenschaften für die Verwendung als Isolationspapier. Nach optimiertem Füllstoffgehalt überbieten deren Zugfestigkeit und elektrische Durchschlagfeldstärkewerte sowohl die kommerziellen Vergleichspapiere als auch alle anderen hier getesteten Papiertypen. Die frequenzabhängige dielektrische Systemantwort zeigte jedoch, vornehmlich bei der Zugabe von ionischer Stärke, erkennbare Beeinträchtigungen.

Literaturhinweise

1 H. Sheppard, „A century of progress in electrical insulation," IEEE Elect. Insul. Mag., Bd. 2, Nr. 5, pp. 20-30, 1986.

2 T. A. Prevost und T. V. Oommen, „Cellulose Insulation in Oil-Filled Power Transformers: Part I – History and Development," IEEE Elect. Insul. Mag., Bd. 22, Nr. 1, pp. 28-35, 2006.

3 M. Schaible, „Electrical Insulation Papers – An Overview," IEEE Elect. Insul. Mag., Bd. 3, Nr. 1, pp. 8-12, 1987.

4 K. Giese, „The Effects of Cellulose Insulation Quality on Electrical Intrinsic Strength," IEEE Electrical Insulation Magazine, Bd. 10, Nr. 5, pp. 38-42, 1994.

5 S. J. Ferrito und R. L. Stegehuis, „High Temperature Reinforced Cellulose Insulation for Use in Electrical Applications," in s Transmission and Distribution Conference and Exposition, 2001.

6 T. V. Oommen und T. A. Prevost, „Cellulose Insulation in Oil-Filled Power Transformers: Part II – Maintainging Insulation Integrity and Life," IEEE Electrical Insulation Magazine, Bd. 22, Nr. 2, pp. 5-14, 2006.

7 S. & B. I. M. GmbH, „Altonit- Bentonite Products for the paper industry," Dec 2005. [Online]. Available: http://www.ikominerals.de/fileadmin/pdf/sb_spezialbentonite_pdfs_german/ALTONIT_Produktinfo_allgemein_deutsch_neu_13.03.2006.pdf. [Zugriff am 19 04 2012].

8 „testXpert® II – Prüfsoftware für alle Anwendungen," Zeick / Roell, 10 04 2012. [Online]. Available: http://www.zwick.de/de/produkte/pruefsoftware/pruefsoftware-fuer-statische-pruefungen.html. [Zugriff am 19 04 2012].

9 I. L. Hosier, A. S. Vaughan und S. G. Swingler, „Structure-property relationships in polyethylene blends: the effect of morphology on electrical breakdown strength," Journal of Materials Science, Bd. 32, pp. 4523-4531, 1997.

Appendix B

Minitab Reports

The following sections provide the complete reports that were generated by the Minitab 16 statistical software. The reports support the analysis in the main body of this thesis, particularly in Chapter 7.

B.1 Sizing Trial

Listing B.1: Minitab Report: Sizing Trial

```
----------------------------
Analysis of Variance for BDS
----------------------------

Source        DF       SS       MS      F      P
Type           2  638.308  319.154  18.52  0.003
Sheet(Type)    6  103.386   17.231   6.38  0.000
Error         45  121.623    2.703
Total         53  863.317


S = 1.64400   R-Sq = 85.91%   R-Sq(adj) = 83.41%


                                 Expected Mean Square
                 Variance  Error  for Each Term (using
   Source       component   term  unrestricted model)
1  Type                        2  (3) + 6 (2) + Q[1]
2  Sheet(Type)       2.421     3  (3) + 6 (2)
3  Error             2.703        (3)


Means

Type          N     BDS
AKD          18  36.161
ASA          18  30.082
Zero-Sheet   18  38.169
```

```
Type         Sheet  N     BDS
AKD          1      6  38.541
AKD          2      6  33.379
AKD          3      6  36.562
ASA          1      6  30.920
ASA          2      6  30.194
ASA          3      6  29.133
Zero-Sheet   1      6  37.029
Zero-Sheet   2      6  38.964
Zero-Sheet   3      6  38.515


Residual Plots for BDS

--------------------------------------
Nested ANOVA: BDS versus Type, Sheet
--------------------------------------

Analysis of Variance for BDS

Source  DF        SS        MS       F      P
Type     2  638.3081  319.1541  18.522  0.003
Sheet    6  103.3857   17.2309   6.375  0.000
Error   45  121.6232    2.7027
Total   53  863.3170


Variance Components

                    % of
Source  Var Comp.  Total  StDev
Type       16.774  76.60  4.096
Sheet       2.421  11.06  1.556
Error       2.703  12.34  1.644
Total      21.898         4.679


Expected Mean Squares

1  Type     1.00(3) +  6.00(2) + 18.00(1)
2  Sheet    1.00(3) +  6.00(2)
3  Error    1.00(3)


------------------------------------------
General Linear Model: BDS versus Type, Sheet
------------------------------------------

Factor       Type   Levels  Values
Type         fixed       3  AKD, ASA, Zero-Sheet
Sheet(Type)  fixed       9  1, 2, 3, 1, 2, 3, 1, 2, 3


Analysis of Variance for BDS, using Adjusted SS for Tests

Source       DF   Seq SS   Adj SS   Adj MS       F      P
Type          2  638.308  638.308  319.154  118.09  0.000
```

```
Sheet(Type)   6  103.386  103.386   17.231    6.38  0.000
Error        45  121.623  121.623    2.703
Total        53  863.317


S = 1.64400   R-Sq = 85.91%   R-Sq(adj) = 83.41%


Unusual Observations for BDS

Obs      BDS      Fit  SE Fit  Residual  St Resid
  5  40.1330  37.0288  0.6712    3.1042      2.07 R
 44  27.0083  30.1939  0.6712   -3.1856     -2.12 R
 50  32.6430  29.1330  0.6712    3.5100      2.34 R

R denotes an observation with a large standardized residual.


Expected Mean Squares, using Adjusted SS

               Expected Mean
               Square for
   Source      Each Term
1  Type        (3) + Q[1, 2]
2  Sheet(Type) (3) + Q[2]
3  Error       (3)


Error Terms for Tests, using Adjusted SS

                                  Synthesis
   Source       Error DF  Error MS  of Error MS
1  Type            45.00     2.703  (3)
2  Sheet(Type)     45.00     2.703  (3)


Variance Components, using Adjusted SS

        Estimated
Source      Value
Error       2.703


Least Squares Means for BDS

Type             Mean  SE Mean
AKD             36.16   0.3875
ASA             30.08   0.3875
Zero-Sheet      38.17   0.3875
(Type)Sheet
 AKD         1  38.54   0.6712
 AKD         2  33.38   0.6712
 AKD         3  36.56   0.6712
 ASA         1  30.92   0.6712
 ASA         2  30.19   0.6712
 ASA         3  29.13   0.6712
 Zero-Sheet  1  37.03   0.6712
 Zero-Sheet  2  38.96   0.6712
 Zero-Sheet  3  38.51   0.6712
```

```
Grouping Information Using Tukey Method and 95.0% Confidence

Type          N   Mean  Grouping
Zero-Sheet   18  38.17  A
AKD          18  36.16     B
ASA          18  30.08        C

Means that do not share a letter are significantly different.


Tukey 95.0% Simultaneous Confidence Intervals
Response Variable BDS
All Pairwise Comparisons among Levels of Type
Type = AKD  subtracted from:

Type          Lower  Center   Upper  -----+---------+---------+---------+-
ASA          -7.408  -6.079  -4.749  (--*--)
Zero-Sheet    0.679   2.009   3.338                  (--*--)
                                    -----+---------+---------+---------+-
                                      -5.0       0.0       5.0      10.0


Type = ASA  subtracted from:

Type         Lower  Center  Upper  -----+---------+---------+---------+-
Zero-Sheet   6.758   8.087  9.416                              (-*--)
                                  -----+---------+---------+---------+-
                                    -5.0       0.0       5.0      10.0


Tukey Simultaneous Tests
Response Variable BDS
All Pairwise Comparisons among Levels of Type
Type = AKD  subtracted from:

            Difference       SE of           Adjusted
Type          of Means  Difference  T-Value   P-Value
ASA             -6.079      0.5480   -11.09    0.0000
Zero-Sheet       2.009      0.5480     3.67    0.0019


Type = ASA  subtracted from:

            Difference       SE of           Adjusted
Type          of Means  Difference  T-Value   P-Value
Zero-Sheet       8.087      0.5480    14.76    0.0000
```

B.2 PVA Trial

Listing B.2: Minitab Report: PVA Trial

```
----------------------------------------
Nested ANOVA: BDS versus Composition, Sheet
----------------------------------------
```

```
Analysis of Variance for BDS

Source         DF          SS         MS       F      P
Composition     7   6567.2440  938.1777   4.533  0.002
Sheet          24   4967.0754  206.9615  13.773  0.000
Error         160   2404.3438   15.0271
Total         191  13938.6632


Variance Components

                         % of
Source       Var Comp.  Total  StDev
Composition     30.467  39.32  5.520
Sheet           31.989  41.28  5.656
Error           15.027  19.39  3.876
Total           77.484         8.802


Expected Mean Squares

1  Composition    1.00(3) +  6.00(2) + 24.00(1)
2  Sheet          1.00(3) +  6.00(2)
3  Error          1.00(3)


General Linear Model: BDS versus Composition, Sheet

Factor              Type   Levels  Values
Composition         fixed       8  1% HR-3010 + (2% starch + 25% Talc), 1%
                                   KL-506 + (2% starch + 25% Talc), 1% Mowiol
                                   56-98 + (2% starch + 25% Talc), 2% HR-3010 +
                                   (2% starch + 25% Talc), 2% KL-506 + (2%
                                   starch + 25% Talc), 2% Mowiol   56-98 + (2%
                                   starch + 25% Talc), Absolute zero (100%
                                   Bleached  softwood pulp), Zero (2% starch +
                                   25% Talc)
Sheet(Composition)  fixed      32  1, 2, 3, 4, 1, 2, 3, 4, 1, 2, 3, 4, 1, 2, 3,
                                   4, 1, 2, 3, 4, 1, 2, 3, 4, 1, 2, 3, 4, 1, 2,
                                   3, 4

-----------------------------------------------------------
Analysis of Variance for BDS, using Adjusted SS for Tests
-----------------------------------------------------------

Source               DF    Seq SS   Adj SS  Adj MS      F      P
Composition           7   6567.24  6567.24  938.18  62.43  0.000
Sheet(Composition)   24   4967.08  4967.08  206.96  13.77  0.000
Error               160   2404.34  2404.34   15.03
Total               191  13938.66


S = 3.87649   R-Sq = 82.75%   R-Sq(adj) = 79.41%


Unusual Observations for BDS

Obs      BDS     Fit  SE Fit  Residual  St Resid
 51  107.812  94.240   1.583    13.573      3.84 R
```

```
 52   83.684  94.240   1.583   -10.556     -2.98 R
 56   67.826  75.565   1.583    -7.739     -2.19 R
 61   79.574  86.834   1.583    -7.260     -2.05 R
 69   90.402  82.869   1.583     7.534      2.13 R
 75   86.182  79.000   1.583     7.182      2.03 R
 80   75.082  88.030   1.583   -12.949     -3.66 R
 84   95.321  88.030   1.583     7.291      2.06 R
 88   69.755  77.797   1.583    -8.042     -2.27 R
 89   85.490  77.797   1.583     7.692      2.17 R
110   68.542  76.726   1.583    -8.184     -2.31 R

R denotes an observation with a large standardized residual.


Expected Mean Squares, using Adjusted SS

                      Expected Mean
                      Square for
   Source             Each Term
1  Composition        (3) + Q[1, 2]
2  Sheet(Composition) (3) + Q[2]
3  Error              (3)


Error Terms for Tests, using Adjusted SS

                                        Synthesis
   Source             Error DF  Error MS  of Error MS
1  Composition          160.00     15.03  (3)
2  Sheet(Composition)   160.00     15.03  (3)


Variance Components, using Adjusted SS

        Estimated
Source      Value
Error       15.03


Least Squares Means for BDS

Composition                                          Mean  SE Mean
1% HR-3010 + (2% starch + 25% Talc)                 83.75   0.7913
1% KL-506 + (2% starch + 25% Talc)                  77.87   0.7913
1% Mowiol   56-98 + (2% starch + 25% Talc)         84.88   0.7913
2% HR-3010 + (2% starch + 25% Talc)                 84.64   0.7913
2% KL-506 + (2% starch + 25% Talc)                  86.52   0.7913
2% Mowiol   56-98 + (2% starch + 25% Talc)         82.07   0.7913
Absolute zero (100% Bleached  softwood pulp)        66.99   0.7913
Zero (2% starch + 25% Talc)                         80.78   0.7913
(Composition)Sheet
 1% HR-3010 + (2% starch + 25% Talc) 1              82.12   1.5826
 1% HR-3010 + (2% starch + 25% Talc) 2              84.41   1.5826
 1% HR-3010 + (2% starch + 25% Talc) 3              81.62   1.5826
 1% HR-3010 + (2% starch + 25% Talc) 4              86.85   1.5826
 1% KL-506 + (2% starch + 25% Talc) 1               77.73   1.5826
 1% KL-506 + (2% starch + 25% Talc) 2               74.76   1.5826
 1% KL-506 + (2% starch + 25% Talc) 3               76.73   1.5826
 1% KL-506 + (2% starch + 25% Talc) 4               82.27   1.5826
```

```
 1% Mowiol   56-98 + (2% starch + 25% Talc) 1    94.24   1.5826
 1% Mowiol   56-98 + (2% starch + 25% Talc) 2    75.57   1.5826
 1% Mowiol   56-98 + (2% starch + 25% Talc) 3    86.83   1.5826
 1% Mowiol   56-98 + (2% starch + 25% Talc) 4    82.87   1.5826
 2% HR-3010 + (2% starch + 25% Talc) 1           96.36   1.5826
 2% HR-3010 + (2% starch + 25% Talc) 2           84.61   1.5826
 2% HR-3010 + (2% starch + 25% Talc) 3           82.80   1.5826
 2% HR-3010 + (2% starch + 25% Talc) 4           74.78   1.5826
 2% KL-506 + (2% starch + 25% Talc) 1            91.81   1.5826
 2% KL-506 + (2% starch + 25% Talc) 2            83.89   1.5826
 2% KL-506 + (2% starch + 25% Talc) 3            83.35   1.5826
 2% KL-506 + (2% starch + 25% Talc) 4            87.05   1.5826
 2% Mowiol   56-98 + (2% starch + 25% Talc) 1    79.00   1.5826
 2% Mowiol   56-98 + (2% starch + 25% Talc) 2    88.03   1.5826
 2% Mowiol   56-98 + (2% starch + 25% Talc) 3    77.80   1.5826
 2% Mowiol   56-98 + (2% starch + 25% Talc) 4    83.45   1.5826
 Absolute zero (100% Bleached  softwood pulp) 1  67.61   1.5826
 Absolute zero (100% Bleached  softwood pulp) 2  58.39   1.5826
 Absolute zero (100% Bleached  softwood pulp) 3  71.57   1.5826
 Absolute zero (100% Bleached  softwood pulp) 4  70.39   1.5826
 Zero (2% starch + 25% Talc) 1                   88.01   1.5826
 Zero (2% starch + 25% Talc) 2                   71.57   1.5826
 Zero (2% starch + 25% Talc) 3                   83.18   1.5826
 Zero (2% starch + 25% Talc) 4                   80.37   1.5826


Grouping Information Using Tukey Method and 95.0% Confidence

Composition                                    N   Mean  Grouping
2% KL-506 + (2% starch + 25% Talc)            24  86.52  A
1% Mowiol   56-98 + (2% starch + 25% Talc)     24  84.88  A B
2% HR-3010 + (2% starch + 25% Talc)           24  84.64  A B
1% HR-3010 + (2% starch + 25% Talc)           24  83.75  A B C
2% Mowiol   56-98 + (2% starch + 25% Talc)     24  82.07    B C
Zero (2% starch + 25% Talc)                   24  80.78      C D
1% KL-506 + (2% starch + 25% Talc)            24  77.87        D
Absolute zero (100% Bleached  softwood pulp)  24  66.99          E

Means that do not share a letter are significantly different.


Tukey 95.0% Simultaneous Confidence Intervals
Response Variable BDS
All Pairwise Comparisons among Levels of Composition
Composition = 1% HR-3010 + (2% starch + 25% Talc)  subtracted from:

Composition                                    Lower  Center   Upper
1% KL-506 + (2% starch + 25% Talc)            -9.31   -5.88   -2.45
1% Mowiol   56-98 + (2% starch + 25% Talc)     -2.31    1.13    4.56
2% HR-3010 + (2% starch + 25% Talc)           -2.55    0.89    4.32
2% KL-506 + (2% starch + 25% Talc)            -0.66    2.77    6.21
2% Mowiol   56-98 + (2% starch + 25% Talc)     -5.12   -1.68    1.75
Absolute zero (100% Bleached  softwood pulp)  -20.20  -16.76  -13.33
Zero (2% starch + 25% Talc)                   -6.40   -2.97    0.46

Composition                                   ---------+---------+---------+-------
1% KL-506 + (2% starch + 25% Talc)                       (--*--)
1% Mowiol   56-98 + (2% starch + 25% Talc)                     (--*--)
2% HR-3010 + (2% starch + 25% Talc)                            (--*--)
```

```
2% KL-506 + (2% starch + 25% Talc)                              (--*--)
2% Mowiol   56-98 + (2% starch + 25% Talc)                  (--*-)
Absolute zero (100% Bleached  softwood pulp)    (--*--)
Zero (2% starch + 25% Talc)                               (--*-)
                                          ---------+---------+---------+-------
                                                -12         0        12
```

Composition = 1% KL-506 + (2% starch + 25% Talc) subtracted from:

Composition	Lower	Center	Upper
1% Mowiol 56-98 + (2% starch + 25% Talc)	3.57	7.01	10.439
2% HR-3010 + (2% starch + 25% Talc)	3.33	6.77	10.200
2% KL-506 + (2% starch + 25% Talc)	5.22	8.65	12.087
2% Mowiol 56-98 + (2% starch + 25% Talc)	0.76	4.20	7.633
Absolute zero (100% Bleached softwood pulp)	-14.32	-10.88	-7.450
Zero (2% starch + 25% Talc)	-0.52	2.91	6.344

```
Composition                               ---------+---------+---------+-------
1% Mowiol   56-98 + (2% starch + 25% Talc)                        (--*--)
2% HR-3010 + (2% starch + 25% Talc)                               (--*-)
2% KL-506 + (2% starch + 25% Talc)                                 (--*--)
2% Mowiol   56-98 + (2% starch + 25% Talc)                      (-*--)
Absolute zero (100% Bleached  softwood pulp)         (--*--)
Zero (2% starch + 25% Talc)                                     (-*--)
                                          ---------+---------+---------+-------
                                                -12         0        12
```

Composition = 1% Mowiol   56-98 + (2% starch + 25% Talc) subtracted from:

Composition	Lower	Center	Upper
2% HR-3010 + (2% starch + 25% Talc)	-3.67	-0.24	3.19
2% KL-506 + (2% starch + 25% Talc)	-1.79	1.65	5.08
2% Mowiol 56-98 + (2% starch + 25% Talc)	-6.24	-2.81	0.63
Absolute zero (100% Bleached softwood pulp)	-21.32	-17.89	-14.45
Zero (2% starch + 25% Talc)	-7.53	-4.10	-0.66

```
Composition                               ---------+---------+---------+-------
2% HR-3010 + (2% starch + 25% Talc)                           (--*--)
2% KL-506 + (2% starch + 25% Talc)                              (-*--)
2% Mowiol   56-98 + (2% starch + 25% Talc)                  (--*--)
Absolute zero (100% Bleached  softwood pulp)   (--*--)
Zero (2% starch + 25% Talc)                                 (--*-)
                                          ---------+---------+---------+-------
                                                -12         0        12
```

Composition = 2% HR-3010 + (2% starch + 25% Talc) subtracted from:

Composition	Lower	Center	Upper
2% KL-506 + (2% starch + 25% Talc)	-1.55	1.89	5.32
2% Mowiol 56-98 + (2% starch + 25% Talc)	-6.00	-2.57	0.87
Absolute zero (100% Bleached softwood pulp)	-21.08	-17.65	-14.22
Zero (2% starch + 25% Talc)	-7.29	-3.86	-0.42

```
Composition                               ---------+---------+---------+-------
2% KL-506 + (2% starch + 25% Talc)                              (--*-)
2% Mowiol   56-98 + (2% starch + 25% Talc)                  (--*--)
```

```
Absolute zero (100% Bleached  softwood pulp)   (--*--)
Zero (2% starch + 25% Talc)                              (--*--)
                                              ---------+---------+---------+-------
                                                     -12         0        12


Composition = 2% KL-506 + (2% starch + 25% Talc)  subtracted from:

Composition                                    Lower  Center   Upper
2% Mowiol   56-98 + (2% starch + 25% Talc)     -7.89   -4.45   -1.02
Absolute zero (100% Bleached  softwood pulp)  -22.97  -19.54  -16.10
Zero (2% starch + 25% Talc)                    -9.18   -5.74   -2.31

Composition                                   ---------+---------+---------+-------
2% Mowiol   56-98 + (2% starch + 25% Talc)               (--*--)
Absolute zero (100% Bleached  softwood pulp)  (--*--)
Zero (2% starch + 25% Talc)                            (--*--)
                                              ---------+---------+---------+-------
                                                     -12         0        12


Composition = 2% Mowiol   56-98 + (2% starch + 25% Talc)  subtracted from:

Composition                                    Lower  Center   Upper
Absolute zero (100% Bleached  softwood pulp)  -18.52  -15.08  -11.65
Zero (2% starch + 25% Talc)                    -4.72   -1.29    2.15

Composition                                   ---------+---------+---------+-------
Absolute zero (100% Bleached  softwood pulp)     (-*--)
Zero (2% starch + 25% Talc)                                (--*--)
                                              ---------+---------+---------+-------
                                                     -12         0        12


Composition = Absolute zero (100% Bleached  softwood pulp)  subtracted from:

Composition                  Lower  Center  Upper
Zero (2% starch + 25% Talc)  10.36   13.79  17.23

Composition                  ---------+---------+---------+-------
Zero (2% starch + 25% Talc)                              (-*--)
                             ---------+---------+---------+-------
                                    -12         0        12


Tukey Simultaneous Tests
Response Variable BDS
All Pairwise Comparisons among Levels of Composition
Composition = 1% HR-3010 + (2% starch + 25% Talc)  subtracted from:

                                           Difference       SE of
Composition                                  of Means  Difference  T-Value
1% KL-506 + (2% starch + 25% Talc)             -5.88       1.119    -5.25
1% Mowiol   56-98 + (2% starch + 25% Talc)      1.13       1.119     1.01
2% HR-3010 + (2% starch + 25% Talc)             0.89       1.119     0.79
2% KL-506 + (2% starch + 25% Talc)              2.77       1.119     2.48
2% Mowiol   56-98 + (2% starch + 25% Talc)     -1.68       1.119    -1.50
Absolute zero (100% Bleached  softwood pulp)  -16.76       1.119   -14.98
Zero (2% starch + 25% Talc)                    -2.97       1.119    -2.65
```

Composition	Adjusted P-Value
1% KL-506 + (2% starch + 25% Talc)	0.0000
1% Mowiol 56-98 + (2% starch + 25% Talc)	0.9730
2% HR-3010 + (2% starch + 25% Talc)	0.9933
2% KL-506 + (2% starch + 25% Talc)	0.2124
2% Mowiol 56-98 + (2% starch + 25% Talc)	0.8054
Absolute zero (100% Bleached softwood pulp)	0.0000
Zero (2% starch + 25% Talc)	0.1451

Composition = 1% KL-506 + (2% starch + 25% Talc) subtracted from:

Composition	Difference of Means	SE of Difference	T-Value
1% Mowiol 56-98 + (2% starch + 25% Talc)	7.01	1.119	6.260
2% HR-3010 + (2% starch + 25% Talc)	6.77	1.119	6.046
2% KL-506 + (2% starch + 25% Talc)	8.65	1.119	7.732
2% Mowiol 56-98 + (2% starch + 25% Talc)	4.20	1.119	3.752
Absolute zero (100% Bleached softwood pulp)	-10.88	1.119	-9.726
Zero (2% starch + 25% Talc)	2.91	1.119	2.600

Composition	Adjusted P-Value
1% Mowiol 56-98 + (2% starch + 25% Talc)	0.0000
2% HR-3010 + (2% starch + 25% Talc)	0.0000
2% KL-506 + (2% starch + 25% Talc)	0.0000
2% Mowiol 56-98 + (2% starch + 25% Talc)	0.0059
Absolute zero (100% Bleached softwood pulp)	0.0000
Zero (2% starch + 25% Talc)	0.1635

Composition = 1% Mowiol 56-98 + (2% starch + 25% Talc) subtracted from:

Composition	Difference of Means	SE of Difference	T-Value
2% HR-3010 + (2% starch + 25% Talc)	-0.24	1.119	-0.21
2% KL-506 + (2% starch + 25% Talc)	1.65	1.119	1.47
2% Mowiol 56-98 + (2% starch + 25% Talc)	-2.81	1.119	-2.51
Absolute zero (100% Bleached softwood pulp)	-17.89	1.119	-15.99
Zero (2% starch + 25% Talc)	-4.10	1.119	-3.66

Composition	Adjusted P-Value
2% HR-3010 + (2% starch + 25% Talc)	1.0000
2% KL-506 + (2% starch + 25% Talc)	0.8210
2% Mowiol 56-98 + (2% starch + 25% Talc)	0.1997
Absolute zero (100% Bleached softwood pulp)	0.0000
Zero (2% starch + 25% Talc)	0.0081

Composition = 2% HR-3010 + (2% starch + 25% Talc) subtracted from:

Composition	Difference of Means	SE of Difference	T-Value
2% KL-506 + (2% starch + 25% Talc)	1.89	1.119	1.69
2% Mowiol 56-98 + (2% starch + 25% Talc)	-2.57	1.119	-2.29
Absolute zero (100% Bleached softwood pulp)	-17.65	1.119	-15.77

```
Zero (2% starch + 25% Talc)                          -3.86       1.119    -3.45


                                                  Adjusted
Composition                                        P-Value
2% KL-506 + (2% starch + 25% Talc)                  0.6960
2% Mowiol   56-98 + (2% starch + 25% Talc)          0.3035
Absolute zero (100% Bleached  softwood pulp)        0.0000
Zero (2% starch + 25% Talc)                         0.0163


Composition = 2% KL-506 + (2% starch + 25% Talc)  subtracted from:

                                                  Difference       SE of
Composition                                         of Means  Difference  T-Value
2% Mowiol   56-98 + (2% starch + 25% Talc)            -4.45       1.119    -3.98
Absolute zero (100% Bleached  softwood pulp)         -19.54       1.119   -17.46
Zero (2% starch + 25% Talc)                           -5.74       1.119    -5.13

                                                  Adjusted
Composition                                        P-Value
2% Mowiol   56-98 + (2% starch + 25% Talc)          0.0026
Absolute zero (100% Bleached  softwood pulp)        0.0000
Zero (2% starch + 25% Talc)                         0.0000


Composition = 2% Mowiol   56-98 + (2% starch + 25% Talc)  subtracted from:

                                                  Difference       SE of
Composition                                         of Means  Difference  T-Value
Absolute zero (100% Bleached  softwood pulp)         -15.08       1.119   -13.48
Zero (2% starch + 25% Talc)                           -1.29       1.119    -1.15

                                                  Adjusted
Composition                                        P-Value
Absolute zero (100% Bleached  softwood pulp)        0.0000
Zero (2% starch + 25% Talc)                         0.9441


Composition = Absolute zero (100% Bleached  softwood pulp)  subtracted from:

                            Difference       SE of           Adjusted
Composition                   of Means  Difference  T-Value   P-Value
Zero (2% starch + 25% Talc)      13.79       1.119    12.33    0.0000


------------------------------------
ANOVA: BDS versus Composition, Sheet
------------------------------------

Factor              Type   Levels
Composition         fixed       8
Sheet(Composition)  fixed       4

Factor              Values
Composition         1% HR-3010 + (2% starch + 25% Talc), 1% KL-506 + (2% starch
+ 25% Talc), 1% Mowiol   56-98 + (2% starch + 25% Talc), 2% HR-3010 + (2% starch
 + 25% Talc), 2% KL-506 + (2% starch + 25% Talc), 2% Mowiol   56-98 + (2% starch
  + 25% Talc), Absolute zero (100% Bleached  softwood pulp), Zero (2% starch
  + 25% Talc)
```

Sheet(Composition) 1, 2, 3, 4

Analysis of Variance for BDS

Source	DF	SS	MS	F	P
Composition	7	6567.24	938.18	62.43	0.000
Sheet(Composition)	24	4967.08	206.96	13.77	0.000
Error	160	2404.34	15.03		
Total	191	13938.66			

S = 3.87649   R-Sq = 82.75%   R-Sq(adj) = 79.41%

	Source	Variance component	Error term	Expected Mean Square for Each Term (using unrestricted model)
1	Composition		3	(3) + Q[1,2]
2	Sheet(Composition)		3	(3) + Q[2]
3	Error	15.03		(3)

Means

Composition	N	BDS
1% HR-3010 + (2% starch + 25% Talc)	24	83.751
1% KL-506 + (2% starch + 25% Talc)	24	77.872
1% Mowiol 56-98 + (2% starch + 25% Talc)	24	84.877
2% HR-3010 + (2% starch + 25% Talc)	24	84.638
2% KL-506 + (2% starch + 25% Talc)	24	86.525
2% Mowiol 56-98 + (2% starch + 25% Talc)	24	82.071
Absolute zero (100% Bleached softwood pulp)	24	66.988
Zero (2% starch + 25% Talc)	24	80.782

Composition	Sheet	N	BDS
1% HR-3010 + (2% starch + 25% Talc)	1	6	82.118
1% HR-3010 + (2% starch + 25% Talc)	2	6	84.412
1% HR-3010 + (2% starch + 25% Talc)	3	6	81.621
1% HR-3010 + (2% starch + 25% Talc)	4	6	86.855
1% KL-506 + (2% starch + 25% Talc)	1	6	77.728
1% KL-506 + (2% starch + 25% Talc)	2	6	74.764
1% KL-506 + (2% starch + 25% Talc)	3	6	76.726
1% KL-506 + (2% starch + 25% Talc)	4	6	82.270
1% Mowiol 56-98 + (2% starch + 25% Talc)	1	6	94.240
1% Mowiol 56-98 + (2% starch + 25% Talc)	2	6	75.565
1% Mowiol 56-98 + (2% starch + 25% Talc)	3	6	86.834
1% Mowiol 56-98 + (2% starch + 25% Talc)	4	6	82.869
2% HR-3010 + (2% starch + 25% Talc)	1	6	96.358
2% HR-3010 + (2% starch + 25% Talc)	2	6	84.608
2% HR-3010 + (2% starch + 25% Talc)	3	6	82.801
2% HR-3010 + (2% starch + 25% Talc)	4	6	74.783
2% KL-506 + (2% starch + 25% Talc)	1	6	91.808
2% KL-506 + (2% starch + 25% Talc)	2	6	83.891
2% KL-506 + (2% starch + 25% Talc)	3	6	83.348
2% KL-506 + (2% starch + 25% Talc)	4	6	87.052

```
2% Mowiol   56-98 + (2% starch + 25% Talc)    1      6  79.000
2% Mowiol   56-98 + (2% starch + 25% Talc)    2      6  88.030
2% Mowiol   56-98 + (2% starch + 25% Talc)    3      6  77.797
2% Mowiol   56-98 + (2% starch + 25% Talc)    4      6  83.455
Absolute zero (100% Bleached  softwood pulp)  1      6  67.607
Absolute zero (100% Bleached  softwood pulp)  2      6  58.388
Absolute zero (100% Bleached  softwood pulp)  3      6  71.569
Absolute zero (100% Bleached  softwood pulp)  4      6  70.390
Zero (2% starch + 25% Talc)                   1      6  88.006
Zero (2% starch + 25% Talc)                   2      6  71.572
Zero (2% starch + 25% Talc)                   3      6  83.178
Zero (2% starch + 25% Talc)                   4      6  80.372


Residual Plots for BDS


Nested ANOVA: BDS versus Composition, Sheet

Analysis of Variance for BDS

Source        DF          SS        MS       F      P
Composition    7   6567.2440  938.1777   4.533  0.002
Sheet         24   4967.0754  206.9615  13.773  0.000
Error        160   2404.3438   15.0271
Total        191  13938.6632


Variance Components

                         % of
Source       Var Comp.  Total  StDev
Composition     30.467  39.32  5.520
Sheet           31.989  41.28  5.656
Error           15.027  19.39  3.876
Total           77.484         8.802


Expected Mean Squares

1  Composition    1.00(3) +  6.00(2) + 24.00(1)
2  Sheet          1.00(3) +  6.00(2)
3  Error          1.00(3)
```

B.3 Guar Gum & Starch Trial

Listing B.3: Minitab Report: Guar & Starch Trial

```
-------------------------------------------------
General Linear Model: BDS versus Talcum, Additive
-------------------------------------------------

Factor    Type   Levels  Values
Talcum    fixed       2  0.00, 0.25
Additive  fixed       4  0.5% Guar Gum, 3% Cationized Starch, 3% Native Starch,
                         None
```

```
Analysis of Variance for BDS, using Adjusted SS for Tests

Source      DF   Seq SS  Adj SS  Adj MS      F      P
Talcum       1   290.29  398.31  398.31  65.83  0.000
Additive     3   326.17  326.17  108.72  17.97  0.000
Error      139   841.09  841.09    6.05
Total      143  1457.55


S = 2.45988   R-Sq = 42.29%   R-Sq(adj) = 40.63%


Unusual Observations for BDS

Obs      BDS      Fit  SE Fit  Residual  St Resid
 26  32.4253  37.4113  0.4349   -4.9860     -2.06 R
 32  43.5842  37.4113  0.4349    6.1729      2.55 R
 33  43.0622  37.4113  0.4349    5.6509      2.33 R
 41  43.3735  37.4113  0.4349    5.9622      2.46 R
 85  28.7823  35.4186  0.4349   -6.6364     -2.74 R
 87  30.0123  35.4186  0.4349   -5.4063     -2.23 R

R denotes an observation with a large standardized residual.


Expected Mean Squares, using Adjusted SS

             Expected Mean
             Square for
   Source    Each Term
1  Talcum    (3) + Q[1]
2  Additive  (3) + Q[2]
3  Error     (3)


Error Terms for Tests, using Adjusted SS

                                 Synthesis
   Source    Error DF  Error MS  of Error MS
1  Talcum      139.00      6.05  (3)
2  Additive    139.00      6.05  (3)


Variance Components, using Adjusted SS

        Estimated
Source      Value
Error       6.051


Least Squares Means for BDS

Talcum                 Mean  SE Mean
0.00                  31.28   0.4349
0.25                  35.35   0.2511
Additive
0.5% Guar Gum         33.38   0.3551
```

```
3% Cationized Starch  30.66   0.5614
3% Native Starch      33.85   0.5614
None                  35.37   0.3551


Grouping Information Using Dunnett Method and 90.0% Confidence

Talcum           N   Mean  Grouping
0.00 (control)  48  31.28  A
0.25            96  35.35

Means not labeled with letter A are significantly different from control level
     mean.


Dunnett 90.0% Simultaneous Confidence Intervals
Response Variable BDS
Comparisons with Control Level
Talcum = 0.00  subtracted from:

Talcum  Lower  Center  Upper  -----+---------+---------+---------+-
0.25    3.242   4.074  4.905  (---------------*----------------)
                              -----+---------+---------+---------+-
                                 3.50      4.00      4.50      5.00


Dunnett Simultaneous Tests
Response Variable BDS
Comparisons with Control Level
Talcum = 0.00  subtracted from:

        Difference       SE of           Adjusted
Talcum    of Means  Difference  T-Value   P-Value
0.25         4.074      0.5021    8.113    0.0000


Grouping Information Using Dunnett Method and 90.0% Confidence

Additive               N   Mean  Grouping
None (control)        48  35.37  A
3% Native Starch      24  33.85
0.5% Guar Gum         48  33.38
3% Cationized Starch  24  30.66

Means not labeled with letter A are significantly different from control level
     mean.


Dunnett 90.0% Simultaneous Confidence Intervals
Response Variable BDS
Comparisons with Control Level
Additive = None  subtracted from:

Additive               Lower  Center   Upper
0.5% Guar Gum         -3.048  -1.993  -0.938
3% Cationized Starch  -6.114  -4.718  -3.323
3% Native Starch      -2.918  -1.522  -0.126

Additive                -+---------+---------+---------+-----
```

```
0.5% Guar Gum                          (----*----)
3% Cationized Starch    (------*------)
3% Native Starch                       (------*------)
                        -+---------+---------+---------+-----
                      -6.0      -4.0      -2.0       0.0


Dunnett Simultaneous Tests
Response Variable BDS
Comparisons with Control Level
Additive = None  subtracted from:

                     Difference       SE of            Adjusted
Additive               of Means  Difference  T-Value    P-Value
0.5% Guar Gum            -1.993      0.5021   -3.968     0.0004
3% Cationized Starch     -4.718      0.6642   -7.104     0.0000
3% Native Starch         -1.522      0.6642   -2.291     0.0641
```

B.4 Polymer Sizing, Dry– and Wet–Strength Agents Trial

Listing B.4: Minitab Report: Polymer Sizing, Dry– and Wet–Strength Agents Trial

```
------------------------------------------------------------
Nested ANOVA: BDS versus Filler, Additive, Sample nr
------------------------------------------------------------

Analysis of Variance for BDS

Source      DF         SS        MS
Filler       1   706.7280  706.7280
Additive     3   935.7696  311.9232
Sample nr   15   459.9809   30.6654
Error      100   465.2923    4.6529
Total      119  2567.7708


Variance Components

                      % of
Source     Var Comp.  Total  StDev
Filler        10.281  33.18  3.206
Additive      11.719  37.82  3.423
Sample nr      4.335  13.99  2.082
Error          4.653  15.01  2.157
Total         30.989         5.567


Expected Mean Squares

1  Filler       1.00(4) +  6.00(3) + 24.00(2) + 38.40(1)
2  Additive     1.00(4) +  6.00(3) + 24.00(2)
3  Sample nr    1.00(4) +  6.00(3)
4  Error        1.00(4)


------------------------------------------------------------
```

General Linear Model: BDS versus Filler, Additive, Sample nr

Factor	Type	Levels	Values
Filler	fixed	2	25% Talc, None
Additive(Filler)	fixed	5	0.4% Polymer Surface sizing, 1% Dry-strength Additive, 2% wet-strength Additive, None, None
Sample nr(Filler Additive)	fixed	20	6.2.1, 6.2.2, 6.2.3, 6.2.7, 6.3.1, 6.3.2, 6.3.3, 6.3.4, 6.4.1, 6.4.2, 6.4.3, 6.4.4, 6.1.1, 6.1.2, 6.1.3, 6.1.7, 6.5.1, 6.5.2, 6.5.3, 6.5.4

Analysis of Variance for BDS, using Adjusted SS for Tests

Source	DF	Seq SS	Adj SS	Adj MS	F	P
Thickness (um)	1	81.61	0.79	0.79	0.17	0.683
Filler	1	819.09	603.50	603.50	128.62	0.000
Additive(Filler)	3	820.65	288.20	96.07	20.47	0.000
Sample nr(Filler Additive)	15	381.92	381.92	25.46	5.43	0.000
Error	99	464.51	464.51	4.69		
Total	119	2567.77				

S = 2.16610 R-Sq = 81.91% R-Sq(adj) = 78.26%

Term	Coef	SE Coef	T	P
Constant	30.16	19.49	1.55	0.125
Thickness (u	0.02035	0.04973	0.41	0.683

Unusual Observations for BDS

Obs	BDS	Fit	SE Fit	Residual	St Resid
17	30.4054	34.6133	0.8868	-4.2079	-2.13 R
28	50.1018	45.5159	0.8955	4.5859	2.33 R
31	44.9757	40.8765	0.8845	4.0992	2.07 R
103	41.5207	35.5533	0.9164	5.9674	3.04 R
104	28.9620	35.3091	0.9534	-6.3471	-3.26 R
106	29.2183	35.5126	0.8955	-6.2943	-3.19 R
108	41.0081	35.3701	0.9083	5.6380	2.87 R

R denotes an observation with a large standardized residual.

Expected Mean Squares, using Adjusted SS

	Source	Expected Mean Square for Each Term
1	Thickness (um)	(5) + Q[1]
2	Filler	(5) + Q[2, 3 , 4]
3	Additive(Filler)	(5) + Q[3, 4]
4	Sample nr(Filler Additive)	(5) + Q[4]
5	Error	(5)

Error Terms for Tests, using Adjusted SS

	Source	Error DF	Error MS	Synthesis of Error MS
1	Thickness (um)	99.00	4.69	(5)
2	Filler	99.00	4.69	(5)
3	Additive(Filler)	99.00	4.69	(5)
4	Sample nr(Filler Additive)	99.00	4.69	(5)

Variance Components, using Adjusted SS

Source	Estimated Value
Error	4.692

Means for Covariates

Covariate	Mean	StDev
Thickness (um)	390.6	10.32

Least Squares Means for BDS

Filler			Mean	SE Mean
25% Talc			41.19	0.2256
None			35.03	0.4773
(Filler)Additive				
25% Talc	0.4% Polymer Surface sizing		44.56	0.7177
25% Talc	1% Dry-strength Additive		37.38	0.6444
25% Talc	2% wet-strength Additive		43.57	0.4437
25% Talc	None		39.25	0.5419
None	None		35.03	0.4773
(Filler Additive)Sample nr				
25% Talc	0.4% Polymer Surface sizing	6.2.1	45.08	1.2788
25% Talc	0.4% Polymer Surface sizing	6.2.2	40.46	1.3587
25% Talc	0.4% Polymer Surface sizing	6.2.3	49.22	0.8878
25% Talc	0.4% Polymer Surface sizing	6.2.7	43.48	0.9645
25% Talc	1% Dry-strength Additive	6.3.1	35.99	1.0466
25% Talc	1% Dry-strength Additive	6.3.2	37.61	1.2675
25% Talc	1% Dry-strength Additive	6.3.3	38.40	0.9022
25% Talc	1% Dry-strength Additive	6.3.4	37.53	0.9133
25% Talc	2% wet-strength Additive	6.4.1	41.39	1.0083
25% Talc	2% wet-strength Additive	6.4.2	43.23	0.9022
25% Talc	2% wet-strength Additive	6.4.3	42.94	0.8843
25% Talc	2% wet-strength Additive	6.4.4	46.73	0.8976
25% Talc	None	6.1.1	39.09	1.0932
25% Talc	None	6.1.2	35.46	0.8846
25% Talc	None	6.1.3	41.72	0.9056
25% Talc	None	6.1.7	40.71	0.9682
None	None	6.5.1	34.58	0.9966
None	None	6.5.2	35.82	0.8848
None	None	6.5.3	34.50	0.9072
None	None	6.5.4	35.22	0.8848

Grouping Information Using Tukey Method and 95.0% Confidence

Filler	N	Mean	Grouping
25% Talc	96	41.19	A

```
None      24  35.03    B

Means that do not share a letter are significantly different.


Tukey 95.0% Simultaneous Confidence Intervals
Response Variable BDS
All Pairwise Comparisons among Levels of Filler
Filler = 25% Talc  subtracted from:

Filler   Lower  Center   Upper  ------+---------+---------+---------+
None    -7.237  -6.159  -5.081  (----*-----)
                               ------+---------+---------+---------+
                                  -6.0      -4.0      -2.0       0.0


Tukey Simultaneous Tests
Response Variable BDS
All Pairwise Comparisons among Levels of Filler
Filler = 25% Talc  subtracted from:

        Difference       SE of           Adjusted
Filler    of Means  Difference  T-Value   P-Value
None        -6.159      0.5431   -11.34    0.0000


Grouping Information Using Tukey Method and 95.0% Confidence

Filler    Additive                       N   Mean  Grouping
25% Talc  0.4% Polymer Surface sizing  24  44.56  A
25% Talc  2% wet-strength Additive     24  43.57  A
25% Talc  None                         24  39.25     B
25% Talc  1% Dry-strength Additive     24  37.38       C
None      None                         24  35.03       C

Means that do not share a letter are significantly different.


Tukey 95.0% Simultaneous Confidence Intervals
Response Variable BDS
All Pairwise Comparisons among Levels of Additive(Filler)
Filler = 25% Talc
Additive = 0.4% Polymer Surface sizing  subtracted from:

Filler    Additive                    Lower  Center   Upper
25% Talc  1% Dry-strength Additive  -10.53  -7.176  -3.818
25% Talc  2% wet-strength Additive   -3.26  -0.989   1.286
25% Talc  None                       -8.31  -5.315  -2.319
None      None                      -11.57  -9.529  -7.488

Filler    Additive                  ---------+---------+---------+-------
25% Talc  1% Dry-strength Additive   (-----*-----)
25% Talc  2% wet-strength Additive               (--*---)
25% Talc  None                         (----*----)
None      None                      (--*---)
                                    ---------+---------+---------+-------
                                          -6.0       0.0       6.0
```

```
Filler = 25% Talc
Additive = 1% Dry-strength Additive  subtracted from:

Filler    Additive                    Lower  Center   Upper
25% Talc  2% wet-strength Additive   3.952   6.187  8.4213
25% Talc  None                       0.070   1.861  3.6510
None      None                      -4.857  -2.353  0.1503

Filler    Additive                  ---------+---------+---------+-------
25% Talc  2% wet-strength Additive                          (--*---)
25% Talc  None                                     (--*--)
None      None                           (---*---)
                                    ---------+---------+---------+-------
                                          -6.0       0.0       6.0


Filler = 25% Talc
Additive = 2% wet-strength Additive  subtracted from:

Filler    Additive   Lower  Center   Upper
25% Talc  None       -6.32  -4.326  -2.335
None      None      -10.32  -8.540  -6.757

Filler    Additive  ---------+---------+---------+-------
25% Talc  None              (---*--)
None      None        (--*--)
                    ---------+---------+---------+-------
                          -6.0       0.0       6.0


Filler = 25% Talc
Additive = None  subtracted from:

Filler  Additive   Lower  Center   Upper  ---------+---------+---------+-------
None    None      -6.427  -4.214  -2.001          (---*---)
                                        ---------+---------+---------+-------
                                              -6.0       0.0       6.0


Tukey Simultaneous Tests
Response Variable BDS
All Pairwise Comparisons among Levels of Additive(Filler)
Filler = 25% Talc
Additive = 0.4% Polymer Surface sizing  subtracted from:

                                  Difference       SE of           Adjusted
Filler    Additive                  of Means  Difference  T-Value   P-Value
25% Talc  1% Dry-strength Additive    -7.176      1.2084    -5.94    0.0000
25% Talc  2% wet-strength Additive    -0.989      0.8187    -1.21    0.7466
25% Talc  None                        -5.315      1.0784    -4.93    0.0000
None      None                        -9.529      0.7345   -12.97    0.0000


Filler = 25% Talc
Additive = 1% Dry-strength Additive  subtracted from:

                                  Difference       SE of           Adjusted
Filler    Additive                  of Means  Difference  T-Value   P-Value
25% Talc  2% wet-strength Additive     6.187      0.8041    7.694    0.0000
```

25% Talc	None	1.861	0.6443	2.888	0.0375
None	None	-2.353	0.9009	-2.612	0.0759

Filler = 25% Talc
Additive = 2% wet-strength Additive subtracted from:

Filler	Additive	Difference of Means	SE of Difference	T-Value	Adjusted P-Value
25% Talc	None	-4.326	0.7167	-6.04	0.0000
None	None	-8.540	0.6414	-13.31	0.0000

Filler = 25% Talc
Additive = None subtracted from:

Filler	Additive	Difference of Means	SE of Difference	T-Value	Adjusted P-Value
None	None	-4.214	0.7964	-5.291	0.0000

Appendix C

Miscellaneous

C.1 Wiring Diagram of the actuator in the TSDC Spectrometer.

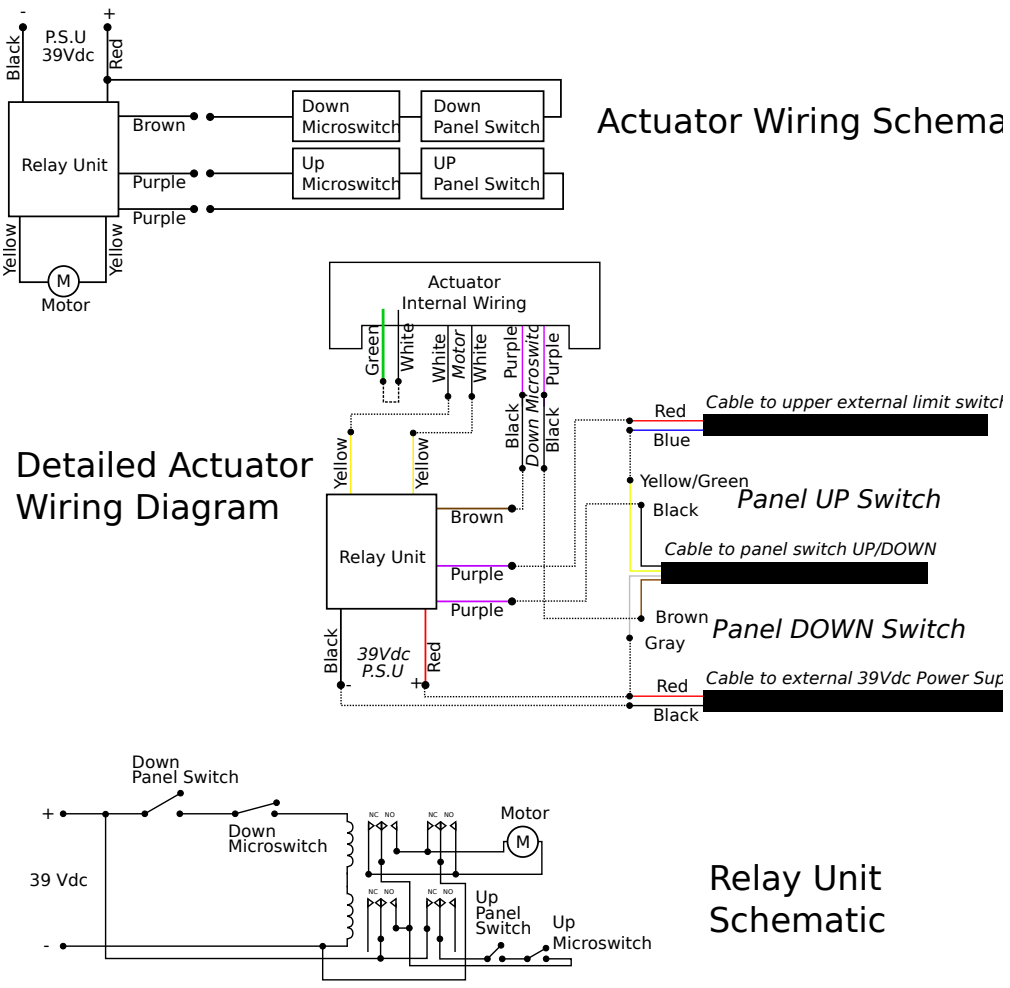

FIGURE C.1: Wiring diagram of the actuator repair.

C.2 LabVIEW Programme Code

LabVIEW code of the custom control programme for the TSDC Spectrometer

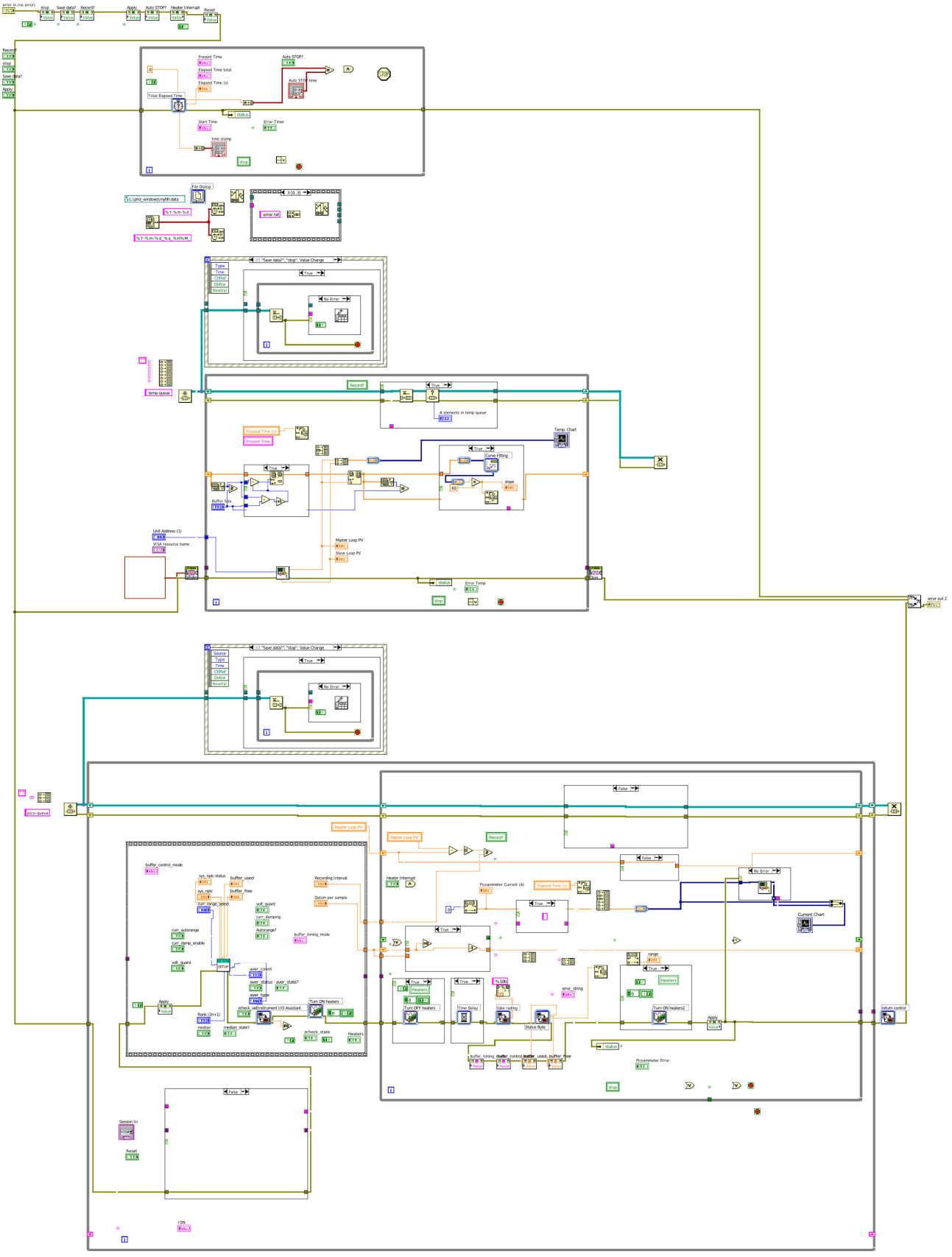

C.3 Mastersizer Report

The following page shows the report on the particle size distribution of the talcum filler employed in this research as determined by the Mastersizer 2000 particle distribution analyser by Malvern Instruments Ltd., Malvern, UK. The red numbers above the graph state the particle size in µm for which 10%, 50% or 90% of the particle distribution are equal or smaller in size.

MASTERSIZER 2000

Result Analysis Report

Sample Name:
talcum, 1. Measurement

SOP Name:
Talc1

Measured:
Thursday, July 26, 2012 4:31:36 PM

Sample Source & type:

Measured by:
bea

Analysed:
Thursday, July 26, 2012 4:31:37 PM

Sample bulk lot ref:

Result Source:
Measurement

Particle Name:
Talc

Accessory Name:
Hydro 2000MU (A)

Analysis model:
General purpose

Sensitivity:
Enhanced

Particle RI:
1.589

Absorption:
0.1

Size range:
0.020 to 2000.000 um

Obscuration:
12.19 %

Dispersant Name:
Wasser

Dispersant RI:
1.330

Weighted Residual:
0.715 %

Result Emulation:
Off

Concentration:
0.0152 %Vol

Span :
2.132

Uniformity:
0.661

Result units:
Volume

Specific Surface Area:
0.679 m²/g

Surface Weighted Mean D[3,2]:
8.838 um

Vol. Weighted Mean D[4,3]:
18.281 um

---

d(0.1): 4.464 um **d(0.5):** 15.123 um **d(0.9):** 36.707 um

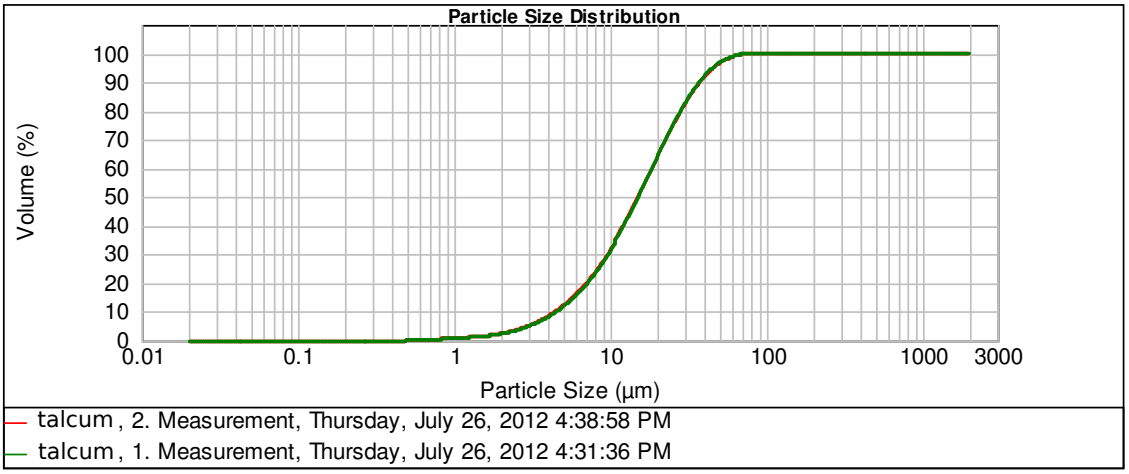

Size (µm)	Volume In %
0.010	0.00
0.011	0.00
0.013	0.00
0.015	0.00
0.017	0.00
0.020	0.00
0.023	0.00
0.026	0.00
0.030	0.00
0.035	0.00
0.040	0.00
0.046	0.00
0.052	0.00
0.060	0.00
0.069	0.00
0.079	0.00
0.091	0.00
0.105	0.00

Size (µm)	Volume In %
0.105	0.00
0.120	0.00
0.138	0.00
0.158	0.00
0.182	0.00
0.209	0.00
0.240	0.00
0.275	0.00
0.316	0.00
0.363	0.00
0.417	0.00
0.479	0.08
0.550	0.14
0.631	0.18
0.724	0.20
0.832	0.20
0.955	0.20
1.096	0.20

Size (µm)	Volume In %
1.096	0.21
1.259	0.25
1.445	0.33
1.660	0.45
1.905	0.61
2.188	0.81
2.512	1.04
2.884	1.32
3.311	1.64
3.802	2.00
4.365	2.40
5.012	2.85
5.754	3.35
6.607	3.89
7.586	4.47
8.710	5.05
10.000	5.63
11.482	

Size (µm)	Volume In %
11.482	6.16
13.183	6.59
15.136	6.88
17.378	6.98
19.953	6.85
22.909	6.48
26.303	5.88
30.200	5.07
34.674	4.14
39.811	3.16
45.709	2.21
52.481	1.37
60.256	0.72
69.183	0.19
79.433	0.03
91.201	0.00
104.713	0.00
120.226	

Size (µm)	Volume In %
120.226	0.00
138.038	0.00
158.489	0.00
181.970	0.00
208.930	0.00
239.883	0.00
275.423	0.00
316.228	0.00
363.078	0.00
416.869	0.00
478.630	0.00
549.541	0.00
630.957	0.00
724.436	0.00
831.764	0.00
954.993	0.00
1096.478	0.00
1258.925	

Size (µm)	Volume In %
1258.925	0.00
1445.440	0.00
1659.587	0.00
1905.461	0.00
2187.762	0.00
2511.886	0.00
2884.032	0.00
3311.311	0.00
3801.894	0.00
4365.158	0.00
5011.872	0.00
5754.399	0.00
6606.934	0.00
7585.776	0.00
8709.636	0.00
10000.000	0.00

Operator notes:

Bibliography

[1] T. Kleemann and S. Badak, "Improvement of Insulating Papers," in *International Munich Paper Symposium*, (Munich), 2012.

[2] T. Kleemann, P. Lewin, S. Badak, and S. Kleemann, "Investigation on Insulation Paper," in *Congresso Aticelca*, (Ascoli Piceno / Italy), 2012.

[3] T. Kleemann, P. Lewin, S. Badak, and S. Kleemann, "Paper & Power: Modifying Electrical Insulation Paper," *Professional Papermaking*, vol. 9, pp. 21–24, 2012.

[4] T. Kleemann, P. Lewin, S. Badak, and S. Kleemann, "Paper & Power: Optimierung von Isolationspapieren," *Wochenblatt für Papierfabrikation*, vol. 6, pp. 468–471, 2012.

[5] E. Kuffel, W. S. Zaengl, and J. Kuffel, *High Voltage Engineering: Fundamentals*. Elsevier Ltd., 2nd ed. ed., 2000.

[6] J. Kolowrotkiewicz, M. Baranski, W. Szeleg, and L. Dlugiewicz, "FE analysis of induction motor working in cryogenic temperature," *COMPEL: The International Journal for Computation and Mathematics in Electrical and Electronic Engineering*, vol. 26, no. 4, pp. 952–964, 2007.

[7] J. Gerhold, "Properties of cryogenic insulants," *Cryogenics*, vol. 38, no. 11, pp. 1063–1081, 1998.

[8] A. Küchler, *Hochspannungstechnik*. Berlin, Heidelberg: Springer Berlin Heidelberg, 2009.

[9] F. Krähenbühl, B. Bernstein, M. Danikas, J. Densley, K. Kadotani, M. Kahle, M. Kosaki, H. Mitsui, M. Nagao, J. Smit, and T. Tanaka, "Properties of Electrical Insulating Material at Cryogenic Temperatures: A Literature Review," *IEEE Electrical Insulation Magazine*, vol. 10, no. 4, pp. 10–22, 1994.

[10] M. Kosaki, M. Nagao, N. Shimizu, and Y. Mizuno, "Solid insulation and its deterioration," *Cryogenics*, vol. 38, pp. 1095–1104, Nov. 1998.

[11] J. Indumathi and J. Bijwe, "Wear of cryo-treated engineering polymers and composites," *Comparative and General Pharmacology*, pp. 343–353, 1999.

[12] D. A. Wigley, *Materials for low temperature use*, vol. 29 of *Engineering Design Guides*. Oxford University Press, 1978.

[13] S. Nishijima and M. Hara, "Mechanical influence on long-term dielectric performance of insulants," *Cryogenics*, vol. 38, no. 11, pp. 1105–1113, 1998.

[14] M. Ieda, "Dielectric Breakdown Process of Polymers," *Electrical Insulation, IEEE Transactions on*, vol. EI-15, pp. 206–224, June 1980.

[15] H. Yamaoka, K. Miyata, and O. Yano, "Cryogenic properties of engineering plastic films," *Cryogenics*, vol. 35, no. 11, pp. 787–789, 1995.

[16] L. A. Dissado and J. C. Fothergill, *Electrical Degradation and Breakdown in Polymers*, vol. 9 of *IEE Materials and Devices Series*. Peter Peregrinus Ltd., London, UK, 1992.

[17] N/S, "This work has been released into the public domain by its author.."

[18] G. Hartwig, *Polymer Properties at Room and Cryogenic Temperatures*. The International Cryogenic Monograph Series, 233 Spring Streek, New York, N.Y. 10013: Plenum Press, 1994.

[19] Y. Mizuno, M. Nagao, M. Kosaki, N. Shimizu, and K. Horii, "Interaction of partial discharge streamers in cryogenic fluids with polymeric films," *Electrical Insulation, IEEE Transactions on*, vol. 23, pp. 689–695, Aug. 1988.

[20] M. Fukuma, K. Fukunaga, and C. Laurent, "Packet-like space charge in polyethylene probed with a 2D-spatial resolution," in *Electrical Insulation and Dielectric Phenomena, 2006 IEEE Conference on*, pp. 748–751, 2006.

[21] M. Fukuma, K. Fukunaga, and C. Laurent, "Two-dimensional structure of charge packets in polyethylene under high dc fields," *Applied Physics Letters*, vol. 88, no. 25, p. 253110, 2006.

[22] F. Boufayed, G. Teyssèdre, C. Laurent, S. Le Roy, L. A. Dissado, P. Ségur, and G. C. Montanari, "Models of bipolar charge transport in polyethylene," *Journal of Applied Physics*, vol. 100, no. 10, p. 104105, 2006.

[23] R. J. Fleming, "Space charge profile measurement techniques: recent advances and future directions," *Dielectrics and Electrical Insulation, IEEE Transactions on*, vol. 12, no. 5, pp. 967–978, 2005.

[24] X. Wang, P. L. Lewin, A. E. Davies, and S. J. Sutton, "Method to determine the trapping level of a polymeric material from thermally stimulated discharge current measurements," *Science, Measurement and Technology, IEE Proceedings* -, vol. 147, no. 1, pp. 2–6, 2000.

[25] O. Yano and H. Yamaoka, "Cryogenic properties of polymers," *Progress in Polymer Science*, vol. 20, no. 4, pp. 585–613, 1995.

[26] W. Weihan and H. Fengnian, "Mechanical and Dielectric Assessment of Ultrahigh Molecular Weight Polyethylene Insulation for Cryogenic Applications," *Electrical Insulation, IEEE Transactions on [see also Dielectrics and Electrical Insulation, IEEE Transactions on]*, vol. 27, no. 3, pp. 504–512, 1992.

[27] W. Weihan and H. Fengnian, "Electrical treeing and stress cracking in polyethylene at cryogenic temperature," in *Properties and Applications of Dielectric Materials, 1991., Proceedings of the 3rd International Conference on*, vol. 1, pp. 322–326, 1991.

[28] Y. S. Touloukian, *Thermal expansion: nonmetallic solids*, vol. 13 of *Thermophysical properties of matter*. New York : IFI/Plenum: New York : IFI/Plenum, 1977.

[29] H. Dominghaus, *Die Kunststoffe und ihre Eigenschaften*. Düsseldorf: VDI Verlag GmbH, 3 ed., 1988.

[30] G. Menges, E. Haberstroh, W. Michaeli, and E. Schmachtenberg, *Werkstoffkunde Kunststoffe*. Carl Hanser Verlag München, 5 ed., 2002.

[31] H. L. Stein, "Ultra High Molecular Weigh Polyethylene (UHMWPE)," 1999.

[32] S. M. Kurtz, *The UHMWPE Handbook: Ultra-High Molecular Weight Polyethylene in Total Joint Replacement*. Elsevier Academic Press, 1968.

[33] E. Neagu and C. Dias, "Charge injection/extraction at a metal-dielectric interface: Experimental validation," *Electrical Insulation Magazine, IEEE*, vol. 25, no. 1, pp. 15–22, 2009.

[34] N. Benrekaa, A. Gourari, M. Bendaoud, R. Saoud, and C. Guerbi, "TSDC study of structural relaxation on polyethylene terephthalate," *Journal of Non-Crystalline Solids*, vol. 352, pp. 4804–4808, Nov. 2006.

[35] R. M. Neagu, E. R. Neagu, I. M. Kalogeras, and A. Vassilikou-Dova, "Evaluation of the dielectric parameters from TSDC spectra: application to polymeric systems," *Materials Research Innovations*, vol. 4, no. 2, pp. 115–125, 2001.

[36] J. C. Canadas, J. A. Diego, J. Sellares, M. Mudarra, and J. Belana, "Cold crystallization effects in PET and PEN by TSDC, DSC and X-ray diffraction," in *Electrets, 1999. ISE 10. Proceedings. 10th International Symposium on*, pp. 103–106, IEEE, 1999.

[37] Y. Gorokhovatsky, D. Temnov, J. N. Marat-Mendes, C. J. M. Dias, and D. K. Das-Gupta, "On the nature of thermally stimulated discharge current spectra in

polyethylene terephthalate," *Journal of Applied Physics*, vol. 83, no. 10, p. 5337, 1998.

[38] R. Kressmann, G. M. Sessler, P. Gunther, and S.-c. Electrets, "Space-charge electrets," *Dielectrics and Electrical Insulation, IEEE Transactions on*, vol. 3, pp. 607–623, Oct. 1996.

[39] Ticona, "Fortron PPS." "http://www.ticona.co.uk/fortron", 2009.

[40] T. Mizutani, Y. Suzuoki, A. Fujii, and T. Suzuki, "Space charge and electrical breakdown in polyphenylene sulfide films," in *Electrical Insulation and Dielectric Phenomena, 1993. Annual Report., Conference on*, pp. 168–173, Oct. 1993.

[41] T. Mizutani, M. Hikita, A. Umemura, and M. Ieda, "Electrical breakdown and space charge of polyphenylene sulfide films," in *Electrical Insulation and Dielectric Phenomena, 1989. Annual Report., Conference on*, pp. 315–320, Nagoya University, 1989.

[42] C. J. Biermann, *Essentials of pulping and papermaking*. Academic Press, 1993.

[43] N. Lavoine, I. Desloges, A. Dufresne, and J. Bras, "Microfibrillated cellulose – Its barrier properties and applications in cellulosic materials: A review," *Carbohydrate Polymers*, vol. 90, pp. 735–764, Oct. 2012.

[44] M. Kouris and A. P. Institute, *Dictionary of paper*. TAPPI Press, 1996.

[45] W. E. Scott, *Principles of Wet End Chemistry*. Tappi Press Publications, Tappi Press, 1996.

[46] ZELLCHEMING Technical Comittee Chemical Additives (CHAD), ed., *Chemical Additives for the Production of Pulp & Paper: Functionally Essential - Ecologically Benefical*. Deutscher Fachverlag, 2008.

[47] G. Teyssedre and C. Laurent, "Charge transport modeling in insulating polymers: from molecular to macroscopic scale," *Dielectrics and Electrical Insulation, IEEE Transactions on*, vol. 12, no. 5, pp. 857–875, 2005.

[48] W. S. Lau, *Simultaneous Space Charge and Current Measurements in Polyethylene Insulation under HVDC Conditions*. PhD thesis, School of Electronics and Computer Science, Faculty of Engineering, Science and Mathematics, University of Southampton, Aug. 2003.

[49] D. L. Reger, S. R. Goode, and D. W. Ball, *Chemistry: Principles and Practice*. Brooks/Cole, Cengage Learning, 2010.

[50] P. J. Harrop, *Dielectrics*. 88 Kingsway, London WC2B 6AB: Butterworth & Co. Ltd., 1972.

[51] S. R. Elliott, *The Physics and Chemistry of Solids*. John Wiley & Sons Ltd., 2005.

[52] T. Blythe and D. Bloor, *Electrical Properties of Polymers*. Cambridge University Press, 2nd ed. ed., 2005.

[53] G. Parker, *Introductory Semiconductor Device Physics*. Institute of Physics Publishing, 2004.

[54] J. William D. CAllister, *Materials Science and Engineering: An Introduction*. 111 River Street, Hoboken, NJ 07030: John Wiley & Sons, Inc., 6th ed. ed., 2003.

[55] A. M. Stoneham, *Theory of Defects in Solids - Electronic Structure of Defects in Insulators and Semiconductors*. Oxford University Press, 1975.

[56] T. J. Lewis, "Electrical Effects at Interfaces and Surfaces," *Electrical Insulation, IEEE Transactions on*, vol. EI-21, pp. 289–295, June 1986.

[57] A. M. Ariffin, *The measurement and modelling of electromluminescence in high voltage polymeric cable insulation*. PhD thesis, School of Electronics and Computer Science, University Road, Southampton SO17 1BJ, 2008.

[58] S. N. F. Mott and E. A. Davis, *Electronic Processes in non-Crystalline Materials*. The International Series of Monographs on Physics, Clarendon Press · Oxford, 2nd ed. ed., 1979.

[59] H. Böttger and V. V. Bryksin, *Hopping Conduction in Solids*. VCH Publishers, 1985.

[60] G. Blaise, "Charge localization and transport in disordered dielectric materials," *Journal of Electrostatics*, vol. 50, pp. 69–89, Jan. 2001.

[61] P. W. Anderson, "Absence of Diffusion in Certain Random Lattices," *Phys. Rev.*, vol. 109, pp. 1492–1505, Mar. 1958.

[62] N. F. Mott, *Metal–Insulator Transitions*. Taylor & Francis Ltd., 2nd ed., 1990.

[63] M. Falck, G. Dreyfus, and J. Lewiner, "Vapor-induced depolarization currents. I. Models," *Phys. Rev. B*, vol. 25, pp. 5499–5508, Apr. 1982.

[64] M. Falck, G. Dreyfus, and J. Lewiner, "Vapor-induced depolarization current . II. Application," *Phys. Rev. B*, vol. 25, pp. 5509–5514, Apr. 1982.

[65] S. Holé, "Recent Developments in the Pressure Wave Propagation Method," *Most*, vol. 25, no. 3, pp. 7–20, 2009.

[66] T. Takada, "Acoustic and optical methods for measuring electric charge distributions in dielectrics," in *Electrical Insulation and Dielectric Phenomena, 1999 Annual Report Conference on*, pp. 1–14, 1999.

[67] N. H. Ahmed and N. N. Srinivas, "Review of Space Charge Measurements in Dielectrics," *Dielectrics and Electrical Insulation, IEEE Transactions on [see also Electrical Insulation, IEEE Transactions on]*, vol. 4, no. 5, pp. 644–656, 1997.

[68] G. Chen, "Space Charge Measurement as a Diagnostic Tool to Monitor Ageing in Polymeric Materials," *Electrical and Electronic Materials, Transactions on*, vol. 7, no. 5, pp. 235–239, 2006.

[69] K. Fukunaga, "Progress and Prospects in PEA Space Charge Measurement Techniques - [Feature Article]," *Electrical Insulation Magazine, IEEE*, vol. 24, no. 3, pp. 26–37, 2008.

[70] J. M. Alison, "A high field pulsed electro-acoustic apparatus for space charge and external circuit current measurement within solid insulators," *Measurement Science and Technology*, vol. 9, no. 10, pp. 1737–1750, 1998.

[71] Y. Li and T. Takada, "Progress in space charge measurement of solid insulating materials in Japan," *IEEE Electr. Insul. M.*, vol. 10, no. 5, pp. 16–28, 1994.

[72] J. Lewiner, S. Holé, and T. Ditchi, "Pressure wave propagation methods: a rich history and a bright future," *Dielectrics and Electrical Insulation, IEEE Transactions on*, vol. 12, no. 1, pp. 114–126, 2005.

[73] T. Maeno, "Three-dimensinal PEA Charge Measurement System," *IEEE Transactions on Dielectrics and Electrical Insulation*, vol. 8, pp. 845–848, Oct. 2001.

[74] T. Maeno, "Portable Space Charge Measurement System Using the Pulsed Electrostatic Method," vol. 10, no. 2, pp. 331–335, 2003.

[75] S. Holé, T. Ditchi, and J. Lewiner, "Non-destructive methods for space charge distribution measurements: what are the differences?," *Dielectrics and Electrical Insulation, IEEE Transactions on*, vol. 10, no. 4, pp. 670–677, 2003.

[76] T. Ditchi, C. Alquié, and J. Lewiner, "Broadband determination of ultrasonic attenuation and phase velocity in insulating materials," *The Journal of the Acoustical Society of America*, vol. 94, no. 6, pp. 3061–3066, 1993.

[77] S. Holé and U. Pierre, "Resolution of Direct Space Charge Distribution Measurement Methods," *IEEE Transactions on Dielectrics and Electrical Insulation*, vol. 15, no. 3, pp. 861–871, 2008.

[78] R. Ono, M. Nakazawa, T. Oda, S. Member, and A. Negatively, "Charge storage in corona-charged polypropylene films analyzed by LIPP and TSC methods," *Industry Applications, IEEE Transactions on*, vol. 40, no. 6, pp. 1482–1488, 2004.

[79] J. Lewiner, O. Naz, T. Ditchi, and C. Alquie, "Study of charge injection in insulators submitted to diverging fields," *Dielectrics and Electrical Insulation, IEEE Transactions on*, vol. 5, pp. 2–8, Feb. 1998.

[80] M. Wübbenhorst and J. Van Turnhout, "Thermal wave methods: some experimental pitfalls," in *Electrets, 1994. (ISE 8), 8th International Symposium on*, pp. 182–187, Sept. 1994.

[81] A. Mellinger, R. Singh, M. Wegener, W. Wirges, R. Gerhard-Multhaupt, and S. B. Lang, "Three-dimensional mapping of polarization profiles with thermal pulses," *Applied Physics Letters*, vol. 86, no. 8, p. 082903, 2005.

[82] S. Bauer and S. Bauer-Gogonea, "Current Practice in Space Charge and Polarization Profile Measurements Using Thermal Techniques," *IEEE Transactions on Dielectrics and Electrical Insulation*, vol. 10, no. 5, pp. 883–902, 2003.

[83] J. Castellon, P. Notingher, S. Agnel, A. Toureille, F. Brame, P. Mirebeau, J. Matallana, and J. F. Brame, "Electric field and space charge measurements in thick power cable insulation," *Electrical Insulation Magazine, IEEE*, vol. 25, no. 3, pp. 30–42, 2009.

[84] S. B. Lang and D. K. Das-Gupta, "A new technique for determination of the spatial distribution of polarization in polymer electrets," *Ferroelectrics*, vol. 60, no. 1, pp. 23–36, 1984.

[85] S. B. Lang, "Laser intensity modulation method (LIMM): review of the fundamentals and a new method for data analysis," *Dielectrics and Electrical Insulation, IEEE Transactions on*, vol. 11, no. 1, pp. 3–12, 2004.

[86] D. Marty-Dessus, L. Berquez, A. Petre, and J. L. Franceschi, "Space charge cartography by FLIMM : a three-dimensional approach," *Integrated Ferroelectrics*, vol. 35, pp. 3249–3256, 2002.

[87] A. Mellinger, R. Singh, and R. Gerhard-Multhaupt, "Fast thermal-pulse measurements of space-charge distributions in electret polymers," *Review of Scientific Instruments*, vol. 76, no. 1, p. 013903, 2005.

[88] A. Mellinger, R. Flores-Suárez, R. Singh, M. Wegener, W. Wirges, R. Gerhard, and S. B. Lang, "Thermal-Pulse Tomography of Space-charge and Polarization Distributions in Electret Polymers," *International Journal of Thermophysics*, vol. 29, pp. 2046–2054, Nov. 2008.

[89] J. M. Reboul, "Simultaneous Space Charge and TSDC Measurements On Polarized Polymer," *IEEE Transactions on Dielectrics and Electrical Insulation*, vol. 13, pp. 1016–1022, Oct. 2006.

[90] K. S. Suh, J. Tanaka, and D. Damon, "What is TSC?," *IEEE Electr. Insul. M.*, vol. 8, no. 6, pp. 13–20, 1992.

[91] C. Lew and M. O. Thompson, "A fast ramp rate thermally stimulated current technique to quantify electronic charge dynamics in thin films.," *The Review of scientific instruments*, vol. 79, p. 43906, Apr. 2008.

[92] C. Lavergne and C. Lacabanne, "A review of thermo-stimulated current," *Electrical Insulation Magazine, IEEE*, vol. 9, no. 2, pp. 5–21, 1993.

[93] R. Gerhard-Multhaupt, "Electrets: Dielectrics with Quasi-Permanent Charge or Polarization," *Electrical Insulation, IEEE Transactions on*, vol. EI-22, no. 5, pp. 531–554, 1987.

[94] J. M. Criado, M. J. Dianez, F. J. Gotor, M. D. Alcala, C. Real, M. D. Alcalá, and L. A. Perez-Maqueda, "Development of an experimental tool for measuring electrical properties of materials from liquid nitrogen temperature up to 1000°C," *Thermochimica Acta*, vol. 351, pp. 125–130, 2000.

[95] A. Roos and J. J. Keyzer, "A helium cryostat for dielectric measurements," *Journal of Physics E: Scientific Instruments*, vol. 16, no. 7, pp. 591–594, 1983.

[96] V. R. Nikitenko, A. Kadashchuk, R. Schmechel, H. V. Seggern, H. von Seggern, and Y. Korosko, "Effect of dispersive transport and partial trap filling on thermally stimulated current in conjugated polymers," *Journal of Applied Physics*, vol. 98, no. 10, p. 103702, 2005.

[97] N.J.Griffiths, M.P.Robinson, U. Betke, C.W.Hill, N. J. Griffiths, M. P. Robinson, and C. W. Hill, *Design and Construction of a Thermally Stimulated Current Spectrometer*. 4th year M.Eng. project report, Faculty of Engineering and Applied Science, University of Southampton, 1994.

[98] J. D. Menczel and R. B. Prime, *Thermal Analysis of Polymers, Fundamentals and Applications*. John Wiley and Sons Ltd., 2007.

[99] G. Teyssedre and C. Lacabanne, "Some considerations about the analysis of thermostimulated depolarization peaks," *Journal of Physics D: Applied Physics*, vol. 28, no. 7, pp. 1478–1487, 1995.

[100] N. A. Nikonorova, T. I. Borisova, E. B. Barmatov, P. Pissis, and R. Diaz-Calleja, "Comparative dielectric and TSDC studies of molecular mobility in liquid-crystalline side-chain poly(methacrylate)," *Polymer*, vol. 43, pp. 2229–2238, Apr. 2002.

[101] F. Henn, J.-C. J.-c. C. Giuntini, M. Cedex, J. Bisquert, and G. Garcia-Belmonte, "An explanation of the peculiar behavior of TSDC peaks at Tg: a simple model of entropy relaxation," *IEEE Transactions on Dielectrics and Electrical Insulation*, vol. 13, pp. 1042–1048, Oct. 2006.

[102] Y. Gorokhovatsky, D. Temnov, J. N. Marat-Mendes, C. J. Dias, and D. K. Das-Gupta, "On the energy spectrum of electrically active defects in polyethylene terephthalate (PET) films," *Electrets, 1999. ISE 10. Proceedings. 10th International Symposium on*, pp. 339–342, 1999.

[103] G. Damamme, C. Le Gressus, and A. S. De Reggi, "Space Charge Characterization for the 21th Century," *IEEE Transactions on Dielectrics and Electrical Insulation, IEEE Transactions on [see also Electrical Insulation, IEEE Transactions on]*, vol. 4, no. 5, pp. 558–584, 1997.

[104] G. Moya, G. Blaise, G.Moya, and G.Blaise, "Charge trapping–detrapping induced thermodynamic relaxation processes," in *Space Charge in Solid Dielectrics* (J. C. Fothergill and L. A. Dissado, eds.), ch. 2, pp. 19–28, The Dielectrics Society, 1997.

[105] S. Holé, A. Sylvestre, O. G. Lavallée, C. Guillermin, P. Rain, and S. Rowe, "Space charge distribution measurement methods and particle loaded insulating materials," *Journal of Physics D: Applied Physics*, vol. 39, pp. 950–956, Mar. 2006.

[106] T. Maeno and K. Fukunaga, "High-resolution PEA Charge Distribution Measurement System," *IEEE Transactions on Dielectrics and Electrical Insulation*, vol. 3, no. 6, pp. 754–757, 1996.

[107] R. E. Collins, "Practical application of the thermal pulsing technique to the study of electrets," *Journal of Applied Physics*, vol. 51, no. 6, pp. 2973–2986, 1980.

[108] D. J. Swaffield, P. L. Lewin, G. Chen, and J. K. Sykulski, "Cryogenic Dielectrics and HTS Power Aparatus: Research at the Univerity of Southampton," *IEEE Electrical Insulation Magazine*, vol. 22, no. 5, pp. 29–37, 2006.

[109] N. Hozumi, H. Suzuki, T. Okamoto, K. Watanabe, and A. Watanabe, "Direct observation of time-dependent space charge profiles in XLPE cable under high electric fields," *IEEE Transactions on Dielectrics and Electrical Insulation*, vol. 1, no. 6, pp. 1068–1076, 1994.

[110] "Model 6514 System Electrometer Instruction Manual," 2003.

[111] SciPy.org, "http://www.scipy.org/Cookbook/FiltFilt [Accessed: 2012-07-05]," 2012.

[112] S. Maeta and K. Sakaguchi, "On the Determination of Trap Depth from Thermally Stimulated Currents," *Japanese Journal of Applied Physics*, vol. 19, pp. 519–526, Mar. 1980.

[113] C. D. Green, "Polyethylene-montmorillonite nanocomposites," Sept. 2008.

[114] G. Sawa, M. Kawade, D. C. Lee, and M. Ieda, "Thermally Stimulated Current from Polyethylene in High-Temperature Region," *Japanese Journal of Applied Physics*, vol. 13, no. 10, pp. 1547–1553, 1974.

[115] A. Thielen, J. Niezette, G. Feyder, and J. Vanderschueren, "Thermally stimulated current study of space charge formation and contact effects in metal-polyethylene terephthalate film-metal systems. II. Influence of polarization conditions," *Journal of Physics and Chemistry of Solids*, vol. 57, no. 11, pp. 1581–1591, 1996.

[116] A. Thielent, J. Niezettet, G. Feyders, and J. Van, "Thermally stimulated current study of space charge formation and contact effects in metal-polyethylene terephthalate film-metal systems. I. Generalities and Theoretical Model," *J.Phys. Chem Solids*, vol. 57, no. 11, pp. 1567–1580, 1996.

[117] A. Thielen, J. Niezette, J. Vanderschueren, G. Feyder, Q. T. Le, and R. Caudano, "Thermally stimulated current study of space-charge formation and contact effects in metal-polyethylene terephthalate films-metal systems. III. Influence of heat treatments," *Journal of Physics and Chemistry of Solids*, vol. 58, no. 4, pp. 607–622, 1997.

[118] V. M. Gun'ko, V. I. Zarko, E. V. Goncharuk, L. S. Andriyko, V. V. Turov, Y. M. Nychiporuk, R. Leboda, J. Skubiszewska-Zieba, a. L. Gabchak, V. D. Osovskii, Y. G. Ptushinskii, G. R. Yurchenko, O. a. Mishchuk, P. P. Gorbik, P. Pissis, and J. P. Blitz, "TSDC spectroscopy of relaxational and interfacial phenomena," *Advances in Colloid and Interface Science*, vol. 131, pp. 1–89, Feb. 2007.

[119] G. A and S. Gubanski, "Thermostimulated depolarization currents in thermally aged polyethylene terephthalate (PET) films," *Properties and Applications of . . .*, pp. 8–10, 1988.

[120] T. Pop, I. Pop, D. Ionescu, R. Ispasoiu, S. Cotescu, and M. Marza, "Dielectric characterization of some low permittivity polymers by thermally stimulated depolarization current method," *Microelectronic Engineering*, vol. 33, no. 1-4, pp. 385–393, 1997.

[121] E. R. Neagu, J. N. Marat-Mendes, D. K. Das-Gupta, R. M. Neagu, and R. Igreja, "Analysis of the thermally stimulated discharge current around glass-rubber transition temperature in polyethylene terephthalate," *Journal of Applied Physics*, vol. 82, pp. 2488–2496, Sept. 1997.

[122] R. E. Mark, *Handbook of physical and mechanical testing of paper and paperboard*. No. v. 1 in Handbook of Physical and Mechanical Testing of Paper and Paperboard, Dekker, 1983.

[123] E. Laredo, D. Newman, A. Bello, and A. J. Müller, "Primary and secondary dielectric relaxations in semi-crystalline and amorphous starch," *European Polymer Journal*, vol. 45, no. 5, pp. 1506–1515, 2009.

[124] T. Mizutani, M. Ieda, S. Ochiai, and M. Ito, "Interfacial polarization in silicone oil-polypropylene insulating system," *Journal of Electrostatics*, vol. 12, pp. 427–433, 1982.

[125] J. B. Whitehead, "The dielectric losses in impregnated paper," *American Institute of Electrical Engineers, Transactions of the*, vol. 52, pp. 667 –681, june 1933.

[126] J. B. Whitehead, I. Part, and E. W. Greenfield, "Dielectric Properties of Cellulose Paper - II," *Electrical Engineering*, pp. 1498–1503, 1934.

[127] T. A. Prevost and T. V. Oommen, "Cellulose Insulation in Oil-Filled Power Transformers : Part I — History and Development," *Electrical Insulation Magazine, IEEE*, vol. 22, no. 1, pp. 28–35, 2006.

[128] T. V. Oommen and T. A. Prevost, "Cellulose Insulation in Oil-Filled Power Transformers : Part II – Maintaining Insulation Integrity and Life," *Electrical Insulation Magazine, IEEE*, vol. 22, no. 2, pp. 5–14, 2006.

[129] M. Schaible, "Electrical Insulation Papers - An Overview," *IEEE Electrical Insulation Magazine*, vol. 3, no. 1, pp. 8–12, 1987.

[130] H. Sheppard, "A century of progress in electrical insulation," *IEEE Electrical Insulation Magazine*, vol. 2, no. 5, pp. 20–30, 1986.

[131] K. Giese, "The Effects of Cellulose Insulation Quality on Electrical Intrinsic Strength," vol. 10, no. 5, pp. 38–42, 2000.

[132] S. J. Ferrito and R. L. Stegehuis, "High Temperature Reinforced Cellulose Insulation for Use in Electrical Applications," vol. 00, no. C, pp. 7285–7288, 2001.

[133] "IEEE Guide for the Statistical Analysis of Electrical Insulation Breakdown Data," Tech. Rep. April, IEEE, 2005.

[134] I. L. Hosier, A. S. Vaughan, and S. G. Swingler, "Structure – property relationships in polyethylene blends : the effect of morphology on electrical breakdown strength," *Journal of Materials Science*, vol. 2, no. 32, pp. 4523–4531, 1997.

[135] A. Anagnostopoulou-Konsta and P. Pissis, "The influence of humidity on the dielectric properties of wood," 1988.

[136] L. Apekis, C. Christodoulides, and P. Pissis, "Dielectric properties of paper as a function of moisture content," 1988.

[137] A. Kirak, H. Yilmaz, S. Güler, and c. Güler, "Dielectric properties and electric conductivity of talc and doped talc," *Journal of Physics D: Applied Physics*, vol. 32, no. 15, p. 1919, 1999.

[138] E. Burdukova, M. Becker, D. J. Bradshaw, and J. S. Laskowski, "Presence of negative charge on the basal planes of New York talc," *Journal of Colloid and Interface Science*, vol. 315, no. 1, pp. 337–342, 2007.

[139] L. Nasrat, M. Abdelwahab, and G. Ismail, "Improvement of Used Transformer Oils with Activated Bentonite," *Engineering*, vol. 03, no. 06, pp. 588–593, 2011.

[140] M. Harun, E. Saion, and A. Kassim, "Dielectric properties of poly (vinyl alcohol)/polypyrrole composite polymer films," *J. Adv. Sci. Arts*, vol. 1, no. 1, pp. 9–16, 2009.

[141] T. G. Abdel-Malik, R. Abdel-Latif, A. Sawaby, and S. Ahmed, "Electrical Properties of Pure and Doped Polyvinyl Alcohol (PVA) Films Using Gold and Aluminum Electrodes," *Journal of Applied Sciences Research*, vol. 4, no. 3, pp. 331–336, 2008.

[142] "Nytro Libra SAFETY DATA SHEET," Tech. Rep. 1907, Nynas AB, Stockholm, 2010.

[143] S. M. Hasheminezhad, E. Ildstad, and A. Nysveen, "Breakdown Strength of Solid | Solid Interface," vol. 0, no. 2, pp. 2–5, 2010.

[144] J. Roberts, *Paper Chemistry*. Chapman & Hall, 1996.

[145] L. L. Barré, A. S. Vaughan, and S. J. Sutton, "On the solid-state ageing behaviour of the polysaccharide, guar gum," *Journal of Materials Science*, vol. 42, no. 14, pp. 5497–5507, 2007.

[146] J. Lee, "Adsorption analysis of cationic guar gum on fibers in closed papermaking systems," *Tappi Journal*, vol. 4, no. 10, pp. 15–19, 2005.

[147] K. Burnfield, "Cationic Starch/cationic Galactomannan Gum Blends as Strength and Drainage Aids," *EP Patent 1,049,832*, vol. 99, no. 19, pp. 1–8, 2002.